The Dissertation Committee for Borje Michael Jacobsson Certifies that this is the approved version of the following dissertation:

MATERIALS DEVELOPMENT FOR STEP AND FLASH IMPRINT LITHOGRAPHY

Committee:

C. Grant Willson, Supervisor

Christopher W. Bielawski

Richard M. Crooks

Brent L. Iverson

Christopher J. Ellison

Materials Development for Step and Flash Imprint Lithography

by

Borje Michael Jacobsson, M.S.; B.S.; B.A.

Dissertation

Presented to the Faculty of the Graduate School of
The University of Texas at Austin
in Partial Fulfillment
of the Requirements
for the Degree of

Doctor of Philosophy

The University of Texas at Austin
August 2011

Dedication

Farfar

&

Mormor

Acknowledgements

First and foremost, I want to express sincere gratitude to Professor C. Grant Willson for his continuous guidance, encouragement and support. Under his supervision, I gained great insight into accomplishing personal aspirations of becoming a better Scientist, leader and person in general. It is this insight that I will carry throughout my life and for which I will remain forever indebted.

I would like to thank Mrs. Kathleen Sparks for her indispensable talents in making group operations run easily and efficiently. Specifically, I want to thank her for lending a helping hand during times of need and for ensuring that every deadline is met. I have immense appreciation for all that she does.

Drs. Frank Palmieri, Mikey Lin, and Kane Jen are a few pioneers of projects with which I have been involved. Thank you for taking me under your wings and for teaching me a considerable amount about imprint lithography. I would still be a novice to all aspects of imprint lithography were it not for your assistance early on during my time at UT. Special thanks belong to Tsuyoshi Ogawa, a visiting scientist from Central Glass Co., whose tenacious work ethic and willingness to help cannot be fully expressed. I am honored to have a friend like you. In addition, I want to thank several other visiting scientists and post-doctoral researchers – Dr. Sangwoong Yoon (Nissan Chemical), Dr. Jianjun Hao (Sachem), Yukio Nishimura (JSR), and Sungyong Bae (Samsung). I also feel fortunate to have had the opportunity to work with very bright and talented undergraduate students such as Will Durand who is currently pursuing his Ph.D. in Chemical Engineering at the University of Texas; Daniel Hellebusch who is currently enrolled in

graduate school at the University of California, Berkeley; and Jason Eubank who is employed at Huntsman. Best of luck to all of you in your future endeavors.

Many thanks are owed to Drs. Jacob Adams, Brian Long, and Jeff Strahan. All were invaluable resources to an incoming first year graduate student as well as great friends. Without them, my graduate career may have ended prematurely. Fellow class members Xinyu Gu and Brandon Rawlings have greatly assisted in understanding engineering related problems that I have encountered. I would especially like to thank Ryan Deschner for his countless number of hours in the clean room giving the "old" Imprio 55 some TLC. I would also like to thank Will Bell for insightful and interesting conversations over breakfast tacos and cups of coffee. In addition, Logan Santos, Dr. Adam Berro, Chris Bates, Ryan Mesch, Chris Chen, and Hao Tang have been great colleagues with whom I have enjoyed working.

I would like to thank the NMR facility, especially Steve Sorey and Dr. Ben Shoulders who have greatly assisted with analysis and interpretation of difficult NMR spectra. I so appreciate Dr. Vince Lynch in the X-ray crystallography facility and Prof. Hugo Steinfink as well as UT glassblower, Mike Ronalter, whose design and repair skills proved helpful on several occasions. Gabriel Glenn of the MER has been a great source of knowledge and assistance in restoring the imprint tool in our laboratory. I have genuinely enjoyed many insightful conversations with Professor Kenneth Liechti regarding modulus measurements. Importantly, Penny Kile's work as chemistry graduate program coordinator has proved invaluable to the many graduate students facing registration deadlines, dues, and job appointments.

During my time at the University of Texas, I have developed friendships with members from Professor Iverson's research group, without which late nights in Welch

Hall and fierce racquetball matches in Gregory Gym would have occurred on a less enjoyable or frequent basis.

I am also grateful to Gunnar Fornander, Hans Chrunak, and Gustaf Johansson for successfully convincing me to attend college in the United States following my completion of secondary education in Sweden.

Finally and most importantly, I have enormous gratitude for my family and loved ones in Sweden, France, and the United States. While my parents and I have lived half a world apart for over thirteen years, they remain steadfast sources of support for personal and professional pursuits. I am also very lucky and grateful for my brilliant big brother, Richard, whose curiosity and many accomplishments within particle physics continue to inspire me. Lastly, I want to thank my wonderful wife, Elizabeth, for her unconditional love and continuous encouragement. This would not have been possible without you by my side.

Materials Development for Step and Flash Imprint Lithography

Publication No._____________

Borje Michael Jacobsson, Ph.D.
The University of Texas at Austin, 2011

Supervisor: C. Grant Willson

The quest for smaller and faster integrated circuits (ICs) continues, but traditional photolithography, the patterning process used to fabricate them, is rapidly approaching its physical limits. Step and Flash Imprint Lithography (S-FIL®) is a low-cost patterning technique which has shown great potential for next generation semiconductor manufacturing. To date, all methods of imprint lithography have utilized a sacrificial resist to produce device features. Our goal has been to develop functional materials such as insulators that can be directly patterned by S-FIL and then remain as a part of the end product. Directly patternable dielectric (DPD) materials must meet multiple mechanical and physical requirements for application in microelectronic devices. In some cases these requirements are conflicting, which leads to material design challenges. Many different materials and curing methods have been evaluated. Thiol-ene based approaches to patterning hyperbranched materials incorporating Polyhedral Oligomeric Silsesquioxanes (POSS) have shown the greatest promise. Thiol-ene polymerization takes place by a free radical mechanism, but it has the advantage over acrylates of not being inhibited by the presence of oxygen. This greatly eases some engineering design challenges for the S-FIL process. A number of thiol-ene formulations have been prepared and their mechanical and electrical properties evaluated.

SFIL-R has been introduced as an alternative technology to SFIL. SFIL-R offers improvements to SFIL in several ways, but requires a high silicon content, low viscosity, planarizing material. Photopolymerizable branched siloxanes were synthesized and evaluated to function as a planarizing topcoat for this technology.

Both SFIL and SFIL-R require a clean separation of the template from the resist material. Fouling of templates is a major concern in imprint lithography and fluorinated materials are used to treat templates to lower their surface energy for better separation. It has been observed that the template treatment degrades over time and needs to be replaced for further imprinting. A fluorinated silazane was designed to repair the degraded areas. This material was evaluated and functions as designed.

Table of Contents

List of Tables

List of Figures

List of Schemes

Chapter 1: Introduction to Nanolithography

1.1 SOCIETAL IMPACT

The domestication of animals, farming with irrigation, the wheel, and penicillin are a few adaptations and discoveries that have had a profound impact on the world, but few discoveries have had a greater impact than the transistor. ENIAC, the first electronic computer, was based on vacuum tube technology. It consisted of approximately 18,000 vacuum tubes, weighed over 30 tons, and occupied an area of about 1800 square feet [1]. Its impressive demonstration of solving mathematical problems led the drive to develop smaller and more efficient computing technology. The transistor was discovered in the middle of the 20th century and rapidly replaced vacuum tubes. The integrated circuit (IC) was developed independently by Robert Noyce of Fairchild Semiconductor and Jack Kilby of Texas Instruments in 1959 and is the basis of today's semiconductor industry. It is an industry that employs several hundreds of thousands of people and touches the lives of billions of people all around the world whether it is through personal computing, communication devices, or medical equipment. Since the introduction of ICs, the development of faster, smaller, and more integrated semiconductor devices has taken place at an astonishing rate, and over the years the semiconductor industry has seen tremendous growth [2].

1.2 MOORE'S LAW

In the 1960's, the co-founder and former CEO of Intel, Gordon Moore, observed a trend in the development and cost for the production of microprocessors. He has been credited with predicting that the number of transistors would double approximately every two years (Figure 1.1). In fact, this conclusion was drawn from Moore's original statement in 1965 that the cost of manufacturing transistors would decrease so newer products could continually be developed at the same price [3].

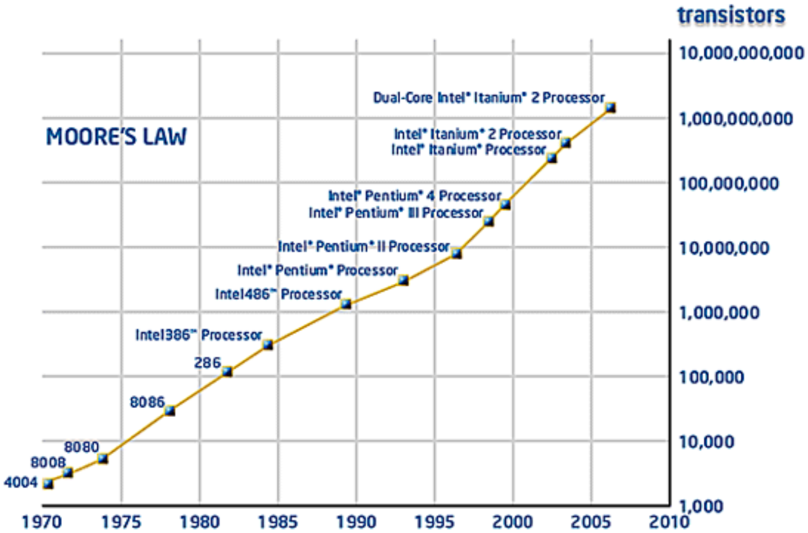

Figure 1.1: The evolution of the microprocessor confirms that Moore's law has held true for the past four decades [4].

By comparison, a cell phone battery with approximately 30 minutes of talk time in the early 1990's [5] would last for about 19 days (of constant talking) in 2010 if it had followed the same trend as microprocessor development. A former graduate student, Jacob Adams, made a more impressive and relevant comparison when comparing the efficiency of the combustion engine from 1978 until the year 2000. He claimed that even though the average car has continually improved its fuel efficiency over the years, it is nowhere near the 26,000 miles per gallon that would be the improvement relative to the transistor density increase that the microelectronic industry was able to achieve over the same time span [6]. The demand for faster and better computing devices is out there, but how has the technology been able to improve at such an incredible pace?

1.3 THE PHOTOLITHOGRAPHIC PROCESS

A major force behind this remarkable evolution has been due to advances in photolithography. The word lithography stems from two Greek words: *lithos*, which translates to *stone*, and *graphia,* which translates to *writing* [7]. The process by which photolithography works is illustrated in Figure 1.2. The basic steps will be briefly discussed to give a better understanding of the technology.

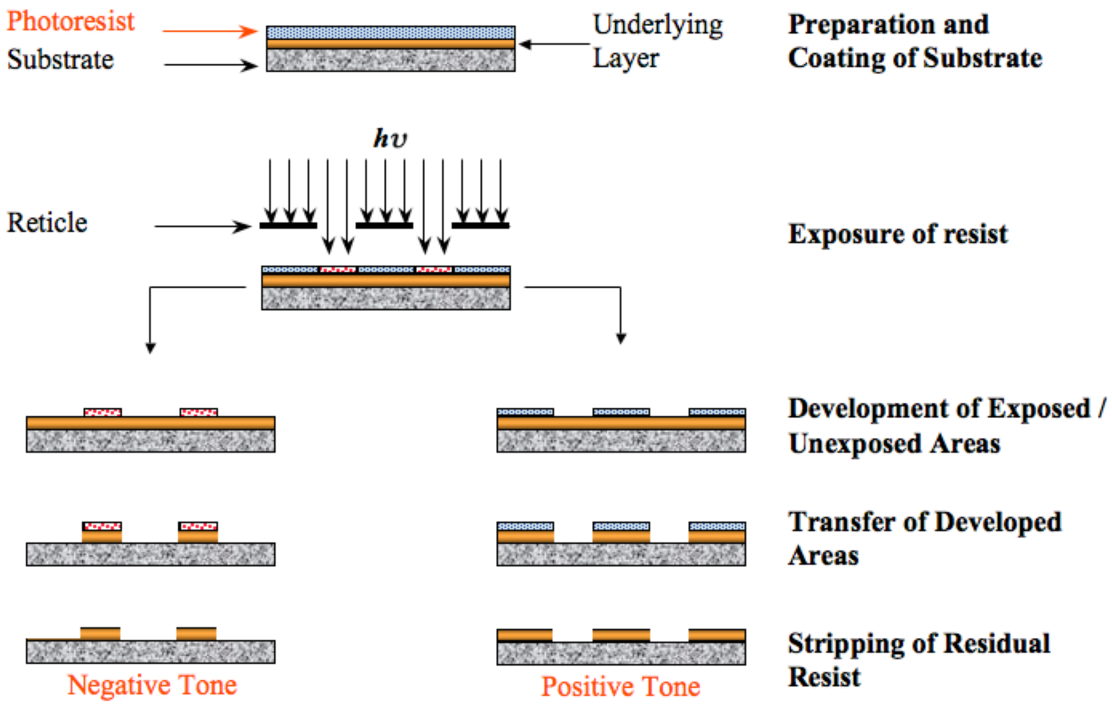

Figure 1.2: Schematic representation of the photolithographic process.

1.3.1 Preparation of Substrate for Projection Lithography

The first step in the process is to prepare the substrate or wafer for optimal resist performance. Silicon wafers are highly reflective, and to avoid reflection of light and exposure of resist in undesirable areas, a bottom anti-reflective coating (BARC) is coated onto the wafer. In addition to a BARC, an adhesion promoter may also be coated on the wafer. The surface of the wafer is highly hydrophilic and by coating a silicon-containing material such as hexamethyldisilazane (HMDS), the hydrophilicity can be decreased to facilitate the adhesion of mainly organic-based (hydrophobic) photoresist.

1.3.2 Deposition of Photoresist Formulations

The resist formulations are prepared by resist vendors and are ready for use upon delivery. Most formulations are trade secrets but generally consist of a photosensitive polymer or a polymer containing reactive functional groups, a low vapor pressure solvent, and some sort of photoacid or photobase generator (PAG or PBG). The acid or base generator is the photosensitive component and is used to locally alter the solubility of the polymer. Common casting solvents include: chlorobenzene, propylene glycol methyl ether acetate (PGMEA), and diglyme. Photoresists are coated onto the wafer by spin-coating, and resist thickness is controlled by the amount of resist dispensed, spin speed, and spin duration.

1.3.3 Post Apply Bake

A soft bake or post apply bake (PAB) is carried out to evaporate any residual solvent from the polymer film. The time and temperature are dependent on the photoresist formulation used for spin-coating. The wafer is now ready to undergo exposure.

1.3.4 Exposure of Photoresist

In order to expose the photoresist, light is passed through a photomask and then focused onto the wafer. As the photons strike the resist material, a photochemical reaction takes place decomposing the PAG or the PBG into an actual acid or base [8]. The exposed area forms a latent image of the photomask with an acid or base concentration that is higher than in the unexposed regions. Light sources for the lithography process have been driven to shorter and shorter wavelengths, from mercury g-line (436 nm) sources in the early 1980's to the ArF excimer laser (193 nm) used in current lithography. Part of the reason for this shortening is because of Rayleigh's equation described later in this chapter. This decrease of wavelength over the years requires newer and more advanced resist formulations to be developed. The conventional resists in use today are sacrificial resists, and have only one purpose: to transfer a pattern replicated from a master photomask into an underlying substrate. When light of an appropriate wavelength is used to expose the resist, a change in dissolution rate (a switch in solubility) occurs with respect to the resist developer. As depicted in Figure 1.2, whether the change makes the resist more or less soluble determines whether the resist is positive or negative in tone, respectively.

1.3.5 Post Exposure Bake

After the exposure has taken place, a post exposure bake (PEB) is carried out. This bake facilitates the controlled diffusion of the acid or the base generated throughout the exposed regions of the film. It is also performed in order to overcome the activation energy barrier required to deprotect or cross-link the polymer. The deprotection of poly(*t*-BOC-styrene), a positive-tone resist component commonly used in 365 nm lithography, is illustrated in Scheme 1.1 [9].

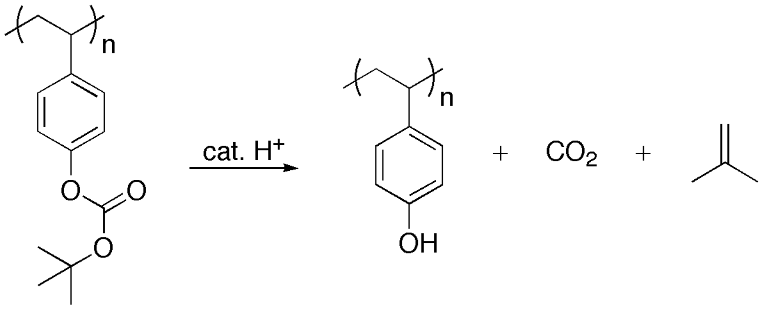

Scheme 1.1: Acid-catalyzed deprotection of poly(*t*-BOC-styrene).

This is the step that produces the solubility switch. The more groups that are deprotected or crosslinked, the greater the difference in solubility; however, a balance needs to be maintained since the acid or base diffuses isotropically and parts of the unexposed regions may start to become soluble.

1.3.6 Develop Exposed or Unexposed Regions

Once the solubility switch has taken place, the more soluble areas are developed away (dissolved) by an efficient solvent. Aqueous mixtures of tetramethylammonium hydroxide are commonly used as developer.

1.3.7 Pattern Transfer

As described before, the term *photoresist* suggests two functions. *Photo* for its photoresponsive nature, and *resist* due to its resistance to some etchant. A reactive ion etch (RIE) is a common way to transfer a photoresist pattern into an underlying layer. Ions are accelerated toward the surface of the substrate where they act to ‘chip’ away the material. The source for the ions is selected to achieve high etch selectivity between the photoresist and the exposed underlying layer. Once the etch process is finished and the pattern has been transferred into the substrate or some other layer (dielectric or insulating layer, polysilicon, etc.), the remaining photoresist is then stripped off.

1.3.8 Damascene

The final stage in the fabrication process step is the deposition of a metal that can efficiently carry an electrical signal. There are two basic structures in the wiring of a microelectronic device: trenches that form the channels for the wires and hole-like vias that connect one wiring layer to the next one located above or below it. This metallization process is referred to as a damascene or dual damascene process depending on whether only via or trench structures or both via and trench structures are metallized simultaneously. Once the metal has been deposited and polished, the entire process is repeated to generate the next layers of a wiring component.

1.4 CHEMISTRY OF RESIST MATERIALS

As with the wavelength of radiation and the miniaturization of feature size, photoresist materials have undergone continuous change [10]. For the photoreaction to take place efficiently, the polymer needs to be transparent to the incident radiation so that photons are only absorbed by the photoactive component, PAC, such as PAG or PBG in the formulation. In addition, to avoid pattern collapse, the material has to have sufficient mechanical strength to withstand a variety of fabrication processes such as heating and cooling cycles, and etch steps. Bis-azides were used in the 1980's as a negative-tone photoresist, meaning that the exposed areas become less soluble than the unexposed areas due to the cross-linking of the polymer. Scheme 1.2 illustrates a generic azide-based photo crosslinking reaction with a reactive nitrene intermediate.

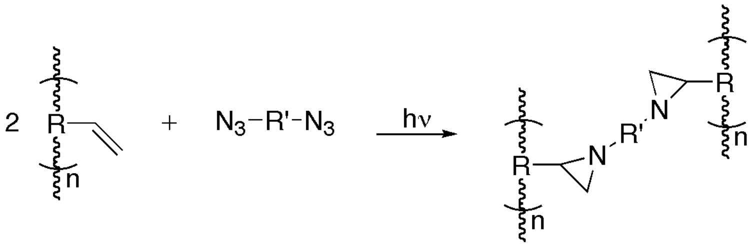

Scheme 1.2: Nominal structure for a bis-azide crosslinking reaction used as negative-tone photoresist.

The nitrene intermediate can undergo a variety of reactions, such as coupling with other nitrenes to form azo compounds, amine formation from hydrogen abstraction, and most importantly, addition to unsaturated functionalities. This crosslinks the material rendering it insoluble in developer. Bis-azide-based photoresists were used for many years, until the development of positive tone resists. Positive tone photoresists generally have greater thermal stability and resolution and exhibit less swelling. Negative tone resists use an organic solvent to dissolve unexposed areas whereas positive tone resists use an aqueous developer to remove exposed regions. Dissolution with organic solvents tends to swell the resist, reducing pattern fidelity. Diazonaphthoquinone – Novolac was one of the first commercial positive tone resists. It consists of a polyphenol matrix (seen in Figure 1.3) with a photoactive dissolution inhibitor mixed in the matrix.

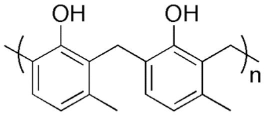

Figure 1.3: Structure of novolac resin.

Novolac is soluble in organic solvent and in aqueous base developer due to the phenolic functionalities. Addition of diazonapthoquinone (DNQ) renders the resin insoluble in aqueous base. The photo-induced decomposition of DNQ that renders exposed regions soluble can be seen in Scheme 1.3.

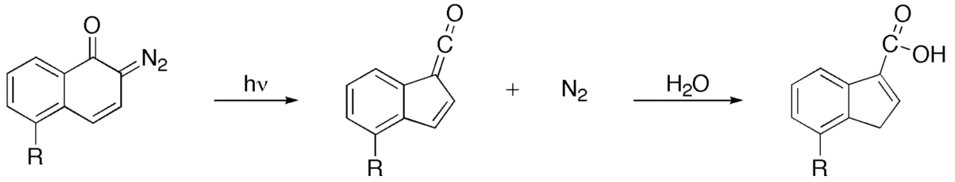

Scheme 1.3: Exposure of diazonaphthoquinone results in a photochemical decomposition ultimately resulting in a carboxylic acid.

As the exposure wavelength was shortened to below 300 nm, the output intensity from the source began to decrease dramatically. There was an imminent need to develop a resist that was much more photosensitive than novolac-based resins. Chemically amplified resists (CARs) were developed at IBM in the 1980’s. CARs function through a two-step process. First, a photoacid generator decomposes upon irradiation to form an acid. Second, a post-exposure bake allows for controlled diffusion of the acid in the photoresist film and provides energy to promote acidolysis of some labile functionality. The deprotection reaction produces more acid, and chemical amplification is achieved. One example, the acid-catalyzed deprotection of a *t*-butyl ester, is shown in Scheme 1.4.

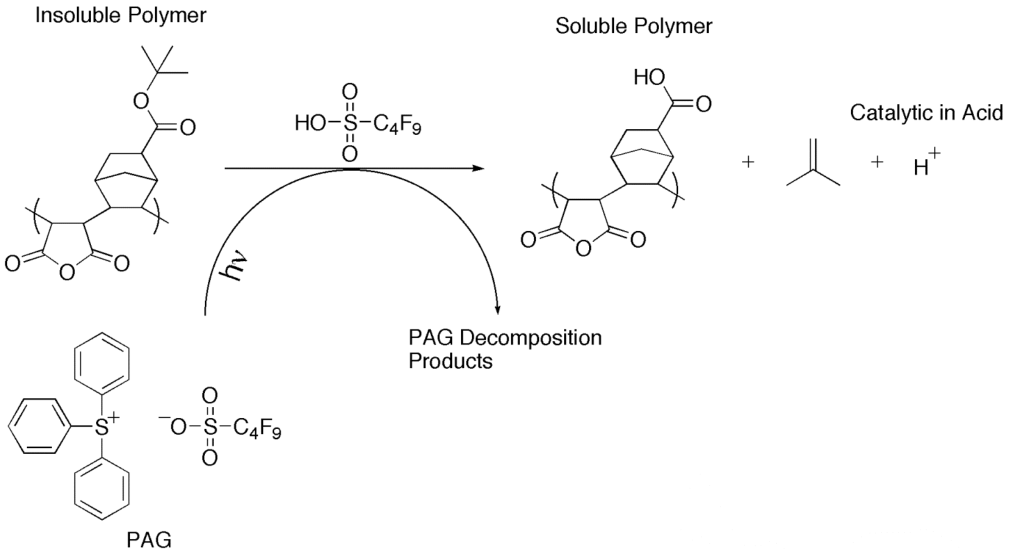

Scheme 1.4: Illustration of the deprotection of a chemically amplified 193 nm resist.

The introduction of chemically amplified resists greatly improved the resist sensitivity and allowed for use of lower power radiation sources.

1.5 THE RAYLEIGH RESOLUTION EQUATION

Resolution can best be described as the smallest feature that can be printed with a certain technology, equipment, and set of conditions [7].

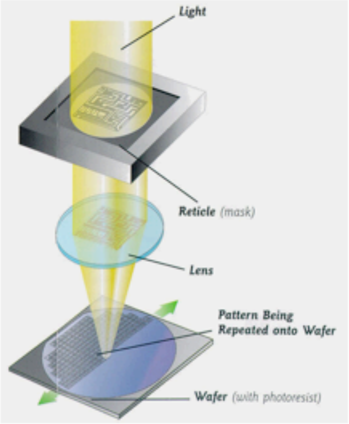

Figure 1.4: Illustration of substrate irradiation through the photomask and objective lens.

The Rayleigh equation, represented by Equation 1.1, describes the optimum resolution that can be obtained in a lithography exposure.

$$R = k_1 \frac{\lambda}{NA} \qquad \text{Eq. 1.1}$$

According to Equation 1.1, resolution, *R,* depends on several variables: a scalable resolution factor, k_1, the wavelength of light, λ, and the numerical aperture of the lens, *NA*. Rayleigh's criterion, k_1, depends on the type of lithography being used and has a physical limit of 0.25. It is not practical to push this "constant" to its limit because this would shrink the process window beyond the point of economic feasibility. Exposure wavelength reduction has been a source of constant improvement. It has helped tremendously in reducing obtainable resolution, but it is rapidly approaching the limits of its usefulness. Current lithography is performed with 193 nm radiation. The numerical aperture is the last variable that can be altered to improve resolution. The numerical aperture depends on the refractive index, *n*, of a material and can be calculated from Equation 1.2.

$$NA = n \sin \theta \qquad \text{Eq. 1.2}$$

Since $\sin\ \theta$ has a maximum value of unity, the numerical aperture cannot exceed the refractive index of the material between the objective lens and the substrate.

Figure 1.5: Illustration of the complexity of the lens system utilized in modern projection lithography tools [11].

With 193 nm light sources currently being used by the semiconductor industry, the best possible resolution attainable according to Rayleigh's Equation is approximately 36 nm. How is it then that Intel recently announced the fabrication and shipment of devices with 22 nm features using optical lithographic techniques? [12]. It is not that they have circumvented Rayleigh's Equation, but rather a more fundamental change in the way transistors are manufactured. First, the numerical aperture has increased with the addition of a liquid between the objective lens and the substrate. Second, there are other methods available known as resolution enhancement techniques (RETs) that allow for the manufacturing of smaller features. However, these techniques alter the structures after photolithography.

1.6 NEXT GENERATION LITHOGRAPHY

As the minimum feature size for microprocessor components has decreased in size, new materials and processes have become necessary. There are many technological challenges with advanced optical lithography, which is the current patterning technology, but its limit may be economical rather than technical [13]. The cost of the exposure tools used in device fabrication has grown enormously since the late 1970's, leading several research groups to explore more cost-effective alternatives as next generation lithography (NGL) technology. For nearly five decades, the microelectronic industry has kept up with Moore's Law. Once the limit of one technology was reached, a new technology had always been ready to replace it. Implementation of these new technologies has come with significant materials, engineering, and financial difficulties. Critics have constantly claimed that the miniaturization of features cannot continue and, in general, they have been proven wrong every time so far. However, this time around, a viable alternative to 193 nm immersion lithography (the current technology of record) has not yet been demonstrated and accepted by industry leaders. Optical projection lithography is rapidly approaching physical limits and, to avoid a stagnation of today's technological growth, new ideas must be implemented.

The technology projected to follow 193 nm was 157 nm lithography. However due to its relatively small reduction in exposure wavelength with respect to the resolution required by the upcoming technology nodes, the need for new masks, and the need for new resist materials, the microelectronic manufacturers cancelled all 157 nm R&D and began to push for extreme UV (11 nm radiation) technology. EUV lithography would have a significant impact on the minimum resolution possible for a lithography process if all other factors could stay constant.

1.6.1 Immersion Lithography

193 nm Immersion Lithography is the current technology being used in the manufacturing of microprocessors. It was started as an extension of traditional 193 nm projection lithography to improve the resolution of the process by increasing its numerical aperture via Rayleigh's Equation. To obtain a greater depth of focus, a liquid is placed in the space between the substrate and the objective lens in the optical lens system to increase the refractive index. It is of utmost importance that the liquid is extremely pure and free of contaminants that can change the refractive index or damage the substrate or the lens. A variety of solvents with high refractive indices and transparency at 193 nm were initially evaluated. Hydrocarbons fulfill both of these criteria, but due to drawbacks such as flammability and high vapor pressure, more suitable alternatives are needed [14].

1.6.2 Extreme Ultraviolet Lithography

Extreme UV lithography has been a technology candidate for over a decade, but its implementation as a production tool has been heavily delayed. The use of 11 nm radiation has posed many challenging problems to researchers. One major problem is the source: molten tin bombarded with powerful lasers in order for it to emit highly energetic photons. This presents another problem as tin is deposited elsewhere in the tool and must be periodically removed. The next issue is the matter of how well the radiation is projected from the mask onto the substrate. At the wavelengths used for EUV, most materials are highly absorbing. Therefore, lenses must be replaced by mirrors that reflect the radiation. As scientists and engineers solve one problem related to the EUV technology, half a dozen new problems are seemingly discovered. Several major chip manufacturers have stopped spending their time and money on a technology that many people believe is not economically feasible.

1.6.3 Electron Beam Lithography

Electron beam lithography is yet another technology that has been around for several decades. It can currently achieve the best resolution of any lithography tool available as it is capable of writing features on the order of a few nanometers. It is a "direct-write" method in which the images are formed serially, pixel by pixel. It takes a beam of electrons a very long time to write one field, let alone all the fields on a 12- or possibly 18-inch wafer. The fact that the technology can achieve such great resolution has made it the best choice for writing masks and templates for other lithographic technologies. In an effort to increase throughput for e-beam processing, it is proposed to use multiple beams grouped together to simultaneously write resist patterns. Two such technologies are called Complementary Electron Beam Lithography (CEBL) and MAPPER. A major concern with using multiple electron beams involves the feasibility of each beam being controlled and moved without affecting the neighboring beams. A large amount of research and development is still needed to convince the lithography community in general that this technology is a viable option for NGL.

1.6.4 Pitch Division Lithography

Pitch division lithography was introduced by our research group in 2009 [15]. It is based on the idea that one can take advantage of a material behaving both as a positive and a negative tone resist by utilizing a specific combination of a PAG and a PBG [15-18]. This technology is shown in comparison to traditional optical lithography in Figure 1.6.

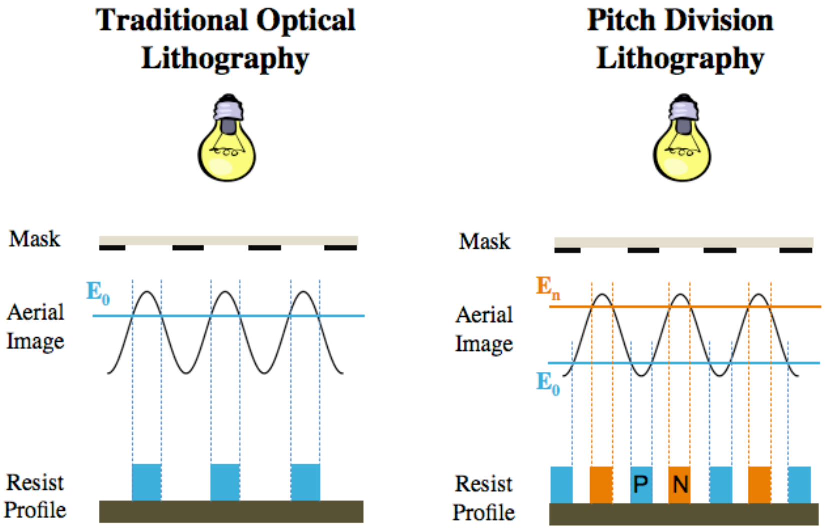

Figure 1.6: Pitch division lithography compared to tradition optical lithography. To achieve the doubling response the photoresist must act as both a positive and negative tone. (Courtesy of Xinyu Gu)

A traditional photoresist requires a certain dose to undergo the photochemical reaction. This energy is referred to as E_0. For pitch division, the formulation contains both a PAG and a PBG. When the exposure dose is below a threshold level, E_0, the resist acts as a positive tone, whereas an exposure dose above E_n switches the behavior of the resist to a negative tone resist. This can be achieved by implementing a latent PBG that quenches the acid once a certain level of dose has been reached [19].

1.6.5 Nanoimprint Lithography

Imprint lithography has been around for over a thousand years [20]. It is based on a technology in which a mold or template is replicated in some medium. A printing press is a simplified example of this technology wherein the mold is replicated by the application of ink to protruding structures thereby transferring the pattern onto paper.

Nanoimprint technology was first introduced in 1996 as a technique for replicating nanostructures in microelectronic device manufacturing. Unlike projection lithography which uses masks and lenses (governed by Rayleigh's Equation), it has been shown that imprint lithography is only limited by the size of the pattern that can be made on the mold [21].

1.7 SUMMARY

The microelectronics industry is made up of scientists and businesspeople from all around the world. At some point in the near future, they all have to come together to answer the question, "What's next?" There are a number of different technologies that are currently being evaluated, some of which have the potential to become the next generation of lithography. Old-timers and hardcore projection lithographers may have to step out of their comfort zone and evaluate alternative, "disruptive" technologies in a non-biased way. The remainder of this dissertation will be focused on one such disruptive technology: nanoimprint lithography. Chapter two gives a brief introduction to imprint technology, specifically step and flash imprint lithography (SFIL). Chapter three covers the synthesis of imprint resist materials, and chapter four covers mechanical and electrical evaluation of the aforementioned resists. Chapter five describes a different version of SFIL and the materials required for its implementation, and chapter six covers the surface modification of molds for SFIL.

1.8 REFERENCES

[1] M. Campbell-Kelly. "Computing". Scientific American, 301, 62-69, 2009.

[2] L. F. Thompson, C. G. Willson and M. J. Bowden. "Introduction to Microlithography"; Ed.; American Chemical Society; Washington D.C., 1983.

[3] G. E. More. "Cramming more components onto integrated circuits". Electronics, 38, 1965.

[4] http://www.intel.com/museum/archives/history_docs/moore.htm. 2011.

[5] http://www.wisegeek.com/how-long-do-cell-phone-batteries-last.htm. 2011.

[6] J. R. Adams. "Organic Materials Development for Advanced Lithographic Applications". Ph.D. Dissertation, The University of Texas, 2009.

[7] C. Mack. "Fundamental Principles of Optical Lithography"; 1st Ed.; John Wiley & Sons, Ltd.; Chichester, West Sussex, 2007.

[8] J. V. Crivello. "The discovery and development of onium salt cationic photoinitiators". Journal of Polymer Science Part A: Polymer Chemistry, 37, 4241-4254, 1999.

[9] S. A. MacDonald, C. G. Willson and J. M. J. Frechet. "Chemical Amplification in High-Resolution Imaging Systems". Accounts of Chemical Research, 27, 151-158, 1994.

[10] C. G. Willson, R. A. Dammel and A. Reiser. "Photoresist Materials: A Historical Perspective". Advances in Resist Technology and Processing XIV, 3049, 1997.

[11] https://asml.picturepark.com/Website/Publisher.aspx?Page=ASML.

[12] http://newsroom.intel.com/community/intel_newsroom/blog/2011/05/04/intel-reinvents-transistors-using-new-3-d-structure. 2011.

[13] M. E. Colburn. "Step and Flash Imprint Lithography: A Low-Pressure, Room-Temperature Nanoimprint Lithography". Ph.D. University of Texas at Austin, 2001.

[14] E. A. Costner. "The Refractive Index and Absorbance of Aqueous and Organic Fluids for Immersion Lithography". Ph.D. Dissertation, The University of Texas, 2009.

[15] X. Gu, C. Bates, Y. Cho, E. Costner, F. Marzuka, T. Nagai, T. Ogata, C. Shi, A. K. Sundaresan, N. J. Turro, R. Bristol, P. Zimmerman and C. G. Willson. "A New Materials-based Pitch Division Technique". Journal of Photopolymer Science and Technology, 22, 773-781, 2009.

[16] X. Gu, Y. Cho, T. Kawakami, Y. Hagawara, B. Rawlings, R. Mesch, T. Ogata, T. Kim, T. Seshimo, W. Wang, A. K. Sundaresan, N. J. Turro, R. Gronheid, J. Blackwell, R. Bristol and C. G. Willson. "Photobase Generator Enabled Pitch Division: A Progress Report". Advances in Resist Materials and Processing Technology XXVIII, 7972, 2011.

[17] X. Gu, C. M. Bates, Y. Cho, T. Kawakami, T. Nagai, T. Ogata, A. K. Sundaresan, N. J. Turro, R. Bristol, P. Zimmerman and C. G. Willson. "Photobase generator assisted pitch division". Advances in Resist Materials and Processing Technology XXVII, 7639, 2010.

[18] Y. Cho, X. Gu, Y. Hagiwara, T. Kawakami, T. Ogata, B. Rawlings, Y. Li, A. K. Sundaresan, N. J. Turro, R. Bristol, J. M. Blackwell and C. G. Willson. "Polymer Bound Photobase Generators and Photoacid Generators for Pitch Division Lithography". Advances in Resist Materials and Processing Technology XXVIII, 7972, 2011.

[19] G. Xinyu. Ph.D. Dissertation, The University of Texas, 2011.

[20] F. L. Palmieri. "Step and Flash Imprint Lithography: Materials and Applications for The Manufacture of Advanced Integrated Circuits". Ph.D. University of Texas at Austin, 2008.

[21] D. J. Resnick, S. V. Sreenivasan and C. G. Willson. "Step & flash imprint lithography". Materials Today, 8, 34-42, 2005.

Chapter 2: Step and Flash Imprint Lithography

2.1 INTRODUCTION TO NANOIMPRINT LITHOGRAPHY

The cost of exposure tools used in the fabrication of microelectronics has substantially increased since the late 1970's, as illustrated in Figure 2.1. Consequently, several research groups have begun to explore low-cost alternatives.

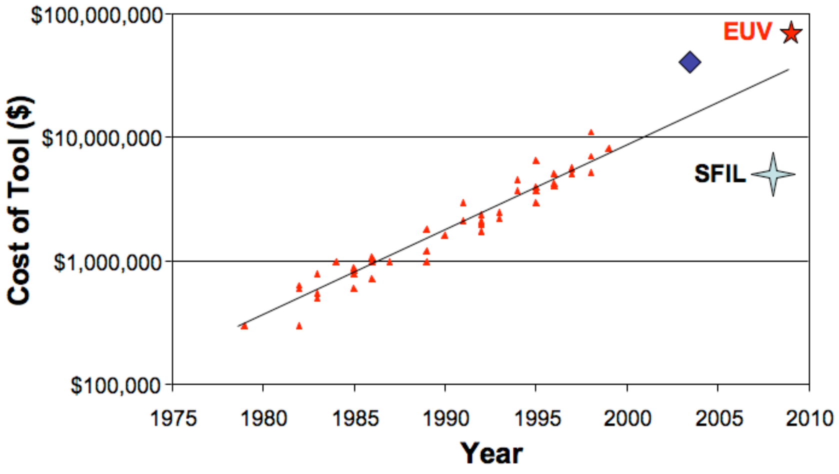

Figure 2.1: Lithography tools – Cost of Ownership.

In 1995, Dr. Stephen Chou and his research group first introduced imprint lithography as a plausible, low-cost Next Generation Lithography (NGL) [1]. Chou *et al.* used thermal embossing to replicate patterns from a silicon master template with PMMA [2]. Today, two main streams of imprint lithography are being explored. One is the aforementioned thermally activated imprinting of a thermoset or thermoplastic material, and the other is the imprinting of a photocurable liquid. The latter was developed at The University of Texas at Austin in 1999 [3]. "Step and Squish Imprint Lithography", as it was first called, was developed into what is today known as Step and Flash Imprint Lithography (S-FIL®), or Jet and Flash™ Imprint Lithography (J-FIL™) as Molecular Imprints, Inc. has renamed the technology. Using this technology, Rogers *et al.*

demonstrated in 2004 that structures as small as 2.4 nm can be reliably replicated [4], which is approximately an order of magnitude better than what is currently in production at leading semiconductor corporations.

One advantage of nanoimprint lithography is the capability of reducing the number of processing steps required to manufacture a semiconductor device. The flow chart in Figure 2.2 illustrates the steps within the lithographic process relating to via and trench structure fabrication. There are two basic structures in microelectronic devices: trenches form the channels for the wires and hole-like vias connect one wiring layer to the next one located above or below it.

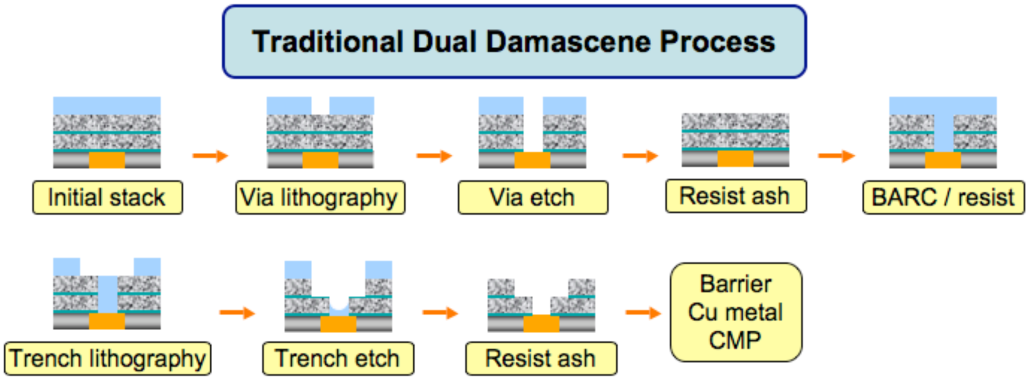

Figure 2.2: An illustration of select process steps for traditional projection lithography in generating via and trench pattern.

For traditional dual damascene, an initial film stack consisting of alternating layers of etch barrier and insulator with the photoresist layered on top is deposited in multiple steps. The alternating layers assist in the etch process for successful pattern transfer. The overall process requires two lithographic steps and several etch steps, whereby additional depositions of bottom anti-reflective coating (BARC) and photoresist films are coated in between the lithography and etch steps. The reduction in the number of steps that can be achieved by using SFIL is depicted in Figure 2.3. This reduction in process steps is attributed to the use of multi-layer templates, which enables production of the structures with far fewer thin-film, lithography, and etch steps.

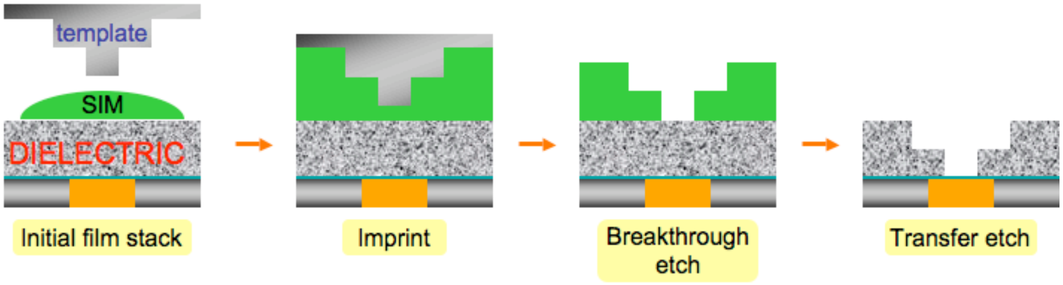

Figure 2.3: Significant reductions in the number of process steps for via and trench pattern generation can produce substantial cost-savings for IC manufacturers.

2.2 THE SFIL PROCESS

Nanoimprint lithography (NIL) is best described as a molding technology that dates back to the ancient method of sealing documents or letters. A mold with a relief pattern is fabricated and used as a stamp to produce an inverse copy of the original mold’s relief features in some recording material. Figure 2.4 illustrates the process flow for SFIL. Each step of the SFIL process is briefly discussed in the following section.

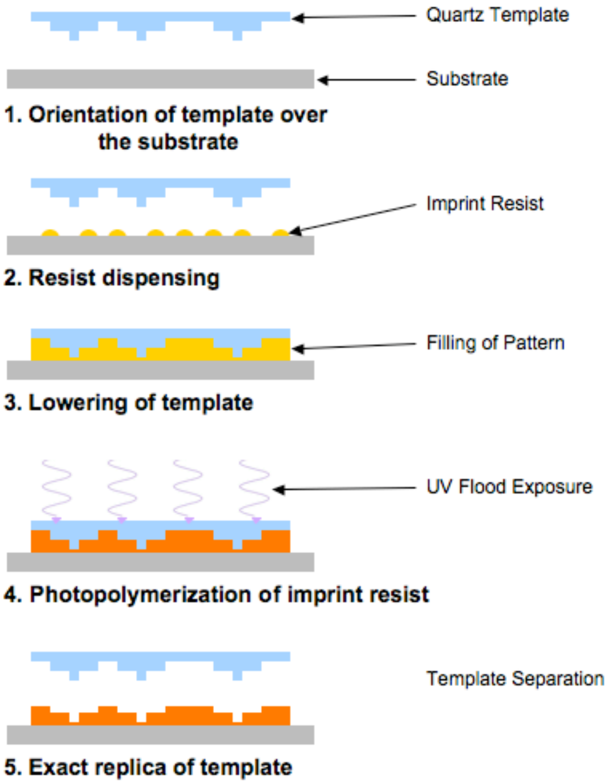

Figure 2.4: Process flow for SFIL.

The initial step after the template and the wafer have been loaded onto the tool is to level and align the template. Newer tools manufactured by Molecular Imprints, Inc. are equipped with manual and automated alignment options that have registration and alignment capability of <10 nm, 3σ [5]. The template chuck is mounted on flexures as this reduces wear on sliding joints that can dislodge particles [6]. The template is leveled and aligned by analysis of marks on the template and substrate as shown in Figure 2.5 [7].

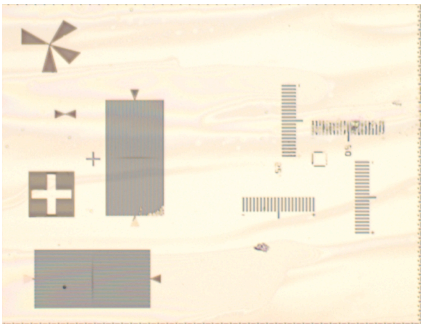

Figure 2.5: Imprinted alignment marks from the template.

The polymerizable monomer is dispensed once the template is aligned. This step is accomplished through a piezoelectric dispense mechanism attached to the imprint tool. The drop pattern is specifically designed to facilitate spreading of the liquid and to avoid trapping air. Therefore, the drop pattern is customized for the type of template used. Two different drop patterns are illustrated in Figure 2.6.

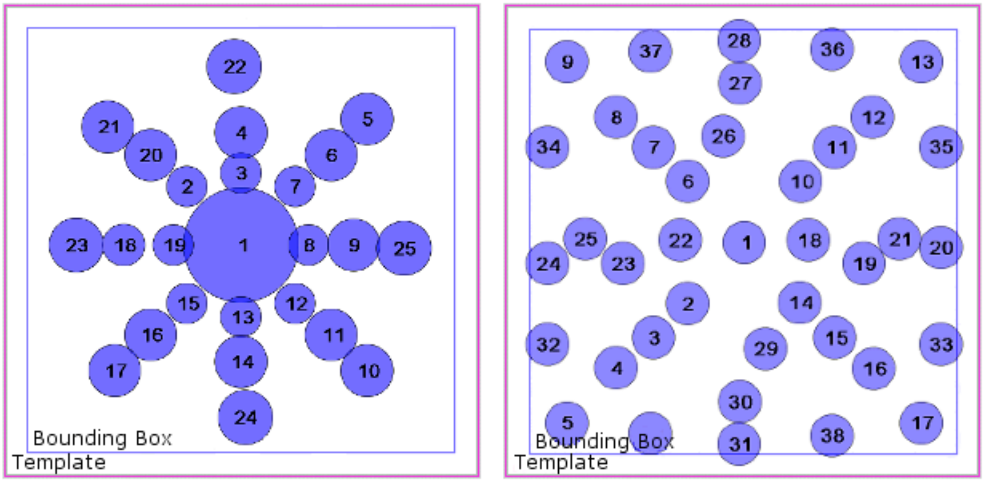

Figure 2.6: Illustrated are two tailored drop patterns that are optimized for different templates for fast fill time and bubble-free imprints.

The amount of resist dispensed can easily be controlled for each droplet. In this way, it is possible to dispense more or less liquid as needed for areas with high or low pattern density.

Once the imprint resist has been dispensed, the template is lowered into the liquid. The force that presses on the template is on the order of a few Newtons compared to the several hundred Newtons that is required for a thermal imprint process. A force vs. time curve for SFIL is shown in Figure 2.7.

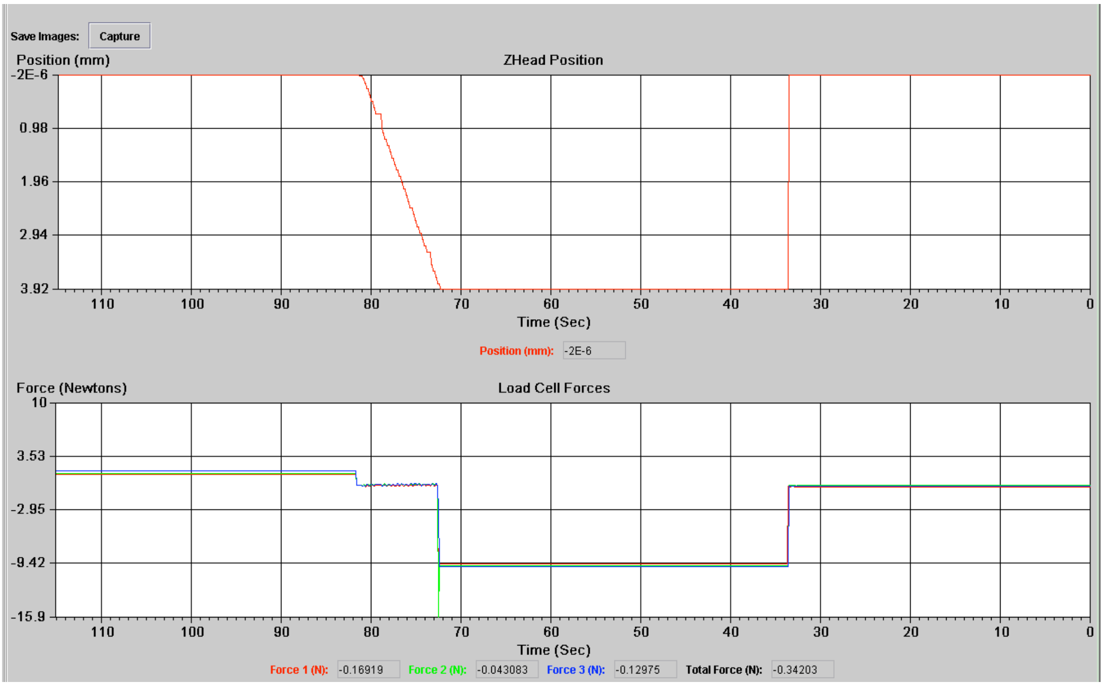

Position (mm): -2E-6

Force 1 (N): -0.16919 Force 2 (N): -0.043083 Force 3 (N): -0.12975 Total Force (N): -0.34203

Figure 2.7: Template approach, fill, cure, and separation.

After allowing a short time for resist spreading, curing of the resist takes place by UV exposure through the backside of the transparent quartz template. The template is then separated from the solidified resist, and the process can be replicated time and again.

It has been repeatedly established that a residual layer of the imprint resist will always be present due to the slowing of flow in the resist as the volume between the substrate and the template decreases. This residual layer can be removed by a selective etch step called a breakthrough etch. Thus, the template never contacts the substrate [8]. The thickness of this layer has been reduced to approximately 10 nm for UV NIL and thinner than 100 nm for thermal NIL [9, 10].

This process produces an inverse copy of the template relief pattern on the substrate. Depending on the composition of the imprint resist, either a halogen etch or an oxygen reactive ion etch (RIE) step can either increase or decrease the aspect ratio of the imprinted features by transferring the pattern into an underlying layer [11]. Once the etch processes are completed, metallization can be carried out to fabricate the actual wires and interconnects.

2.3 TEMPLATE DESIGN

Whereas SFIL tools themselves are inexpensive in comparison to optical projection tools, templates are not. The high cost of templates derives from costs associated with template manufacturing. The templates for NIL are different than the masks used in projection lithography. Unlike projection lithography masks, the template has to be in scale since there is no opportunity to reduce the feature sizes. Electron beam lithography (e-beam) is a direct-write technique that is used in template manufacturing [12, 13]. In essence, every line and space is written in the scale of the final IC pattern. Figure 2.8 depicts one method of utilizing electron beam lithography for template manufacturing.

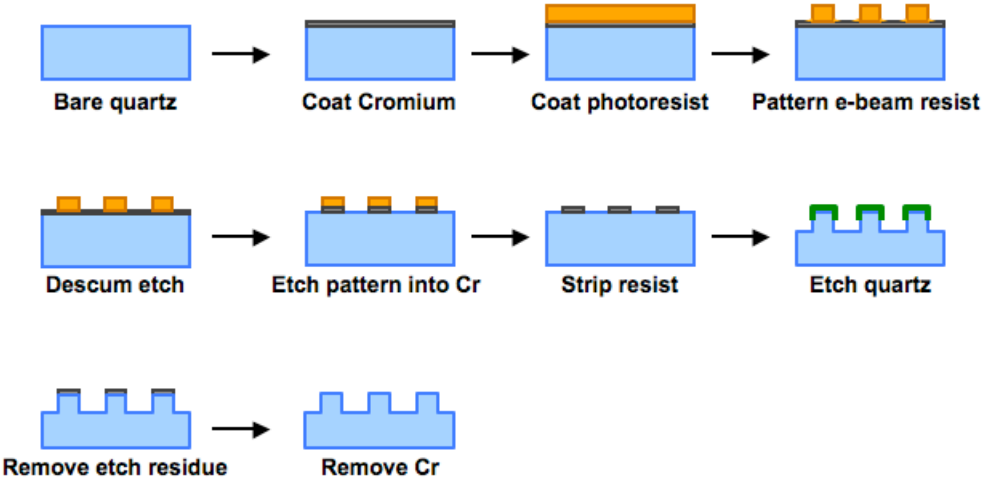

Figure 2.8: Template manufacturing process.

2.4 DUAL DAMASCENE

The term, damascene, stems from the ancient method of fabricating decorative structures in a metal, e.g. knives, swords, jewelry, etc. The method by which it works consists of overfilling a pre-patterned surface then polishing off excess metal as illustrated in Figure 2.9.

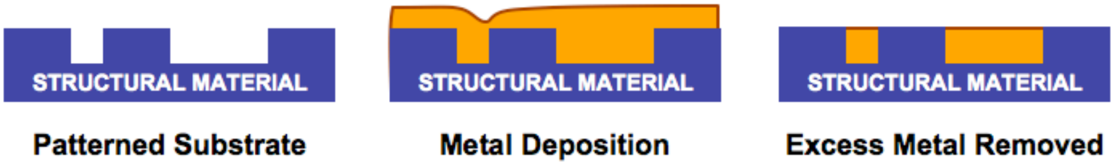

Figure 2.9: Illustration of the damascene process in which a substrate is patterned, coated with a noble metal, and excess metal is polished off.

In lithography for microelectronics, damascene refers to the process for creating interconnect wiring. At the time when copper was incorporated, there was no efficient way to etch copper [14]. It was therefore necessary to fabricate both via and trench before the metallization took place, and hence the technique is referred to as dual damascene. As previously mentioned, NIL can produce both the wire and the via layers simultaneously by using a multi-tier template.

2.5 MATERIALS

The materials used in NIL can be divided into two different categories: thermal and UV-curable materials. There are subcategories of materials within these two groups, which are briefly discussed in the following section.

2.5.1 Thermally Activated Materials

Thermal materials can consist of two basic types: polymers or thermally curable pre-polymers / monomers, or a combination of the two. A polymer, such as polymethyl methacrylate (PMMA) can be used in NIL by spin-coating. The polymer can then be heated above the glass transition temperature (T_g), inducing flow when the template is lowered and pressed into it as shown in Figure 2.10.

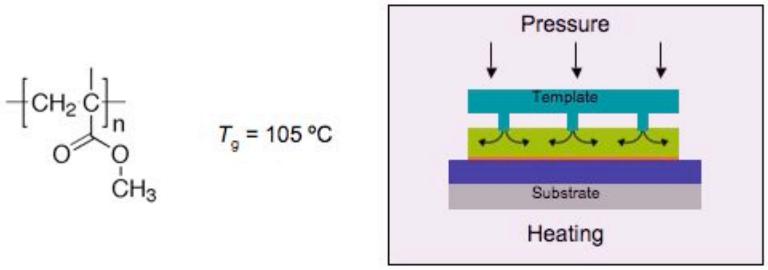

Figure 2.10: PMMA use in thermal embossing.

High pressure is needed to displace the molten polymer since the viscosity of such materials is fairly high. Once the polymer has spread and filled the pattern, the system is cooled down, which allows the polymer to solidify before the template is removed. The high pressure required to improve the throughput can easily cause irreparable defects to the template if particles are present. They can “chip” the pattern. A thermally curable material is also a possibility for use as an imprint resist. The substrate does not need to be heated for extended periods of time to aid in spreading of a polymer. Instead, the monomer can flow unassisted and then be cured. While this method is seemingly simple, serious potential complications must be avoided. Specifically, the coefficients of thermal expansion (CTE) must match in order to prevent stress and strain from building up inside the different materials. This can cause cracks to form, which will ruin the device. In addition to the CTEs, the elevated temperature and pressure required can result in imprecise overlay, leading to non-functional circuits [6, 7].

2.5.2 UV Activated Sacrificial Materials

Using UV cross-linkable liquid polymers or monomers in the SFIL process has shown great promise. Curable materials can be formulated in a way that overcomes underlying concerns with thermal imprinting. Lowering the viscosity makes it possible to operate the system at low pressure and ambient temperature, which improves alignment accuracy and throughput.

In the early stages of SFIL, the technology took advantage of standard photopolymerizable resist materials that were readily available. One such formulation is illustrated in Table 2.1.

Component	Structure	Wt%
EGDA		37.0
nBA	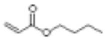	19.6
IBA	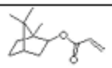	37.0
Darocur® 1173	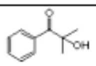	3.9

Table 2.1: A typical resist formulation for imprint lithography.

With traditional projection lithography, the resist used is ultimately removed as it only functions as a transfer layer. These organic-based resists are called sacrificial imprint resists. An improvement to the sacrificial resists occurred when de-crosslinkable groups were incorporated into the material. Templates are repeatedly exposed to the resist formulations and are susceptible to fouling as resist material can adhere to the template, which requires cleaning of the template. A piranha etch is commonly performed and, in some cases, an alkali solution cleaning is performed as well. Both of these methods are aggressive and slowly etch the template and change the critical dimension (CD) of the features [15]. A de-crosslinkable material has the advantage of undergoing depolymerization and can be removed much more easily. The idea was to incorporate a cross-linking unit that contains a degradable functionality [16, 17]. Figure 2.11 illustrates how one such material works.

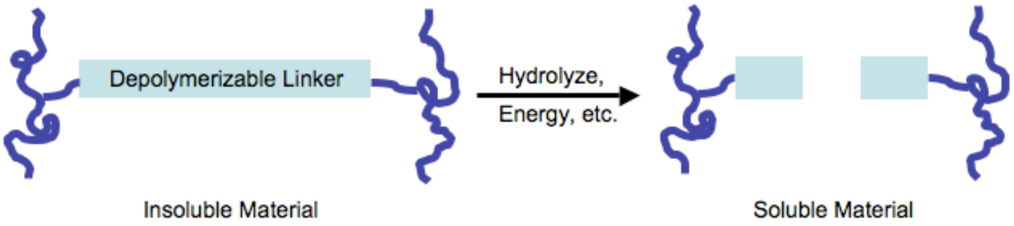

Figure 2.11: De-crosslinkable polymers can be removed from a template surface in several different ways [16].

Crosslinkable acetals along with reversible Diels-Alder groups were investigated and the results showed that the acetals readily undergo hydrolysis under acidic conditions and fouled templates were easily cleaned. Scheme 2.1 provides examples of degradable acetal and thermally degradable Diels-Alder reaction-based de-crosslinking chemistries.

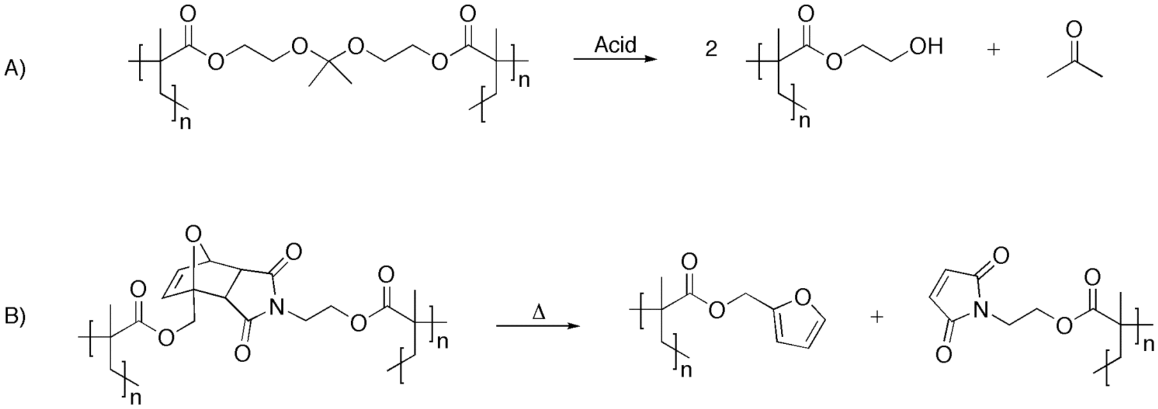

Scheme 2.1: Shown are two schemes for degradable polymers. A significant increase in solubility occurs when the polymer is decomposed into smaller segments. A) Acid hydrolysis of acetal, and B) retro Diels-Alder.

2.5.3 UV Functional Materials

Although the number of process steps involved in the manufacturing of ICs is reduced significantly through the use of the SFIL process (Figure 2.12), there are additional steps that could be removed by implementing an imprint resist that become a functional part of the final device [18-20].

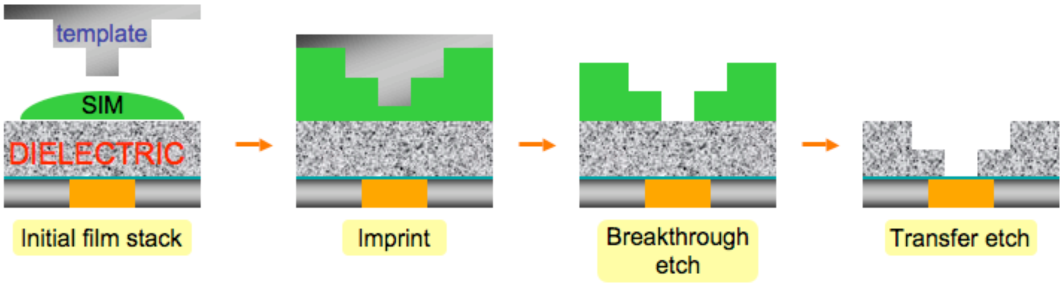

Figure 2.12: Imprint lithography with SIM requires etch barrier and dielectric films to be deposited in an initial stack.

A functional resist that is also an interlayer dielectric (ILD) has the potential to remove additional steps as seen in Figure 2.13. In this case, instead of dispensing a sacrificial material on top of a film stack, the ILD is directly dispensed and imprinted.

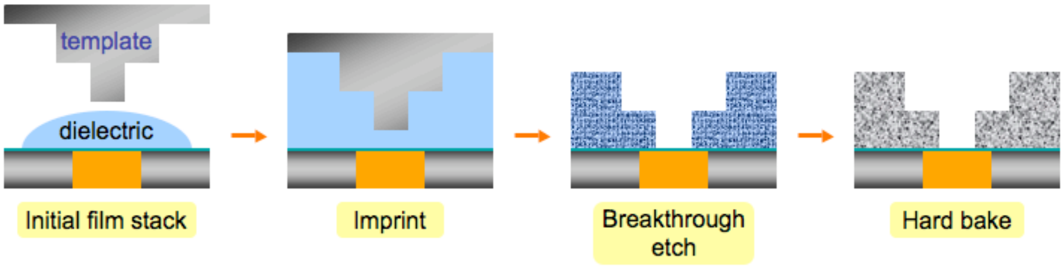

Figure 2.13: Imprinting using a functional material that will become an integral part of the final product.

These functional resists or directly patternable dielectric (DPDs) materials will be discussed in greater detail in the following chapter.

2.6 NIL LIMITATIONS?

Despite the tremendous progress in materials and tool development that has already occurred, NIL has many skeptics who point to overlay, throughput, and defect limitations. From a personal viewpoint, most of the resistance comes from researchers and managers that have invested billions of dollars in a non-functional, non-performing, and much delayed EUV technology. However, the resistance does raise an interesting point regarding throughput. Projection lithography can now process approximately 100 wafers per hour, whereas SFIL has only been able to reach around 20 wafers per hour. It is true that imprint does not have the capacity for high volume manufacturing because imprint is fundamentally a slower process. However, their argument falls short if one considers that EUV will be implemented as a NGL even though throughput is even worse for EUV.

Another point that is constantly brought up by skeptics of NIL is that of defects. Defectivity was a valid point when NIL was first introduced, but thanks to the work of several independent research groups, defectivity, while still a concern, has seen significant improvement. One study demonstrated that even though a template had become fouled, after several imprints the template had self-cleaned and the defects did not propagate further [21, 22]. As demoralizing as these limitations may seem, there is much room for improvement that can be achieved through industrial collaboration if a fraction of the money spent on EUV were to be allocated to NIL.

2.7 SUMMARY

Thermal imprint has slowly lost its initial attraction due to the fact that it is constrained by having multiple slow heating cycles and mismatched CTEs. SFIL has had tremendous growth and momentum over the past decade as a potential candidate for NGL. It has been illustrated that nanoimprint lithography can outperform optical projection lithography by repeatedly replicating features that are half the size of what has been achieved through immersion lithography, and at a fraction of the cost. Templates are commercially available and progress in their manufacturing has been made. Imprinting of smaller features is currently limited by the template manufacturing process. Thus, production e-beam tools are being pushed near their limits to pattern features that are several carbon atoms in width. There has been a great improvement in the materials used for SFIL and several research groups are working on a variety of polymerization techniques.

2.8 REFERENCES

[1] S. Y. Chou, P. R. Krauss and P. J. Renstrom. "Imprint of sub-25 nm vias and trenches in polymers". Appl. Phys. Lett., 67, 1995.

[2] S. Y. Chou, P. R. Krauss and P. J. Renstrom. "Nanoimprint lithography". The 40th international conference on electron, ion, and photon beam technology and nanofabrication, 14, 1996.

[3] M. Colburn, S. C. Johnson, M. D. Stewart, S. Damle, T. C. Bailey, C. Bernard, M. Wedlake, T. B. Michaelson, S. V. Sreenivasan, J. G. Ekerdt and C. G. Willson. "Step and flash imprint lithography: a new approach to high-resolution patterning". 3676, 1999.

[4] F. Hua, Y. Sun, A. Gaur, M. A. Meitl, L. Bilhaut, L. Rotkina, J. Wang, P. Geil, M. Shim, J. A. Rogers and A. Shim. "Polymer Imprint Lithography with Molecular-Scale Resolution". Nano Lett., 4, 2467-2471, 2004.

[5] W. M. Tong, S. D. Hector, G.-Y. Jung, W. Wu, R. S. Williams, J. Ellenson, K. Kramer, T. Hostetler and S. K. Richards. "Nanoimprint lithography: the path toward high-tech, low-cost devices". Emerging Lithographic Technologies IX, SPIE, 2005.

[6] B. J. Choi, S. V. Sreenivasan, S. Johnson, M. Colburn and C. G. Willson. "Design of orientation stages for step and flash imprint lithography". Journal of the International Societies for Precision Engineering and Nanotechnology, 25, 192-199, 2001.

[7] B. J. Choi, M. Meissl, M. Colburn, T. Bailey, P. Ruchhoeft, S. V. Sreenivasan, F. Prins, S. Banerjee, J. G. Ekerdt and C. G. Willson. "Layer-to-Layer Alignment for Step and Flash Imprint Lithography". Emerging Lithographic Technologies V, 2001.

[8] C. Perret, C. Gourgon, G. Micouin and J. P. Grolier. "Influence of Thermal Properties of Polymers on NanoImprint Lithography Performance". Jpn. J. Appl. Phys., 41, 4203-4207, 2002.

[9] L.-R. Bao, X. Cheng, X. D. Huang, L. J. Guo, S. W. Pang and A. F. Yee. "Nanoimprinting over topography and multilayer three-dimensional printing". J. Vac. Sci. Technol. B, 20, 2881-2886, 2002.

[10] M. Vogler, S. Wiedenberg, M. Muhlberger, I. Bergmair, T. Glinsner, H. Schmidt, E.-B. Kley and G. Grutzner. "Development of a novel, low-viscosity UV-curable polymer system for UV-nanoimprint lithography". Microelectronic Engineering, 84, 984-988, 2007.

[11] B. H. Chao, F. Palmieri, W.-L. Jen, D. H. McMichael, C. G. Willson, J. Owens, R. Berger, K. Sotoodeh, B. Wilks, J. Pham, R. Carpio, E. LaBelle and J. Wetzel. "Dual damascene BEOL processing using multilevel step and flash imprint lithography". Emerging Lithographic Technologies XII, 6921, 2008.

[12] S. Johnson, D. J. Resnick, D. Mancini, K. Nordquist, W. J. Dauksher, K. Gehoski, J. H. Baker, L. Dues, A. Hooper, T. C. Bailey, S. V. Sreenivasan, J. G. Ekerdt and C. G. Willson. "Fabrication of multi-tiered structures on step and flash imprint lithography templates". Microelectronic Engineering, 67-68, 221-228, 2003.

[13] S. Sasaki, T. Hiraka, J. Mizuochi, Y. Nakanishi, S. Yusa, Y. Morikawa, H. Mohri and N. Hayashi. "UV-NIL template making and imprint evaluation". 7271, 2009.

[14] C. Mack. "Fundamental Principles of Optical Lithography"; 1st Ed.; John Wiley & Sons, Ltd.; Chichester, West Sussex, 2007.

[15] M. Pritschow, J. Butschke, M. Irmscher, L. Parisoli, T. Oba, T. Iwai and T. Nakamura. "Evaluation of the CD-SEM Vistec LWM90xx for line-width measurement of nanoimprint templates". Alternative Lithographic Technologies, 7271, 2009.

[16] W. H. Heath, F. Palmieri, J. R. Adams, B. K. Long, J. Chute, T. W. Holcombe, S. Zieren, M. J. Truitt, J. L. White and C. G. Willson. "Degradable Cross-Linkers

and Strippable Imaging Materials for Step-and-Flash Imprint Lithography". Macromolecules, 2008.

[17] F. Palmieri, J. Adams, B. Long, W. Heath, P. Tsiartas and C. G. Willson. "Design of Reversible Cross-Linkers for Step and Flash Imprint Lithography Imprint Resists". ACS Nano, 1, 307-312, 2007.

[18] M. D. Stewart and C. G. Willson. "Imprint Materials for Nanoscale Devices". MRS Bulletin, 30, 947-951, 2005.

[19] F. L. Palmieri. "Step and Flash Imprint Lithography: Materials and Applications for The Manufacture of Advanced Integrated Circuits". Ph.D. University of Texas at Austin, 2008.

[20] W.-L. K. Jen. "Materials and Processes for Advanced Lithography Applications". Ph.D. Dissertation, The University of Texas at Austin, 2009.

[21] T. Bailey, B. Smith, B. J. Choi, M. Colburn, M. Meissl, S. V. Sreenivasan, J. G. Ekerdt and C. G. Willson. "Step and flash imprint lithography: Defect analysis". J. Vac. Sci. Technol. B, 19, 2806-2810, 2001.

[22] T. Bailey, B. J. Choi, M. Colburn, M. Meissl, S. Shaya, J. G. Ekerdt, S. V. Sreenivasan and C. G. Willson. "Step and flash imprint lithography: Template surface treatment and defect analysis". Papers from the 44th international conference on electron, ion, and photon beam technology and nanofabrication, 18, 2000.

Chapter 3: Directly Patternable Dielectrics

3.1 INTRODUCTION TO DIRECTLY PATTERNABLE DIELECTRICS

Step and Flash Imprint Lithography (SFIL) can be used with the dual damascene interconnect process to create imprintable dielectrics. This term, coined by Stewart and Willson in 2005 [1], refers to a dielectric material that can be patterned to form multi-level structures. If successful, this process could remove as many as 100 unit process steps from the manufacturing of advanced microprocessors. Independent cost analysis studies have shown that this process could save between 20% and 60% of the cost of manufacturing such devices. This dramatic cost saving can be realized by new materials that are compatible with current microelectronic processing equipment.

Imprintable dielectric materials are comprised of a photopolymerizable precursor that upon light exposure reacts to form a thermally stable insulator with a low dielectric constant and has the properties required for implementation in the manufacturing of microelectronic devices. The material must meet not only the requirements for use in SFIL, but also the end use requirements for on-chip interlayer dielectric applications. First, the material needs to be photocurable and possess a low viscosity. Low viscosity imprint formulations are needed for acceptable throughput since they flow and spread faster than high viscosity materials [2]. At the same time the materials must have low vapor pressures to avoid resist loss due to evaporation. There are restrictions on the polymerization as well; to avoid formation of cracks and pattern distortion, the cured film must not shrink significantly. In addition to these requirements, the dielectric constant has to be below three to properly function as an insulator [3]. For this reason, the material cannot absorb water since this would alter the dielectric constant. The material must also tolerate elevated temperatures and have a coefficient of thermal expansion (CTE) close to that of copper and other material components of a device. The matching of CTEs is important to avoid stress buildup within materials due to expansion/shrinkage. Lastly, for the material to be functional, it must have a sufficient tensile modulus to withstand CMP processes. These requirements are listed in Figure 3.1.

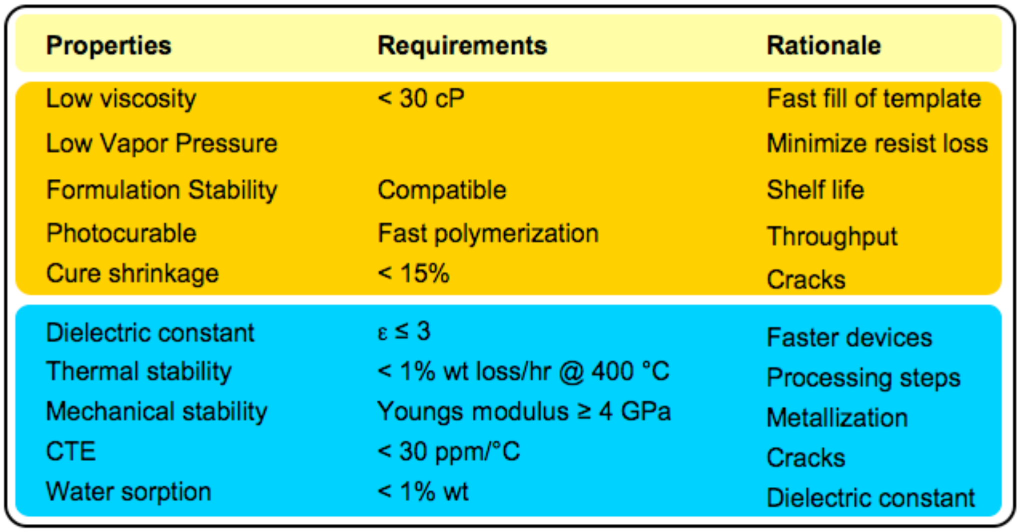

Properties	Requirements	Rationale
Low viscosity	< 30 cP	Fast fill of template
Low Vapor Pressure		Minimize resist loss
Formulation Stability	Compatible	Shelf life
Photocurable	Fast polymerization	Throughput
Cure shrinkage	< 15%	Cracks
Dielectric constant	$\varepsilon \leq 3$	Faster devices
Thermal stability	< 1% wt loss/hr @ 400 °C	Processing steps
Mechanical stability	Youngs modulus ≥ 4 GPa	Metallization
CTE	< 30 ppm/°C	Cracks
Water sorption	< 1% wt	Dielectric constant

Figure 3.1: List of material requirements for implementation into the semiconductor manufacturing as an ILD [4].

3.2 METHODS FOR DEPOSITING DIELECTRICS

There are two basic methods that semiconductor manufacturers use to deposit ILDs: spincoating (spin-on) and vapor deposition. Typically, chemical vapor deposition (CVD) is employed. Historically, silicon dioxide (SiO_2) has been used as a dielectric and is deposited by CVD [5]. Most dielectric materials are based on doped SiO_2 that are deposited by the same technology. Spin-on dielectrics is a concept that gained momentum in 2001 [5]. Spincoating is not a new technology, but one the semiconductor industry is very familiar with since it is used to deposit films of photoresist. Spin-on dielectrics consist of organic polymers, inorganic materials, or combinations of the two. Over time, interest in spin-on dielectrics has slowly diminished, as improved materials can still be deposited either through CVD or physical vapor deposition (PVD). A third possible method to deposit low-*k* dielectric films is to imprint directly into the material, as with DPDs or imageable dielectrics [1, 3, 6-8].

3.3 MATERIALS

Directly patternable dielectric (DPD) materials will not be removed from the substrate but instead become an integral part of the final device. A number of approaches have been explored for the design of such materials, and it has been concluded that siloxane-based materials have promise for this application.

3.3.1 Sol-gel

Palmieri *et al*. developed a sol-gel based pre-polymer for use as an imprint resist. The material was based on the incomplete condensation of alkoxy-silanes through sol-gel reactions. A great variety of formulations were made from a set of methacryloyl substituted precursors and evaluated [3, 9]. These were prepared by mixing the materials and subjecting the mixture to acid-catalyzed condensation for a specific period of time. Scheme 3.1 below depicts one such formulation. This pre-polymer, only a nominal structure, was functionalized with photopolymerizable methacrylate groups.

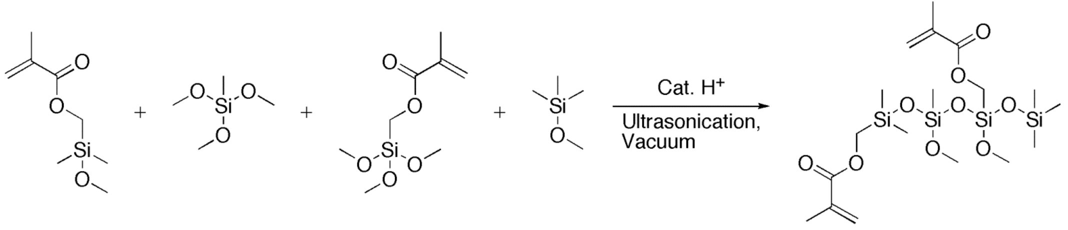

Scheme 3.1: Sol-gel components and a nominal structure for a crosslinkable pre-polymer [3].

The sol-gel materials produced good quality imprints and were processed through metal deposition, plating, and CMP processes to produce via chain test structures that demonstrated electrical connectivity.

Several formulations were evaluated and the best candidate met almost all end use criteria except that it exhibited significant shrinkage along the z-axis upon exposure and possessed a low modulus [3]. The effect of the low modulus can be seen in the metal patterns below manifested as “dishing” between the metal lines (Figure 3.2).

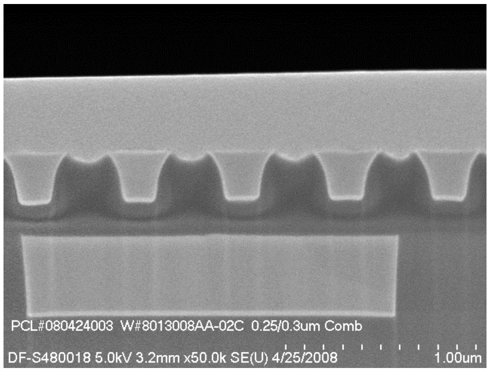

Figure 3.2: Dishing is clearly visible between the metal wires (Courtesy of Dr. F. Palmieri).

3.3.2 Polyhedral Oligomeric Silsesquioxanes

Commercially available ILDs or insulators such as Black Diamond (Applied Material) or Coral (Novellus) are proprietary materials composed mainly of silicon dioxide that has been doped with carbon or organic substituents to lower the overall dielectric constant [5]. For silicon dioxide to be used as a DPD in SFIL, it must be dissolved in a liquid, or rendered a liquid and polymerizable. Polyhedral oligomeric silsesquioxane are of the general formula $RSiO_{1.5}$ and are great candidates to use as DPD (Figure 3.3).

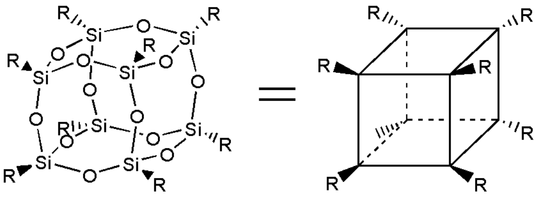

Figure 3.3: Structure of the POSS cage core.

POSS materials assemble into cubic structures commonly referred to as cages. When the R groups are oxygen atoms the molecule is referred to as Q_8, which refers to each of the eight core silicon atoms being bonded to four oxygen atoms. A superscript is commonly used to describe the terminal group such as Q_8^H indicating a terminal hydrosilane. Q_8^H describes a POSS cage with R = -O-SiMe$_2$H. POSS cages have shown high thermal stability, high modulus, and the compatibility to be incorporated into low-*k* materials [10]. Unsubstituted Q_8 derivatives are highly crystalline solids. However, the corners are readily functionalized with a variety of polymerizable groups. In this way, we can hope to achieve low viscosity due to limited entanglement and low vapor pressure due to high molecular weight.

3.3.3 Epoxide Functionalized POSS

Epoxides are one type of functional group crosslinkable by acid or base. This is advantageous for semiconductor applications because PAGs can be used to give the material photoreactivity. The epoxide functionalized POSS is shown in Figure 3.4.

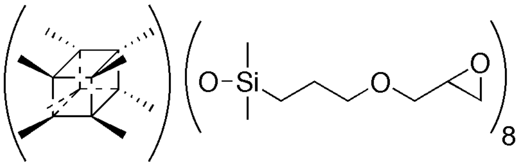

Figure 3.4: Structure of epoxide functionalized cage obtained from Prof. Laine at The University of Michigan.

Though the material was quit viscous, imprinting was carried out successfully [6]. Unfortunately, upon heating, the pattern started to decompose at unexpectedly low temperatures. It was speculated that scrambling and decomposition of the siloxane backbone catalyzed by residual PAG and acid in the film was the cause. This hypothesis was tested and verified by exposing the films after polymerizations to ammonia gas to quench any residual acid. This increased the overall thermal stability, but due to the early onset of decomposition and high viscosity, another method for polymerizing POSS cages was needed.

3.3.4 Methacrylate Functionalized POSS

A free radical polymerization mechanism could have less impact on the stability of the films generated since there would be no residual acid present. The POSS cage was functionalized through a hydrosilylation reaction between allyl methacrylate and Q_8^H (Figure 3.5). The material was unstable under laboratory conditions, and its viscosity was unsuitable for the imprinting processes. The fully functionalized methacrylate POSS was abandoned not only due to the lack of storage stability, but also because methacrylates have a tendency to have poor thermal properties and to shrink upon curing, leading to stress and defects in the films.

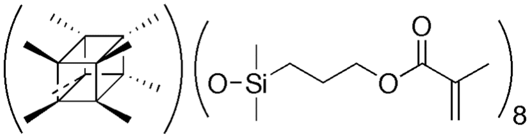

Figure 3.5: Methacrylate functionalized cage.

3.3.5 Dually Functionalized POSS

Because the methacrylate functionalized POSS cage was too unstable, it was speculated that several methacrylates could be replaced by a thermally curable functionality. Q_8 was first symmetrically substituted with a disiloxane that terminates in a hydrosilane. This lowered the melting point of the structure and allowed for materials to be a liquid at STP. Allyl methacrylate was determined to be an excellent photocurable segment and benzocyclobutene an effective thermal crosslinker. Scheme 3.2 shows the functionalized material for S-FIL and DPD, and the two different paths to crosslinking.

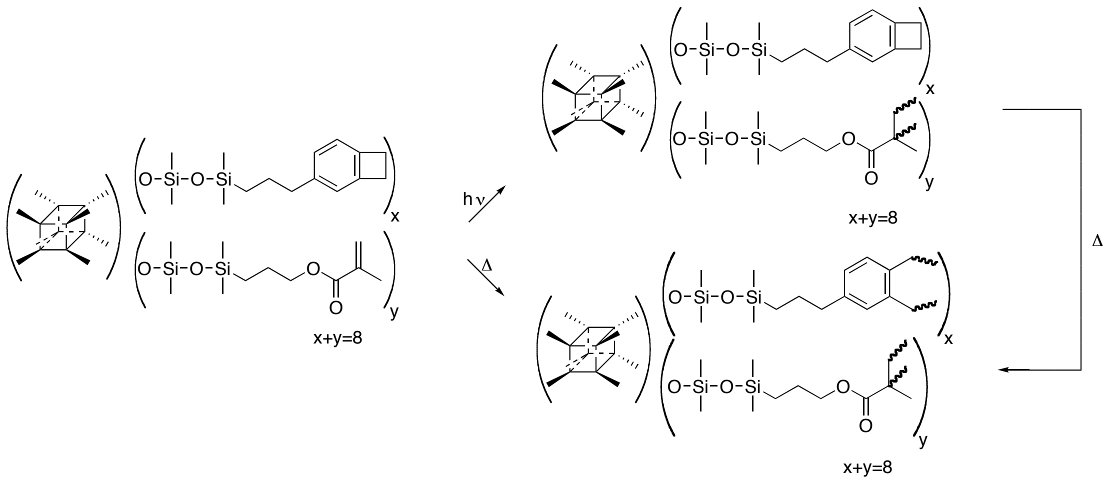

Scheme 3.2: Structure and two paths to polymerizing dually functionalized POSS.

The POSS was functionalized with allyl benzocyclobutene and allyl methacrylate [11]. This produces a mixture of substitutional isomers that is a viscous liquid. The methacrylate enables free radical-mediated photopolymerization, but that linkage is not very thermally stable and the polymerization through this group introduces shrinkage. The benzocyclobutene functionality is used to vitrify the structure by thermal curing subsequent to printing. This thermal cure proceeds via a ring-opening reaction producing thermally stable linkages and is not accompanied by large shrinkage. The optimum ratio of the two substituents was determined to be five BCBs to three methacrylates. This was determined by using the minimum amount of methacrylate to render the material a solid upon photopolymerization. This POSS formulation meets many of the end use criteria but suffers from very high viscosity (~600 cP) and a lower than desirable modulus (2-5 GPa) [3]. The material also seems to have a limited shelf life, as older samples gel within in a few days. The quality of the imprints from this material is acceptable as seen below (Figure 3.6).

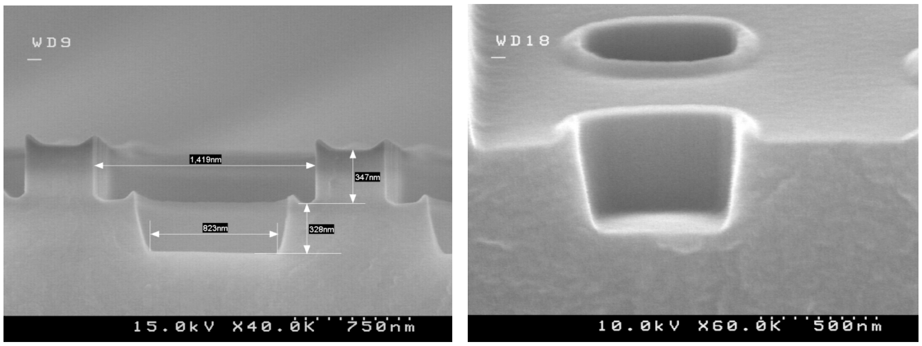

Figure 3.6: SEM images of imprinted BA5x3. The apparent dishing is actually micro-faceting. This faceting is due to imperfections on the template that SFIL reproduces faithfully.

Clearly there is a need for new approaches to the design of these materials. We need to greatly reduce the viscosity. We also need to improve the material's mechanical properties and solve the shelf life problem.

3.3.6 Nitrene Based Photopolymerization

Another class of DPD POSS materials that was investigated is based on polymerization reactions of vinylsiloxanes. A model system based on nitrene chemistry was tested. Nitrene based polymerization, which has been used in photolithography in the past (in g-line negative resist formulations), is based on the photolysis of azides to form nitrenes [12]. Nitrenes undergo addition to olefins readily resulting in cross-linking of materials as illustrated in Scheme 3.3.

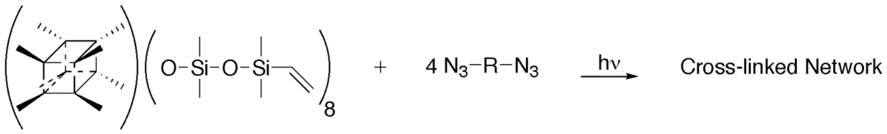

Scheme 3.3: Nitrene based polymerization of vinyl POSS.

A major difference in the type of reactions described previously is that the azide mediated reaction is not catalytic. It was shown that model systems underwent crosslinking, but due to the release of nitrogen gas, bubble formation was observed and incomplete pattern transfer resulted when imprints were carried out.

3.3.7 Thiol-ene Based Photopolymerization

The thiol-ene reaction is another potential polymerization mechanism that was explored. The use of the thiol-ene chemistry for curing has two advantages over acrylates. The reaction is not inhibited by the presence of oxygen [13], and it avoids the shelf life problems common with multifunctional acrylates and methacrylates. Thiols undergo homolytic cleavage when exposed to deep UV light [14, 15]; the radicals formed can then undergo addition to olefins as shown in Scheme 3.4 [13].

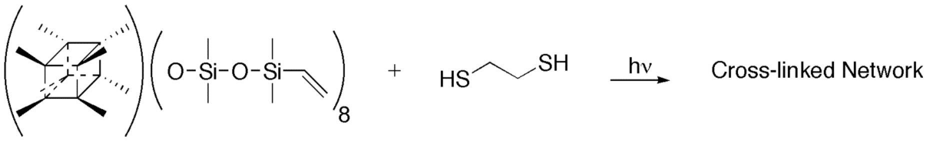

Scheme 3.4: Thiol-ene based photopolymerization of vinyl POSS.

Thiols initiate a free radical reaction and can therefore be used in sub-stoichiometric amounts and still generate high conversion of monomers to polymers.

3.4 RESULTS AND DISCUSSION

3.4.1 Polyhedral Oligomeric Silsesquioxane

The preparation of the tetramethylammonium silicate cage structure was carried out according to literature procedures [16, 17]. The highest overall yield and purity (97% yield) was obtained by following Moran and Cuadrado's procedure [16] (Scheme 3.5).

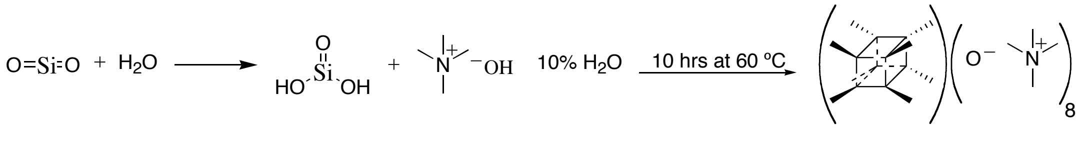

Scheme 3.5: Preparation of silicate salt.

In accordance with the same literature, the silicate salt was then converted to Q_8^H (cage) without any unexpected results, except for a disappointing yield of 28.6% (literature value reports 85% yield [16], but after closely inspecting their results an error must have been made in their calculations). The solid product was re-crystallized from hexanes to remove POSS cages that were not fully condensed and other impurities, yielding fairly large, clear crystals of Q_8^H (Scheme 3.6*)*.

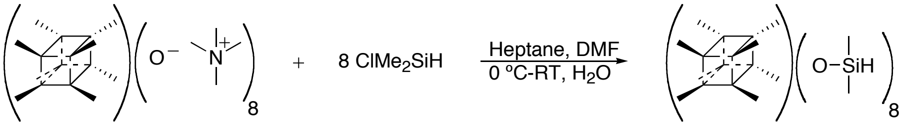

Scheme 3.6: Synthesis of Q_8^H.

For the preparation of Q_8^{OSiH}, Q_8^H was oxidized. The hydrolysis was carried out by the use of palladium on carbon and water to form the silanol Q_8^{OSiOH} shown in Scheme 3.7 [18]. No attempt was made to isolate and purify the silanol since it was only an intermediate in the path to the final product.

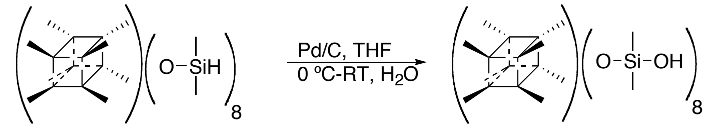

Scheme 3.7: Silanol synthesis.

The freshly made silanol was slowly added to a solution of chlorodimethylsilane (Scheme 3.8). After careful optimization the product was obtained in 62% yield as a clear gelatinous material. The liquid and the gelatinous solid were both analyzed by Matrix Assisted Laser Desorption/Ionization (MALDI). It was observed that the less viscous material contained a significant amount of partially functionalized corners while the gelatinous solid appeared to be a single product (see Appendix A for MALDI spectra). Sublimation was attempted at high vacuum (<40 mTorr) and elevated temperature (135

°C) for 8 hrs. It was observed that the liquid remained at the bottom of the vessel and that a solid was "crawling" up the sides of the sublimer instead of collecting on the cold finger. IR analysis showed hydroxyl groups in the product (broad peak at 3446 cm^{-1} was observed).

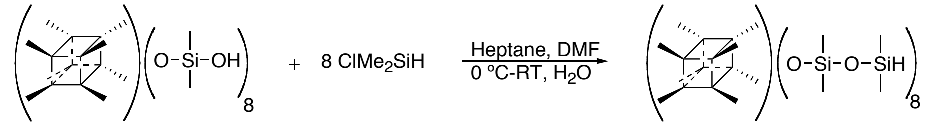

Scheme 3.8: Silane synthesis, extension of siloxane chains.

3.4.2 Benzocyclobutene

The synthesis of 4-allyl-1,2-dihydrocyclobutabenzene (allylbenzocyclobutene) was carried out and optimized in collaboration with a visiting scientist from JSR, Yukio Nishimura. Reduction of 2-bromophenyl acetic acid was carried out with borane in THF. This is illustrated in Scheme 3.9. The product was isolated in 62% as a clear liquid and purified by distillation.

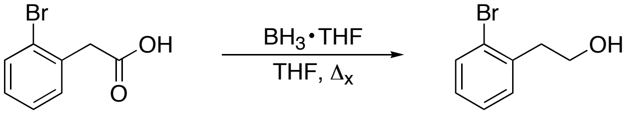

Scheme 3.9: Synthesis of 2-(2-bromophenyl)ethanol.

Toluenesulfonyl chloride (TsCl) was used to convert the hydroxyl group into a better leaving group (Scheme 3.10). Product was isolated as a crystalline solid in 69%.

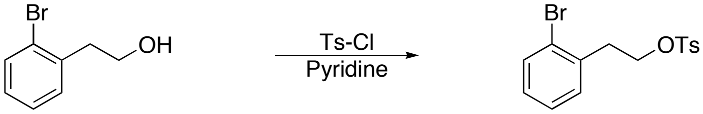

Scheme 3.10: Synthesis of 2-(2-bromophenyl)ethyl 4-methylbenzenesulfonate.

As can be seen in Scheme 3.11, lithium bromide was used to displace the tosyl group in refluxing acetone. The product was obtained after column chromatography as a slightly yellowish liquid in 60%.

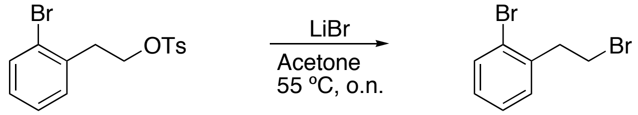

Scheme 3.11: Synthesis of 1-bromo-2-(2-bromoethyl)benzene.

A lithium halogen exchange using *n*-butyllithium in THF at -78 °C lead to ring closing to form benzocyclobutene (BCB), illustrated in Scheme 3.12.

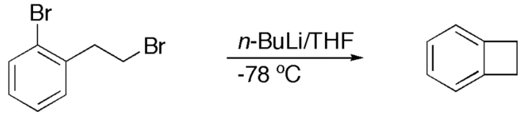

Scheme 3.12: Ring-closing reaction to obtain benzocyclobutene (BCB).

One of the most facile ways to functionalize BCB is by bromination of the phenyl ring to result in 4-bromo-benzocyclobutene (Scheme 3.13). Following column chromatography, the product was obtained as a clear liquid in 58%.

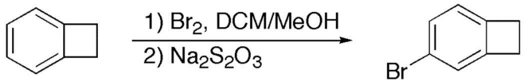

Scheme 3.13: Bromination of BCB.

There were two separate paths investigated to render 4-bromo-BCB functional in order to be appended to POSS; both are shown in Scheme 3.14.

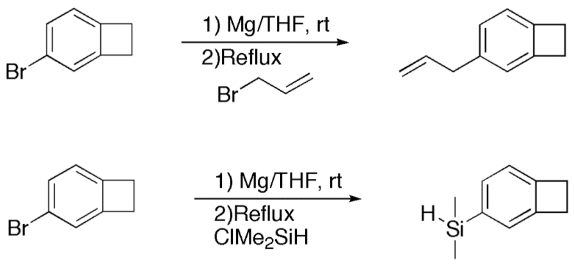

Scheme 3.14: Two synthetic paths to prepare BCB to be appended onto two different POSS, hydrosilane and vinylsilane terminated.

3.4.3 Functionalizing POSS cages

Once all starting materials were available, trial and model reactions were carried out. First, the Q_8^H cage was homo-functionalized with allyl acetate (Scheme 3.15) to provide a stable analogue to the photocurable allyl methacrylate. Allyl acetate was used for characterization studies. The hydrosilylation reaction was done in collaboration with Dr. Jianjun Hao. Using Karstedt's catalyst [Pt(dvs)], a silane (Si-H) can be added to a terminal olefin [19, 20].

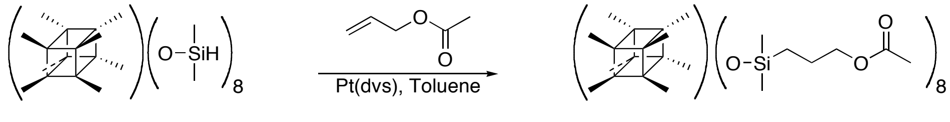

Scheme 3.15: Attempted hydrosilylation of Q_8^H with allyl acetate.

Allylbenzene was used as a model to BCB. The same reaction procedure was performed and after two silica gel columns led to the product, a slightly yellow-colored, viscous oil in 73% (Scheme 3.16).

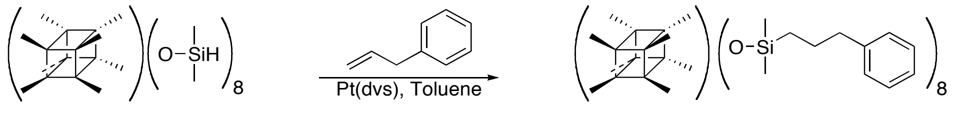

Scheme 3.16: Hydrosilylation of Q_8^H with allylbenzene.

A reaction with allyl methacrylate was also attempted (illustrated in Scheme 3.17) with hydroquinone present (radical inhibitor). Upon removal of the solvent, the material formed an insoluble, thick gel. A miniscule amount was dissolved in a fairly large quantity of deuterated chloroform, and an NMR spectra was collected. Proton NMR spectra indicates that product is present but mixed with impurities.

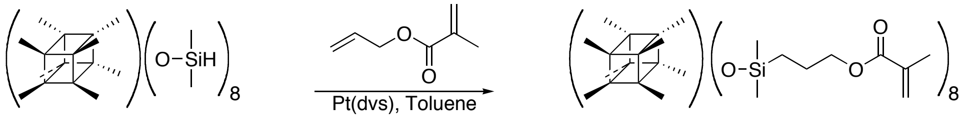

Scheme 3.17: Synthesis of octa functionalized Q_8^H with allyl methacrylate resulted in a material with very poor shelf stability.

Q_8^{OSiH} was reacted with BCB (Scheme 3.18) using the same procedure. A short (2 inches) silica gel plug was used to purify the product, which is a slightly yellow viscous oil (81%).

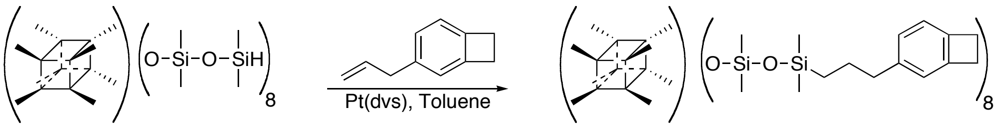

Scheme 3.18: Octa allylBCB functionalized POSS cage resulted in a viscous thermally crosslinkable material.

3.4.4 Dually Functionalized POSS

Since the method for carrying out the hydrosilylation reaction was established, it was time to dually-functionalize the $Q_8M_8^{OSiH}$ POSS. Because there are eight corners available to append side groups. Many combinations were tried to determine the correct ratio of the two substituents in order to generate a product with the above-mentioned mechanical and chemical properties. It was determined that a ratio of five allylbenzocyclobutenes to three allyl methacrylates groups attached to the cage (BA5x3) gave the best properties for the material. The two functional groups were appended

(Scheme 3.19) using the same hydrosilylation method as for the other reactions described above. One main difference being that hydroquinone was added to inhibit premature radical polymerization. A critical problem yet to be overcome is how to purify the final product. This is because it has a statistical distribution of the two functional groups. This was modeled by Dr. Kane Jen and verified by MALDI. ^{1}H-NMR can only show an average of what is appended to the core cage, but MALDI data gives insight into the distribution of products.

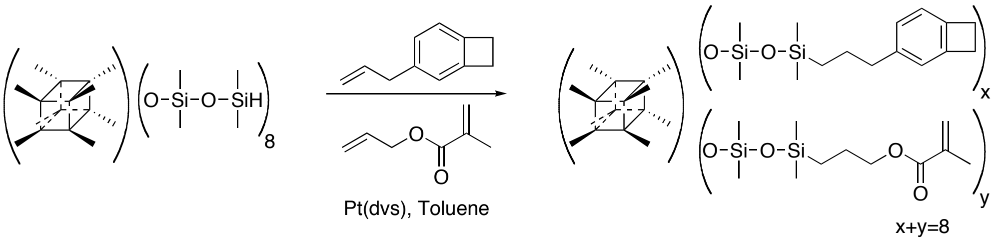

Scheme 3.19: Hydrosilylation of POSS cage with allylBCB and allyl methacrylate to render the material photocrosslinkable and thermally stable.

The reason for appending the two functional groups was described in Scheme 3.2. With BA5x3, a network polymer can be produced by first curing the material with UV and then vitrifying by heating to fully crosslink the material. Several batches were tested by hand imprinting with assistance from Dr. Frank Palmieri. Figure 3.7 below shows the result of a successful imprint. In order to obtain those patterns, several issues needed to be overcome, such as adhesive and/or cohesive failure (material sticking to the template and not releasing or material tearing). These problems were worked out by optimizing the surface treatments on the wafer and the template. The best process included AP410 as an adhesion promoter and a fluorinated self-assembled monolayer (FSAM) to promote template release.

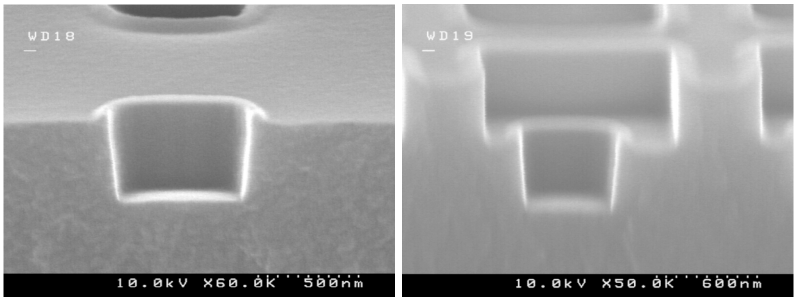

Figure 3.7: SEM images from hand imprint of BA5x3. Microfaceting is replicated from defects created during manufacturing of the template used.

3.4.5 Vinyl POSS with Azides

Ultimately homo-functionalized material was explored to provide a single, pure substance rather than a mixture and to avoid the instability of the acrylate functionality. One such material was POSS with terminal vinyl groups. The vinyl group is not sufficiently reactive to enable polymerization but can undergo crosslinking by the addition of nitrenes. All of the same steps described above to synthesize Q_8^H were used to synthesize the vinyl cage. Instead of using chlorodimethylsilane, vinyldimethylchlorosilane was used in the last step. The reaction is illustrated in Scheme 3.20. The product is a crystalline solid that was obtained in moderate yield (46%). Purification was carried out in a manner similar to that described above.

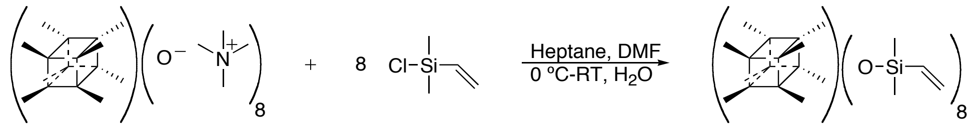

Scheme 3.20: Synthesis of vinyl terminated Q_8 (Q_8^{vinyl}).

As with the silane POSS, Q_8^H was hydrolyzed and reacted with vinyldimethylchlorosilane to extend the siloxane linkages from each corner. The reaction was carried out with the same observations as in the preparation of Q_8^{OSiH}. The product

PS_2V ($Q_8^{OSiVinyl}$, seen in Scheme 3.21), is a colorless viscous liquid that was obtained in 52% yield. Spectral analysis along with HRMS verified the structure.

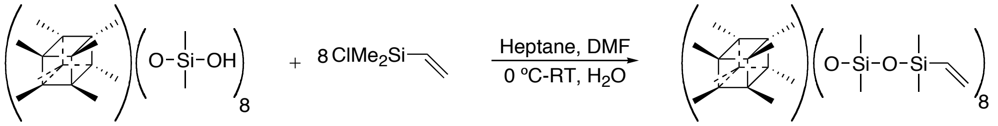

Scheme 3.21: Preparation of PS_2V cage ($Q_8^{OSiVinyl}$).

In order to study the chemistry of the vinyl POSS, benzyldimethyl(vinyl)silane was used as a model compound (Scheme 3.22). The colorless liquid product was obtained in 83%. Analysis compared to published data confirmed the structure [21].

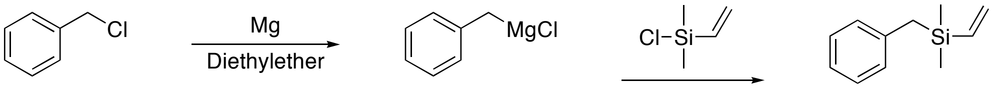

Scheme 3.22: Synthesis of benzyldimethyl(vinyl)silane.

Benzyloxydimethyl(vinyl)silane was also synthesized as a model compound as shown in Scheme 3.23. The product was obtained as a colorless liquid in 61%.

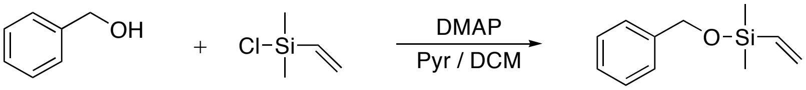

Scheme 3.23: Synthesis of benzyloxydimethyl(vinyl)silane.

As for the azide model compounds, two simple azides were synthesized (according to slightly modified published procedures [22, 23]: azidobenzene and benzylazide (Scheme 3.24).

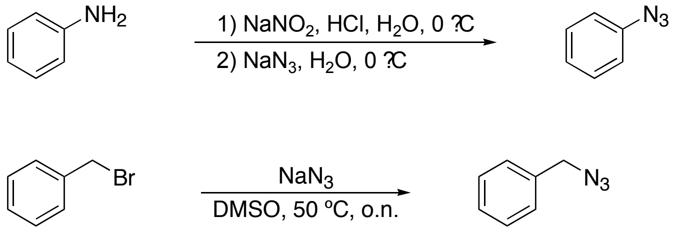

Scheme 3.24: Synthesis of model azide compounds.

These azide compounds were mixed with the model vinylsilanes between two IR plates and exposed to UV irradiation. Reactions were monitored at first by IR to observe the disappearance of the azide group. Later, mixtures of model compounds were dissolved in deuterated acetonitrile and exposed to UV in a quartz cuvette. In this way the reactions could be monitored by NMR (appearances and shifts of signals).

A difunctional azide or an azide appended onto POSS is necessary to achieve crosslinking. A diazide, 1,3-bis(azidomethyl)-1,1,3,3-tetramethyldisiloxane (bisazide), was synthesized by a slight modification of a literature procedure [24]. A colorless liquid (99%) was isolated upon aqueous workup (Scheme 3.25).

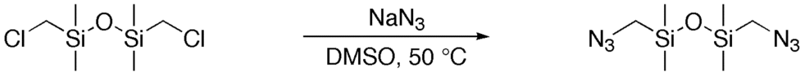

Scheme 3.25: Synthesis of bisazide crosslinker.

A polyfunctional azide can also mediate crosslinking. 4-Azidostyrene (*p*-azidostyrene), was therefore synthesized in collaboration with a visiting scientist, Dr. Sangwoong Yoon according to Scheme 3.26 [25]. This azide can be appended to a POSS cage by hydrosilylation and tested as a crosslinker.

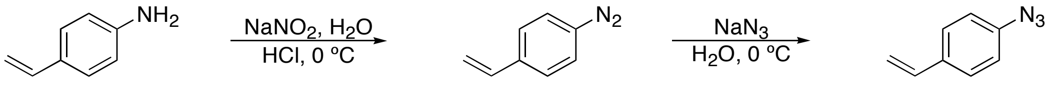

Scheme 3.26: Synthesis of 4-azidostyrene.

4-Azidobenzyl alcohol was also prepared in collaboration with Dr. Yoon (illustrated in Scheme 3.27) [26]. The idea for the design of this molecule was to append it to the POSS cage or various chlorosilanes.

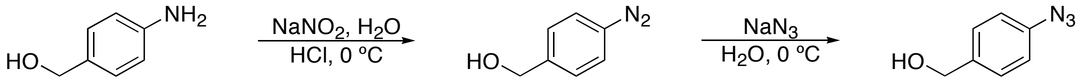

Scheme 3.27: Synthesis of 4-azidobenzyl alcohol.

UV exposures were carried out on glass slides to see if a solid film would form from formulations of bisazide and PS_2V (shown in Scheme 3.28). Solid films formed when drops were dispensed on glass slides and exposed.

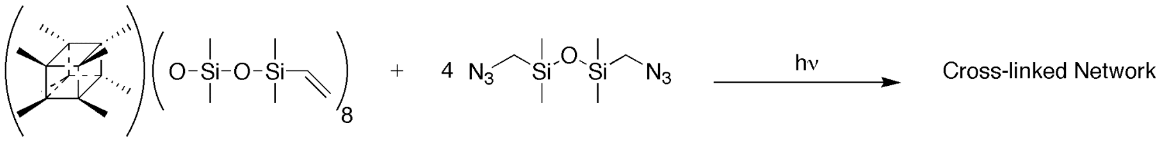

Scheme 3.28: POSS containing imprint formulations based on azide chemistry.

Hand imprints were tried with quartz templates. Adhesive and cohesive failure was catastrophic. Closer attention to the actual UV exposure was made and large bubbles were observed forming between the wafer and the template. Occasionally these bubbles forced the template off the wafer. It was determined that the amount of nitrogen gas generated from the reaction was too large to diffuse through the material and that nitrene chemistry would not work for imprint lithography.

3.4.6 Vinyl POSS with Thiols

Thiol-ene chemistry has been known for over a century [13] It is similar to click chemistry in that it forms products in nearly quantitative yield. The reaction takes place as a free radical reaction. Another attractive characteristic of this chemistry is that it is not inhibited by oxygen.

Benzyldimethyl(vinyl)silane, trimethylvinylsilane, and vinyltetramethyldisiloxane model compounds were formulated with ethanethiol, 1,2-ethanedithiol, and thiophenol and tested. Reactions were monitored by the disappearance of the vinylic and thiol protons and the appearance of methylene groups in NMR spectra. It was observed that the thiophenol formulation crosslinked while being stored in a dark cabinet. This could obviously become a problem if one cannot store the mixture, and shelf-life studies need to be carried out. None of the products were characterized by techniques other than NMR.

A formulation of PS_2V and 1,2-ethanedithiol (Scheme 3.29) was successfully patterned by hand imprinting. However, the two components of this initial formulation phase-separated and further trials were abandoned.

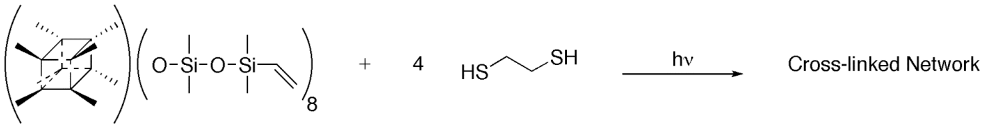

Scheme 3.29: Initial thiol-ene based imprint formulation solidified upon exposure, but phase separate upon storage.

Pentaerythritol tetrakis(3-mercaptopropionate) was tried as well but was not miscible with PS_2V either.

Because of the initial success with 1,2-ethanedithiol the synthesis of potentially phase compatible multi-thiols was investigated. Initially, 1,2-bis(mercaptomethyl)-1,1,3,3-tetramethyldisiloxane (bisthiol) was synthesized according to a slightly modified and adapted thiouronium salt procedure (see Scheme 3.30) [27]. The product, a colorless, low-viscosity liquid, was obtained in 51%.

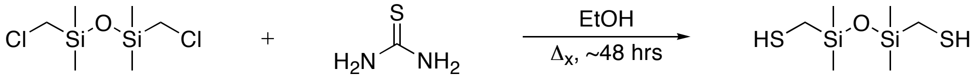

Scheme 3.30: Synthesis of 1,3-bis(mercaptomethyl)-1,1,3,3-tetramethyldisiloxane crosslinker.

An additional path to the thiol involved first carrying out a displacement of the chloride by thioacetate as illustrated in Scheme 3.31.

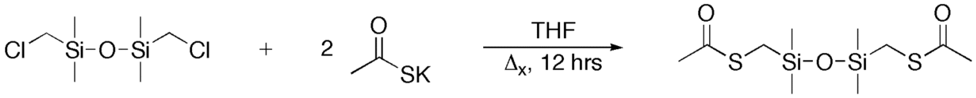

Scheme 3.31: Synthesis of 1,3-bis(methylene ethanethioate)-1,1,3,3-tetramethyldisiloxane.

This procedure converted starting material to product in nearly quantitative yield. Hence attempts toward cleaving the acetate to provide the free thiol. There are only a few alkyl halide terminated silanes and siloxanes commercially available. However, there are a large number of commercially available vinyl-terminated silanes and siloxanes. So, it would be convenient to find an efficient way to synthesizing thiols directly from such starting materials. Several methods of installing thiols were explored and are illustrated in Scheme 3.32.

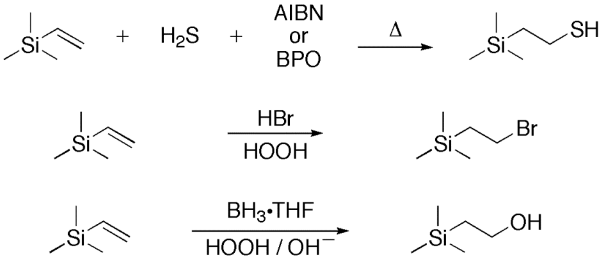

Scheme 3.32: Various unsuccessful methods attempted to install thiols directly or indirectly.

Various conditions were attempted to add hydrogen sulfide directly to a vinyl silane. No conversion of starting material was observed. Displacement of the alkyl halide with either thiourea or thioacetate resulted in modest to almost quantitative yields. Several methods were tried to add a halide in anti-markovnikov fashion with little success. Reduction of the vinyl functionality with borane was also attempted without success. There was much disappointment when the above reactions did not proceed to any appreciative conversion or not at all. Fortunately the reaction between the various vinyl terminated compounds and thioacetic acid to yield thioacetates as seen in Scheme 3.33 produced in excellent yield.

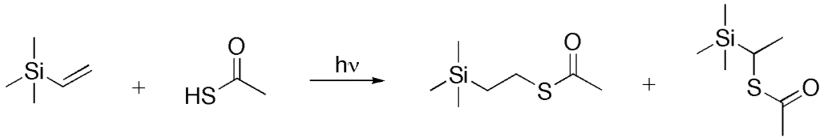

Scheme 3.33: Thiol-ene reaction producing a thioester. Although the anti-Markovnikov is the major product, the B-addition is shown as it is produced in small quantity.

Cleavage of the thioesters would yield the desired thiols.

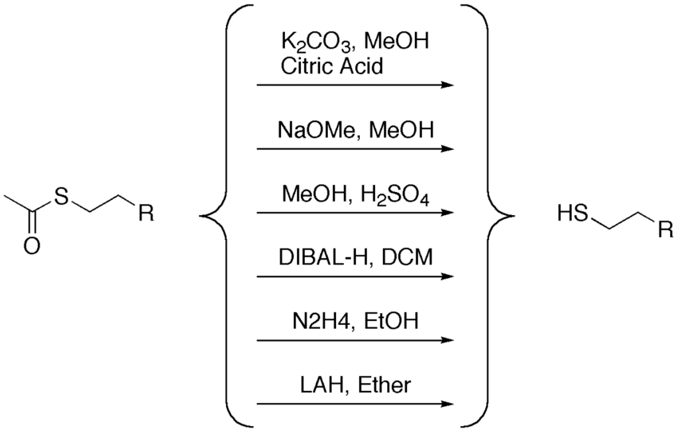

Scheme 3.34: Attempts to cleave thioesters. The LAH procedure worked best and even then only in meager yields.

Several methods were attempted but there was little success in cleaving the thioacetate. Heating the thioester to reflux in alcoholic potassium hydroxide lead to formation of thiols in model compounds. However, this method is not suitable for cleaving thioesters from siloxane derivatives as the basic conditions scramble the siloxane linkages. Reduction of the thioesters with LAH, provided a series of thiols in low yield as illustrated in Figure 3.8.

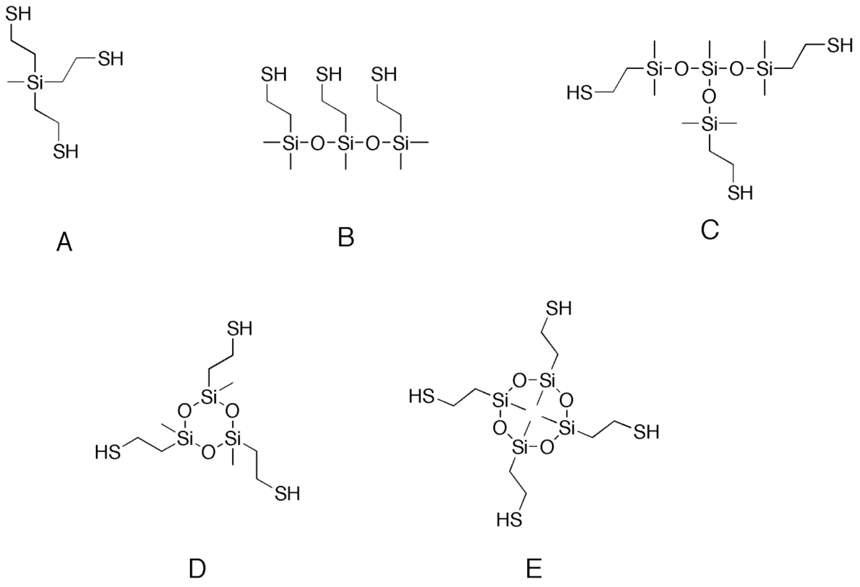

Figure 3.8: Attempted synthesis of multi-thiols containing silane and siloxanes.

The new multi-thiols were fully characterized and evaluated for compatibility with PS_2V (Scheme 3.34). Unfortunately, only multi-thiol B, and C were phase compatible with the vinyl cage.

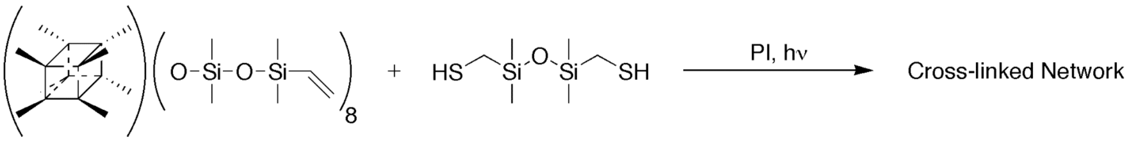

Scheme 3.35: Crosslinking of PS_2V and bisthiol formulation under UV exposure.

Imprint images were examined by scanning electron microscope (SEM). Results can be seen in Figure 3.9.

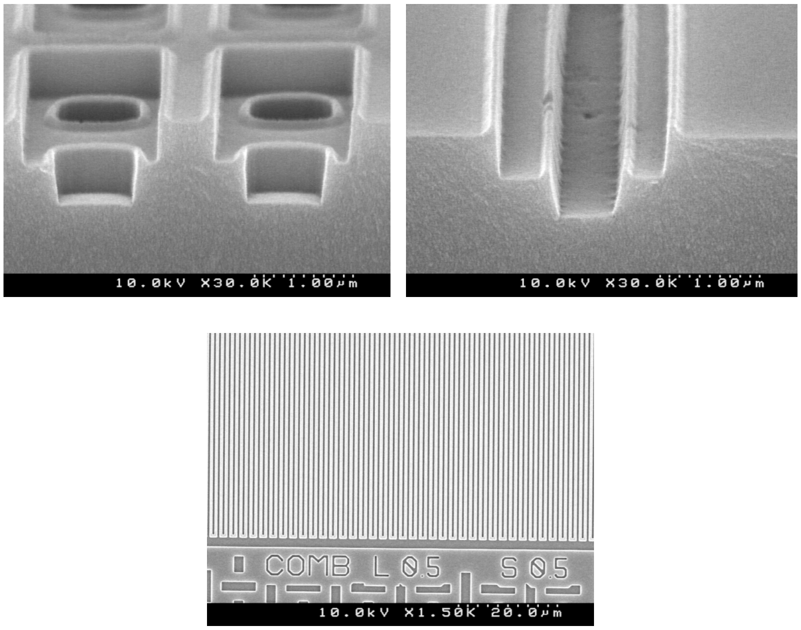

Figure 3.9: SEM images of hand imprinted patterns with PS_2V–bis(mercaptomethyl)-tetramethyldisiloxane formulation.

3.4.7 Reactive Diluents

As noted, POSS cages have a tendency to be crystalline or viscous liquids. For these materials to be useful for high volume manufacturing (HVM), the time required to fill the template before curing must be minimized. Solvents cannot be used to reduce viscosity as they evaporate over time and change the composition of the films. However, a nonvolatile solvent that is reactive could be used to lower the viscosity. Figure 3.10 shows several commercially available and synthesized reactive diluents that were tested in various imprint formulations.

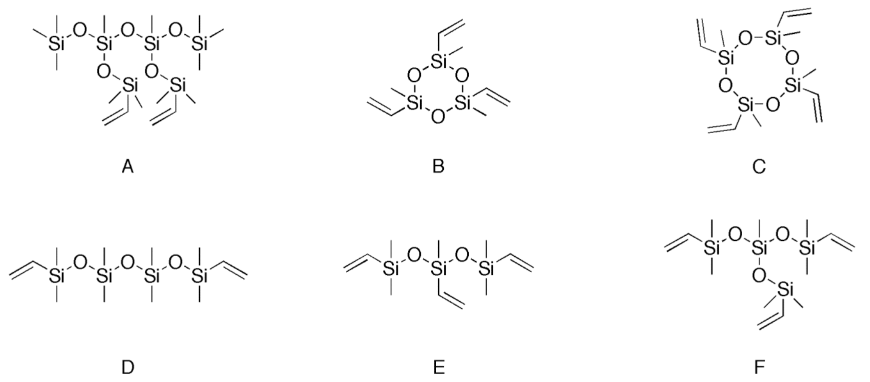

Figure 3.10: Various reactive diluents evaluated in formulations. Compound A and D were synthesized whereas the rest are commercially available. As a side note, many of these reactive diluents were used in the preparation of the above multi-thiols.

The addition of a reactive diluent can alter the viscosity of formulations tremendously. It was determined by viscometry, thermal stability tests, and the ability to solidify upon exposure that compound B and C are the two most promising candidates. Reactive diluents become a permanent part of the film and will therefore impact its physical properties after photopolymerization. It was observed that a loading of any reactive diluent greater than 15 wt.%, produced films that were sticky and rubbery.

3.5 IMPRINTING OF RESIST FORMULATIONS

An optimum imprint resist formulation consisting of PS_2V, bisthiol, compound C in Figure 3.10 above, and a photo initiator was chosen and used in imprint tests on an Imprio 55. The resist formulation is based on the lowest possible viscosity while maintaining the highest possible thermal stability. The formulation used can be seen in Table 3.1.

Component	Structure	wt.%
PS2V	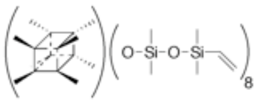	**65.0**
Bisthiol	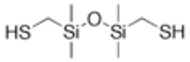	**20.0**
RD	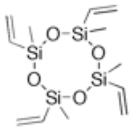	**10.0**
Darocur® 1173	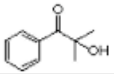	**5.0**

Table 3.1: Best performing imprint resist formulations used in imaging attempts on an Imprio 55.

3.8 SUMMARY

Several polymerization techniques have been evaluated to provide a functional DPD material. Each new method has brought us closer to discovering a formulation that meets all of the requirements set by the microelectronic industry. The development of a thiol-ene based formulation has shown great promise. Unfortunately, the viscosity of current formulations is too high for high-volume manufacturing. Higher concentrations of a reactive diluent solves the viscosity problem but compromises other requirements a material must meet. A more advanced formulation consisting of additional components will be required to meet all the criteria set on ILD materials.

3.9 REFERENCES

[1] M. D. Stewart and C. G. Willson. "Imprint Materials for Nanoscale Devices". *MRS Bulletin,* 30, 947-951, 2005.

[2] M. W. Lin. "Simulation and Design of Planarizing Materials and Interfacial Adhesion Studies for Step and Flash Imprint Lithography". *Ph.D. University of Texas at Austin,* 2008**.**

[3] F. L. Palmieri. "Step and Flash Imprint Lithography: Materials and Applications for The Manufacture of Advanced Integrated Circuits". *Ph.D. University of Texas at Austin,* 2008**.**

[4] D. J. Resnick, S. V. Sreenivasan and C. G. Willson. "Step & flash imprint lithography". *Materials Today,* 8, 34-42, 2005.

[5] M. McCoy. "Deciding on a Dielectric". *Chemical & Engineering News,* 79, 43-46, 2001.

[6] M. D. Stewart, J. T. Wetzel, G. M. Schmid, F. Palmieri, E. Thompson, E. K. Kim, D. Wang, K. Sotoodeh, K. Jen, S. C. Johnson, J. Hao, M. D. Dickey, Y. Nishimura, R. M. Laine, D. J. Resnick and C. G. Willson. "Direct Imprinting of Dielectric Materials for Dual Damascene Processing". *Emerging Lithographic Technologies IX*, 5751, 2005.

[7] G. M. Schmid, M. D. Stewart, J. Wetzel, F. Palmieri, J. Hao, Y. Nishimura, K. Jen, E. K. Kim, D. J. Resnick, J. A. Liddle and C. G. Willson. "Implementation of an imprint damascene process for interconnect fabrication". *Journal of Vacuum Science & Technology B: Microelectronics and Nanometer Structures,* 24, 1283-1291, 2006.

[8] W.-L. K. Jen. "Materials and Processes for Advanced Lithography Applications". *Ph.D. Dissertation, The University of Texas at Austin,* 2009**.**

[9] F. Palmieri, M. D. Stewart, J. Wetzel, J. Hao, Y. Nishimura, K. Jen, C. Flannery, B. Li, H.-L. Chao, S. Young, W. C. Kim, P. S. Ho and C. G. Willson. "Multi-level Step and Flash Imprint Lithography for Direct Patterning of Dielectrics ". *Proc. of SPIE,* 6151, 2006.

[10] M. A. Wahab, K. Y. Mya and C. He. "Synthesis, Morphology, and Properties of Hydroxyl Terminated-POSS/Polyimide Low-*k* Nanocomposite Films". *Journal of Polymer Science Part A: Polymer Chemistry,* 46, 5887-5896, 2008.

[11] J. Hao, M. W. Lin, F. Palmieri, Y. Nishimura, H.-L. Chao, M. D. Stewart, A. Collins, K. Jen and C. G. Willson. "Photocurable Silicon-Based Materials for Imprint Lithography". *Proc. of SPIE,* 6517, 2007.

[12] L. F. Thompson, C. G. Willson and M. J. Bowden. "Introduction to Microlithography"; Ed.; American Chemical Society; Washington D.C., 1983.

[13] C. E. Hoyle, T. Y. Lee and T. Roper. "Thiol–Enes: Chemistry of the Past with Promise for the Future". *J. Polym. Sci. Part A: Polym. Chem.,* 42, 5301-5338, 2004.

[14] W. A. Pryor and E. G. Olsen. "Homolytic Displacement at Sulfur by the Hydrogen Atom. Formation of Hydrogen Sulfide in the Liquid-Phase Photolysis of Thiols". *J. Am. Chem. Soc.,* 100, 2852-2856, 1978.

[15] J. D. Coyle. "Photochemistry of Organic Sulphur Compounds". *Chemical Society Reviews,* 523-532, 1975.

[16] M. Moran, C. M. Casado and I. Cuadrado. "Ferrocenyl Substituted Octakis(dimethylsiloxy)octasilsesquioxanes: A New Class of Supramolecular Organometallic Compounds. Synthesis, Characterization, and Electrochemistry". *Organometallics,* 12, 4327-4333, 1993.

[17] A. Provatas, M. Luft, J. C. Mu, A. H. White, J. G. Matisons and B. W. Skelton. "Silsesquioxanes: Part I: A key intermediate in the building of molecular composite materials". *Journal of Organometallic Chemistry,* 565, 159-164, 1998.

[18] H. Uchida, Y. Kabe, K. Yoshino, A. Kawamata, T. Tsumuraya and S. Masamune. "General Strategy for the Systematic Synthesis of Oligosiloxanes. Silicone Dendrimers". *Journal of American Chemistry Society,* 112, 7077-7079, 1990.

[19] E. Markovic, M. Ginic-Markovic, S. Clarke, J. Matisons, M. Hussain and G. P. Simon. "Poly(ethylene glycol)-Octafunctionalized Polyhedral Oligomeric Silsesquioxane: Synthesis and Thermal Analysis". *Macromolecules,* 40, 2694-2701, 2007.

[20] L. N. Lewis and N. Lewis. "Platinum-Catalyzed Hydrosilylation-Colloid Formation as the Essential Step". *J. Am. Chem. Soc.,* 108, 7228-7231, 1986.

[21] W. B. Motherwell, G. Begis, D. E. Cladingboel, L. Jerome and T. D. Sheppard. "Observations on the direct amidocyclopropanation of alkenes using organozinc carbenoids". *Tetrahedron,* 63, 6462-6476, 2007.

[22] L. Barr, S. F. Lincoln and C. J. Easton. "A Cyclodextrin Molecular Reactor for the Regioselective Synthesis of 1,5-disubstituted-1,2,3-triazoles". *Supramolecular Chemistry,* 17, 547-555, 2005.

[23] L. Campbell-Verduyn, P. H. Elsinga, L. Mirfeizi, R. A. Dierckx and B. L. Feringa. "Copper-free 'click': 1,3-dipolar cycloaddition of azides and arynes". *Organic & Biomolecular Chemistry,* 6, 3461-3463, 2008.

[24] V. V. Dorsselaer, D. Schirlin, P. Marchal, F. Weber and C. Danzin. "Silicon-Mediated Inactivation of Diamine Oxidase". *Bioorganic Chemistry,* 24, 178-193, 1996.

[25] N.-H. Nguyen, J. W.Apriletti, J. D. Baxter and T. S. Scanlan. "Hammett Analysis of Selective Thyroid Hormone Receptor Modulators Reveals Structural and Electronic Requirements for Hormone Antagonists". *J. Am. Chem. Soc.,* 127, 4599-4608, 2005.

[26] J. T. Spletstoser, P. T. Flaherty, R. H. Himes and G. I. Georg. "Synthesis and Anti-Tubulin Activity of a 3'-(4-Azidophenyl)-3'-dephenylpaclitaxel Photoaffinity Probe". *J. Med. Chem.,* 47, 6459-6465, 2004.

[27] E. Block, J.-A. Laffitte and V. Eswarakrishnan. "Synthesis and Reactions of 3-Mercaptocyclobutanol and Derivatives. Preparation of a 2,4-Dithiabicyclo[3.1.1]heptane". *JOC,* 51, 1986.

[28] D. D. Perrin and W. L. F. Armarego. "Purification of Laboratory Chemicals"; 3rd Ed.; Butterworth-Heinemann Ltd; 1988.

[29] J. P. Wolfe, R. A. Rennels and S. L. Buchwald. "Intramolecular Palladium-Catalyzed Aryl Amination and Aryl Amidation". *Tetrahedron,* 52, 7525-7546, 1996.

[30] M. G. Banwell, B. L. Flynn, D. C. R. Hockless, R. W. Longmore and A. D. Rae. "Assessment of Double-Barrelled Heck Cyclizations as a Means for Construction of the 14-Phenyl-8,9-dihydro-6H-[1]benzopyrano[4',3':4,5]pyrrolo[2,1-a]isoquinolin-6-one Core Associated with Certain Members of the Lamellarin Class of Marine Natural Product". *Aust. J. Chem.,* 52, 755-765, 1998.

[31] F. Bilodeau, M.-C. Brochu, N. Guimond, K. H. Thesen and P. Forgione. "Palladium-Catalyzed Decarboxylative Cross-Coupling Reaction Between Heteroaramatic Carboxylic Acids and Aryl Halides". *Journal of Organic Chemistry,* 75, 1550-1560, 2010.

[32] J. B. F. Lloyd and P. A. Ongley. "The Electrophilic Substitution of Benzocyclobutene-II". *Tetrahedron,* 21, 245-254, 1965.

[33] A. R. Bassindale, C. Eaborn and D. R. M. Walton. "Aromatic Reactivity. Part XXXVIII. Protodesilylation of 1,2-Dihydrobenzocyclobutene, Indan, and Tetralin". *J. Chem. Soc. (B),* 12-15, 1969.

[34] J. T. Spletstoser, P. T. Flaherty, R. H. Himes and G. I. Georg. *J. Med. Chem.,* 47, 2004.

[35] C. Zhang and R. M. Laine. "Silsesquioxanes as synthetic platforms. II. Epoxy-functionalized inorganic-organic hybrid species". *Journal of Organometallic Chemistry,* 521, 199-201, 1996.

[36] T. I. Ito and W. P. Weber. "Synthesis and Mass Spectra of *w*-(trimethylsilyl)alkyl Methyl Sulfides and Sulfones". *JOC,* 39, 1694-1697, 1974.

[37] A. L. Schwan, D. Brillon and R. Dufault. "Synthesis, reactions, and interconversions of some 2-(trimethylsilyl)ethyl substituted sulfur compounds". *Can. J. Chem.,* 72, 325, 1994.

3.10 SYNTHESIS OF MATERIALS

General experimental procedures and comments. Chemicals were purchased and used in reactions without further purification unless otherwise indicated. Solvents were dried and distilled according to commonly used literature procedures [28]. All reactions were performed under a dry nitrogen atmosphere unless otherwise indicated. Q_8^{OH} was not isolated, but instead run through a celite plug and a micro filter to remove catalyst, and used directly in subsequent reactions.

^{1}H NMR spectra were obtained on a Varian Mercury (400 MHz), Varian (400 MHz System, Direct Drive), Varian INOVA (500 MHz) or Unity plus (300 MHz) instruments referenced to deuterated chloroform (7.24 ppm), deuterated DMSO (2.49 ppm) or deuterated water (4.79 ppm). Chemical shifts are reported in delta units (∂), parts per million, and coupling constants (*J*) are reported in Hertz (Hz). ^{13}C spectra were obtained on a Varian Mercury (100 MHz), Varian (100 MHz System, Direct Drive), Varian INOVA (125 MHz) or a Unity plus (75 MHz) instruments referenced to 77.000 ppm for deuterated chloroform, or 39.5 ppm for deuterated DMSO. ^{13}C NMR spectra were routinely run with broadband decoupling. ^{29}Si spectra were obtained on a Varian INOVA (75 MHz) or a Unity plus (60 MHz). Low-resolution mass spectra were obtained on an Agilent GC/MS 6890N Gas Chromatograph and 5973 Mass Spectrometer, or a Finnigan LCQ instrument. High-resolution mass spectroscopy analyses were carried out on an ION-SPEC, FT-ICR/MS instrument. FT-IR spectra were obtained on a Nicolet Avatar 360 FT-IR instrument. Thermal stability and melting points were measured on a MEL-TEMP II or a TA instruments DSC Q_{100} / TGA Q_{500}. UV exposures were either carried out on a The Southern N.E. Ultraviolet Co. Rayonet Photochemical Reactor (16 bulbs, 300 nm) or a JH Technoligies Novacure® 2100 System (High Pressure 100 W Mercury Vapor Short Arc Lamp, ~250-500 nm).

Preparation of tetramethylammonium silicate [16]. Tetramethylammonium hydroxide pentahydrate (17.187 g, 0.095 mol, 1.3 eq.) was added to a 250 mL single necked round-bottom flask equipped with a magnetic stir bar and a rubber septum. To this was added distilled water (85 mL) and then silicic acid (5.684 g, 0.073 mol, 1.0 eq.) slowly portion wise. The white cloudy mixture was stirred at room temperature for 7 hours and then heated to 60 °C overnight. The resulting clear colorless solution was concentrated in vacuo and cooled to 0 °C to obtain a wet white solid. The solid was isolated by filtration and dried further under high vacuum to yield 10.1 g, 97% of tetramethylammonium silicate. Decomposition occurs above 380 °C. ^{1}H-NMR (500 MHz, D_2O): δ 3.086 (t, *J* = 0.6 Hz, 96H). ^{13}C-NMR (125 MHz, D_2O): δ 55.435 (t). ^{29}Si-NMR (100 MHz, D_20): δ -72.020 (s). FT-IR (KBr): 3196 (br), 1457, 1375, 1107, 1060, 1002, 948, 881, 705 cm^{-1} (m).

Preparation of Q_8^H (POSS) [16]. A mixture of dried heptane (200 mL), dimethylformamide, (400 mL), and dimethylchlorosilane (200 mL, 188.6 g, 2 mol) was prepared in a 2 L single necked round-bottom flask equipped with a septum and a magnetic stir bar. The mixture was stirred for about 15 min. at room temperature and then cooled to 0 °C before tetramethylammonium silicate (9.528 g, 0.0084 mol) was added slowly to the mixture. The resulting mixture was stirred for 15 min. before ~1 L of chilled distilled water was added drop wise through an addition funnel at a rate of a few drops/s. The organic layer was separated from the aqueous layer, then washed with distilled water (3x400 mL) until the organic layer was neutralized. The solvent was removed under reduced pressure at 50 °C to leave a white solid that was purified by crystallization from hexanes and isolated to yield 2.435 g (29%) of product which sublimes between 166-245 °C (modulated mode, modulation temperature amplitude: +/- 5° C, modulation period: 200s, heating rate: 2° C/min). Spectral data corresponds well with reported values [16]. ^{1}H NMR (500 MHz, $CDCl_3$): δ 4.710 (t sep., *J* = 2.8 Hz, J_{SiH} = 105 Hz, 8H), 0.24-0.22 (m, 48H). ^{13}C-NMR (75 MHz, $CDCl_3$): δ 0.042 (s). ^{29}Si-NMR (100 MHz, $CDCl_3$): δ -1.368 (dp, *J* = 7.2/209.9 Hz), -108.630 (d, *J* = 1.9 Hz). FT-IR (KBr): 2963, 2361, 2359, 837 (m), 2144, 1096, 901, 771, 552 cm-1 (s). HRMS (CI+, $[M-1]^+$) calcd. for $C_{16}H_{55}O_{20}Si_{16}$: 1014.9595, found = 1014.9595.

Preparation of Q_8^{OH} (POSS silanol). Palladium on carbon (0.04 g) was weighed into a 250 mL single necked round-bottom flask equipped with a magnetic stir bar. Distilled water (2.0 mL, 0.111 mol) was added along with THF (30 mL) to the reaction flask. An addition funnel was fitted on the reaction flask containing a solution of $Q_8M_8^H$ (2.0 g, 1.96 mmol) dissolved in THF (70 mL). $Q_8M_8^H$ which was slowly added drop wise over several hours while the temperature was kept at 0 °C. The resulting mixture was then stirred for 8 hrs at room temperature. The product was kept in the THF mixture and used directly in subsequent reactions.

Preparation of Q_8^{OSiH} (POSS) [11]. A mixture of heptane (160 mL), DMF (320 mL), and dimethylchlorosilane (50 mL, 47.2 g, 0.50 mol) was stirred at 0 °C for 15 minutes in a 1 L round-bottom flask equipped with a magnetic stir bar. The freshly made POSS silanol (~2 g, 2 mmol) in THF was poured into an addition funnel that was fitted on the reaction flask. Nitrogen was flushed through the system for a few minutes before the silanol was slowly added drop wise into the reaction flask at a rate of ~1 drop/s. After all the silanol was added the reaction mixture was stirred for an additional 15-20 minutes before quenching the reaction by drop wise addition of chilled distilled water (~350 mL). The reaction flask was kept in an ice bath during the entire addition of silanol and water. The organic layer was separated out and washed with distilled water (3x500 mL) until the organic layer was neutralized. The solvent was removed under reduced pressure over several hours to give a gelatinous colorless product in 1.98 g, 62% yield. ^{1}H NMR (400 MHz, $CDCl_3$): δ 4.710 (sep., *J* = 2.7 HZ, J_{SiH} = 102.6 Hz, 8H), 0.199 (d, *J* = 2.7 Hz, 48H), 0.123 (s, 48H). ^{13}C-NMR (100 MHz, $CDCl_3$): δ 0.618, 0.313. ^{29}Si-NMR (75 MHz, $CDCl_3$): δ -4.09 (d sep., *J* = 7.2/205.3 Hz), -16.97 (dp, *J* = 1.4/7.4 Hz), -110.00 - -110.14 (m). FT-IR (neat): 3054, 2964, 2130 (m), 3446 (br), 1265, 1114, 1060, 913, 847, 746 cm-1 (s). HRMS (CI+, $[M-1]^+$) calcd. for $C_{32}H_{103}O_{28}Si_{24}$: 1607.1099, found = 1607.1091.

Preparation of 2-(2-bromophenyl)ethanol. A 250 mL three necked round bottomed flask was equipped with a magnetic stir bar, rubber septa, and an addition funnel with a rubber septum. The setup was flame dried under vacuum. 2-Bromophenylacetic acid (4.039 g, 18.8 mmol, 1 eq.) was dissolved in freshly distilled THF (60 mL) and the solution was transferred to the reaction flask via canula. Borane in THF (24 mL, 1.0 M, 24 mmol) was added to the addition funnel via canula and slowly added dropwise into the reaction flask. After addition of BH_3·THF, the solution was stirred at room temperature for 1 h and then heated at 100 °C for 2 h. After this time, the solution was cooled to room temperature, and a mixture of THF and water (20 mL) was added slowly. Potassium carbonate was then added (a full spatula tip, along with diethyl ether (60 mL). The organic layer was separated from the mixture, and washed with water (60 mL), aqueous $NaHCO_3$ (60 mL), and brine (60 mL) before it was dried over magnesium sulfate, filtered, and concentrated to give the crude product. Residue was purified by distillation and the product 2.34 g, 62% was collected at 115 °C and 10 Torr as a colorless oil. Spectral data corresponds well with reported values [29]. ^{1}H NMR (400 MHz, DMSO-*d6*): δ 7.549 (d, *J* = 8.0 Hz, 1H), 7.346-7.267 (m, 2H), 7.147-7.109 (t, *J* = 7.5, 1H), 4.760-4.734 (t, *J* = 5.3 Hz, 1H), 3.618-3.569 (dd, *J* = 6.9/5.7 Hz, 2H), 2.869-2.833 (t, *J* = 7.1 Hz, 2H). ^{13}C NMR(100 MHz, DMSO-*d6*): δ 138.366, 132.362, 131.462, 128.180, 127.615, 123.932, 60.333, 39.068. FT-IR (neat): 3341 (br), 3057, 1567, 1337 (w), 2959, 2880, 659 (m), 1471, 1440, 1041, 750 cm^{-1} (s). HRMS (CI+, $[M-1]^+$) calcd. for C_8H_8OBr: 198.9759, found = 198.9761.

Preparation of 2-(2-bromophenyl)ethyl 4-methylbenzenesulfonate. 2-Bromophenethyl alcohol (1.852 g, 9.2 mmol, 1.0 eq.) was dissolved in freshly distilled pyridine (25 mL) in a 200 mL three-necked round-bottom flask equipped with a rubber septa and a magnetic stir bar the. The reaction flask was flushed for several minutes with nitrogen while stirring in an ice bath. Recrystallized *p*-toluenesulfonyl chloride (3.520 g, 18.46 mmol, 2.0 eq.) was added in small amounts via spatula over 5 minutes and the mixture was stirred at 0 ºC for several hours. DCM (50 mL) was added and the organic layer was thoroughly washed with dilute HCl (aq.), water, saturated sodium carbonate, water and brine, dried over magnesium sulfate, filtered, and concentrated in vacuo. The product 3.26 g, 69% was isolated as a crystalline solid. Melting point = 41-43 °C (lit. 39-39.5 °C) and spectral data corresponds well with reported values [30]. ^{1}H NMR (400 MHz, $CDCl_3$): δ 7.669 (app. d, *J* = 8.4 Hz, 2H), 7.441 (dd, *J* = 0.9/7.9 Hz, 1H), 7.257 (app. d, *J* = 7.8 Hz, 2H), 7.157-7.241 (comp., 2H), 7.049-7.092 (m, 1H), 4.231 (t, *J* = 6.9 Hz, 2H), 3.071 (t, *J* = 6.9 Hz, 2H), 2.413 (s, 3H). ^{13}C NMR (100 MHz, $CDCl_3$): δ 144.595, 135.414, 132.780, 132.661, 131.426, 129.700, 128.613, 127.713, 127.505, 124.261, 68.645, 35.550, 21.533. FT-IR (neat): 3735, 3565, 2737, 2279 (w), 3669, 2586, 1805, 1732, 1650 (m), 3064, 2955, 2916, 2893, 2866, 1922, 1600, 1565 (s), 1491 cm^{-1} (br). HRMS (CI+, $[M+1]^+$) calcd. for $C_{15}H_{16}O_3SBr$: 355.0004, found = 354.9997.

Preparation of 1-bromo-2-(2-bromoethyl)benzene. 2-(2-Bromophenyl)ethyl 4-methylbenzenesulfonate (2.237 g, 6.3 mmol, 1.0 eq.) was added to a flame dried 50 mL single-necked round-bottom flask. Freshly distilled acetone (15 mL) and lithium bromide (1.106 g, 12.7 mmol, 2.0 eq.) was added to the reaction flask. The reaction was refluxed overnight. The resulting solid was removed via vacuum filtration and washed with acetone. The acetone was evaporated under reduced pressure and the resulting oil was dissolved in diethyl ether, washed with sodium carbonate. The aqueous layer was extracted once more with diethyl ether and the combined organic layers were washed with brine, dried over magnesium sulfate and rotary evaporated. The residue was purified by column chromatography with hexanes on silica gel to give the product 0.99 g, 60% as a slightly yellowish liquid. Spectral data corresponds well with reported values [31]. ^{1}H NMR (400 MHz, $CDCl_3$): δ 7.553 (s, *J* = 8.0 Hz, 1H), 7.255-7.279 (m, 2H), 7.109-7.161 (m, 1H), 3.575-3.613 (app. t, *J* = 7.6 Hz, 2H), 3.277-3.315 (t, *J* = 7.6 Hz, 2H). ^{13}C-NMR (100 MHz, $CDCl_3$): δ 138.348, 133.296, 131.450, 129.017, 127.849, 124.605, 39.845, 31.334. FT-IR (neat): 2858, 1950, 1918, 1798, 1693, 1158, 921, 852, 822 (w), 3010, 1592, 1182, 1138, 944, 867 (m), 3060, 2959, 1565, 1472, 1437, 1320, 1293, 1257, 1217, 1095, 1045, 1024, 751, 662, 644 cm^{-1} (s). HRMS (CI+, $[M+1]^+$) calcd. for $C_8H_9Br_2$: 262.9071, found = 262.9071.

Preparation of 4-bromo-benzocyclobutene [32, 33]. Benzocyclobutene (0.46 g, 4.4 mmol, 1.0 eq.), methanol (0.43 mL), and DCM (2.15 mL) were added to a 10 mL round bottom flask and immersed in an ice bath. Bromine (0.72 g, 4.5 mmol, 1.0 eq.) was slowly added dropwise by a syringe into the flask. The resulting mixture was stirred for 16 hrs. Aqueous sodium bisulfate solution was then added and the aqueous layer was extracted with diethyl ether twice. The combined organic layer was washed with brine, dried with magnesium sulfate, filtered and the solvent was removed under reduced pressure. The residue was purified by column chromatography with hexanes on silica gel. The product 0.47 g, 58 % was recovered as a clear liquid. ^{1}H NMR (400 MHz, $CDCl_3$): δ 7.353 (d, *J* = 7.6 Hz, 1H), 7.211 (s, 1H), 6.938 (d, *J* = 8 Hz, 1H), 3.190 (app. t, *J* = 4.4 Hz, 2H), 3.126 (app. t, *J* = 4.4 Hz). ^{13}C-NMR (100 MHz, $CDCl_3$): δ 147.214, 144.134, 129.826, 125.860, 124.283, 120.466, 29.442, 29.427, 29.166, 29.151. FT-IR (neat): 2969, 2825, 1740 (weak), 2932, 1579, 1303, 1249, 1201, 1136, 1094, 1038 (medium), 1455, 866, 813, 688 cm^{-1} (strong). HRMS (CI+, $[M+1]^+$) calcd. for C_8H_8Br: 182.9809, found = 182.9809.

Preparation of 4-allyl-benzocyclobutene. 4-bromo-benzocyclobutene (0.59 g, 3.2 mmol, 1.0 eq.) was added to a 50 mL three-necked round-bottom flask equipped with a magnetic stir bar and a reflux condenser. The setup was stirred under vacuum for approximately 60 minutes before vented with nitrogen gas. Freshly distilled THF was added by a canula. Magnesium (0.09 g, 3.6 mmol, 1.1 eq.) was added and the reaction was stirred for 30–60 min at room temperature. The reaction vessel was immersed in an ice bath at 0 °C and allyl bromide (0.79 g, 6.5 mmol, 2.0 eq.) was slowly added by syringe. The resulting mixture was removed from the ice bath and warmed to room temperature then heated to reflux for 60 minutes. The solvent was evaporated under reduced pressure and the remaining liquid was poured into cold DI water, extracted with diethyl ether, and the organic layer was washed with brine, dried over magnesium sulfate and concentrated on a rotary evaporator. The product was isolated by column chromatography with hexanes on silica gel as a clear liquid 0.15 g, 32%. ^1H NMR (400 MHz, $CDCl_3$): δ 6.993–7.240 (m, 2H), 6.936 (s, 1H), 5.938–6.039 (m, 1H), 5.050–5.129 (m, 2H), 3.387 (d, *J* = 6.8 Hz 2H), 3.171 (s, 4H). ^{13}C-NMR (100 MHz, $CDCl_3$): δ 145.897, 143.367, 138.620, 138.070, 127.043, 122.802, 122.408, 115.340, 40.863, 29.330, 29.189. FT-IR (neat): 3075, 3002, 1602, 1203 (weak), 2963, 2829, 802, 705 (medium), 2928, 1638, 1473, 1432, 993, 826 cm^{-1} (strong). HRMS (CI+, $[M+1]^+$) calcd. for $C_{11}H_{13}$: 145.1017, found = 145.1017.

Preparation of *p*-azidostyrene [25]. 4-vinylaniline (1.192g 0.010 mol, 1.0 eq.) and dioxane (10 mL) were added to a 250 mL single necked round-bottom flask. The mixture was cooled to 0 ºC before adding an aqueous HCl solution (2 M, 50 mL) while stirring. Sodium nitrite (0.691 g, 0.010 mol, 1.0 eq.) dissolved in water (10 mL) was then added and the resulting mixture was stirred for 30 min at 0 ºC. During this time the solution changed color to a dark yellow and an orange solid precipitated while gas evolved. Sodium azide (0.792, 0.012 mol, 1.2 eq.) dissolved in water (10 mL) was slowly added and more gas was produced. The reaction mixture was stirred at 0 ºC for 1hr and then slowly warmed to room temperature by removing the ice bath. Saturated $NaHCO_3$ (aq.) was added to pH 7. The organic phase was extracted with ethyl acetate (3x30 mL) and washed with water (3x30 mL) and brine (3x30 mL), dried over magnesium sulfate and concentrated on a rotary evaporator. Column chromatography with *n*-pentane on silica gel afforded the product as a slightly yellow liquid 0.494, 34% yield. ^{1}H NMR (300 MHz, $CDCl_3$): δ 7.154-7.188 (app. d, *J* = 8.8 HZ, 2H), 6.747-6.782 (app. d, *J* = 8.8 Hz, 2H), 6.461-6.532 (dd, *J* = 11.0/17.6 Hz, 1H), 5.506-5.552 (dd, *J* = 0.8/17.6 Hz, 1H), 5.053-5.082 (dd, *J* = 0.8/11.0 Hz, 1H). ^{13}C NMR (75.5 MHz, $CDCl_3$): δ 139.082, 135.629, 134.275, 127.348, 118.867, 113.227. FT-IR (neat): 3220, 3088, 3035, 3008, 2981, 2926, 1963, 1893, 1820 (w), 2418, 2257, 2043, 1629, 1571, 1407, 1206, 1182, 1129, 1117, 751 (m), 2101, 1603, 1505, 1295, 989, 907, 836 cm^{-1} (s). HRMS (CI+, $[M+1]^+$) calcd. for $C_8H_8N_3$: 146.0718, found = 146.0715.

Preparation of *p*-azidobenzyl alcohol [26, 34]. 4-aminobenzyl alcohol (1.23 g, 10 mmol, 1.0 eq.) was dissolved in 2 M aqueous HCl (30 mL) at 0 ºC in a 250 mL single-necked round-bottom flask equipped with a magnetic stir bar. Sodium nitrite (1.035 g, 15 mmol, 1.5 eq.) in water (10 mL) was slowly added and the reaction was stirred for 15 min at 0 ºC. Sodium azide (15 mmol) dissolved in water (10 mL) was carefully added at 0 ºC with gas evolution. The reaction mixture was stirred for 1h at room temperature. A brownish oil separated from the aqueous solution. Diethyl ether (50 mL) was added and the organic layer was dried over magnesium sulfate and concentrated on a rotary evaporator. Column chromatography with ether/*n*-pentane (30% → 90%) on silica gel afforded the product as a brownish oil 1.08 g, 65%. Spectroscopic data matched literature values. ^{1}H NMR (400 MHz, $CDCl_3$): δ 7.184-7.205 (d, *J* = 8.4 Hz, 2H), 6.885-6.906 (d, *J* = 8.4 Hz, 2H), 4.460 (s, 3H). ^{1}H NMR (300 MHz, DMSO-d_6): δ 7.340-7.369 (app. d, *J* = 8.7 Hz, 2H), 7.039-7.082 (dt, *J* = 2.1/8.7 Hz, 2H), 5.208-5.246 (t, *J* = 5.74 Hz, 1H), 4.476-4.495 (d, *J* = 5.7 Hz, 2H). ^{13}C-NMR (100 MHz, $CDCl_3$): δ 138.561, 137.147, 127.944, 118.465, 63.481. FT-IR (in $CDCl_3$): 3343 (br), 3033, 1894, 1458, 1368, 1112, 938 (w), 2928, 2875, 2411, 2255, 1582, 1420, 1209, 1180, 774 (m), 2106, 1609, 1507, 1291, 1129, 1012, 815 cm^{-1} (s). HRMS (CI+, $[M+1]^+$) calcd. for $C_7H_8ON_3$: 150.0667, found = 150.0662.

Preparation of aB8x POSS (octa functionalized Q_8^H with allylbenzene). Q_8^H (2.014 g, 1.98 mmol, 1.0 eq.), allylbenzene (2.6 mL, 0.0196 mol, 9.9 eq.), and freshly distilled toluene (10 mL) were added to a 25 ml round bottom flask. Karstedt's catalyst (0.5 mL, 2mM solution in xylenes) was slowly added at 0 °C. The reaction mixture was stirred at room temperature for 6 hours before filtering through celite (2 mL) and a micro filter (0.45 μ). Solvent was removed under reduced pressure and the product was placed on high vacuum for ~24 hrs. The crude product was purified by column chromatography on silica gel. First 100% hexanes were used to collect 2 fractions then a second column was run with 50% ethyl acetate in hexanes as eluent. The product 3.082 g, 79% as thick yellow oil. ^{1}H NMR (400 MHz, $CDCl_3$): δ 7.132-7.224 (m, 16H), 7.037-7.089 (m, 24H), 2.497 (t, *J* = 7.6 Hz, 16H), 1.513-1.593 (m, 16H), 0.506-0.548 (m, 16H), -0.016-0.029 (m, 48H). ^{13}C-NMR (100 MHz, $CDCl_3$): δ 142.475, 128.457, 128.212, 125.593, 39.508, 24.985, 17.440, -0.327. ^{29}Si-NMR (100 MHz, $CDCl_3$): δ 12.632-12.914 (m), -108.768 (s). FT-IR (neat): 3731, 3646, 1739, 1681, 1654(w), 3110, 2792, 1937, 1864, 1797, 1580 (m), 3083, 3059, 3021, 2959, 2920, 2854, 1599, 1494, 1452, 1405, 1343, 1249, 1172, 1090, 838, 698 cm^{-1} (s). HRMS (CI+, $[M+1]^+$) calcd. for $C_{88}H_{137}O_{20}Si_{16}$: 1961.6012, found = 1961.6016

Preparation of B8x POSS (octa functionalized Q_8^{OSiH} with allylbenzocyclobutene). The same procedure for the preparation and isolation of aB8x was used here. Q_8^{OSiH} (0.563 g, 0.35 mmol, 1.0 eq.), freshly distilled toluene (5 mL) allylbenzocyclobutene (0.813 g, 5.6 mmol, 16 eq.), and Karstedt's catalyst (0.45 mL, 2 mM) were combined in a 25 mL round bottom flask as described above. After workup product was isolated as slightly yellowish liquid. TLC showed two spots that were easily separated using a short silica plug with hexanes and ethyl acetate. The product 0.777 g was obtained in 81% as a slightly yellowish oil. ^{1}H NMR (400 MHz, $CDCl_3$): δ 6.812-6.887 (dd, *J* = 15.3 Hz, *J* = 7.5 Hz, 16H), 6.759 (s, 8H), 3.006 (s, 32H), 2.463-2.501 (t, *J* = 7.6 Hz, 16H), 1.484-1.564 (m, 16H), 0.484-0.526 (m, 16H), 0.000-0.015 (2 overlapping signals, 96H). ^{13}C-NMR (75 MHz, $CDCl_3$): δ 145.525, 142.750, 141.292, 126.991, 122.616, 122.185, 40.357, 29.300, 29.137, 25.960, 17.991, 0.722, 0.186. ^{29}Si-NMR (100 MHz, $CDCl_3$): δ 8.921 (s), -18.318 (s), -109.748 (s). FT-IR (neat): 2858, 1475, 1410, 704 (w), 2960, 2926 (m), 1259, 1112, 1056, 846, 802 (s), 446 cm^{-1} (br). HRMS, MALDI calcd. for $C_{108}H_{194}O_{28}Si_{24}$ = 2760.8688 found = 2783.934).

Imprint Formulation BA5x3. Two to three drops of BA5x3 was added to an eppendorf tube. A very small amount (two to three millimeter in the tip of a Pasteur pipette) of Darocur® 1173 (2-hydroxy-2-methyl-1-phenyl-1-propanone) was added to the eppendorf tube. Aluminum foil was used to wrap the eppendorf tube to avoid light exposure and the mixture was shaken on a Maxi Mix II Type 37600 Mixer. A wafer cleaned with acetone and 2-propanol was coated with adhesion promoter AP410. Templates were soaked in a piranha bath, rinsed with water, quickly dipped in aqueous potassium hydroxide solution (25%), rinsed with water and placed under oxygen plasma for 15-20 min. A crystallization dish was prepared with a 1 wt.% solution of toluene and (tridecafluoro-1,1,2,2-tetrahydrooctyl)dimethylchlorosilane. The template was soaked in the solution for at least 24 hrs before imprints were carried out. Hand imprints were performed by placing a drop of the mixture on a wafer shard and slowly lowering the template into the liquid. Care was taken to make sure that no air was trapped between the wafer and the template. The liquid completely filled the surface under the template then the material was flood exposed through the quartz template. The template was removed from the substrate by carefully prying a razorblade between the two. Successfully transferred patterns were inspected by SEM.

Preparation of vinyl Q_8 [35]. A mixture of heptane (70 mL) and freshly distilled DMF (100 mL), and vinyldimethylchlorosilane (28 mL, 0.20 mol, 60 eq.) was added to a 500 mL single necked round bottomed flask and stirred at 0 °C. Tetramethylammonium silicate (3.85 g, 3.39 mmol, 1.0 eq.) was slowly added by a spatula over 10 minutes. The reaction was stirred for about 15 minutes before 1 L of chilled distilled water was slowly added. The organic layer was separated and washed with water until neutral pH was reached. The solvent was removed under reduced pressure on a rotary evaporator at 50 °C. The residue 1.911 g, 46% of white crystals was recrystallized by slow evaporation of hexanes. ^{1}H NMR (400 MHz, $CDCl_3$): δ 6.062-6.150 (dd, J = 20.1/14.9 Hz, 8H), 5.919-5.967 (app. dd, J = 3.9/14.9 Hz, 8H), 5.739-5.800 (app. dd, J = 3.9/20.2 Hz, 8H), 0.186 (s, 48H). ^{13}C-NMR (100 MHz, $CDCl_3$): δ 137.929, 132.467, -0.223. ^{29}Si-NMR (60 MHz, $CDCl_3$): δ 0.522, -109.116. FT-IR (neat): 3052, 3014, 2901, 734, 699, 517 (w), 2963, 1410, 1254, 1002, 955, 614 (m), 1091, 839, 784, 555 cm^{-1} (s). HRMS (CI+, $[M-CH_3]^+$) calcd. for $C_{31}H_{69}O_{20}Si_{16}$: 1209.0691, found = 1209.0702.

Preparation of PS_2V "vinyl cage"[35]. A mixture of heptane (170 mL), DMF (350 mL), and vinyldimethylchlorosilane (20 mL, 0.15 mol) was stirred at 0 °C in a 1 L round-bottom flask equipped with a magnetic stir bar. The reaction flask was purged with nitrogen gas for approximately 5 minutes. Then Q_8^{OH} in THF was added dropwise at a rate of 1 drop/s. The reaction mixture was stirred for 3 hrs before dropwise addition of chilled distilled water (250 mL). The reaction was kept in an ice bath during the addition of both silanol and water. The organic layer was separated, and washed with distilled water (3x500 mL) until pH = 7. The solvent was removed under reduced pressure and pumped on for several hours to give a highly viscous colorless liquid in 3.886 g, 52% yield. ^{1}H NMR (400 MHz, $CDCl_3$): δ 6.07-5.97 (dd, *J* = 20.1/15.0 Hz, 8H), 5.86-5.80 (app. dd, *J* = 4.1/14.9 Hz, 8H), 5.67 - 5.59 (app. dd, *J* = 4.2/20.1 Hz, 8H), 0.156 (s), 0.100 (s). ^{13}C-NMR (75 MHz, $CDCl_3$): δ 139.0, 131.8, 0.7, 0.2. ^{29}Si-NMR (100 MHz, $CDCl_3$): δ -2.8- -3.29 (m), -17.69 - -18.20 (m), -110.07 - -110.20 (m). FT-IR (neat): 3013, 2904, 1051, 846, 801, 707 (m), 3052, 2963, 1406, 1259, 956 cm-1 (s). HRMS (CI+, $[M-CH_3]^+$) calcd. for $C_{47}H_{117}O_{28}Si_{24}$: 1801.2194, found = 1801.2192.

Preparation of benzyldimethyl(vinyl)silane [21]. Freshly grounded magnesium (0.250, 10.3 mmol, 1.3 eq.) and a small crystal of iodine were added along with distilled THF (30 mL) to a flame dried 100 mL single necked round-bottom flask. Benzylchloride (1.0 g, 7.9 mmol, 1.0 eq.) was slowly added via syringe to the flask. The reaction was gently heated and then stirred at RT for ~2-3 hrs. Vinyldimethylchlorosilane (1.91 g, 15.8 mmol, 2.0 eq.) was added slowly and the mixture was stirred overnight, carefully poured into chilled water (100 mL), and extracted with diethyl ether (2x30 mL). The combined organic layers were washed with water (2x30 mL) and brine (2x30 mL), dried over magnesium sulfate, filtered, and concentrated to give 1.17 g, 83% of crude product as a colorless liquid. Spectral data corresponds well with reported values [21]. ^{1}H NMR (400

MHz, $CDCl_3$): δ 7.7.124-7.161 (m, 2H), 6.987-7.023 (m, 1H), 6.935-6.957 (m, 2H), 6.029-6.116 (dd, *J* = 20.2/14.7 Hz, 1H), 5.884-5.930 (dd, *J* = 3.9/14.7 Hz, 1H), 5.577-5.637 (dd, *J* = 3.9/20.2 Hz, 1H), 2.089 (s, 2H), 0.000 (s, 6H). ^{13}C-NMR (100 MHz, $CDCl_3$): δ 139.804, 138.129, 132.155, 128.204, 128.092, 124.000, 25.766, -3.735. ^{29}Si-NMR (60 MHz, $CDCl_3$): δ -6.280 (s). FT-IR (neat): 3082, 667 (w), 3049, 2892, 1452, 903 (m), 3026, 2957, 1601, 1493, 1405, 1248, 1207, 1156, 1057, 1008, 952, 832, 793, 760, 698 cm^{-1} (s). HRMS (CI+, $[M+1]^+$) calcd. for $C_{11}H_{17}Si$: 177.1100, found = 177.1102.

Preparation of benzyloxydimethyl(vinyl)silane. A 100 mL single necked round-bottom flask was flame dried under vacuum. To the reaction vessel was added dimethylaminopyridine (DMAP, 0.04 g, 0.33 mmol, 4 mol%), freshly distilled benzyl alcohol (0.9 mL, 8.7 mmol, 1.0 eq.), vinyldimethylchlorosilane (3.0 mL, 22 mmol, 2.6 eq.), freshly distilled DCM (30 mL), and pyridine (30 mL). The resulting mixture was stirred for 14 hrs. The solid was filtered and washed with DCM. The organic layer was washed with saturated aqueous cupric sulfate solution several times to remove pyridine, then washed with water (50 mL), and brine (50 mL) before it was dried over magnesium sulfate, filtered, and concentrated to leave 1.018 g, 61% of a colorless liquid. ^{1}H NMR (400 MHz, $CDCl_3$): δ 7.361 (d, *J* = 4.5 Hz, 4H), 7.256-7.310 (m, 1H), 6.157-6.244 (dd, *J* = 20.0/14.9 Hz, 1H), 6.064-6.101 (dd, *J* = 4.3/14.9 Hz, 1H), 5.828-5.889 (dd, *J* = 4.1/20.0 Hz, 1H), 4.741 (s, 2H), 0.266 (s, 6H). ^{13}C-NMR (100 MHz, $CDCl_3$): δ 140.778, 137.177, 133.397, 128.212, 127.058, 126.508, 64.783, -2.083. ^{29}Si-NMR (60 MHz, $CDCl_3$): δ 7.539. FT-IR (neat): 3087, 2730 (w), 3049, 3025, 2862, 2357, 2338, 1495, 1452, 1406, 1375, 1208, 1029, 1006, 955 (m), 2959, 1254, 1095, 1068, 839, 784, 726, 695 cm^{-1} (s). HRMS (CI+, $[M+1]^+$) calcd. for $C_{11}H_{17}OSi$: 193.1049, found = 193.1047.

Preparation of Azidobenzene [22]. A stock solution of 2M aqueous HCl (100 mL, 0.2 mol, 2.8 eq.) was added to a 250 mL single necked round-bottom and cooled to 0

°C. Aniline (6.6 mL, 0.073 mol, 1.0 eq.) was added to HCl solution. Sodium nitrite (10.5g, 0.15 mol, 2.1 eq.) was dissolved in a small quantity of water before added very slowly it to the mixture at 0 °C. The reaction was stirred at 0 °C for 45 minutes then sodium azide (14.1 g, 0.217 mol, 3.0 eq.) dissolved in a small amount of water was added very carefully as gas evolved. The reaction was slowly poured into saturated sodium carbonate (~200 mL) then extracted with pentane. The organic layer was washed with water (150 mL), brine (150 mL) before it was dried over magnesium sulfate, filtered, and concentrated to give the crude product. The residue was purified by column chromatography with ethyl acetate and hexanes on silica gel to give 4.9 g, 57% of a deep reddish brown liquid. Spectral data corresponds well with reported values [22]. ^{1}H NMR (400 MHz, $CDCl_3$): δ 7.340-7.392 (m, 2H), 7.133-7.187(m, 1H), 7.030-7.063 (m, 2H). ^{13}C-NMR (100 MHz, $CDCl_3$): δ 139.929, 129.673, 124.784, 118.944. FT-IR (neat): 1938 (w), 3245, 3064, 3036, 2418, 2257, 1129, 1076 (m), 2128, 1594, 1492, 1296 cm^{-1} (s).

Preparation of Benzylazide [23]. Benzylbromide (10 mL, 84 mmol, 1.0 eq.), DMSO (150 mL), and sodium azide (18.1 g, 0.278 mol, 3.3 eq.) were added to a 250 mL single necked round-bottom flask. The reaction was heated to 50 °C for 12 hrs. The reaction mixture was cooled and poured into water (300 mL). Product was extracted with ether (3x50 mL) and washed with water (100 mL), and brine (100 mL) before it was dried over magnesium sulfate, filtered, and concentrated to give the product. The product 4.632 g, 41% as a yellow liquid. Spectral data corresponds well with reported values [23]. ^{1}H NMR (400 MHz, $CDCl_3$): δ 7.335-7.452 (m, 5H), 4.346 (s, 2H). ^{13}C-NMR (100 MHz, $CDCl_3$): δ 135.266, 128.702, 128.168, 128.091, 54.628. FT-IR (neat): 3066, 3032, 2932, 2877, 1496, 1455, 1349, 1202 (m), 2094 cm^{-1} (s).

Preparation of Bis(azidomethyl)-1,1,3,3-tetramethyldisiloxane (Bisazide). Bis(chloromethyl)-1,1,3,3-tetramethyldisiloxane (2.78 g, 0.012 mol, 1.0 eq.) was added to 250 mL single necked round bottomed flask was equipped with a magnetic stir bar and a septum. Dimethylsulfoxide (DMSO, 80 mL) was added along with sodium azide (11.72 g, 0.180 mol, 15.0 eq.). The resulting mixture was heated at 50 °C and stirred for 14 hrs. Water (100 mL) was used to dissolve the solid and diethyl ether (3x50 mL) was used for extraction. The ether layer was washed with water (50 mL) and brine (50 mL) before it was dried over magnesium sulfate, filtered, and concentrated to leave 2.92 g, 99% of a colorless liquid. ^{1}H NMR (400 MHz, $CDCl_3$): δ 2.702 (s, 4H), 0.161 (s, 12H). ^{13}C-NMR (100 MHz, $CDCl_3$): δ 41.964, -0.885. ^{29}Si-NMR (60 MHz, $CDCl_3$): δ 5.012. FT-IR (neat): 2961, 2888, 2187, 1411, 1291, 840 (m), 2094, 1258, 1067 cm^{-1} (s). HRMS (ESI, $[M]^+$) calcd. for $C_6H_{16}N_60Si_2Na^{+1}$: 267.0816, found = 267.0819.

General Procedure for UV Exposure of Model Compounds for Vinyl and Azide Cross-Linking. The vinyl compound was weighed into an aluminum wrapped 6 mL vial. The vial was then tared again and the azide was weighed into the vial with the molar ratio of 1:1 (olefin:azide). The mixture was shaken rigorously for 1-2 minutes and examined for evidence of phase separation. Exposures and reactions were carried out in deuterated acetonitrile and monitored by NMR or neat between NaCl IR plates. The appearance of methylene groups and the disappearance of vinylic and thiol protons in NMR spectrum indicate that a reaction took place.

Imprint Formulation with Vinyl POSS and Bisazide. The same procedure described for the imprinting of BA5x3 was utilized here. A 1:1 molar ratio of azide to vinyl was initially used. Wafer and template were treated the same way as described for BA5x3. The exposure was carried out for 10 min. Imprints were only inspected by the naked eye.

Preparation of 1,3-Bis(mercaptomethyl)-1,1,3,3-tetramethyldisiloxane. Thiourea (3.64 g, 47.7 mmol, 4.0 eq.) was weighed into a 100 mL round bottom flask.

Ethanol (48 mL) and bis(chloromethyl)-1,1,3,3-tetramethyldisiloxane (2.72 g, 11.8 mmol, 1.0 eq.) were added. A condenser was attached and mixture was refluxed for 48 hrs. The ethanol was evaporated on a rotary evaporator and the resulting white solid was dissolved in water (24 mL) and stirred for one hour before 40 % aqueous sodium hydroxide (48 mL) was added. The resulting mixture was stirred for less than 30 seconds then extracted with diethyl ether (2x30 mL). The aqueous layer was acidified with 1.0 M HCl (aq.) and diethyl ether was once again used for extraction (1x40 mL). The combined organic layers were washed with water and brine (50 mL each time). Dried over magnesium sulfate and evaporated to produce 1.353 g, 51% of a colorless liquid. ^{1}H NMR (400 MHz, $CDCl_3$): δ 1.591-1.621 (dd, *J* = 1.2/7.2 Hz, 4H), 1.113-1.152 (dt, *J* = 1.2/7.2 Hz, 2H), 0.138 (d, *J* = 1.2 Hz, 12H). ^{13}C NMR(60 MHz, $CDCl_3$): δ 8.899, -0.796. ^{29}Si-NMR (100 MHz, $CDCl_3$): δ 5.289 (s). FT-IR (neat): 2955, 2897, 1390, 1157, 687 (m), 1258, 1068, 843, 800 (s), 2551, 1573 cm^{-1} (w). HRMS (CI+, $[M+1]^+$) calcd. for $C_6H_{19}OSi_2S_2$: 227.0416, found = 227.0418.

Synthesis of *S,S'*((1,1,3,3-tetramethyldisiloxane-1,3-diyl)bis(methylene))-diethanethioate. A 250 mL round bottom flask was charged with 1,3-bis(chloromethyl)-1,1,3,3-tetrametyldisiloxane (0.63 g, 2.7 mmol, 1.0 eq.), potassium thioacetate (0.71 g, 6.2 mmol, 2.3 eq.), and 100 ml dry THF. The reaction was heated to reflux and stirred overnight, cooled to room temperature and the resulting solid was filtered out. The organic layer was washed water, brine then dried over magnesium sulfate, and rotary evaporated to leave 0.81 g, 96% of a brownish liquid. ^{1}H NMR (400 MHz, $CDCl_3$): δ 0.076 (d., *J* = 1.2 Hz, 12H), 2.028 (d., *J* = 1.2 Hz, 4H), 2.266 (d., *J* = 1.4 Hz, 6H). ^{13}C-NMR (100 MHz, $CDCl_3$): δ -0.1, 14.9, 30.0, 196.2. ^{29}Si-NMR (60 MHz, $CDCl_3$): δ 4.854. FT-IR (neat): 2959, 2900 (weak), 1354, 1138, 954, 695 (medium), 1688, 1254, 1054, 838 cm^{-1} (strong). HRMS (CI+, [M+Na]$^+$ calcd. = 333.0440, found = 333.0441). $C_{10}H_{22}NaO_3S_2Si_2$

Preparation of *S*-2-(trimethylsilyl)ethyl ethanethioate [36]. Trimethylvinylsilane (1.13 g, 11.3 mmol, 1 eq.) and thioacetic acid (0.84 mL, 12 mmol, 1.1 eq.) were added to a 25 mL quartz test tube. The reaction vessel was flushed with nitrogen gas for approximately one minute while the mixture was gently swirled. The reaction vessel was placed in the Rayonet UV exposure box and exposed for approximately 12 hrs, removed from the UV reactor and added to water (20 mL), extracted with diethyl ether (2x20 mL), and the combined organic layer was washed with aqueous $NaHCO_3$ (2x20 mL), water (2x20 mL), and brine (60 mL) before it was dried over magnesium sulfate, filtered, and concentrated in vacuo. The residue was purified by column chromatography with ethyl acetate and hexanes on silica gel to give the product 0.964 g, 49% as a colorless liquid. It is worth noting that spectral data indicates an approximate 10% β-addition. ^{1}H NMR (400 MHz, $CDCl_3$): δ 2.797–2.841 (m, 2H), 2.222 (s, 3H), 0.763–0.807 (m, 2H), -0.031 (s, 9H). ^{13}C-NMR (100 MHz, $CDCl_3$): δ 196.290, 30.550, 25.342, 17.262, -1.889. FT-IR (neat): 2953, 2926, 2897 (weak), 1412, 1353, 1012, 953, 750 (medium), 1687, 1248, 1134, 837 cm^{-1} (strong).

Preparation of 2-(trimethylsilyl)ethanethiol [36]. Trimethylvinylsilane (6.20 g, 35.1 mmol, 1.0 eq.) and potassium hydroxide (100 mL, 10 wt.% in ethanol) were added to a 250 mL round bottom flask. The solution was then refluxed for two hours, cooled to room temperature and neutralized with acetic acid. Pentene (3x50 mL) was added, and the organic portion was washed with water and then with brine, dried over magnesium sulfate and the solvent was removed under reduced pressure. The residue was purified by distillation at 55 °C and 25 mmHg (lit. 52-54 °C [37]). The product 2.99 g, 63% was collected as a colorless liquid. ^{1}H NMR (400 MHz, $CDCl_3$): δ 2.528–2.589 (m, 2H), 1.457 (t, *J* = 6.7 Hz, 1H), 0.889–0.933 (m, 2H), -0.024 (s, 9H). ^{13}C-NMR (100 MHz, $CDCl_3$): δ 23.065, 20.640, -1.815. FT-IR (neat): 2897, 2561, 1124 (weak), 2953, 1414, 1170, 1017 (medium), 1248, 835, 692 cm^{-1} (strong). HRMS (CI+, $[M-1]^+$) calcd. for $C_5H_{13}SiS$: 133.0507, found = 133.0504.

Preparation of *S',S'',S'''*-2,2,2-(methylsilanetriyl)tris(ethane-2,1-diyl)-triethane-thioate (Trithioestermethylsilane). The same procedure as that used in the preparation of *S*-2-(trimethylsilyl)ethyl ethanethioate was implemented here. Trivinylmethylsilane (11.3 g, 90.7 mmol, 1 eq.) and thioacetic acid (43 mL, 0.60 mmol, 6.7 eq.) were added to a 100 mL quartz test tube. Product was distilled using a Kugelrohr at 135 °C and less than 1 Torr as a slightly yellowish oil 25.67 g, 80.3%. ^{1}H NMR (400 MHz, $CDCl_3$): δ 2.846–2.890 (m, 6H), 2.274 (s, 9H), 0.923–0.967 (m, 6H), 0.098 (s, 3H). ^{13}C-NMR (100 MHz, $CDCl_3$): δ 195.955, 30.573, 24.777, 14.502, -5.595. ^{29}Si-NMR (60 MHz, $CDCl_3$): δ 2.636. FT-IR (neat): 2924, 1274, 1255, 1170 (weak), 1409, 1352, 1006, 875 (medium), 1682, 1132, 1103, 952 cm^{-1} (strong). HRMS (CI+, $[M-1]^+$ calcd. for $C_{13}H_{25}SiO_3S_3$ = 353.0732, found = 353.07296).

Preparation of 2,2,2-(methylsilanetriyl)triethanethiol. The same procedure used in preparation of 2-(trimethylsilyl)ethanethiol was implemented here. Trithioestermethyl silane (22.8 g, 64.8 mmol, 1.0 eq.) and alcoholic potassium hydroxide (300 mL 10 wt.%) were added to a 1 L round-bottom flask. Product was distilled at 104-118 °C at 3-5 Torr to provide 9.457 g, 64% of product as a slightly yellowish oil. ^{1}H NMR (400 MHz, $CDCl_3$): δ 2.512–2.572 (m, 6H), 1.502 (t, *J* = 6.8 Hz, 3H), 0.942–0.985 (m, 6H), 0.011 (s, 3H). ^{13}C-NMR (100 MHz, $CDCl_3$): δ 20.178, 19.873, -5.401. FT-IR (neat): 2950, 2552, 1127 (weak), 2926, 1413, 1173, 807 (medium), 1276, 1254, 1011, 908, 728 cm^{-1} (strong). HRMS (CI+, $[M-1]^+$ calcd. for $C_7H_{17}SiS_3$ = 225.0262, found = 225.0261).

Preparation of *S,S'*-((3-(((2-(acetylthio)ethyl)dimethylsilyl)oxy)-1,1,3,5,5-pentamethyltrisiloxane-1,5-diyl)bis(ethane-2,1-diyl))diethanethioate (Tris(thioester-dimethylsiloxy)methylsilane). The same procedure used in preparation of *S*-2-(trimethylsilyl)ethyl ethanethioate was implemented here. Tris(vinyldimethylsiloxy)methylsilane (10.4 g, 30.1 mmol 1.0 eq.) and thioacetic acid (15 mL, 0.21 mol, 7 eq.) were added to a 100 mL quartz test tube. Product 15.6 g, 90% was carried on without further purification to the next step. ^{1}H NMR (400 MHz, $CDCl_3$): δ 2.852–2.902 (m, 6H), 2.665 (s, 9H), 0.849–0.901 (m, 6H), 0.102 (s, 12H), 0.018(s, 3H). ^{13}C-NMR (100 MHz, $CDCl_3$): δ 196.037, 30.543, 24.524, 18.676, -0.014, -2.239. ^{29}Si-NMR (60 MHz, $CDCl_3$): δ 6.587, -64.024. FT-IR (neat): 2957, 2926, 1009, 755, 703 (weak), 1412, 1353, 1169, 1134, 1102, 953, 880 (medium), 1687, 1253, 1042, 835, 783 cm^{-1} (strong). HRMS (ESI+, $[M+Na]^+$ calcd. for $C_{19}H_{42}O_6NaSi_4S_3$ = 597.1118, found = 597.1111).

Preparation of 2,2'-(3-(((2-mercaptoethyl)dimethylsilyl)oxy)-1,1,3,5,5-pentamethyltrisiloxane-1,5-diyl)diethanethiol ,Tris(2-mercaptoethyldimethylsiloxy)-methylsilane). Lithium aluminum hydride (10.2 g, 0.27 mmol, 7.2 eq.) was added to a flame dried 1 L three-necked round-bottom flask equipped with a reflux condenser, a magnetic stir bar, and rubber septa. Dry diethyl ether (400 mL) was added to the flask and the suspension was heated to reflux for 1 hour, cooled and held at 0 °C while tristhioester (21.4 g, 37.2 mmol, 1.0 eq.) was added dropwise via a syringe. The mixture was then refluxed for 12 hours, cooled to room temperature and poured onto ice. The aqueous layer was acidified and extracted with diethyl ether. The diethyl ether layers were combined, washed with water and brine, dried over magnesium sulfate and the solvent was evaporated to give a clear liquid 4.947 g, 30%. ^{1}H NMR (400 MHz, $CDCl_3$): δ 2.552–2.626 (m, 6H), 1.501 (t, J = 7.2 Hz, 3H), 0.932–1.004 (m, 6H), 0.083 (s, 18H), -

0.021(s, 3H). ^{13}C-NMR (100 MHz, CDCl$_3$): δ 24.382, 19.784, 0.112, -2.187. ^{29}Si-NMR (60 MHz, CDCl$_3$): δ 6.050, -64.277. FT-IR (neat): 2930, 2562, 1440, 1395, 755, 700 (weak), 2958, 1172 (medium), 1252, 1044, 833, 785 cm^{-1} (strong). HRMS (CI+, [M-1]$^+$ calcd. for $C_{13}H_{37}O_3Si_4S_3$ = 449.0982, found = 449.0987).

Preparation of *S,S',S''*-((1,1,3,5,5-pentamethyltrisiloxane-1,3,5-triyl)tris(ethane-2,1-diyl))triethanethioate (trithioestertrisiloxane).

The same procedure used in the preparation of *S*-2-(trimethylsilyl)ethyl ethanethioate was implemented here. 1,3,5-trivinyl-1,1,3,5,5-pentamethyltrisiloxane (10.0 g, 36.7 mmol 1.0 eq.) and thioacetic acid (18 mL, 0.26 mmol, 7.0 eq.) were added to a 100 mL quartz test tube, irradiated and was carried on to the next step.

Preparation of 2,2',2''-(1,1,3,5,5-pentametyltrisiloxane-1,3,5-triyl)triethanethiol, (1,3,5-Tri(2-mercaptoethyl)-1,1,3,5,5-pentamethyltrisiloxane). The same procedure used in the preparation of tristhiol was implemented here. Lithium aluminum hydride (15.2 g, 0.40 mol, 5.7 eq.) was added to a flame dried 1 L three-necked round-bottom flask equipped with a reflux condenser, a magnetic stir bar, and rubber septa. Dry diethyl ether (400 mL) was added and the suspension was refluxed for 1 hour. The reaction vessel was cooled and held at 0 °C while *S,S',S''*-((1,1,3,5,5-pentamethyltrisiloxane-1,3,5-triyl)tris(ethane-2,1-diyl))triethanethioate (11.7 g, 23.3 mmol, 1.0 eq.) was added dropwise via a syringe. The product 2.824 g, 31% was isolated as a clear liquid. ^{1}H NMR (400 MHz, CDCl$_3$): δ 2.497–2.596 (m, 6H), 1.488 (m, 3H), 0.843–0.967 (m, 6H), 0.068 (d, *J* = 0.8 Hz, 12H), 0.007(s, 3H). ^{13}C-NMR (100 MHz, CDCl$_3$): δ 24.338, 23.698, 19.747, 19.509, 0.253, -0.126. ^{29}Si-NMR (60 MHz, CDCl$_3$): δ 6.174, -24.426. FT-IR (neat): 2562, 1435, 1278, 700 (weak), 2956, 1411, 1174, 834 (medium), 1255, 1043, 780 cm^{-1} (strong). HRMS (CI+, [M-1]$^+$ calcd. for $C_{11}H_{31}Si_3O_2S_3$ = 375.0794, found = 375.0795).

Preparation of 1,7-divinyl-3,5-bis(trimethylsiloxy)hexamethyltetrasiloxane, RD Si-6. Palladium on carbon (0.04 g), distilled water (0.4 mL, 0.02 mol, 3 eq.), and THF (75 mL) were added to a 250 mL single-necked round bottom flask. The resulting mixture was cooled to 0 °C. 1,3-Bis(trimethylsiloxy)-1,3-dimethyldisiloxane (2.0 g, 7.1 mmol, 1 eq.) dissolved in THF (25 mL) was then added by an addition funnel. The mixture was stirred for approximately 30 minutes at 0 °C then 3 hours at room temperature. To a clean and dry 500 ml single-necked round-bottom flask equipped with a magnetic stir bar, a nitrogen inlet needle and a rubber septum and flushed with nitrogen gas was added diethyl ether (200 mL) via syringe along with freshly distilled triethylamine (8.89 mL). Vinyldimethylchlorosilane (5.87 mL, 42.5 mmol, 6 eq.) was added via a graduated cylinder and a lot of white solid formed. The mixture was cooled in an ice bath and equipped with a 125 mL addition funnel previously flushed with nitrogen. The hydrolyzed silane (silanol) was filtered through celite and then added to an addition funnel. The reaction flask was stirred for 5 minutes at 0 ºC before addition of silanol was started. The rate of addition was set to roughly one drop per second. After addition was complete the reaction was kept in the ice bath for an additional 15 minutes then stirred over night at room temperature. 500 mL of cold distilled water was added via the addition funnel slowly into the reaction flask to quench excess chlorosilane. A separatory funnel was used to separate the organic layer from the aqueous layer and the organic layer was washed with approximately 750 mL of additional distilled water. The organic layer was dried over magnesium sulfate and rotary evaporated to leave a clear liquid of low viscosity. The product 1.57 g, 46% yield was isolated by distillation at 10 Torr and 135 °C. ^{1}H NMR (400 MHz, $CDCl_3$): δ 6.115 (dd, J = 14.8 Hz, 20 Hz, 2H), 5.912 (dd, J = 3,6 Hz, 15 Hz, 2H), 5.731 (dd, J = 4 Hz, 20.4 Hz, 2H), 0.150 (s, 12H), 0.083 (s, 18H), 0.018 (s, 6H). ^{13}C-NMR (100 MHz, $CDCl_3$): δ 139.156, 131.708, 1.674, 0.157, -2.217. ^{29}Si-NMR (60 MHz, $CDCl_3$): δ 7.756, -3.845, -65.814. FT-IR (neat): 1735, 1313 (weak), 1912, 956, 840, 787, 706 (medium), 3052, 2960, 2902, 1596, 1407, 1252, 1050 cm^{-1} (strong). HRMS (CI+, $[M-1]^+$ calcd. for $C_{15}H_{39}O_5Si_6$ = 467.1413, found = 467.1412).

Preparation of 1,7-divinyl-1,1,3,3,5,5,7,7-octamethyltetrasiloxane, RD Si-4(Vi,Vi). The procedure used to prepare RD Si-6 was implemented here. 1,1,3,3-Tetramethyldisiloxane (5.0 g, 37mmol, 1.0 eq.) was hydrolyzed with palladium on carbon (0.205 g), water (2.0 mL, 0.11 mol, 3.0 eq.) in THF (175 mL). The silanol was reacted with vinyldimethylchlorosilane (31 mL, 0.22 mol, 6.0 eq.) in triethylamine (46.7 mL, 9.0 eq.) and diethyl ether (400 mL). The product was purified by distillation at 106-107 °C and 10 Torr. Product 3.15 g, 25% as a clear liquid. ^{1}H NMR (400 MHz, $CDCl_3$): δ 6.113 (dd, *J* = 20.2/14.9 Hz, 2H), 5.918 (dd, *J* = 14.9/3.9 Hz, 2H), 5.720 (dd, *J* = 20.2/3.9 Hz, 2H), 0.142 (s, 6H), 0.041 (s, 6H). ^{13}C-NMR (100 MHz, $CDCl_3$): δ 139.342, 131.642, 1.169, 0.261. ^{29}Si-NMR (60 MHz, $CDCl_3$): δ -3.820 – -4.423 (m), -20.980 (p, *J* = 7.4 Hz). FT-IR (neat): 3053, 2904, 1699, 1596, 1008 (weak), 2962, 1407, 954, 836, 705 (medium), 1257, 1031, 790 cm^{-1} (strong). HRMS (ESI, $[M+Na]^+$ calcd. for $C_{12}H_{30}O_3NaSi_4$ = 357.1170, found = 357.1164).

General Procedure for UV Exposure of Model Compounds for Thiol-Ene formulations. A vinyl compound was weighed into an aluminum wrapped 6 mL vial. The vial was tared and the thiol containing molecule was weighed into the vial with the molar ratio of 1:1 (olefin:thiol). The mixture was shaken rigorously for 1-2 minutes. The mixture was examined for phase compatibility. The reaction was carried out in either an NMR tube in $CDCl_3$ (reaction monitored by NMR), or a small droplet was placed on a glass slide and exposed to broadband UV radiation.

Imprio 55. The normal inkjet and the viscous dispense mechanisms were temporarily out of order and the imprint formulations had to be dispensed manually through a micropipette. This lead to several issues as it is nearly impossible to manually dispense droplets on the order of nanoliters. Instead, fewer larger droplets were dispensed in a star pattern. To circumvent the Imprio 55's system manual imprinting had to be carried out with a combination of automatated and manual functions. A wafer substrate treated with AP410 adhesion promoter was manually loaded and automatically leveled. A surface treated (to facilitate separation from resist) template was loaded automatically and aligned and leveled. The manual imprint window was used to give full control of the process. All steps were carried out manually so a blank dispense was carried out before the wafer chuck was given coordinates to move the wafer to the front. The imprint resist was manually dispensed and the wafer chuck was moved back to its original coordinates to allow an imprint to be carried out. Successfully transferred patterns were inspected by SEM.

Preparation of Chloromethyl $Q_8^{OSiMeCl}$. The procedure used in the synthesis of vinyl Q_8^{OSiVi},was applied here. Heptane (70 mL), DMF (100 mL), and chloromethyldimethylchlorosilane (25 g, 0.18 mol, 53 eq.) was stirred at 0 °C in a 500 mL single-necked round-bottom flask. Tetramethylammonium silicate (3.71 g, 3.26 mmol, 1.0 eq.) was added slowly via spatula. A yield of 14 grams of material was isolated after workup. A few crystals were isolated from liquid after 6 hrs on high vacuum (<500 mTorr). The crystals were separated and distillation was carried out on the remaining liquid. Fractions 1 (38-44 °C) and 2 (44-45 °C) were collected at 1.8 Torr, oil bath at 60 °C. Fraction 3 (45 °C) was collected at 1.8 Torr and oil bath at 70 °C. The distillation flask went dry and a white solid was left behind. The product, a semi-crystalline solid, 1.205 g, 26% was isolated. Sublimation occurred between 237-338 °C (modulated method described above). ^{1}H NMR (300 MHz, CDCl$_3$): δ 2.773 (s, 16H), 0.274 (s, 48H). ^{13}C-NMR (75 MHz, CDCl$_3$): δ 29.884, -1.939. ^{29}Si-NMR (60 MHz, CDCl$_3$): δ 7.302, -109.407. FT-IR (KBr): 2930, 1397 (w), 2965, 1258, 803, 754, 676, 606 (m), 1090, 853, 555 cm^{-1} (s). HRMS (CI+, [M+1]$^+$) calcd. for $C_{24}H_{65}Cl_8O_{20}Si_{16}$: 1400.7886, found = 1400.7898.

Fractions 2-4 collected from distillation of above mentioned compound are pure bis(chloromethyl)tetramethyldisiloxane, which is a commercially available substance (all spectral data were compared to purchased substance from Gelest Inc.). ^{1}H NMR (300 MHz, CDCl$_3$): δ 2.695 (s, 4H), 0.179(s, 12H). ^{13}C-NMR (75 MHz, CDCl$_3$): δ 30.580, -1.490. ^{29}Si-NMR (60 MHz, CDCl$_3$): δ 3.512. FT-IR (neat): 469 (br), 651, 621, 601 (w), 2924, 745, 679 (m), 2963, 1394, 1258, 1180, 1075, 846, 819 cm^{-1} (s). HRMS (CI+, [M+1]$^+$) calcd. for $C_6H_{17}Cl_2OSi_2$: 231.0195, found = 231.0197.

Preparation of *p*-Tolyl Q_8^{Tolyl} (POSS). A mixture of dried heptane (100 mL) and chlorodimethyl(*p*-tolyl)silane (10.0 g, 54.1 mmol) was prepared in a 250 mL single necked round-bottomed flask equipped with a septum and a magnetic stir bar. The mixture was stirred for about 15 minutes at room temperature then cooled to 0° C before the tetramethylammonium silicate (2.04 g, 1.79 mmol) was added slowly to the mixture via a spatula. The reaction mixture was stirred for about 15 minutes with no visible change as the solid was stirring at the bottom of the flask. As the reaction was slowly brought to room temperature the mixture turned slightly cloudy. Upon addition of a few drops of triethylamine, a large quantity of white solid formed. The reaction was stirred for 12 hrs then the solid was removed by vacuum filtration. The organic layer was washed with distilled water and brine. The solvent was removed on a rotary evaporator at 50 °C to leave 7.063 g of a reddish liquid. Crystals were isolated from the liquid after a few hours on high vacuum (<500 mTorr). The white crystalline solid was purified by recrystallized from hexanes and an analytical sample 0.058 g was isolated. ^{1}H NMR (400 MHz, $CDCl_3$): δ 7.413 (d, 2H, *J* = 8 Hz), 7.049 (dd, 2H, *J* = 0.8 Hz, and *J* = 8 Hz), 2.274 (s, 3H), 0.287 (s, 6H). ^{13}C-NMR (100 MHz, $CDCl_3$): δ 139.112, 134.967, 133.040, 128.509, 21.451, 0.313. ^{29}Si-NMR (60 MHz, $CDCl_3$): δ 2.221, -108.4.

The reddish transparent liquid that was isolated in 7.063 g corresponds to 83% is bis(*p*-tolyl)tetramethyldisiloxane, a commercially available substance (all spectral data match previously published results). ^{1}H NMR (400 MHz, $CDCl_3$): δ 7.498 (d, 2H, *J* = 7.6 Hz), 7.220 (dd, 2H, *J* = 0.6, 8.0 Hz), 2.398 (s, 3H), 0.362 (s, 6H). ^{13}C-NMR (100 MHz, $CDCl_3$): δ 139.045, 136.321, 133.070, 128.494, 21.488, 0.953. ^{29}Si-NMR (60 MHz, $CDCl_3$): δ -1.356. FT-IR (neat): 3068, 2922 (weak), 2981, 1604, 1392, 1020 (medium), 1252, 1111, 1042, 831, 776 cm^{-1} (strong). HRMS (CI+, $[M]^+$) calcd. for $C_{18}H_{26}OSi_2$: 314.1522, found = 314.1520.

Chapter 4: Mechanical and Electrical Evaluation of Imprint Formulations

4.1 INTRODUCTION TO MODULUS

As mentioned earlier, an ILD must meet many industrial requirements. One of these requirements is a modulus greater than 4 GPa. One of the reasons for this modulus value can best be described by the illustration in Figure 4.1.

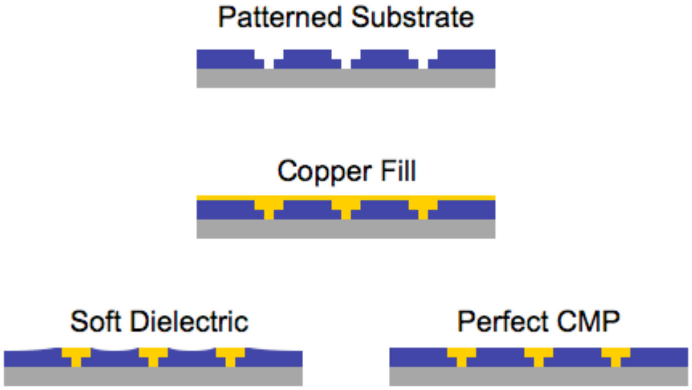

Figure 4.11: Illustration of the metallization process and CMP. As seen in the bottom left structure, dishing (an indentation of the dielectric surface) has occurred that will ultimately lead to a failed circuit.

Once the substrate has been patterned and is ready to undergo a metallization process, the entire surface is coated with metal and the pattern is overfilled. The excess metal is then removed by CMP, which physically etches away the top metal layer. CMP uses a slurry containing dispersed abrasive particles on the order of a few nanometers to several hundred nanometers in size and a polishing pad to remove the excess metal in a rotary grinding process. The mechanical polishing by itself leaves residue and a rough surface behind, therefore a chemical etch is carried out simultaneously. However, if the

ILD is of insufficient modulus, a defect known as dishing can result, as illustrated in Figure 4.1. Dishing can ultimately lead to complete device failure.

4.2 MODELS FOR NANOINDENTATION

The elasticity of a material can be determined from its tensile strength by measuring the sample elongation experimentally under an applied force. However, these bulk data cannot be transferred reliably to thin films, as thin films can exhibit unexpected property changes such as deviations from the bulk glass transition temperature [1]. The materials tested herein are functional ILDs, and it would be beneficial to measure their moduli as thin film samples. There are two common techniques for measuring the modulus of a material in thin film form. Surface acoustic wave spectroscopy, SAWS, can be used to measure the modulus and density of the sample. However, this method is highly sensitive to variations in film thickness and materials are preferably deposited via spincoating. Spincoating of imprint formulations with multiple components is not possible due to separation by centripetal forces and evaporation of higher vapor pressure components. Indentation is the second technique. Since the development of the nanoindentation tool, the technique has become the standard for such measurements. Nanoindentation measurements can be carried out using an atomic force microscope (AFM) [2, 3], a nanoindenter [4], or an interfacial force microscope (IFM) [5]. There are many different models for contact indentation; however, only the three most common will be discussed. The different models are based on the shape of the tip that makes the actual indentation. H. J. Hertz first proposed a model in 1882 describing a spherical tip indenting a surface as illustrated in Figure 4.2 [6]. The required force can be calculated from Equation 4.1, where R is the radius of curvature of the sphere and δ is the depth of the indentation.

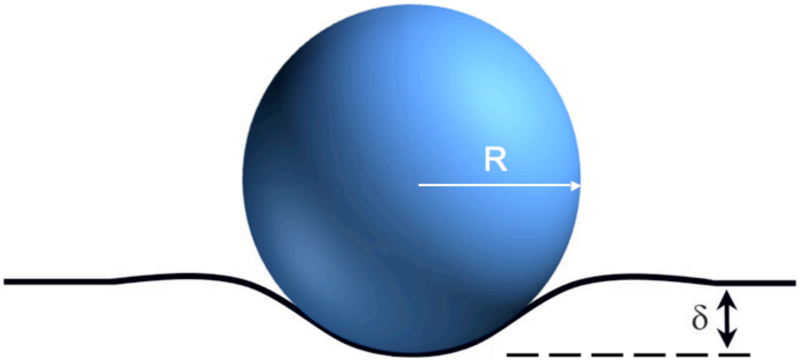

Figure 4.12: A sphere indenting a flat surface was initially studied by Hertz and is referred to as the Hertz model [7].

$$F = (K^2 R \delta^3)^{1/2} \qquad \text{Eq. 4.1}$$

The value of K can be expressed as Equation 4.2 where ν is the Poisson ratio and E is the modulus.

$$K = \frac{4}{3}\left(\frac{1-\nu_s^2}{E_s} + \frac{1-\nu_t^2}{E_t}\right)^{-1} \qquad \text{Eq. 4.2}$$

One can assume that the modulus of the sphere or tip (E_t) is significantly greater than that of the sample (E_s), and therefore the second term becomes zero [7]. This new K, $K = \frac{4}{3}\left(\frac{1-\nu_s^2}{E_s}\right)^{-1}$ expression can be inserted into Equation 4.3 to solve for the spherical indentation model.

$$F = \frac{4 E_s R^{1/2}}{3(1-\nu^2)} \delta^{3/2} \qquad \text{Eq. 4.3}$$

From Equation 4.3 the modulus can be obtained from the slope of the indentation (F vs. $\delta^{3/2}$), which is equivalent to $\frac{4E_s R^{\frac{1}{2}}}{3(1-\nu^2)}$.

Several decades later, I. N. Sneddon published a set of models that are able to describe an indentation carried out by tips of various shapes [8]. In addition to Hertz's spherical indentation model, two of the more commonly used shapes are cylindrical and conical. The two types of indentations are illustrated in Figures 4.3 and 4.4.

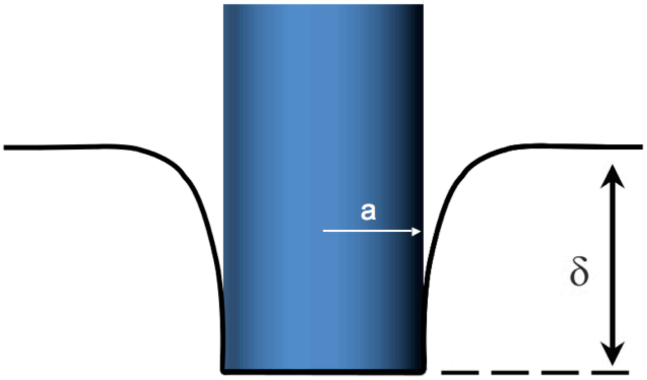

Figure 4.13: Sneddon's cylinder model depends on the radius of the cylinder and the depth of the indentation [7].

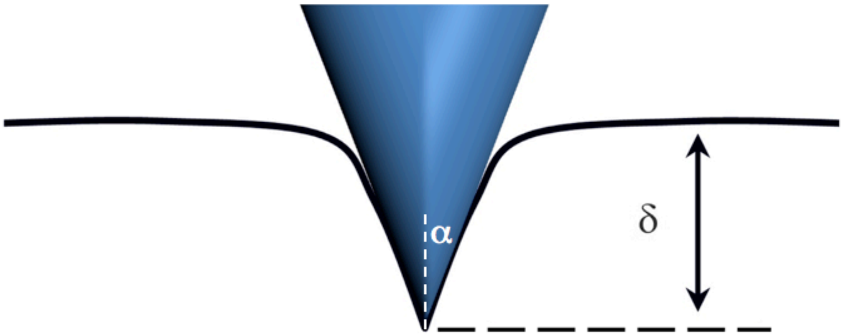

Figure 4.14: Sneddon's pyramidal model takes the angle of the tip and the indentation depth into consideration when calculating the modulus of a material [7].

For simplicity, the cylindrical tip will be referred to as a flat-bottom tip. The force of an indentation can be described by Equation 4.4 for the cylindrical model and Equation 4.5 for the pyramidal indentation [7].

$$F = \frac{4E_s a}{(1-\nu)}\delta \qquad \text{Eq. 4.4}$$

$$F = \frac{4E_s \cot(\alpha)}{\pi(1-\nu)}\delta^2 \qquad \text{Eq. 4.5}$$

The different geometries of the tips give different expressions for the indentation. For the flat-bottom indentation, the slope can be expressed as F vs. δ, or $\frac{4E_s a}{(1-\nu)}$, where *a* is the radius of the cylinder. For the pyramidal shaped tip, the slope is expressed as F vs. δ^2, or $\frac{4E_s \cot(\alpha)}{\pi(1-\nu)}$, where α is the approach angle of the pyramidal shaped tip.

When utilizing an AFM, the majority of tips are mounted on a flexible cantilever. This adds to the complexity of the measurements, as it has to be taken into consideration when calculating the modulus of a material. As described in Equation 4.2 above, it is assumed that the modulus of the tip is significantly greater than that of the film to be measured, and the contribution from the tip equals zero. However, when a tip is mounted on a cantilever, the deflection of the cantilever must be considered during indentation of the surface. This is illustrated in Figure 4.5 below.

Figure 4.15: Illustration of a cantilever flexing while the tip is indenting a sample.

Figure 4.6 illustrates a generic data plot for an indentation. The slope of the pressure vs. indentation depth plot corresponds to the flexing of the cantilever and the modulus or the total spring constant.

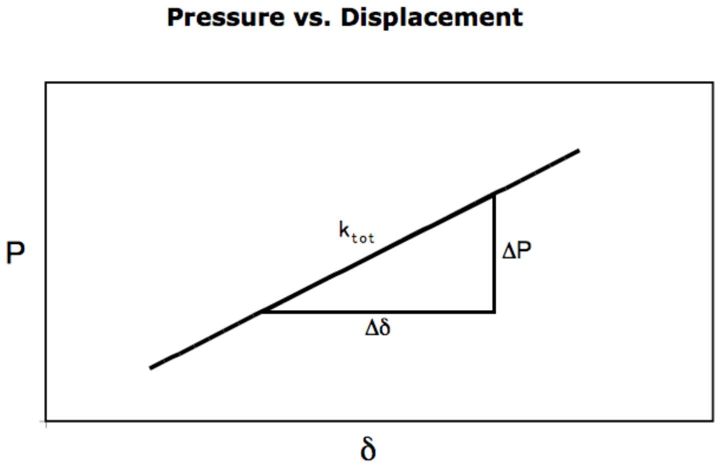

Figure 4.6: Generic pressure versus displacement slope from AFM indentation while in contact with the sample.

To extract the modulus of the material, one must first separate the deflection of the cantilever from the indentation into the sample. This can be accomplished by treating the problem as two springs in series using Hooke's law. As shown in Figure 4.7, the force required to stretch or compress the two springs involves the spring constant of the sample (k_s), the spring constant of the cantilever (k_c), and the distance that each is displaced.

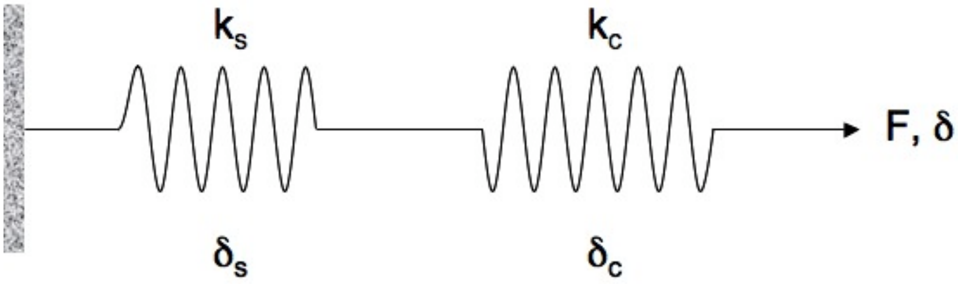

Figure 4.7: A two springs in series model illustrates the variables involved in determining the force and elongation / compression [9].

The total stretch or compression of the two springs is the sum of each spring's deformation as described in Equation 4.6.

$$\delta_{tot} = \delta_s + \delta_c \qquad \text{Eq. 4.6}$$

As the pressure is equal throughout the system, one can divide the displacement by pressure as shown in Equation 4.7.

$$\frac{\delta_{tot}}{P} = \frac{\delta_c}{P} + \frac{\delta_s}{P} \qquad \text{Eq. 4.7}$$

This expression is the inverse of the slope seen in Figure 4.6 above, and by using Hooke's law, it can be expanded further to Equation 4.8.

$$\frac{1}{k_{tot}} = \frac{\delta_{tot}}{P} \qquad \text{Eq. 4.8}$$

From this we see that each term in Equation 4.7 can be rewritten as Equation 4.9 and the spring constant of the cantilever can be calculated separately and subtracted from the data to obtain the modulus of the material.

$$\frac{1}{k_{tot}} = \frac{1}{k_s} + \frac{1}{k_c} \qquad \text{Eq. 4.9}$$

4.3 EXPERIMENTAL

4.3.1 Materials and Instrumentation

Materials were either synthesized and purified or purchased and used without further purification. Darocur® 1173 was obtained from Ciba Specialty Chemicals Inc. 1,3,5-trivinyl-1,3,5-trimethylcyclotrisiloxane and 1,3,5,7-tetravinyl-1,3,5,7-tetramethyl-cyclotetrasiloxane were purchased from Gelest Inc. Silicon wafers were purchased from Silicon Quest International, Inc. Two different models of AFM tips were obtained from Veeco, Inc. The first was a silicon probe (Model MPP-21120) with a reported spring constant of 3 N/m. The second was a silicon probe (Model TESPA) with a spring constant of 20 – 80 N/m. Both models have a backside coating of 50 ± 10 nm of aluminum. Two other models were obtained from Nano World. The first was model NVLR-SPL, Series-10, with a spring constant of 48 N/m. The second was a silicon probe model NCHR-50 with a spring constant of 42 N/m. Again, both of these models have their detector side coated with an aluminum layer. AFM experiments were carried out with assistance from Prof. Ed Yu’s research group in the department of Electrical and Computer Engineering at The University of Texas at Austin. Nanoindentation experiments were carried out at the Texas A&M University’s Materials Characterization Facility (TAMU MCF). SEM images were obtained on a Zeiss Supra 40 VP Scanning Electron Microscope. The Poisson’s ratios were unknown for the materials tested; therefore, the moduli are reported as reduced moduli.

4.3.2 Film Preparation

It was shown by Matthew Colburn that if the indentation reached a depth of ten percent of the film thickness or greater, the underlying substrate had a great impact on the modulus [7]. For this reason, films with thicknesses of several microns were prepared. Imprint resist formulations were drop casted onto clean ~0.5 square inch silicon wafer substrates for use in the AFM experiments (Table 4.1) and Nanoindenter experiments (Table 4.2). All values are reported as weight percent.

	% PS2V	% Bisthiol	% PI	% RD
AFM-F-1	84.4	10.7	4.9	0
AFM-F-2	72.6	11.3	5.0	11.1[a]
AFM-F-3	74.7	10.0	5.3	10.0[b]

Table 4.1: Formulations for AFM experiments. Reactive diluent [a] 1,3,5-trivinyl-1,3,5-trimethylcyclotrisiloxane and [b] 1,3,5,7-tetravinyl-1,3,5,7-tetramethylcyclotetrasiloxane.

	% PS2V	% Bisthiol	% PI	% RD
NI-F-1	84.4	10.7	4.9	0
NI-F-2	74.7	10.0	5.3	10.0

Table 4.2: Formulations for nanoindenter experiments. Reactive diluent is 1,3,5,7-tetravinyl-1,3,5,7-tetramethylcyclotetrasiloxane.

The liquid was allowed to spread unassisted, then it was cured with a JH Technologies Novacure® 2100 System with a high pressure, 100 W mercury vapor short arc lamp (exposure wavelength of ~250-500 nm). Film thicknesses were determined by scoring a film with a razor blade and then taking measurements with a stylus profilometer. A profilometry cut of this type on an imprint resist film is illustrated in Figure 4.8. On the left side at the bottom of the cut is the bare wafer and on the right is the polymer film. In this case the thickness is approximately 5.5 μm. All films were several micrometers thick, which is advantageous for indentation measurements as substrate interference can be avoided.

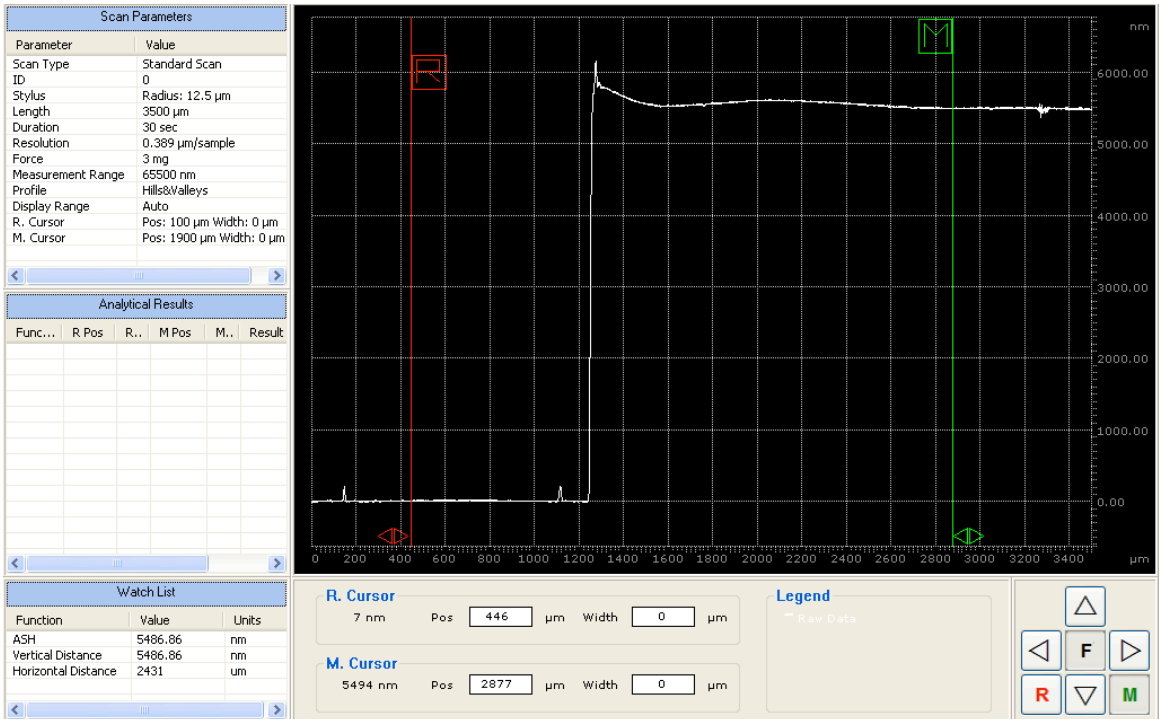

Scan Parameters

Parameter	Value
Scan Type	Standard Scan
ID	0
Stylus	Radius: 12.5 µm
Length	3500 µm
Duration	30 sec
Resolution	0.389 µm/sample
Force	3 mg
Measurement Range	65500 nm
Profile	Hills&Valleys
Display Range	Auto
R. Cursor	Pos: 100 µm Width: 0 µm
M. Cursor	Pos: 1900 µm Width: 0 µm

Analytical Results

Func...	R Pos	R..	M Pos	M..	Result

Watch List

Function	Value	Units
ASH	5486.86	nm
Vertical Distance	5486.86	nm
Horizontal Distance	2431	um

R. Cursor
7 nm Pos 446 µm Width 0 µm

M. Cursor
5494 nm Pos 2877 µm Width 0 µm

Figure 4.8: Stylus profilometer trace across a cut in the material shows the thickness of the polymer-coated film to be approximately 5.5 µm.

Half of the films were baked under vacuum at 200 °C for 30 minutes and cooled to room temperature overnight. The slow cooling process was used to circumvent formation of cracks. The other films were left untouched after exposure. A reference sample for AFM measurements was prepared by spin coating a solution of PMMA in PGMEA to a thickness of 360 nm as measured by ellipsometry.

4.3.3 Atomic Force Microscope

A Bruker Veeco Icon Dimension with Scan Asyst AFM was run in peak-force contact mode. The different probes that were used had varying spring constants and different radii of curvature but were all made from silicon. The tips were calibrated according to a slightly modified procedure from Veeco [10]. The deflection sensitivity was first determined using a clean wafer as an infinitely hard surface. A built-in thermal tuning function evaluates the spring constant of the tips as the reported values from tip manufacturers are approximations. This information was required to calculate the modulus of the materials being evaluated. It is also critical to know the complete geometry of the tips to obtain reproducible results. There are several methods for measuring the tip radius. A few instruments have a function called tip-evaluation software that can determine the geometry of the tip being used. Another, very simple method uses a reference sample with a known modulus. By using the latter method, a reference can be chosen to match the estimated modulus of the samples being evaluated. This allows one to test a tip at frequent intervals to verify its robustness to change. A 360 nm thick PMMA film was used as the reference material to extract the radius of each tip. The reference film was used at the very beginning and at the very end to verify that the shape of the tips had not changed during the measurements.

A typical data plot is illustrated in Figure 4.9 when the tip is retracted from the sample.

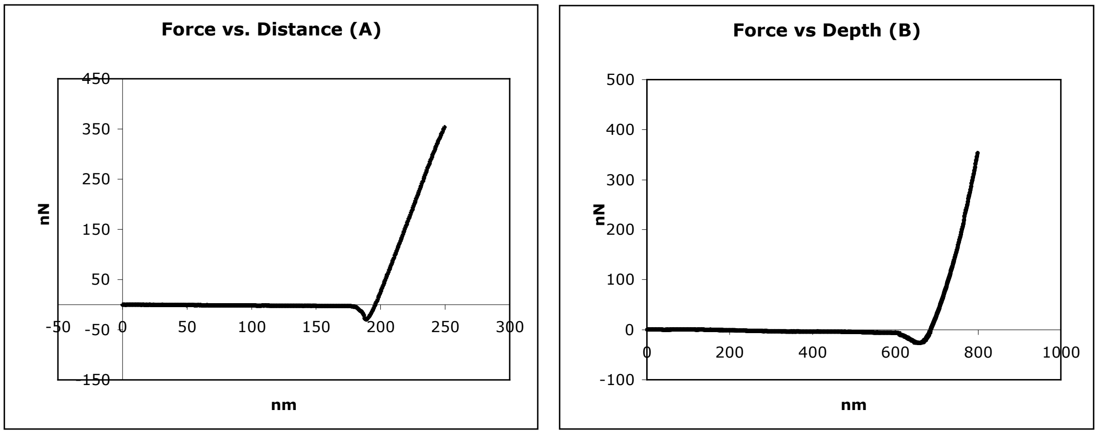

Figure 4.9: Tip retracting from, A) PMMA, and B) imprint formulation.

Since Figure 4.9 illustrates the retracting of a tip, the graph is analyzed from right to left. Initially the force decreases linearly as the indentation becomes smaller. Adhesive forces hold the tip to the material until it snaps away from the sample, as seen by the change in the slope. Once the tip is no longer in contact with the sample, the force remains constant. Looking at the indentation portion of the graph, the three different models can be applied and the fit for all three is excellent as illustrated in Figures 4.10, 4.11, and 4.12 with R^2 values all very close to 0.99.

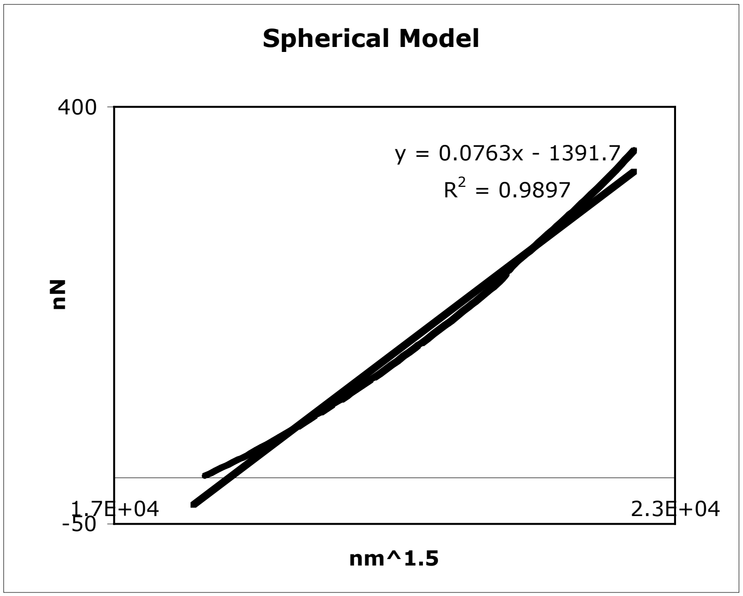

Figure 4.10: Hertz model describing a spherical tip retracting from a sample surface.

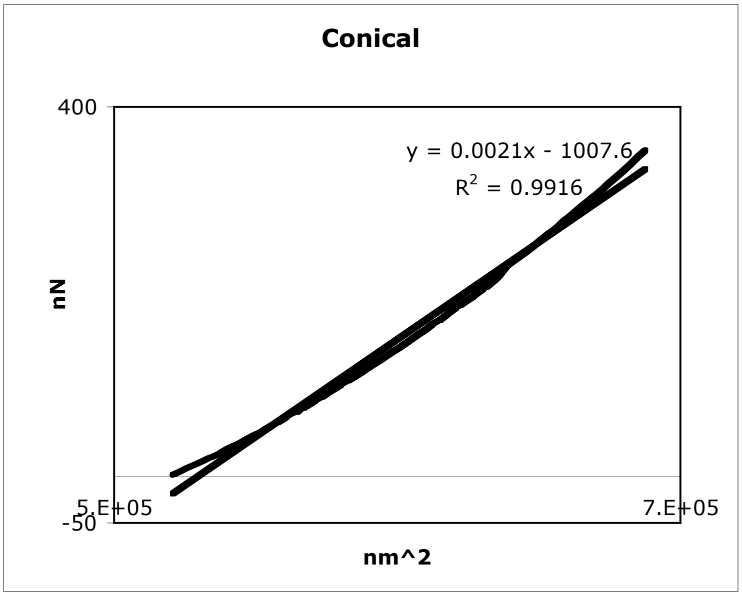

Figure 4.11: Sneddon's Conical Model.

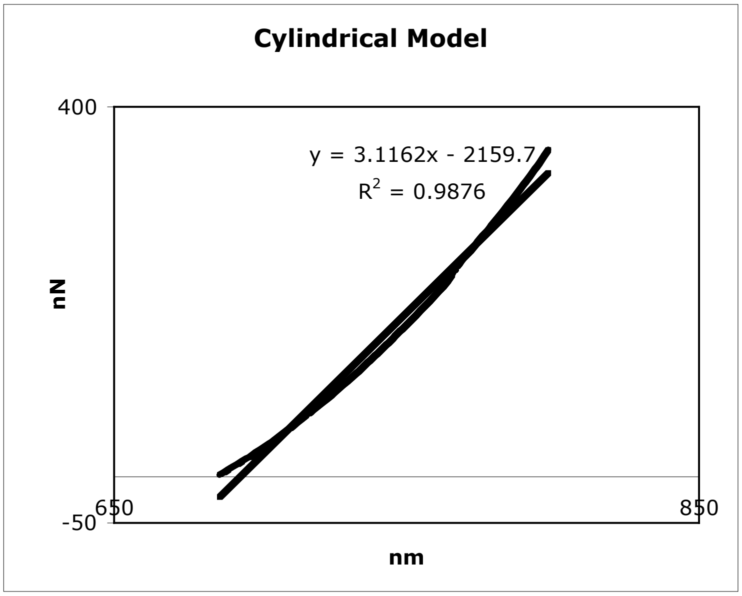

Figure 4.12: Sneddon's cylindrical indentation model.

From these models, the slope of the indentation can be calculated and used to determine the overall modulus of the material. Moduli values are reported in Table 4.3.

	% PS2V	% Bisthiol	% PI	% RD	Modulus
AFM-F-1	84.4	10.7	4.9	0	128 MPa
AFM-F-1-Baked					173 MPa
AFM-F-2	72.6	11.3	5.0	11.1[a]	67.3 MPa
AFM-F-2-Baked					142 MPa
AFM-F-3	74.7	10.0	5.3	10.0[b]	97.6 MPa
AFM-F-3-Baked					141 MPa

Table 4.3: Modulus results from AFM measurements. [a] The reactive diluent in this formulation is 1,3,5-trivinyl-1,3,5-trimethylcyclotrisiloxane. [b] The reactive diluent for this formulation is 1,3,5,7-tetravinyl-1,3,5,7-tetramethyl-cyclotetrasiloxane.

It was noted that the greater the spring constant of the tip, the more consistent the data. This is believed to be caused by a decreased deflection of the cantilever and therefore the indentation reading comes from indenting the surface. However, it was also observed that the modulus did change over the duration of the measurements by comparing the data collected from the PMMA standard. The tips were analyzed by scanning electron microscopy and it was clear that the tip geometries had changed drastically as shown in Figure 4.13.

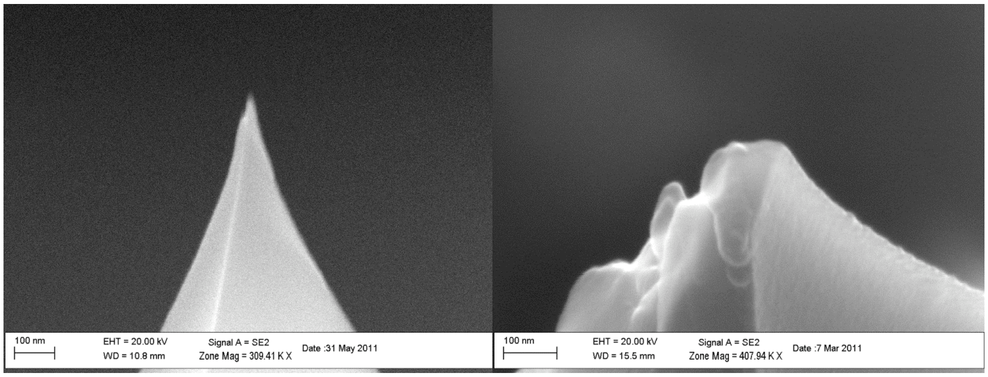

Figure 4.13: Images of AFM tip before and after indentation experiments clearly indicate that the tip geometry has changed during the measurements.

4.3.4 Nanoindenter

Due to the inconsistent data obtained from traditional AFM measurements another method for analysis was selected. A nanoindenter is very similar to an atomic force microscope. One of the major differences between the two instruments has to do with the tips used. On an AFM, the tip is mounted on the edge of a flexible cantilever while, on a nanoindenter, the tip is mounted on an inflexible indentation probe [11]. For these experiments, a Hysitron Triboindenter Nanoindenter (341-F) was run in indentation mode with a Berkovitch diamond tip with three sides each with an angle of 142.35° (curvature of radius ~150 nm). An aluminum sample was used to calibrate the microscope with the indentation stage so the area of indentation could be visually inspected for defects. Three indentations were carried out in a row then repeated parallel to the first indentations. The indentation stage was moved into the field of view of a camera for inspection and a seventh indentation was done in the center of the two parallel lines to generate an H pattern. This was carried out to calibrate the X and Y distances from the center of the stage. A thick polystyrene sample was used as a reference sample and an image of an indentation can be observed on a rough surface in Figure 4.14.

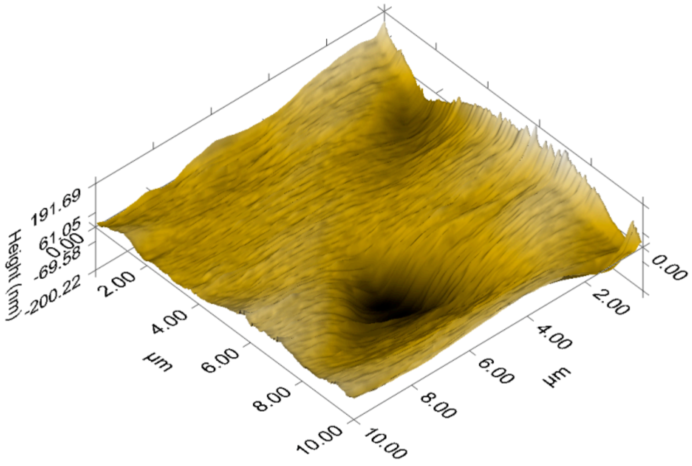

Figure 4.14: A topographic image of indentations in polystyrene.

The instrument was configured to stop a measurement if a depth of 5 μm was reached. To ensure that this depth was not reached, various peak forces were tested on the samples, and it was found that 1000 μN was the highest force that could be used. Each sample was indented nine times in various locations on the film to obtain a reliable value. A plot of force versus distance that is generated by such an indentation experiment is provided as Figure 4.15; all nine data points overlap nicely.

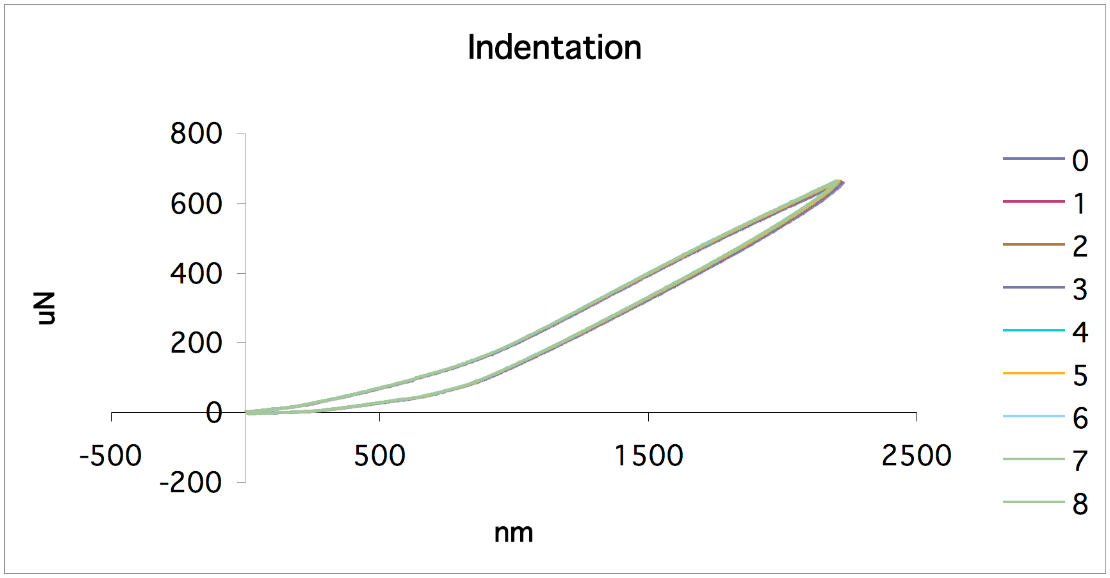

Figure 4.15: A typical result from an indentation experiments illustrates an elastic response.

Nanoindentation was used to measure the modulus of two different formulations shown in Table 4.4. Samples were prepared as described above, and half were baked at 200 ºC under vacuum for 30 minutes before being cooled back to room temperature.

	% PS2V	% Bisthiol	% PI	% RD*	Modulus
NI-F-1	84.4	10.7	4.9	0	22.0 ± 0.4 MPa
NI-F-1-Baked					69.3 ± 0.7 MPa
NI-F-2	74.7	10.0	5.3	10.0	13.9 ± 0.2 MPa
NI-F-2-Baked					28.4 ± 0.5 MPa

Table 4.4: Formulations used along with modulus values from nanoindentation experiments. *Reactive diluent used in the formulations is 1,3,5,7-tetravinyl-1,3,5,7-tetramethylcyclotetrasiloxane.

4.4 SUMMARY OF MODULUS EVALUATION

The choice of AFM tip is critical for indentation applications. It is important to recognize that if a low spring constant cantilever (AFM probe) is used on a hard surface, the deflection observed is mainly due to the flexing of the cantilever and not due to an indentation to the surface. Therefore, higher spring constant cantilevers are preferred for these measurements. However, even though sturdier cantilevers were used, consistent data was hard to obtain, and nanoindentation is much better if available.

As anticipated, from the modulus data obtained from both the AFM and the nanoindenter measurements, it is clear that the baked samples have increased hardness than the cured-only materials. However, the materials are far too soft for implementation as ILDs, so new formulations must be evaluated.

4.5 INTRODUCTION TO DIELECTRIC CONSTANTS

The dielectric constant, also known as the relative permittivity, is an important factor for manufacturing ILD materials, as it affects the electrical signal that is sent through the ICs. The dielectric material must prevent current leakage and limit cross-talk between wires [12]. Therefore, a lower dielectric constant can lead to smaller and faster devices because of better insulating capability and less charge buildup. The dielectric constant can be determined from capacitance measurements.

Capacitance is a measure of a material's ability to store charge. A capacitor is basically two electrodes separated by an insulating material. The capacitance is influenced by the area of the electrodes, the thickness of the material separating the electrode, and the dielectric constant of the insulator according to the Equation 4.10 below.

$$C = \varepsilon_r \varepsilon_0 \frac{S}{d} \qquad \text{Eq. 4.10}^{1}$$

ε_r is the dielectric constant, ε_0 is the electrical constant, also known as the permittivity of free space, (~8.854e^{-12} Fm^{-1}), S is the area of the electrodes, and d is the thickness of the insulating material separating the electrodes. This equation can be rearranged to solve for the dielectric constant of the insulating material.

4.6 EXPERIMENTAL

4.6.1 Instrumentation

Film thicknesses were measured on either a J.A. Woollam ellipsometer, or a Stylus Profilometer. The experimental setup was tested by purchasing four capacitors of known capacitance. Initially, a box consisting of four contact points for easy attachment of commercial capacitors and four input/output jacks for source measure unit (SMU) connectors were used to measure the capacitance. However, since thin films would be tested, the box was only used to verify the reported capacitance of the purchased capacitors. For the thin film capacitors, a Karl Suss probe station was used. The wafers were held with a vacuum chuck to facilitate the probes touching the top and bottom electrodes. The blunt end of the probes were used to make a connection to the electrodes as the sharp point can punch through the metal and cause an inaccurate reading of the capacitance.

---

[1] Traditionally the capacitance is calculated from $C = \varepsilon \frac{A}{d}$, where A is the area of the electrodes, d is the thickness of the insulating material separating the electrodes, and ε is the permittivity. The dielectric constant, ε_0, can be determined from $\varepsilon = \varepsilon_r \varepsilon_0$.

4.6.2 CV Analysis

The capacitance versus voltage measurements were carried out on a Keithley 4200 SCS equipped with a Keithley 590 CV Analyzer (experimental setup can be seen in APPENDIX B). The test equipment was connected to a Karl Suss Probe Station equipped with a wafer chuck to hold the wafers in place and to facilitate the connection between the substrate and the probes. Measurements were carried out between -5 and 5 V and a typical CV graph is shown in Figure 4.16 for a purchased capacitor.

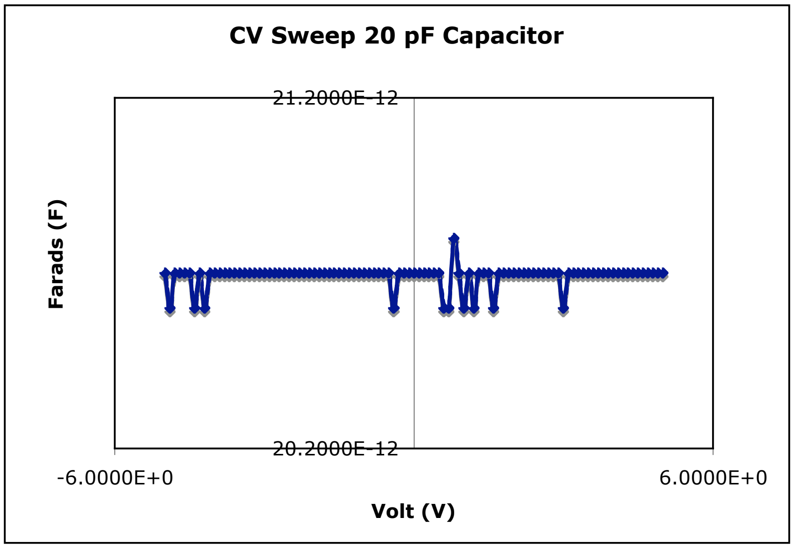

Figure 4.16: A CV graph illustrating the classical behavior of a capacitor with a reported value of 20 pF.

The measurement resulted in an average capacitance of 20.7 pF, comparable to the reported capacitance of 20 pF. Control measurements were carried out with additional 20 pF and 820 pF capacitors with an accuracy within +/- 5% of reported values.

4.6.3 Preparation of Parallel Plate Capacitors

Before imprint formulations were tested, MIM (metal insulator metal) capacitors were generated with aluminum / polystyrene / copper or copper / polystyrene / copper as shown in Figure 4.17.

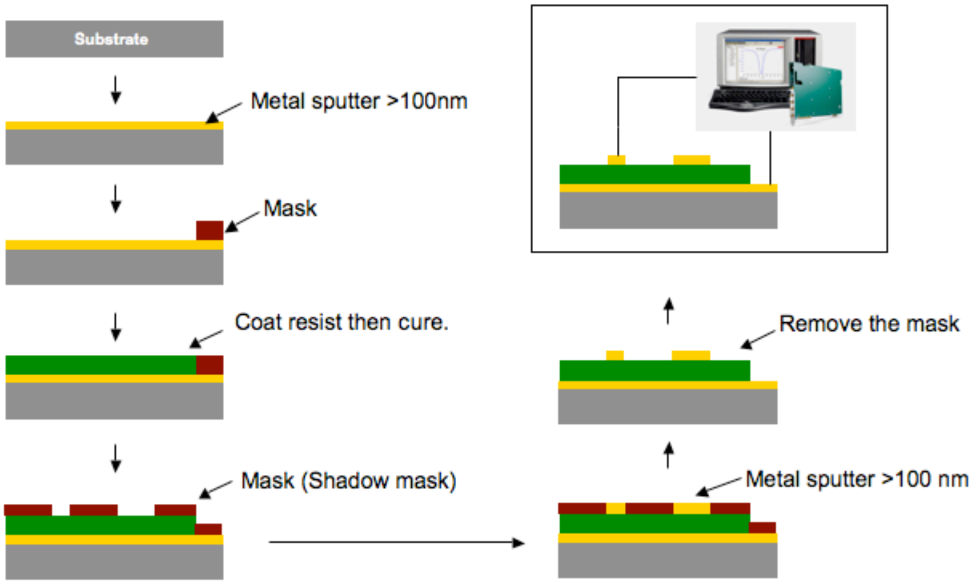

Figure 4.17: Process for making MIMs and measuring capacitance.

Bottom electrodes were either deposited by thermal evaporation or by e-beam sputtering to a thickness of approximately 100 nm on a silicon wafer. The thickness was verified by a microbalance during the deposition and by a stylus profilometer by scratching the film surface once the deposition was done. It is crucial for capacitance measurements to have a uniform and known thickness, and this was accomplished by spin coating the polymers. Spin coating imprint resists from solution could alter resist composition due to the differing evaporation rates of the components therefore spin coating cannot be used to produce films under these circumstances. Instead, imprints with a 25 mm x 25 mm blank mesa template were used. Polystyrene was spin coated at approximately 1400 rpm from a 7.0 wt.% solution in toluene to a thickness of 280 nm.

The thickness of the polymer film was measured by profilometry and ellipsometry after a 60 second bake at 110 °C to evaporate residual solvent. A 3 by 3 inch aluminum plate was used as a shadow mask with four holes of four different dimensions drilled through it as illustrated in Figure 4.18. Different diameters of holes were used to vary the area of the electrodes.

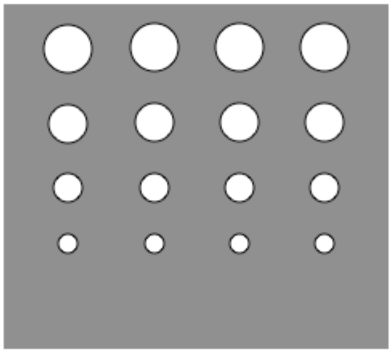

Figure 4.18: Aluminum shadow mask for deposition of top electrodes.

The top electrodes were deposited by sputtering copper to a thickness of approximately 100 nm. The top electrode was deposited thicker than 100 nm to give enough mechanical stability to avoid damage by the probes when capacitance measurements were carried out. The diameters of the top electrodes were confirmed by profilometry.

Figure 4.19 is a profilometry trace of a MIM on a wafer, where two of the top electrodes with different diameters are clearly observed. The jagged edges of the electrodes result from the metal deposition step.

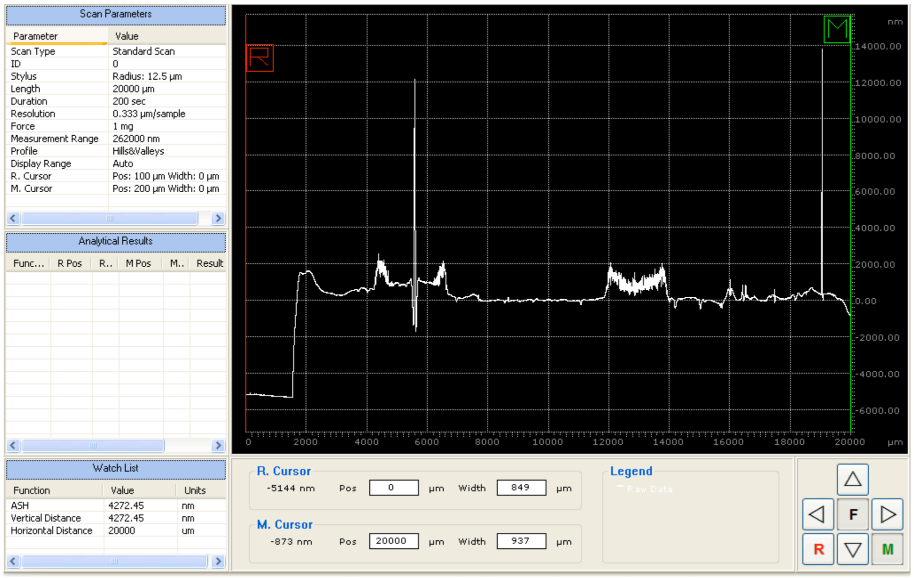

Scan Parameters

Parameter	Value
Scan Type	Standard Scan
ID	0
Stylus	Radius: 12.5 µm
Length	20000 µm
Duration	200 sec
Resolution	0.333 µm/sample
Force	1 mg
Measurement Range	262000 nm
Profile	Hills&Valleys
Display Range	Auto
R. Cursor	Pos: 100 µm Width: 0 µm
M. Cursor	Pos: 200 µm Width: 0 µm

Analytical Results

Func...	R Pos	R..	M Pos	M..	Result

Watch List

Function	Value	Units
ASH	4272.45	nm
Vertical Distance	4272.45	nm
Horizontal Distance	20000	um

R. Cursor
-5144 nm Pos 0 µm Width 849 µm

M. Cursor
-873 nm Pos 20000 µm Width 937 µm

Figure 4.19: A profilometry trace of a MIM profile with thick top electrodes clearly seen.

Imprint formulations, shown in Table 4.5, were dispensed onto metal-coated substrates and cured under a mesa-only template. Film thicknesses were measured by a stylus profilometer over several millimeters to verify film uniformity. A film thickness variation of around 10-15 % was observed over approximately 15 mm. Capacitances were measured before and after a bake. The dielectric constants reported in Table 4.5 were calculated from average capacitance measurements of different-sized electrodes.

	% PS2V	% Bisthiol	% PI	% RD*	Dielectric Constant
Polystyrene					2.10 ± 0.06
CV-F-1	84.4	10.7	4.9	0	2.92 ± 0.05
CV-F-1-Baked					3.00 ± 0.02
CV-F-2	74.7	10.0	5.3	10.0	2.94 ± 0.05
CV-F-2-Baked					2.98 ± 0.04

Table 4.5: Formulations with average dielectric values presented. Reactive diluent used in the formulations is 1,3,5,7-tetravinyl-1,3,5,7-tetramethylcyclotetrasiloxane.

4.7 SUMMARY OF DIELECTRIC CONSTANT EVALUATION

The reported capacitance values for purchased capacitors versus values obtained experimentally fall within approximately a 5 % range. The dielectric constant for the PMMA sample was on average ~8 % lower than the reported value of 2.3 [13]. This systematic offset error was consistent for repeat experiments with new samples. For the imprint resist formulations, there is no statistically significant difference in the dielectric constant between the two formulations whether they were exposed to a PEB or not. This indicates that there is no significant change in material composition while baking the samples. The errors reported with the dielectric values do not take into consideration any variation of film thickness or discrepancy in electrode area. The measured dielectric constants of the imprint materials are comparable to reported POSS based ILDs [14].

4.8 HOW TO GET AN ACCEPTABLE MATERIAL

Illustrated in this chapter are the modulus and dielectric values obtained from various imprint formulations. It is clear from modulus evaluation that the materials do not measure up to the ILD requirements set by the semiconductor industry. It has been shown that the higher the POSS content is, the lower the resulting modulus [15]. It is speculated that this is due to the lowering of the density of the cured material [15]. To achieve an acceptable material, the solution could be the addition of another cross-linking agent, thereby lowering the overall weight percentage of vinyl POSS. Previous studies have illustrated that a combination of methacrylates and a thermally curable group (BCB) resulted in a modulus much closer to 4 GPa [14, 15]. Since the dielectric constant of the materials tested are below the requirements, nothing has to be adjusted to lower these values. Since current ILD materials are silicon dioxide-doped with carbon or organic components, the addition of a cross-linkable functionality may actually lower the dielectric constant even further.

4.9 REFERENCES

[1] S. Napolitano, A. Pilleri, P. Rolla and M. Wubbenhorst. "Unusual Deviations from Bulk Behavior in Ultrathin Films of Poly(tert-butylstyrene): Can Dead Layers Induce a Reduction of Tg?" *ACS Nano,* 4, 841-848, 2010.

[2] J. Domke and M. Radmacher. "Measuring the Elastic Properties of Thin Polymer Films with the Atomic Force Microscope". *Langmuir,* 14, 3320-3325, 1998.

[3] A. C.-M. Yang. "Young's moduli of materials in polymer deformation zones by an AFM deflection technique". *Materials Chemistry and Physics,* 41, 295-298, 1995.

[4] D. J. Shuman, A. L. M. Costa and M. S. Andrade. "Calculating the elastic modulus from nanoindentation and microindentation reload curves". *Materials Characterization,* 58, 380-389, 2007.

[5] M. Wang, K. M. Liechti, J. M. White and R. M. Winter. "Nanoindentation of polymeric thin films with an interfacial force microscope". *Journal of the Mechanics and Physics of Solids,* 52, 2329-2354, 2004.

[6] H. J. Hertz. "Ueber die Berührung fester elastischer Körper". *Journal Fur Die Reine Und Angewandte Mathematik,* 156-171, 1882.

[7] M. E. Colburn. "Step and Flash Imprint Lithography: A Low-Pressure, Room-Temperature Nanoimprint Lithography". *Ph.D. University of Texas at Austin,* 2001.

[8] I. N. Sneddon. "The relation between load and penetration in the axisymmetric boussinesq problem for a punch of arbitrary profile". *International Journal of Engineering Science,* 3, 47-57, 1965.

[9] K. M. Liechti. Personal Communication. 2011.

[10] G. M. Schmid. Personal Communication. 2011.

[11] A. Henkes-Young. Personal Communication. 2011.

[12] S. Franssila. "Introduction to Microfabrication"; 2nd Ed.; John Wiley & Sons, Ltd.; Chichester, West Sussex, 2010.

[13] G. Odian. "Principles of Polymerization"; 4 Ed.; John Wiley & Sons, Ltd.; Chichester, 2004.

[14] F. L. Palmieri. "Step and Flash Imprint Lithography: Materials and Applications for The Manufacture of Advanced Integrated Circuits". *Ph.D. University of Texas at Austin,* 2008**.**

[15] H. Lin, X. Wan, X. Jiang, Q. Wang and J. Yin. "A Nanoimprint Lithography Hybrid Photoresist Based on the Thiol-Ene System". *Advanced Functional Materials,* 21, 2011.

Chapter 5: Planarizing Materials for SFIL-R

5.1 INTRODUCTION TO SFIL-R AND THE NEED FOR PLANARIZING MATERIALS

UV nanoimprint lithography has made many advances in the past decade. One of these advances is the development of reverse-tone SFIL (SFIL-R) technology. Figure 5.1 illustrates how SFIL-R differs from traditional SFIL.

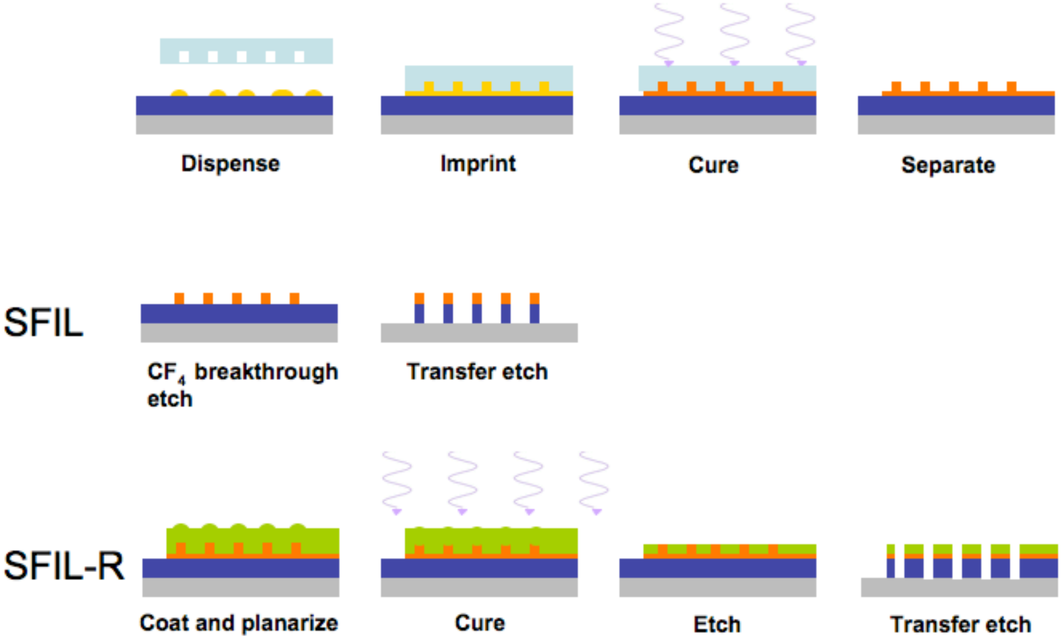

Figure 5.1: Schematic flow of SFIL and SFIL-R.

It was first developed and demonstrated by Molecular Imprints, Inc. in 2005 as a simplification and improvement of certain processing steps related to traditional SFIL [1]. Such improvements include more accurate template alignment, lower susceptibility to forming defects by allowing imprinting of lower-aspect ratio features with thicker residual layers, and the potential for higher throughput as lower-aspect ratio patterns require less fill time due to the smaller quantity of liquid that needs to be redistributed to form the uniform residual layer [2]. Instead of a silicon-containing imprint resist, SFIL-R uses an organic resist as a medium for printing the template pattern features. Organic resist formulations are more versatile than traditional SFIL resists because there are more component options to tailor the vapor pressure and viscosity of the formulations as a whole, and templates used with these resists are generally easier to clean. This resist option, however, requires a planarizing top layer to be deposited by some deposition technique such as spincoating, CVD, CMP, etc. This topcoat functions as a hard etch mask and must have high silicon content to achieve the etch selectivity desired [1].

Once the liquid planarizing topcoat has been deposited, it is then cured to solidify it into a thin film. An etch step is then carried out to remove excess topcoat and expose the features in the imprint resist layer. It is important to note that this etch step does not affect the features that were originally imprinted and full control of the feature sizes is maintained. After the imprinted features have been exposed, an anisotropic oxygen reactive ion etch (RIE) is performed. This allows for high-selectivity etching of the organic imprint resist material. Accordingly, high aspect ratio features can be achieved if thick organic resist films are used or additional layers were previously deposited before imprinting. SFIL-R reverses the imprinted pattern and produces an exact copy of the template.

There are many requirements for planarizing materials that are often conflicting. These requirements include: high silicon content for etch selectivity, photolytically or thermally curable functional groups for polymerization, low volatility to limit evaporation during coating, and low viscosity for fast flowing and planarization [3].

5.2 PLANARIZING TECHNIQUES

There are basically four different methods by which planar surfaces can be obtained. The main concern for these methods is their cost due to the additional processing required, their low throughput, and the fact that they require additional expensive equipment.

5.2.1 Chemical Mechanical Polishing

One such technique is chemical mechanical polishing (CMP), a method frequently used in the manufacturing of microelectronics, especially for planarizing various metal and oxide layers. As the name implies, the technology uses a chemical solution in combination with a rotating polishing pad to obtain planar surfaces [4]. Significant advances in the development of advanced abrasive slurries and polishing pads has been achieved, but this has led to a significant increase in cost of ownership (CoO) for the process.

5.2.2 Polymer Melt

Another method for obtaining planar surfaces is the deposition of a polymer or pre-polymer that is then heated to a temperature above its T_g [5]. The polymer can then flow freely and self-planarize driven by capillary, surface tension, and gravitational forces. Once a critical degree of planarization (DOP) is obtained, the temperature is allowed to return to room temperature and the polymer hardens again. This technology presents itself as a cheap alternative to CMP. The planarizing forces are small and they diminish asymptotically as the film approaches planarity. There are other factors that must be met as well, including the matching of the coefficients of thermal expansion (CTE) for the different films in order to avoid stresses from building up within the film stack leading to the generation of cracks.

5.2.3 Imprinting of an Optical Flat

A third method comprises imprinting an optical flat on top of a pre-patterned substrate. An optical flat template can be pressed onto a curable liquid or pre-polymer that is heated above its T_g. Brewer Science has commercialized this technology and demonstrated its use on pre-patterned features [6]. The most viable option is to use a polymerizable liquid in order to avoid heating and cooling cycles, but this requires additional templates and imprint tools which further increase the processing costs. These three methods are illustrated in Figure 5.2 below.

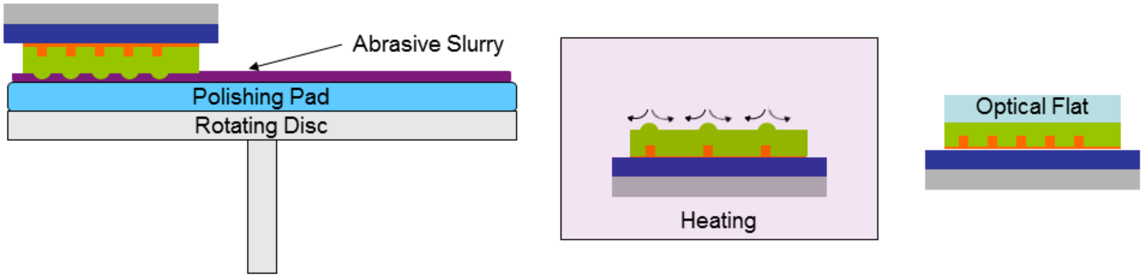

Figure 5.2: Illustration of the three methods for obtaining planar surfaces. From left to right, using CMP to polish the surface, heating a pre-polymer to decrease viscosity and allowing for the material to self-planarize, and imprinting an optical flat [5].

5.2.4 Curable Planarizing Liquids

The last method is a technique in which a non-volatile pre-polymer is spincoated over a patterned surface. This method has several advantages over the three previous techniques as it allows for the use of low-cost equipment and requires no additional instrumentation with the exception of a spincoater. Spincoating to obtain planar surfaces has been studied in great detail; simulations and experimental data have been previously published by Lin, *et al*. [2, 5, 7].

The importance of using non-volatile polymerizable liquids becomes clear when the process is studied in greater detail. To achieve successful reverse-tone imprinting, it is important that the planarizing material reaches a certain degree of planarization over the patterned substrate (Figure 5.3) [7]. It has been shown that spincoating a material over a pre-patterned surface causes the material to essentially conform to the pattern [5]. If the material being spincoated does not freely flow after spinning has stopped, the rate of planarization is simply too slow to be used as a manufacturing operation.

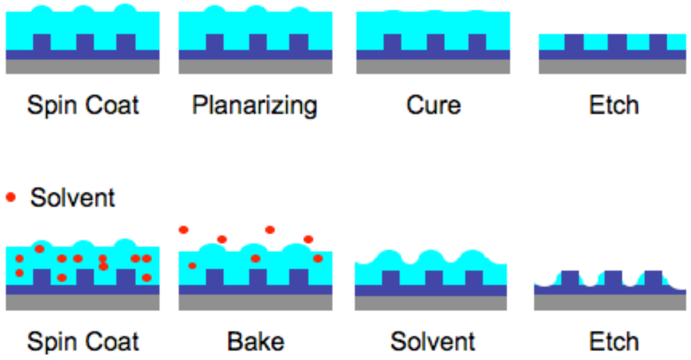

Figure 5.3: Importance of forming a planar layer for successful etch pattern transfer [5].

If a non-volatile, polymerizable, low-viscosity liquid is used, then it can planarize more quickly after the target thickness has been reached by spincoating. The polymerizable material never reaches perfect planarization, but a critical degree of planarization can be defined which allows for successful etch and pattern transfer processes. The material can then be cured thermally or photolytically. However, if a polymer is dissolved in a solvent and then spincoated, the solvent evaporates as the film becomes thinner, which causes an increase in viscosity and slower redistribution of the material across the wafer. Eventually, all the solvent evaporates and the polymer forms a conformal layer on top of the pre-patterned substrate [5]. SEM images of a poorly planarized polymer layer over a patterned substrate are shown in Figure 5.4.

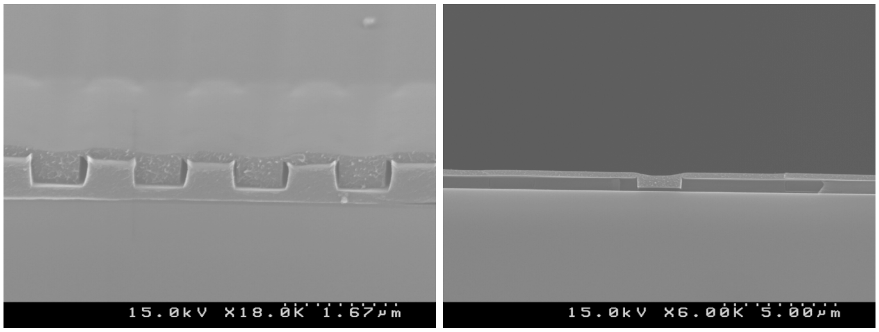

Figure 5.4: An uneven surface obtained by spincoating a solution with a volatile solvent over a patterned substrate is clearly visible over lines and trenches as well as isolated trenches. This would ultimately lead to defects after the etch process is completed.

5.3 MATERIALS

As mentioned previously, a planarizing liquid must meet several requirements to be implemented into the SFIL-R process. In certain cases these characteristics conflict, which adds to the challenges of synthesizing a suitable material. Several siloxane-based materials have been investigated as photocurable, planarizing liquids since they meet the aforementioned requirements [8]. Branched materials were chosen in order to produce lower viscosities while maintaining a low vapor pressure. The first material, named Si-14 (1H,23H-11,13-bis(trimethylsiloxy)docosamethyldodecasiloxane, shown in Figure 5.5), was synthesized, and its planarizing properties were evaluated in detail [5, 8, 9].

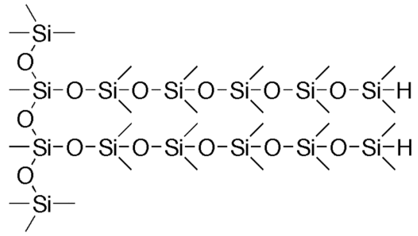

Figure 5.5: Structure of Si-14 (so-named because of its 14 silicon atoms).

Si-14 was functionalized with methacrylate groups to render it polymerizable. Methacrylate groups were chosen due to their synthetic accessibility and the large amount of literature on their use in semiconductor applications. Hyperbranched polymers represent another area that has potential as a planarizing material. Both epoxide and thiol-ene functional groups were considered and evaluated as polymerizable moieties. Synthesis of asymmetrically and symmetrically substituted monomers of thiol-ene type AB_2, A_2B_2, and AB_3 or epoxide type A_2, A_3, and A_4 was attempted for evaluation as planarizing materials.

5.4 EXPERIMENTAL

5.4.1 Instrumentation

The materials were characterized as described in the synthesis section and evaluated using a variety of techniques. Film thicknesses were determined using a J. A. Woollam ellipsometer. Viscosities were determined using a Physica MCR 500 Rheometer. SEM images were taken on a Zeiss Neon 40 installed at The University of Texas Micro Electronics Research Facility (MER). Imprints were performed on an Imprio 100® (Molecular Imprints, Inc.) and etching was carried out using an Oxford Plasmalab 80 Plus; both also installed at MER. Vapor pressures were determined by initially exposing the samples to a series of freeze-pump-thaw cycles before allowing the material to reach equilibrium at room temperature while pressure in the container was measured. A Varian Diffusion Pump set-up was built with a MKS HPS® 943 Vacuum Gauge Controller and a 423 I-Mag Vacuum Sensor.

5.4.2 Si-14

The first material investigated for this role was Si-14. The synthesis involved two steps that were repeated multiple times to produce the desired product. The commercially available 3H,5H-octamethyltetrasiloxane was hydrolyzed to a silanol and then reacted with chlorodimethylsilane (Scheme 5.1) to extend the siloxane backbone by two units to form Si-6 (H,H).

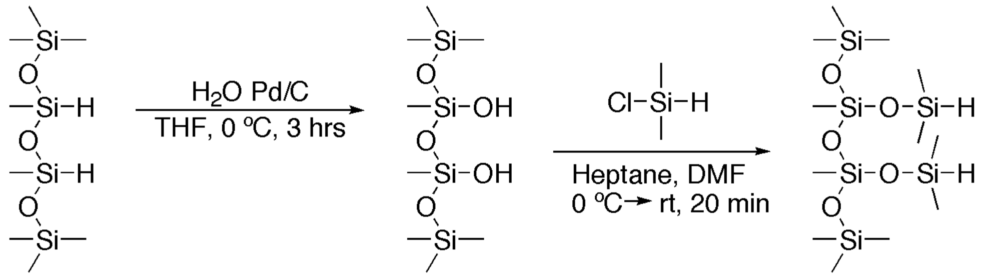

Scheme 5.1. The palladium-assisted hydrolysis of Si-4 (H,H) and subsequent reaction with chlorodimethylsilane to yield Si-6 (H,H).

Si-6 (H,H) was functionalized with allyl methacrylate by hydrosilylation to render it polymerizable (Scheme 5.2).

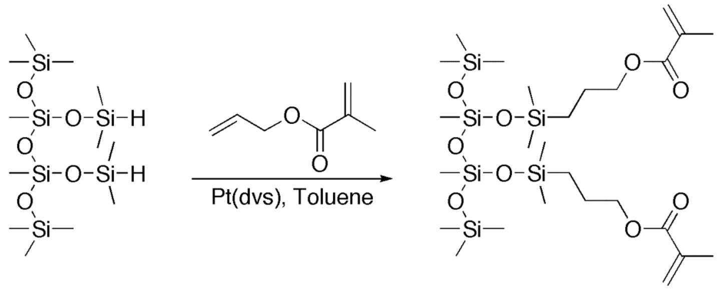

Scheme 5.2. Polymerizable Si-6 obtained after hydrosilylation of Si-6 (H,H) and allyl methacrylate.

This methacrylate-functionalized siloxane was deposited via spincoating, but the material evaporated too rapidly and was deemed unsuitable due to its high vapor pressure. Thus, the hydrolysis and chlorosilane reaction steps were repeated four more times to yield Si-14 (H,H) as illustrated in Scheme 5.3.

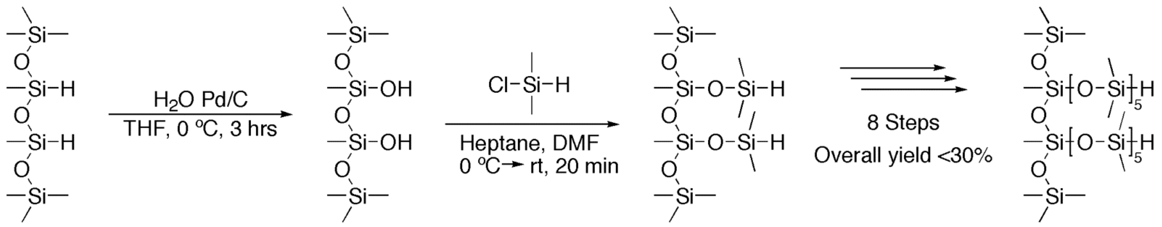

Scheme 5.3. Repetitive steps in the full synthesis of Si-14 (H,H).

Si-14 was functionalized with the same polymerizable group as Si-6 to be evaluated as a planarizing material. Results from complete evaluation of this material have been published elsewhere and are shown in Table 5.1.

Name	**Methacryl Si-14**
Structure	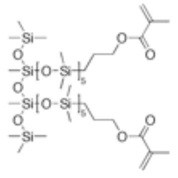
Silicon content	**30.8 %**
Vapor pressure	**0.75 Torr**
Viscosity	**15 cP**
UV shrinkage	**~5.1 %**

Table 5.1: Properties of functionalized Si-14.

5.4.3 Si-12

The synthesis of Si-14 was successful, but it was a tedious process, so a more efficient alternative route was investigated. Polydimethylsiloxane (PDMS) can be synthesized by a ring opening polymerization of hexamethylcyclotrisiloxane (D_3) [10], and it was found that cyclic siloxanes can also be opened to provide asymmetrically substituted siloxanes (Scheme 5.4) [3, 11, 12].

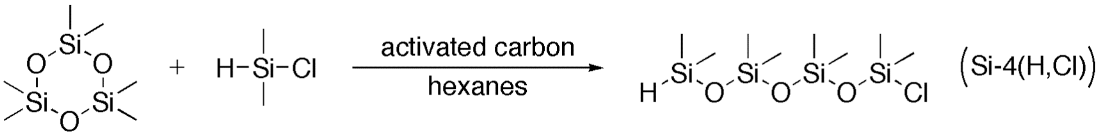

Scheme 5.4. Ring opening of hexamethylcyclotrisiloxane with chlorodimethylsilane to render the asymmetrically substituted Si-4 (H,Cl).

This asymmetrically substituted chlorosiloxane can be used to synthesize Si-12 (1H,19H-9,11-bis(trimethylsiloxy)octadecamethyldecasiloxane) in a total of three steps (Scheme 5.5) [11].

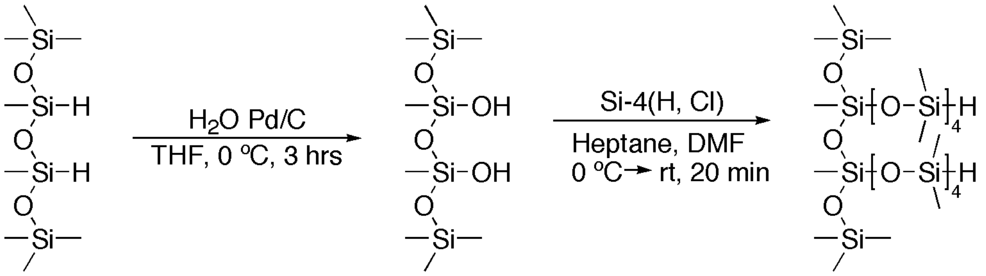

Scheme 5.5. Synthesis of Si-12 utilizes the asymmetric product obtained from the ring opening reaction of D_3.

Si-12 was functionalized with either epoxide or methacrylate groups via a platinum catalyzed hydrosilylation reaction (Scheme 5.6).

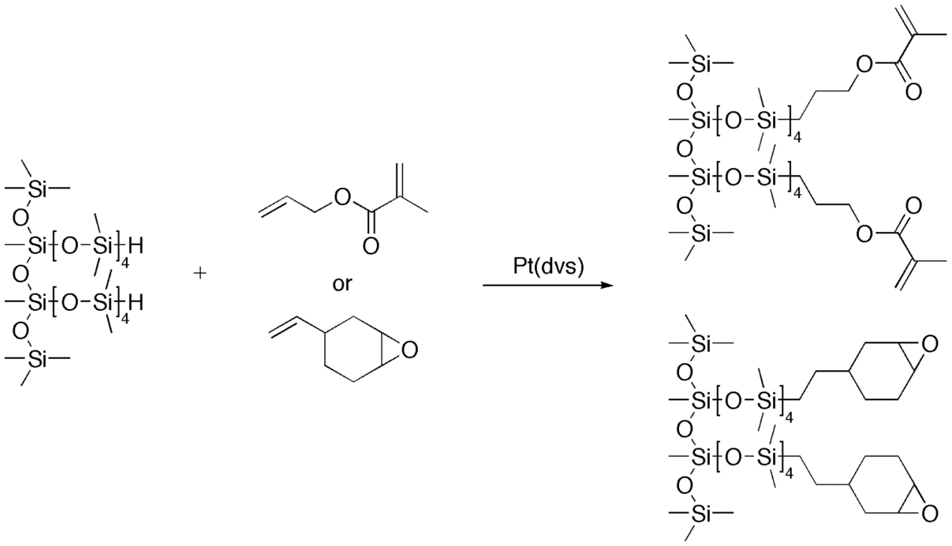

Scheme 5.6. Platinum catalyzed functionalization of Si-12 with either methacrylate or epoxide.

Both materials were evaluated and the results are illustrated in Table 5.2 [3, 11].

Name	**Methacryl-Si-12**	**Epoxy-Si-12**
Structure	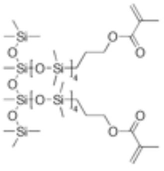	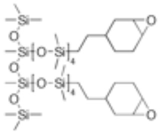
Si content	**29.9 %**	**30.0 %**
Vapor pressure	**1.26 Torr**	**0.65 Torr**
Viscosity	**20 cP**	**29 cP**
UV shrinkage	**~8.0 %**	**~2.2 %**

Table 5.2: Physical properties of functionalized Si-12.

In addition to the complete evaluation of functionalized Si-12 as a planarizing material, the epoxide-substituted version of Si-12 was tested in an SFIL-R experiment.

5.4.4 SFIL-R Study with Epoxide Si-12

After all the material requirements were met by Si-12, it was time to test it in an actual SFIL-R imprint study. Epoxide Si-12 was chosen for its lower vapor pressure and resistance to shrinkage, which would allow for the spincoating of a thinner planarizing layer. Clean wafers were coated with an organic adhesion layer (NCI-NIL-01, Nissan Chemical Industries, Ltd.) to function as the underlayer for imprint lithography. A template was made at The University of Texas at Austin consisting of 80 nm lines and 180 nm spaces. The template was exposed to tridecafluoro-1,1,2,2-tetrahydrooctyldimethyl-chlorosilane to function as a release layer. Imprints were made in an organic resist formulation (Table 5.3).

Component	Structure	
EGDA		38.2
nBA	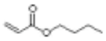	19.8
IBA	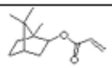	38.0
Darocur® 1173	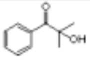	4.0

Table 5.3: Organic resist formulation used in the SFIL-R experiments.

An SEM image of the imprinted pattern (Figure 5.6) indicates that 80 nm lines and 180 nm spaces were clearly patterned. Epoxide functionalized Si-12 was then spincoated over the pre-patterned substrate before being cured by UV light. Figure 5.7 shows the planarized Si-12 over the patterned substrate.

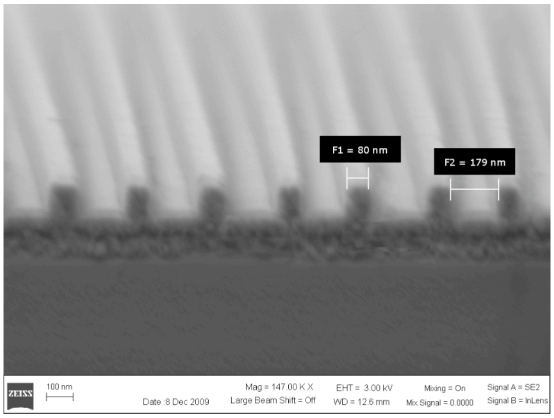

Figure 5.6: Imprinted lines and spaces in the organic resist referred to as F1 and F2.

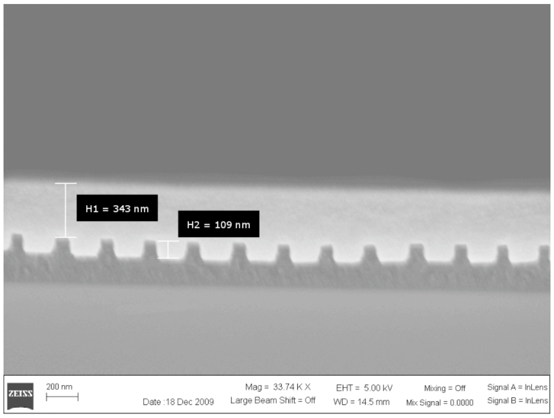

Figure 5.7: Epoxy-Si-12 planarized over the patterned substrate.

A timed blanket etch was carried out using CHF_3 to remove excess Si-12 and to expose the top of the imprinted pattern. At this point, the etch conditions were changed to an oxygen etch in order to selectively etch the organic resist since the high silicon content of Si-12 would function as an etch mask. Figure 5.8 illustrates the etch transfer into the organic resist. As the exposed organic material was etched away, a reverse tone image was generated giving 180 nm lines and 80 nm spaces.

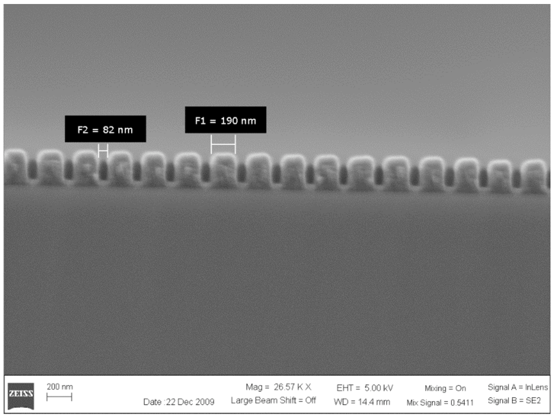

Figure 5.8: Final pattern transfer into the organic resist after blanket etching to obtain the reverse tone features (an exact replica of the template).

5.4.5 Hyperbranched Monomers

As an alternative to the first materials evaluated, it was believed that hyperbranched polymers would have lower viscosities resulting in thinner layers during spincoating. The synthesis of hyperbranched polymers demands AB_2 type monomers or something similar. A few such siloxane precursor materials are available from chemical suppliers, but they can also be synthesized. Three approaches to the hyperbranched materials were considered. The first is based on work by Jean Frechet and David Son's groups, where the propagation step is a platinum-catalyzed hydrosilylation reaction [13-15]. This reaction requires the presence of a metal catalyst for polymerization. The semiconductor industry goes to great lengths to remove metal to levels that are on the parts per billion scale. Consequently, this polymerization mechanism was not investigated. The second approach is based on work done by James Crivello [16, 17], in which the propagation step for multi-epoxide functionalized materials is an acid catalyzed epoxide-opening reaction. The epoxide-based polymerization technique is very common in the manufacturing of microelectronics, and several photoresists exist that are based on epoxides. The third approach is the addition reaction of thiol-ene based materials. Examples of target monomers for hyperbranched polymers based on this chemistry are shown in Figure 5.9 below.

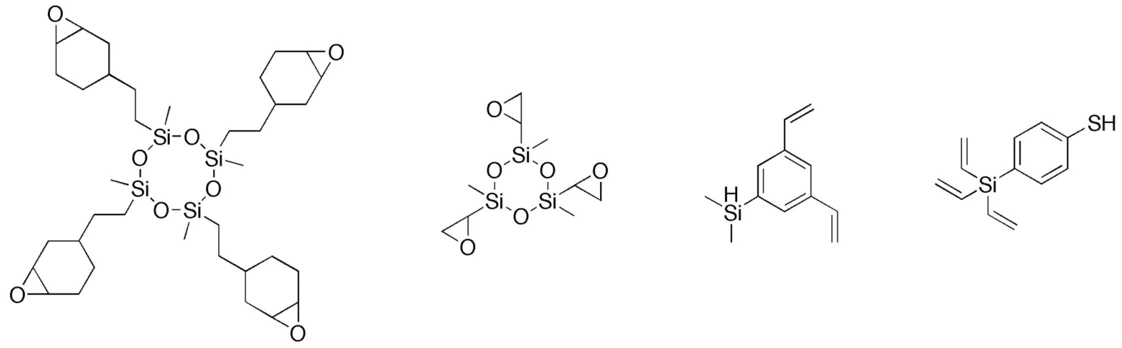

Figure 5.9: Monomer candidates for hyperbranched polymers.

Figure 5.10 illustrates three potential epoxides. The first two are commercially available, whereas the third has to be synthesized.

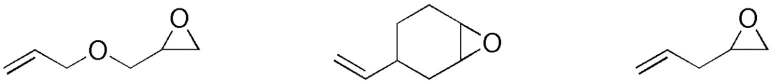

Figure 5.10: Two commercially available epoxides and a third candidate that can be appended onto a siloxane backbone through a hydrosilylation reaction.

2-Allyloxirane (allylepoxide) was synthesized using the procedure illustrated in Scheme 5.7 [18].

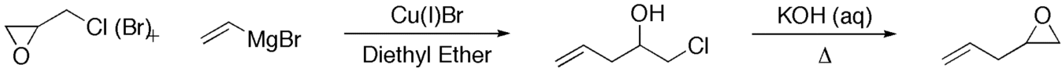

Scheme 5.7: Synthesis of 2-allyloxirane.

Starting materials are commercially available for a variety of multifunctional siloxane precursors and the following species were purchased (Figure 5.11).

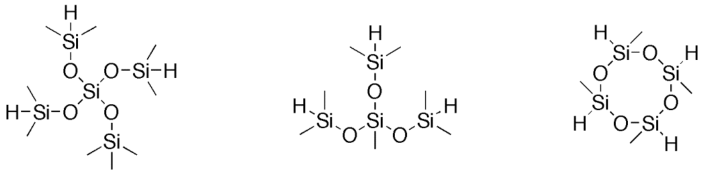

Figure 5.11: Various hydrogen terminated siloxanes.

With the starting materials in hand, epoxide-functionalized siloxanes were prepared according to a procedure published by Crivello *et al.* [19-21] as illustrated in Scheme 5.8.

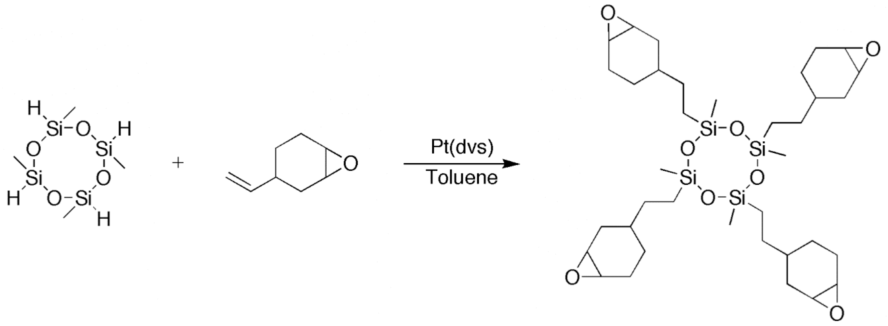

Scheme 5.8: Platinum catalyzed hydrosilylation to obtain multi-epoxide functionalized siloxanes [16].

In addition to the candidates above, epoxides can be synthesized from vinyl functionalities. Epoxidation of vinylsiloxanes was carried out with *m*-CPBA, or peracetic acid as shown in Scheme 5.9.

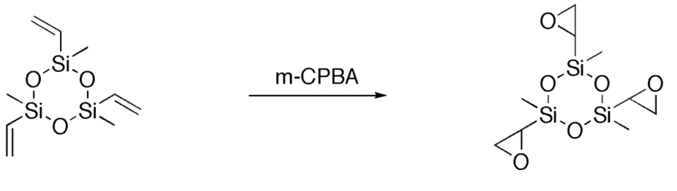

Scheme 5.9: Example of epoxide structure from epoxidation of vinylsiloxane.

To our surprise, it was observed that all of the epoxide-functionalized materials were highly viscous. Due to the high viscosity, this approach was abandoned.

The second group of materials investigated was the asymmetrically substituted molecules designed for the thiol-ene reaction. The thiol-ene reaction requires multifunctional thiol monomers which provide the maximum thermal stability possible while contributing to the reduction of the formulation's viscosity. These materials must have reasonably low vapor pressure. Blending the thiols with multi-ene compounds offers freedom to achieve the desired properties in the formulation.

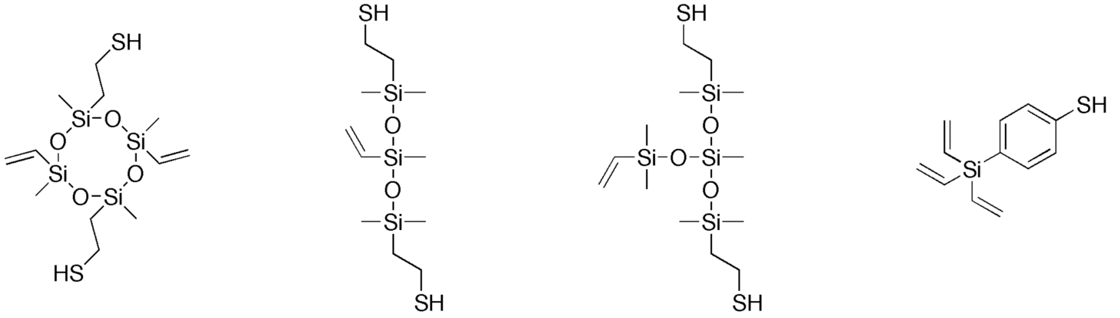

Figure 5.12: Asymmetrically substituted thiol-ene monomers for use in hyperbranched polymers.

Attempts were made to synthesize the first three materials in Figure 5.12 in two steps as indicated in Scheme 5.10.

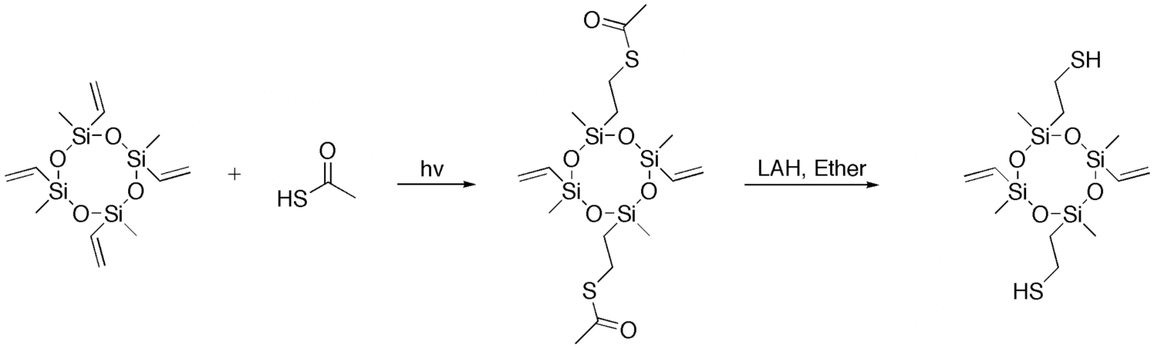

Scheme 5.10: Synthesis of asymmetrically substituted thiol-ene monomers through a two-step path.

Various efforts were also made to synthesize 4-(trivinylsilyl)benzenethiol shown in Figure 5.12 (and product in Scheme 5.11) by protecting the thiol functionality before appending the vinylsilane by employing a Grignard reaction. A variety of protecting groups were attempted with little success. Consequently, a reduction in yield was deemed acceptable by skipping the protection of the thiol and carrying out the Grignard reaction directly as illustrated in Scheme 5.11.

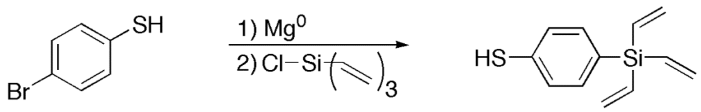

Scheme 5.11: One possible synthetic route to obtain the AB_3 monomer.

However, upon isolation of the product, it was noted that the thiol functionality seemed to react with the vinyl moieties even in the absence of light and the presence of a radical inhibitor. This was confirmed by following the reduction of the thiol proton and the appearance of methylene protons in NMR experiments.

5.5 RESULTS AND CONCLUSIONS

Methacrylate-functionalized Si-14 illustrates excellent planarizing properties. It meets all of the specified material requirements. However, the initial synthesis is lengthy and costly as two steps must be repeated multiple times and yields are low. Although the material served as a great candidate in a university research setting, it is not suitable for industrial scale-up. For this purpose, a simplified path was needed. The significantly shorter synthetic path of the precursor to Si-14, Si-12, was discovered, and the material was functionalized with polymerizable groups and fully evaluated. Si-12 also meets all the specified material requirements. It was scaled up by a chemical company and was tested as a planarizing material for a SFIL-R demonstration. The SFIL-R demonstration was successful in that the final features of the multiple etch processes were inverted to provide an exact replica of the template (reverse tone SFIL). The dually functionalized monomers of the thiol-ene type species all had vapor pressures that were too high and were unsuccessfully spincoated onto substrates. In addition, due to the dual functionality, dimerization and polymerization took place even in dark and cold storage conditions.

5.6 FUTURE WORK

Si-12 was successfully demonstrated as a planarizing liquid, but there is room for improvement. In order to achieve high throughput, it is important to reach the critical degree of planarization as rapidly as possible. Materials with even lower viscosities could accomplish this. When spincoating materials without a volatile solvent, the thickness depends on the spin time and the amount of material dispensed on the substrate. The thiol-ene based materials have the potential of becoming great planarizing materials if this viscosity can be kept low while molecular weight is increased to lower the vapor pressure.

5.7 REFERENCES

[1] S. V. Sreenivasan, I. McMackin, F. Xu, D. Wang, N. Stacey and D. Resnick. "Reverse Tone Bi-Layer Etch in UV Nanoimprint Lithography". *Micro Magazine,* 2005.

[2] M. W. Lin, H.-L. Chao, J. Hao, E. K. Kim, F. Palmieri, W. C. Kim, M. Dickey, P. S. Ho and C. G. Willson. "Planarization for Reverse-Tone Step and Flash Imprint Lithography". *SPIE*, 6151, Emerging Lithographic Technologies X, 2006.

[3] T. Ogawa, S. Takei, B. M. Jacobsson, R. Deschner, W. Bell, M. W. Lin, Y. Hagiwara, M. Hanabata and C. G. Willson. "Planarizing material for reverse-tone step and flash imprint lithography". *Alternative Lithographic Technologies II*, 7637, 2010.

[4] S. Franssila. "Introduction to Microfabrication"; 2nd Ed.; John Wiley & Sons, Ltd.; Chichester, West Sussex, 2010.

[5] M. W. Lin. "Simulation and Design of Planarizing Materials and Interfacial Adhesion Studies for Step and Flash Imprint Lithography". *Ph.D. University of Texas at Austin,* 2008.

[6] J. E. L. III, M. Daffron, R. Hopper, M. Whittaker and S. Scott. "Planarizing Difficult Topographies Using Contact Planarization". *Solid State Technology,* 46, 2003.

[7] M. W. Lin, B. Chao, J. Hao, K. Osberg, P. S. Ho and C. G. Willson. "Simulation and design of planarizing materials for reverse-tone step and flash imprint lithography". *Journal of Micro/Nanolithography, MEMS and MOEMS,* 7, 023008, 2008.

[8] J. Hao, M. W. Lin, F. Palmieri, Y. Nishimura, H.-L. Chao, M. D. Stewart, A. Collins, K. Jen and C. G. Willson. "Photocurable Silicon-Based Materials for Imprint Lithography". *Proc. of SPIE,* 6517, 2007.

[9] W.-L. Jen, F. Palmieri, B. Chao, M. Lin, J. Hao, J. Owens, K. Sotoodeh, R. Cheung and C. G. Willson. "Multi-level Step and Flash Imprint Lithography for Direct Patterning of Dielectrics". *Proc. of SPIE,* 6517, 2007.

[10] S. Boileau. "Anionic Polymerization of Cyclosiloxanes with Cryptates as Counterions". Ring-Opening Polymerization. 1985.

[11] T. Ogawa, B. M. Jacobsson and C. G. Willson. "Novel synthetic route to UV curable branched siloxanes for nano imprint lithography". *239th ACS National Meeting*, 2010.

[12] K. Yoshino, A. Kawamata, H. Uchida and Y. Kabe. "A Convenient Synthesis of a,w-Difunctionalized Linear Dimethylsiloxanes with Definite Chain Lengths". *Chemistry Letters,* 2133-2136, 1990.

[13] J. F. Miravet and J. M. J. Frechet. "New Hyperbranched Poly(siloxysilanes): Variation of the Branching Pattern and End-Functionalization". *Macromolecules,* 31, 3461-3468, 1998.

[14] Y. Xiao, R. A. Wong and D. Y. Son. "Synthesis of a New Hyperbranched Poly(silylenevinylene) with Ethynyl Functionalization". *Macromolecules,* 33, 7232-7234, 2000.

[15] K. Yoon and D. Y. Son. "Syntheses of Hyperbranched Poly(carbosilarylenes)". *Macromolecules,* 32, 5210-5216, 1999.

[16] J. V. Crivello and M. Ranjit. "Synthesis and photoinitiated cationic polymerization of monomers with the silsesquioxane core". *Journal of Polymer Science Part A: Polymer Chemistry,* 35, 407-425, 1997.

[17] J. V. Crivello. "The discovery and development of onium salt cationic photoinitiators". *Journal of Polymer Science Part A: Polymer Chemistry,* 37, 4241-4254, 1999.

[18] A. De Camp Schuda, P. H. Mazzocchi, G. Fritz and T. Morgan. "A Short and Efficient Synthesis of 4,5-Disubstituted-1-pentenes". *Synthesis,* 1986, 309-312, 1986.

[19] J. V. Crivello and J. L. Lee. "The Synthesis, Characterization, and Photoinitiated Cationic Polymerization of Silicon-Containing Epoxy Resins". *Journal of Polymer Science Part A: Polymer Chemistry,* 28, 479-503, 1990.

[20] J. V. Crivello. "The Synthesis and Cationic Polymerization of Novel Epoxide Monomers". *Polymer Engineering and Science,* 32, 1662-1665, 1992.

[21] J. V. Crivello, M. Fan and D. Bi. "The Electron Beam-Induced Cationic Polymerization of Epoxy Resins". *Journal of Applied Polymer Science,* 44, 9-16, 1992.

[22] D. D. Perrin and W. L. F. Armarego. "Purification of Laboratory Chemicals"; 3rd Ed.; Butterworth-Heinemann Ltd; 1988.

5.8 SYNTHESIS OF MATERIALS

General experimental procedures and comments. Chemicals were purchased from various sources and used in reactions without any further purification unless otherwise indicated. Solvents were dried and distilled according to commonly used literature procedures [22]. All reactions were performed under a dry nitrogen atmosphere unless otherwise indicated.

^{1}H NMR spectra were obtained on a Varian Mercury (400 MHz), Varian (400 MHz System, Direct Drive), Varian INOVA (500 MHz) or Unity plus (300 MHz) instruments referenced to deuterated chloroform (7.24 ppm), deuterated DMSO (2.49 ppm) or deuterated water (4.79 ppm). Chemical shifts are reported in delta units (∂), parts per million, and coupling constants (J) are reported in Hertz (Hz). ^{13}C spectra were obtained on a Varian Mercury (100 MHz), Varian (100 MHz System, Direct Drive), Varian INOVA (125 MHz) or a Unity plus (75 MHz) instruments referenced to 77.000 ppm for deuterated chloroform, or 39.5 ppm for deuterated DMSO. ^{13}C NMR spectra were routinely run with broadband decoupling. ^{29}Si spectra were obtained on a Varian INOVA (75 MHz) or a Unity plus (60 MHz). Low-resolution mass spectra were obtained on an Agilent GC/MS 6890N Gas Chromatograph and 5973 Mass Spectrometer, or a Finnigan LCQ instrument. High-resolution mass spectroscopy analyses were carried out on an ION-SPEC, FT-ICR/MS instrument. FT-IR spectra were obtained on a Nicolet Avatar 360 FT-IR instrument. Thermal stability and melting points were measured on a MEL-TEMP II or a TA instruments DSC Q_{100} / TGA Q_{500}. UV exposures were either carried out on a The Southern N.E. Ultraviolet Co. Rayonet Photochemical Reactor (16 bulbs, 300 nm) or a JH Technologies Novacure® 2100 System (High Pressure 100 W Mercury Vapor Short Arc Lamp, ~250-500 nm).

Preparation of 3,5-Bis(dimethylsiloxy)octamethyltetrasiloxane or 1H,7H-3,5-bis(trimethylsiloxy)hexamethyltetrasiloxane (Si-6). Palladium on carbon (0.10 g), distilled water (9.0 mL, 0.50 mol, 14 eq.), and THF (300 mL) were added to a 500 mL round bottom flask equipped with a magnetic stir bar and a rubber septum. 1,3-Bis(trimethylsiloxy)-1,3-dimethyldisiloxane (10.0 g, 35 mmol, 1.0 eq.) in THF (50 mL) was slowly added via an addition funnel and the reaction was stirred for ~8 hrs. To a clean and dry 1 L round-bottomed flask equipped with a magnetic stir bar, a nitrogen inlet needle, a rubber septum, and flushed with nitrogen gas was added heptane (100 mL) via syringe along with freshly distilled DMF (100 mL). Dimethylchlorosilane (44 mL, 0.4 mol, 11.0 eq.) was added via a volumetric cylinder and as gas evolved it was flushed out with a stream of nitrogen. The round-bottomed flask was then cooled in an ice bath and equipped with a large addition funnel previously flushed with nitrogen. The hydrolyzed silane in the 500 mL flask was filtered through celite and then added to the large addition funnel attached to the 1 L reaction flask. The reaction flask was stirred for 5 minutes at 0 °C before addition of silanol was started. The rate of addition was set to roughly one drop per second. After addition was complete the reaction was kept in the ice bath for an additional 15 minutes before cold distilled water was added slowly via the addition funnel to quench excess chlorosilane. A separatory funnel was used to separate the organic layer from the aqueous layer and the organic layer was washed with approximately 1.5 L of distilled water to remove DMF. The organic layer was dried over magnesium sulfate before being placed on a rotary evaporator and under high vacuum to remove solvents. TLC indicated two spots with large difference in R_f value. The residue was chromatographed through a short plug run with 100% hexanes to yield a clear liquid with low viscosity in 12.3 g, 80.4% yield. ^{1}H NMR (400 MHz, $CDCl_3$): δ 4.707 - 4.748 (sep, J = 2.739 Hz, 2H), 0.197 (d, J = 2.738, 12H), 0.110 (s, 18H), 0.048 (s, 6H). ^{13}C-

NMR (100 MHz, $CDCl_3$): δ 1.652, 0.573, -2.552. ^{29}Si-NMR (60 MHz, $CDCl_3$): δ 8.013 (s), -6.596 (d, *J* = 207 Hz), -65.108. IR (neat): 2903, 1417 (w), 2961, 2132, 800, 770 (m), 1253, 1061, 909, 843 cm^{-1} (s). HRMS (CI+, $[M-1]^+$) calcd. for $C_{12}H_{37}O_5Si_6$: 429.1257, found = 429.1259.

Preparation of Functionalized Si-6 with Allyl Methacrylate. Allyl methacrylate (2.4 mL, 18 mmol, 2.4 eq.), and 1H,7H-3,5-bis(trimethylsiloxy)hexamethyltetrasiloxane (3.161 g, 7.3 mmol, 1 eq.) were added to a flame dried nitrogen flushed 25 mL round-bottom flask equipped with a magnetic stir bar and a rubber septum. Freshly distilled toluene was added via syringe as well as Karstedt's catalyst (0.5 mL). The reaction was stirred for 48 hrs under N_2 at RT. A 10 mL plastic syringe equipped with a 0.2 micro filter and about 2 mL of celite was used to filter the product. The toluene was evaporated and the crude product was recovered in 3.555 g, 71% yield. Column chromatography with ethyl acetate and hexanes 10/90 as eluent gave product in 5%, (0.273 g). ^{1}H NMR (400 MHz, $CDCl_3$): δ 6.064-6.057 (q, *J* = 1.0 Hz, 2H), 5.507-5.492 (p, *J* =1.6 Hz, 2H), 4.081-4.046 (t, *J* = 7.0 Hz, 4H), 1.906-1.900 (dd, *J* = 0.6 Hz, *J* = 1.0 Hz, 6H), 1.710-1.632 (m, 4H), 0.523-0.566 (m, 4H), 0.05-0.074 (m, 30H), -0.020-0.001 (m, 6H). ^{13}C-NMR (100 MHz, $CDCl_3$): δ 167.421, 136.489, 125.059, 67.101, 22.510, 18.272, 13.934, 1.606, -0.114, -2.279. ^{29}Si-NMR (60 MHz, $CDCl_3$): δ 7.776 (s), -65.898 (s). IR (neat): 2899 (w), 1639, 1455, 1406, 1321, 1296, 939 (m), 2959, 1722, 1253, 1164, 1056, 844, 791 cm^{-1} (s). HRMS (CI+, $[M-CH_3]^+$) calcd. for $C_{25}H_{55}O_9Si_6$: 667.2462, found = 667.2465.

Preparation of 1H,11H-5,7-bis(trimethylsiloxy)decamethylhexasiloxane (Si-8). The procedure used for the preparation and isolation of Si-6 was utilized here. Palladium on carbon (0.10 g), distill water (9 mL, 0.50 mol, 17 eq.), and THF (300 mL) were added and stirred in a 500 mL round bottom flask. 1H,7H-3,5-

bis(trimethylsiloxy)hexamethyltetrasiloxane, Si-6, (12.46 g, 29 mmol, 1.0 eq.) was added dropwise. Dimethylchlorosilane (45 mL, 0.4 mol, 14 eq.), heptane (100 mL), and DMF (100 mL) were added to a 1 L single necked round bottom flask equipped with an addition funnel. The hydrolyzed Si-6 was added to the addition funnel and slowly added to the reaction to obtain the product Si-8 as a colorless low viscosity liquid (12.768 g, 76% yield). ^{1}H NMR (400 MHz, $CDCl_3$): δ 4.687-4.722 (sep, *J* = 2.7 Hz, 2H), 0.184 (d, *J* = 2.7 Hz, 12H), 0.108 (s, 18H), 0.079 (s, 12H), 0.059 (s, 6H). ^{13}C-NMR (75 MHz, $CDCl_3$): δ 1.683, 0.785, 0.732, -2.295. ^{29}Si-NMR (100 MHz, $CDCl_3$): δ 7.855 (s), -6.872 (d, *J* = 202 Hz), -20.020, -66.845 (s). IR (neat): 2903, 1414 (w), 757 (m), 2962, 2129, 1260, 1050, 913, 843, 797 cm^{-1} (s). HRMS (CI+, $[M-1]^+$) calcd. for $C_{16}H_{49}O_7Si_8$: 577.1633, found = 577.1626.

Preparation of 1H,15H-7,9-bis(trimethylsiloxy)tetradecamethyloctasiloxane (Si-10). The procedure used for the preparation and isolation of Si-6 was utilized here. Palladium on carbon (0.05 g), distill water (3.3 mL, 0.18 mol, 14 eq.), and THF (150 mL) were added to a 500 mL flask. Dimethylchlorosilane (29 mL, 0.26 mol, 20 eq.), DMF (150 mL), and heptane (150 mL) were stirred at 0 °C while hydrolyzed Si-8 (7.62 g, 13.2 mmol, 1.0 eq.) was slowly added to the flask. Product (Si-10) was obtained as a colorless low viscosity liquid (7.16 g, 74.7% yield). ^{1}H NMR (400 MHz, $CDCl_3$): δ 4.677-4.718 (sep., *J* = 2.7 Hz, 2H), 0.173 (d, *J* = 2.7 Hz, 12H), 0.046-0.108 (m, 48H). ^{13}C-NMR (75 MHz, $CDCl_3$): δ 1.674, 0.968, 0.878, 0.700, -2.269. ^{29}Si-NMR (60 MHz, $CDCl_3$): δ 7.855, -6.872 (d, *J* = 202 Hz), -19.783, -21.836, -66.924. IR (neat): 1414, 690 (w), 2128, 766 (m), 2962, 1261, 1043, 913, 842, 800 cm^{-1} (s). HRMS (CI+, $[M-1]^+$) calcd. for $C_{20}H_{61}O_9Si_{10}$: 725.2008, found = 725.2003. Elemental analysis calcd. for $C_{20}H_{62}O_9Si_{10}$: C: 33.02%, H: 8.59%, found: C 33.16%, H: 8.65%.

Preparation of 1H,19H-9,11-bis(trimethylsiloxy)octadecamethyldecasiloxane (Si-12). The procedure used for the preparation and isolation of Si-6 was utilized here Palladium on carbon (0.06 g), distill water (4.5 mL, 0.25 mol, 14 eq.), and THF (200 mL) were added to a 500 mL round bottom flask. Si-10 (13.18 g, 18.1 mmol, 1.0 eq.) was slowly added to the mixture. Dimethylchlorosilane (40 mL, 0.36 mol, 20 eq.), DMF (200 mL), and heptane (200 mL) were added to a 1 L round bottom flask and stirred at 0 °C while the hydrolyzed Si-10 was slowly added. Product, Si-12, was obtained as a colorless low viscosity liquid (10.83 g, 68% yield). ^{1}H NMR (400 MHz, $CDCl_3$): δ 4.698 (sep, *J* = 2.7 Hz, 2 H), 0.172 (d, *J* = 2.7 Hz, 12 H), 0.108-0.044 (m, 60 H). ^{13}C-NMR (75 MHz, $CDCl_3$): δ 1.682, 1.057, 0.990, 0.975, 0.863, 0.700, -2.254. ^{29}Si-NMR (60 MHz, $CDCl_3$): δ 7.815, -5.212, -8.607, -19.898, -21.871, -66.875. IR (neat): 2904, 1413 (w), 2128, 766 (m), cm^{-1} 2963, 1661, 1034, 913, 802 (s). HRMS (CI+, $[M-1]^+$) calcd. for $C_{24}H_{73}O_{11}Si_{12}$: 873.2384, found = 873.2380.

Preparation of 1H,23H-11,13-bis(trimethylsiloxy)docosamethyldodecasiloxane (Si-14). The same procedure used for the preparation and isolation of Si-6 was employed here. Palladium on carbon (0.040 g), water (2.0 mL, 0.11 mol, 14 eq.), and THF (100 mL) were stirred together in a 250 mL single necked round bottom flask. Dimethylchlorosilane (20 mL, 0.18 mol, 23 eq.), DMF (100 mL), and heptanes (100 mL) were added and stirred at 0 °C in a 500 mL flask. Si-12 (6.96 g, 7.9 mmol, 1.0 eq.) was slowly added to the reaction vessel. Product Si-14 as a colorless low viscosity liquid 5.525 g, 68% yield. ^{1}H NMR (400 MHz, $CDCl_3$): δ 4.648 (t sep., 2H, *J* = 2.7/102 Hz), 0.128 (d, *J* = 2.9 Hz, 12 H), 0.071 - 0.00 (m, 72 H). ^{13}C-NMR (75 MHz, $CDCl_3$): δ 1.667-1.481 (m), 1.012-0.558 (m), -2.284 (s), -2.660 (d). IR (neat): 767, 690 (m), 2962, 2128, 1261, 1028, 913, 801 cm-1 (s). HRMS (CI+, $[M-1]^+$) calcd. for $C_{28}H_{85}O_{13}Si_{14}$: 1021.2760, found = 1021.2756. Elemental analysis calcd. for $C_{28}H_{86}O_9Si_{14}$: C: 32.84%, H: 8.46%, found: C 32.77%, H: 8.61%.

Preparation of Functionalized Si-14 with Allyl Methacrylate. The procedure used for the preparation and isolation of functionalized Si-6 was employed here. Allyl methacrylate (1.3 mL, 9.6 mmol, 2.7 eq.), Si-14 (3.61 g, 3.5 mmol, 1 eq.), and toluene (20 mL) were added together to a 50 mL round bottom flask. The mixture was flushed for several minutes with nitrogen before Karstedt's catalyst (0.5 mL) was added via syringe. Reaction was stirred for 48 hrs under N_2 and RT. A 10 mL plastic syringe was equipped with a 0.2 micro filter and about 2 mL of celite before the reaction mixture was carefully added and filtered into a tared 25 mL flask. Toluene was evaporated and a slightly yellowish liquid was recovered. No yield quoted as product is impure by proton NMR. Additional attempts to purify were unsuccessful and often led isolation of insoluble gels. ^{13}C-NMR (75 MHz, $CDCl_3$): δ 167.504, 136.537, 125.116, 67.142, 22.597, 18.318, 14.077, 1.652, 1.124, 1.042, 0.968, 0.298, 0.060, -2.284.

Synthesis of asymmetric linear siloxane, Si-4[H,Cl]. Hexamethylcyclotrisiloxane, D_3, (116.7 g, 0.524 mol), activated carbon (2.15 g) and hexane (330 mL) were added to a 2 L round bottom glass flask equipped with a 250 mL addition funnel. Dimethylchlorosilane (88.5 mL, 0.795 mol) in hexane (110 mL) were added to the addition funnel and slowly added dropwise over 1 hour at room temperature. The reaction was allowed to stir overnight. The reaction was monitored by GC/MS periodically, and if un-reacted D_3 was still present over 20%, additional activated carbon and dimethylchlorosilane was added. The solution was filtered through a 0.2 micro PTFE filter to remove the activated carbon. Then the solvent was evaporated on a rotary evaporator. Distillation at 10 Torr and 75 °C was carried out to obtain the product 129.6 g 78% as a colorless liquid. ^{1}H NMR ($CDCl_3$): δ 4.69 (m, 1H), 0.43 (s, 6H), 0.17 (d, J = 2.8

Hz, 6H), 0.11 (s, 6H), 0.06 (s, 6H). ^{13}C NMR ($CDCl_3$): δ 4.06, 0.88, 0.80, 0.68. ^{29}Si NMR ($CDCl_3$): δ 3.75, -6.63 (d, J = 204 Hz), -18.94, -19.27.

Synthesis of 1H,19H-9,11-bis(trimethylsiloxy)octadecamethyldecasiloxane (Si-12, preferred method). Palladium on carbon (0.16 g), water (1.9 g, 0.11 mol) and THF (175 mL) were added to a 500 mL round bottom glass flask equipped with an addition funnel. 1,3-Bis(trimethylsiloxy)-1,3-dimethyldisiloxane (10.0 g, 35 mmol) and THF (75 mL) were added to the addition funnel. The solution was slowly added dropwise into the flask and stirred at RT for 6 hours. The solution was filtered through celite. Si-4[H,Cl] (56.4 g, 0.178 mol), triethylamine (27.8 g, 0.275 mol) and diethyl ether (700 mL) were added to a 3 L round bottom glass flask equipped with a 250 mL addition funnel. The filtrate from above was added to the addition funnel and slowly dripped into the flask at 0 °C. The suspension was stirred overnight at RT. Water (1 L) was added to the solution to quench excess Si-4[H,Cl] and then the organic layer was separated from the aqueous layer. The organic layer was washed with water and dried over anhydrous magnesium sulfate. The solvent was removed under reduced pressure. Distillation using a Kugelrohr apparatus at 170 °C and <1 Torr was carried out to remove impurities. Product was obtained 28.9 g 93% as a colorless liquid. Spectral data corresponds well with data obtained from previous Si-12 synthesis.

Synthesis of epoxide functionalized Si-12. Si-12 (12.7 g, 14.5 mmol), 4-vinyl-1-cyclohexene 1,2-epoxide (4.8 g, 38 mmol) and toluene (130 mL) were added to a 500 mL round bottom glass flask. The flask was flushed with nitrogen gas for several minutes before 25 drops of Karstedt's catalyst was added to the solution with vigorous stirring. The solution turned to a yellowish hue and was allowed to stir overnight. The solvent was removed under reduced pressure, and the excess epoxide was removed under high vacuum (<1 Torr) at room temperature. 14.1 g of slightly yellowish liquid was obtained as 86.7 % yield. ^{1}H NMR (CDCl$_3$): δ 3.104–3.140 (m, 4H), 0.793–2.178 (comp. m, 18H) 0.442–0.486 (m, 4H), 0.015–0.093 (m, 72Hz, 12H), 0.06 (s, 12H), 0.05 (s, 12H), 0.03 (s, 6H). ^{13}C NMR (CDCl$_3$): δ 53.280, 52.752, 52.008, 51.963, 35.409, 32.269, 31.525, 30.394, 30.096, 29.531, 26.726, 25.372, 24.025, 23.571, 15.074, 14.970, 1.660, 1.169, 1.094, 0.975, 0.023, -2.276. FT-IR (neat): 2916, 2850, 1436, 1413, 1338 (w), 2961, 840, 685 (m), 1257, 1019, 788 cm^{-1} (s). HRMS (ESI+, [M+Na]$^+$) calcd. for $C_{40}H_{98}O_{13}Si_{12}$: 1145.4131, found = 1145.4117.

Synthesis of methacrylate functionalized Si-12. Si-12 (12.0 g, 13.7 mmol), allyl methacrylate (4.41 g, 34.9 mmol) and toluene (130 mL) were added to a 500 mL round bottom glass flask. Karstedt's catalyst (25 drops) was added to the solution. The solution turned to a yellow color and was allowed to stir overnight covered with aluminum foil. The solvent was removed under reduced pressure and the excess allyl methacrylate was removed under high vacuum (<1 Torr) at room temperature to provide the product. No yield quoted as product was impure by NMR. HRMS (ESI+, [M+Na]$^+$) calcd. for $C_{38}H_{94}O_{15}Si_{12}$: 1149.3716, found = 1149.3718.

Synthesis of 5-Chloro-4-hydroxy-1-pentene [18]. Cu(I)Br (0.90 g, 6.3 mmol) and diethyl ether (200 mL) were added to a 1 L single necked round bottom flask. The solution was cooled to -73 °C in a dry ice 2-propanol bath. Vinylmagnesium bromide (60 mL of a 1 M THF solution, 1.1 eq.) was added via a syringe. Epichlorohydrin (5.03g, 54.3 mmol 1.0 eq.) was slowly added via syringe and the reaction was stirred at -73 °C for 3 hrs. The cooling bath was removed and mixture was stirred at room temperature for ~12 hrs. The reaction was added to 150 mL of water and stirred for 5 minutes. The two layers were separated in a separatory funnel and the aqueous layer was extracted twice with 100 mL diethyl ether. The ether layers were combined and dried over sodium sulfate before the solvent was removed *in vacuo*. Distillation of the product yielded a colorless liquid. ^{1}H NMR (400 MHz, $CDCl_3$): δ 5.723-5.827 (m, 1H), 5.094-5.157 (m, 2H), 3.809-3.878 (m, 1H), 3.590 (dd, J = 11 Hz, 3.7 Hz, 1H), 3.473 (dd, J = 11.2 Hz, 6.7 Hz, 1H), 2.426 (d, J = 4.9 Hz, 1H), 2.289-2.337 (m, 2H). ^{13}C-NMR (100 MHz, $CDCl_3$): δ 133.219, 118.576, 70.534, 49.307, 38.616. HRMS (CI+, $[M-1]^+$ calcd. for C_5H_8OCl = 119.0264, found = 119.0266).

Synthesis of tetraepoxycyclotetrasiloxane (2,4,6,8-tetrakis(2-(7-oxabicyclo-[4.1.0]heptan-3-yl)ethyl)-2,4,6,8-tetramethyl-1,3,5,7,2,4,6,8-tetraoxatetrasilocane). 1,3,5,7-tetramethylcyclotetrasiloxane (10.33 g, 43.0 mmol, 1.0 eq.) and freshly distilled toluene (250 mL) were added to a 500 mL round bottom flask. The flask was purged with nitrogen gas for a couple of minutes before 4-vinyl-1-cyclohexene 1,2-epoxide (34 mL, 0.26 mol, 6.0 eq., mixture of isomers) was added. Karstedt's catalyst was slowly added (0.1 mL, 2 mM solution in xylenes) to the reaction mixture. The reaction was stirred for six hours before filtering through celite and a micro filter (0.45 μ). Solvent was removed under reduced pressure and the product was placed on high vacuum overnight. The crude product contained vinyl-epoxide residue and was distilled under vacuum (5-10 Torr) at 110 °C. Product was obtained as yellowish highly viscous oil. ^{1}H NMR (400 MHz, $CDCl_3$): δ 3.102–3.132 (m, 8H), 0.777–2.155 (m, 36H), 0.406–0.426 (m, 8H), 0.003 (s, 12H). ^{13}C-NMR (100 MHz, $CDCl_3$): δ 53.176, 52.663, 51.911, 51.829, 35.119, 35.074, 32.053, 32.016, 31.532, 31.495, 30.320, 29.799, 29.263, 26.726, 25.290, 23.988, 23.527, 14.048, 13.996, 13.891, 13.839, -0.796, -0.863. ^{29}Si-NMR (60 MHz, $CDCl_3$): δ -19.933. HRMS (CI+, $[M-1]^+$ calcd. for $C_{36}H_{65}O_8Si_4$= 737.3757, found = 737.3745).

Synthesis of 1,1,3,3-tetramethyl-1,3-bis(3-(oxiran-2-ylmethoxy)propyl)disiloxane. 1,1,3,3-tetramethyldisiloxane (0.44 g, 3.3 mmol, 1.0 eq.) and DCM (30 mL) were added to a 100 mL round bottom flask. The flask was flushed with nitrogen gas. Allyl glycidyl ether (1.5 mL, 13 mmol, 3.9 eq.) was added to the reaction vessel via a syringe. The reaction was cooled to 0 °C before the platinum catalyst was slowly added via a syringe (5 drops). The reaction was removed from the ice bath and stirred at RT overnight, conversion was monitored by GC. Residue was filtered through a celite plug, followed by a 0.2 micro filter, and then chromatographed through a short silica plug. The product was isolated as a light yellow oil 0.617 g, 52%. ^{1}H NMR (400 MHz, $CDCl_3$): δ 3.65 (dd, *J* = 3 Hz, 11 Hz, 2H), 3.296–3.431 (m, 6H), 3.073–3.106 (m, 2H), 2.721–2.752 (m, 2H) 2.536–2.562 (m, 2H), 1.492–1.596 (m, 4H), 0.423–0.480 (m, 4H), -0.005 (s, 12H). ^{13}C-NMR (100 MHz, $CDCl_3$): δ 74.212, 71.330, 50.759, 44.207, 23.377, 14.113, 0.167. ^{29}Si-NMR (60 MHz, $CDCl_3$): δ 7.68 (m). IR (neat): 2955, 2931, 2870, 1729, 1480, 1413, 1186, 1159 (w), 1338, 1104, 909, 699 (m), 1252, 1043, 836 cm^{-1} (s). HRMS (CI+, $[M+1]^+$ calcd. for $C_{16}H_{35}O_5Si_2$= 363.2023, found = 363.2016).

Preparation of 1,1,3,3,5,5,7,7-octamethyl-1,7-di(oxiran-2-yl)tetrasiloxane. *m*-CPBA (3.201 g, 77%, 14 mmol, 9.5 eq.) and DCM (15 mL) were added to a flame dried 50 mL round bottom flask. The suspension was stirred at 0 °C and 1,7-divinyl-1,1,3,3,5,5,7,7-octamethyltetrasiloxane (0.502 g, 1.5 mmol, 1 eq.) was slowly added. The reaction was allowed to stir at 0 °C for 30 minutes before removing the cooling bath. Stirring was continued for 72 hours at RT. Solid residue was filtered out and washed with DCM. Organic layer was washed with aqueous sodium bisulfite, sodium bicarbonate, water and brine before dried over magnesium sulfate. No yield quoted as residual aromatic protons were observed in NMR. Additional attempts to purify the product were unsuccessful. HRMS (CI+, $[M-C_2H_3]^+$ calcd. for $C_{10}H_{27}O_4Si_4$ = 323.0986, found = 323.0989).

Synthesis of 5.1 (A_xB_y thioester). Trivinylmethylsilane (23.04 g, 185.4 mmol, 1.0 eq.) and thiolacetic acid (24 mL, 0.34 mol, 1.8 eq.) were added to a large quartz test tube. The test tube was placed in a Rayonet UV reactor and allowed to be irradiated for approximately 14 hrs. Residue was added to water (100 mL) and extracted with diethyl ether. Organic layer was washed with aqueous sodium bicarbonate, water, and brine before being dried over magnesium sulfate. Solvent was removed under reduced pressure and product was obtained as a slightly yellowish viscous liquid 41.463 g, 85%. NMR analysis indicated a mixture with a ratio of vinyl to methylene spacer of approximately1.2:1.8 (vinyl to thioester).

Synthesis of 5.2 (A_xB_y thiol-ene). Lithium aluminum hydride (1.28 g, 33.7 mmol) was added to a flame dried 100 mL three-necked round-bottom flask equipped with a reflux condenser, a magnetic stir bar, and rubber septa. Dry diethyl ether (25 mL) was added to the flask and suspension was heated to reflux for 2 hour. Reaction vessel was cooled and kept at 0 °C for 5 minutes before compound **5.1** (8.542 g) was added dropwise via a syringe. Reaction was stirred overnight before poured onto ice. Aqueous layer was acidified and extracted with diethyl ether. Organic layers were combined and washed with water and brine before drying over magnesium sulfate. Solvent was evaporated to give product as a clear liquid 4.1 g. NMR analysis indicated a mixture with a ratio of vinyl to thiol of approximately 1.2:1.8 (vinyl to thiol).

Synthesis of 5.3 (A_2B_2 thioester). 1,3,5,7-tetramethylcyclo-tetrasiloxane (30.145 g, 87.5 mmol, 1.0 eq.) and thiolacetic acid (12.5 mL, 175.4 mmol, 2.0 eq.) were added to a large quartz test tube. The test tube was placed in a UV reactor and allowed to be irradiated for approximately 6 hrs. Residue was added to water (100 mL) and extracted with diethyl ether. Organic layer was washed with aqueous sodium bicarbonate, water and brine before being dried over magnesium sulfate. Solvent was removed under reduced pressure and product was obtained as a slightly yellowish viscous liquid 39.5 g, 91%. NMR analysis indicated a mixture with a ratio of vinyl to methylene spacer a distribution of 1:1 (vinyl to thioester).

Synthesis of 5.5 (A_xB_y thioester). Tris(vinyldimethylsiloxy)methylsilane (10.4 g, 30.1 mmol) and thioacetic acid (3.8 mL, 53 mmol) were added to a large quartz test tube. The test tube was placed in a UV reactor and allowed to be irradiated for approximately 14 hrs. Residue was added to water (100 mL) and extracted with diethyl ether. Organic layer was washed with, aqueous sodium bicarbonate, water and brine before being dried over magnesium sulfate. Solvent was removed under reduced pressure and product was obtained as a slightly yellowish viscous mixture 12.742 g, 88%. NMR analysis indicated product as a mixture with a ratio of vinyl to methylene spacer of approximately 1.2:1.8 (vinyl to thioester).

Synthesis of 5.6 (A_xB_y thiol-ene). Lithium aluminum hydride (3.31 g, 87.3 mmol) was added to a flame dried 500 mL three-necked round-bottom flask equipped with a reflux condenser, a magnetic stir bar, and rubber septa. Dry diethyl ether (250 mL) was added to the flask and suspension was heated to reflux for 2 hour. Reaction vessel was cooled and kept at 0 °C for 5 minutes before compound **5.5** (5.013 g) was added dropwise via a syringe. Reaction was stirred overnight before poured onto ice. Aqueous layer was acidified and extracted with diethyl ether. Organic layers were combined and washed with water and brine before drying over magnesium sulfate. Solvent was evaporated to give product as a clear liquid. Product was obtained as a mixture with a ratio of vinyl to thiol of approximately 1.2:1.8 (vinyl to thiol).

Preparation of benzyl(4-bromophenyl)sulfane. Sodium hydride (60% in oil, 0.60 g, 15 mmol, 1.3 eq.) and freshly distilled THF (100 mL) was added to a flame dried 250 mL round bottom flask and cooled to 0 °C. 4-bromo-thiophenol (2.105 g, 11.1 mmol, 1.0 eq.) was added very slowly via a syringe. Reaction was stirred at 0 °C for 30 minutes before benzyl bromide (1.5 mL, 12.5 mmol, 1.1 eq.) was added dropwise. Reaction was removed from ice bath and heated in an oil bath at 60 °C overnight. Reaction was cooled to 0 °C before residue was carefully poured into chilled water (100 mL). Saturated aqueous ammonium chloride (100 mL) was added. The solution was extracted with diethyl ether and washed with water and then brine before being dried over magnesium sulfate. Solvent was removed under reduced pressure and product isolated as an off white solid 1.913 g, 62%, MP = 61-63 °C. ^{1}H NMR (400 MHz, $CDCl_3$): δ 7.519–7.541 (m, 2H), 7.238–7.288 (m, 3H), 7.174–7.196 (m, 2H), 6.943–6.963 (m, 2H), 4.020 (app. m, 2H). ^{13}C-NMR (100 MHz, $CDCl_3$): δ 141.753, 131.939, 130.295, 128.517, 128.487, 128.368, 125.965, 125.540, 63.310. IR (neat): 3063, 3040, 2846, 1340, 1183, 917 (weak), 2921, 1434, 1239, 1112, 1025, 1003 (medium), 1493, 1473, 1454, 1386, 1089, 1070, 807, 780, 710, 696 cm^{-1} (strong). HRMS (CI+, $[M-1]^+$ calcd. for $C_{13}H_{11}SBr$ = 277.9765, found = 277.9761).

Preparation of (4-(benzylthio)phenyl)trivinylsilane. Magnesium turnings (0.094 g, 3.9 mmol, 1.0 eq.) and distilled THF (20 mL) were added to a flame dried 100 mL round bottom flask. Benzyl(4-bromophenyl)sulfane (1.05 g, 3.8 mmol, 1.0 eq.) was dissolved in THF (20 mL) in a flame dried 50 mL conical shaped flask before being slowly added via syringe to the reaction vessel containing the magnesium. A heat gun was used to bring the reaction to refluxing conditions and allowed to stir for 3 hrs. Trivinylchlorosilane (0.72 g, 4.9 mmol, 1.3 eq.) was slowly added via syringe into the reaction flask. Upon completion of addition, reaction was stirred overnight. The reaction was cooled in an ice bath and dilute aqueous HCl was slowly added until mixture was slightly acidic. Product was extracted with diethyl ether, washed with water and brine before dried over magnesium sulfate. Solvent was removed under reduced pressure. No yield quoted as compound was impure by NMR. HRMS (CI+, $[M]^+$ calcd. for $C_{19}H_{20}SSi$ = 308.1055, found = 308.1050).

Preparation of 4-(trivinylsilyl)benzenethiol, AB_3. Freshly ground magnesium turnings (0.11 g, 4.6 mmol, 1.0 eq.) and distilled THF (15 mL) was added to a flame dried 50 mL three necked round bottom flask. Trivinylchlorosilane (0.82 g, 5.6 mmol, 1.2 eq.) was slowly added dropwise. 4-bromo-thiophenol (1.08 g, 5.7 mmol, 1.2 eq.) was dissolved in 5 mL of dry THF and slowly added via syringe. A heat gun was used to bring the reaction to refluxing conditions. Let reaction stir overnight. Cool the reaction in an ice bath and slowly add dilute aqueous HCl until mixture is slightly acidic. Extract with diethyl ether, wash with water and brine before drying the organic layer over magnesium sulfate. Solvent was removed under reduced pressure. No yield quoted as product was impure and observed to crosslink by NMR. HRMS (CI+, $[M-1]^+$ calcd. for $C_{12}H_{13}SSi$ = 217.0507, found = 217.0509).

Spincoating of asymmetrically-substituted thiol-ene-based monomer. Silicon wafers were first cleaned with acetone and IPA and then adhesion promoter AP410 was spincoated to a thickness of about 10 nm. A drop of either 5.2 or 5.6 was dispensed onto the wafer and spin-coated at approximately 2000 rpm for 30 s. Film thicknesses were determined by ellipsometry. It was observed that evaporation occurred as the thickness of the films decreased over time, and uneven surfaces resulted from spincoating for longer durations.

Chapter 6: Surfactant Effect on S-FIL Adhesion

6.1 INTRODUCTION TO SURFACE TREATMENT AND MODIFICATION

While SFIL has many advantages over traditional optical lithography, one concern unique to imprint lithography is the fouling of templates. Template fouling is an adverse occurrence that has been studied in great detail [1-3] and can be very costly in terms of system downtime, defective imprints, and template removal and cleaning. Template contamination occurs when the template is separated after curing of the imprint resist. In order for template separation to take place, a crack must propagate at the interface of the resist film [4]. Figure 6.1 illustrates three different outcomes resulting from the separation of two interfaces.

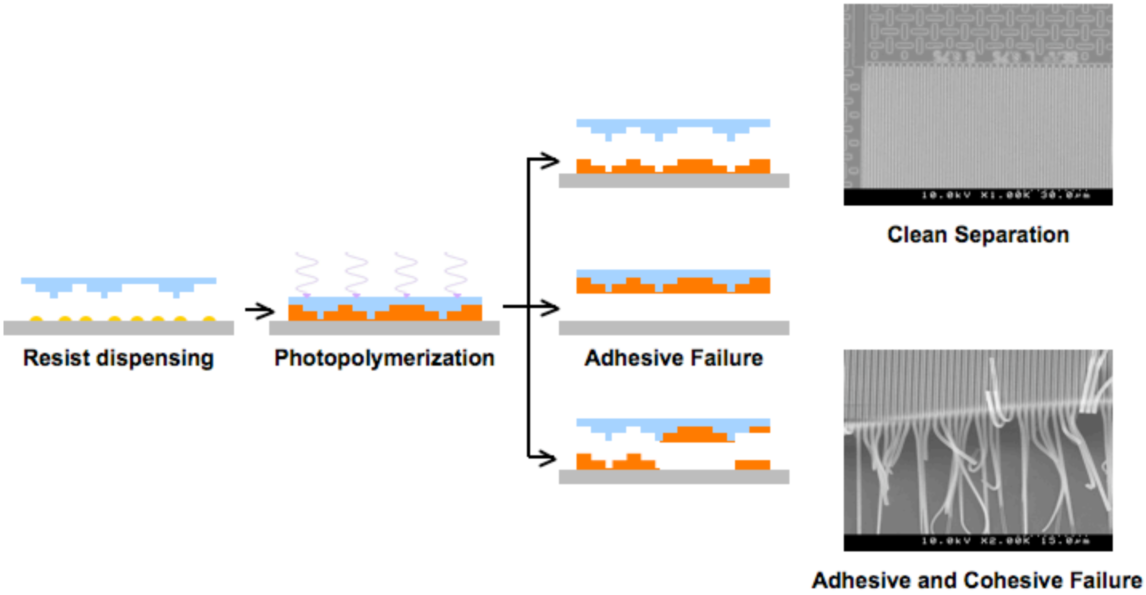

Figure 6.1: Three possible outcomes from template and resist separation [5].

In order to obtain a clean separation without defects or template fouling, forces required for the crack to propagate at the interface must be lower than the forces holding the resist to the substrate. On the other hand, if the force for separation is greater than the adhesion of the resist to the substrate, a complete lift-off from the substrate can occur. Cohesive failure due to separation forces being greater than the cohesive forces in the cured resist lead to partial pattern transfer. This type of defect can be very small and hard to observe.

It is well understood what criteria must be met in order to facilitate the separation of the template from an imprinted resist pattern. However, there are very few known materials and solutions that meet such criteria. One approach to improving separation is to treat the substrate with a material that facilitates and increases the adhesion of the resist to the substrate. Such materials are designed to accommodate a variety of formulations and types of resists (organic, inorganic, etc.), although only a few are commercially available. Nevertheless, while this addresses the issue of adhesion to the substrate, it does not aid in template separation. The second solution is to treat the template with a material that facilitates release and decreases adhesion of the resist to the template [6]. To date, the best material is (tridecafluoro-1,1,2,2-tetrahydrooctyl)dimethylchlorosilane, which forms a Fluorinated Self Assembled Monolayer (FSAM) on the surface [7]. Both of these treatments can be seen in Figure 6.2. Note that the FSAM is covalently bound to the surface of the template [2], while the adhesion promoter layer interacts with the substrate through van der Waals forces.

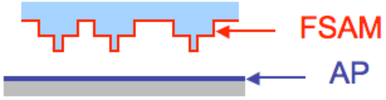

Figure 6.2: Illustration of surface treatment promoting adhesion (AP) to substrate and release from template (FSAM).

The adhesion layer in Figure 6.2 can be designed in a way so as to provide multiple functions including adhesion promoter and etch barrier. The release agent only needs to lower the adhesive forces of the template. While this design seemingly has its advantages, it has been observed that surface treatments degrade over time [8] and need to be replaced. Causes of degradation include: mechanical failure from physical contact and separation of the resist (at which point chain entanglement may occur [9]), chemical degradation upon exposure to UV radiation, and / or reactive species such as radicals that are generated under exposure [10].

Initially it was thought that adding a surfactant to the imprint resist in order to facilitate clean separation could slow degradation [4]. It has been shown that fluorinated materials migrate to certain boundaries based on interaction parameters of different molecules [11]. This has been illustrated both experimentally and in theory [11, 12]. This phenomenon is shown in Figure 6.3.

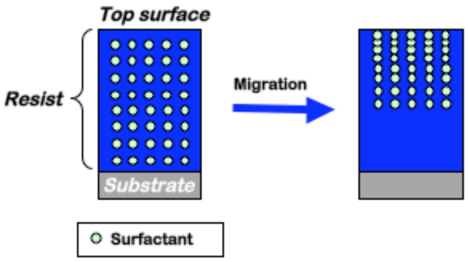

Figure 6.3: Possible migration of fluorinated materials to the resist / air- or template interface.

Ideally, a fluorinated layer forms at the interface between the template and the resist as this facilitates clean and easy template separation. This lowers the surface energy without affecting the overall bulk properties of the film. In addition, it lowers the interaction of the FSAM layer and the polymer resist allowing for slower degradation of the template treatment [4].

To test the hypothesis of a surfactant migrating in an imprint resist, Lin *et al.* tested two different molecules [4]. These molecules are shown in Figure 6.4. The gradient that is expected is illustrated in green and dark green indicates a higher concentration of the surfactant. As anticipated, migration occurs and the process is explained in the experimental section below [3, 4, 7].

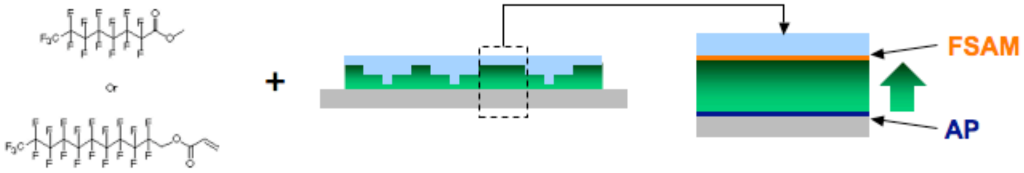

Figure 6.4: Two surfactants added to resist formulations to facilitate template separation. As it migrates towards the template-resist interface, a concentration gradient develops in the film [5].

The idea of replenishing the degraded FSAM layer was developed a few years ago by Michael Lin, a former member of the Willson group. This process was termed “Self Replenishing Fluorinated Self Assembling Monolayer” (SeRFSAM). The concept is illustrated in Figure 6.5.

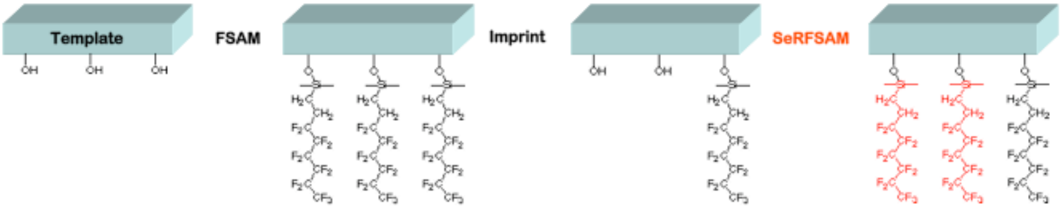

Figure 6.5: Pretreatment of the template and degradation while imprinting. SeRFSAM could be a solution as it replenishes the degraded FSAM [5].

Specifically, the template is first treated to form the FSAM layer. This layer eventually wears down causing defects after multiple imprints. However, imprinting can continue uninterrupted if a fluorinated species is added to the imprint resist. This fluorinated species can migrate toward the low surface energy FSAM layer to repair the release layer in the degraded regions of the template surface treatment.

The criteria that a SeRFSAM material must meet are described in Table 6.1.

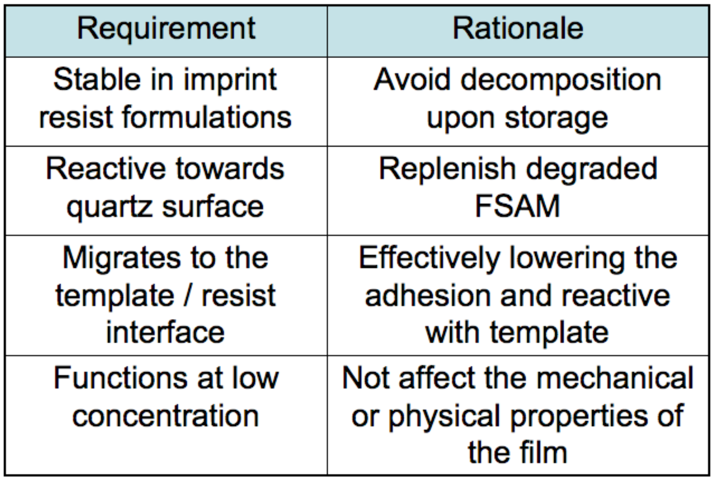

Requirement	Rationale
Stable in imprint resist formulations	Avoid decomposition upon storage
Reactive towards quartz surface	Replenish degraded FSAM
Migrates to the template / resist interface	Effectively lowering the adhesion and reactive with template
Functions at low concentration	Not affect the mechanical or physical properties of the film

Table 6.1: Criteria for replenishing surface materials.

6.2 EXPERIMENTAL

All materials for imprint formulations and methyl perfluorooctanoate were purchased from Sigma-Aldrich and used without further purification. FSAM (tridecafluoro-1,1,2,2-tetrahydrooctyl) dimethylchlorosilane was purchased from Gelest Inc. F-Silazane was obtained from Central Glass Co., Ltd. Silicon wafers were purchased from Silicon Quest International, Inc. AP410 was purchased from Silicon Resources and Darocur® 1173 was purchased from Ciba Specialty Chemicals. Exposures were carried out under a UV cut off filter lighting before photopolymerization of imprint resist. XPS analysis was carried out at the Texas Materials Institute. Imprinting was carried out in a cleanroom at the Microelectronics Research Center (MER) at The University of Texas at Austin.

6.2.1 Materials

As previously mentioned, several different materials have been screened for use as surfactants or additives to replace degraded FSAM. It was shown that a fluorinated, non-reactive material (methyl perfluorooctanoate) assists in the separation of the template from the resist polymer by lowering the adhesive forces after photopolymerization [4]. However, the problem of FSAM degradation still exists, which eventually leads to defects; unreactive additives do very little to prevent this. To overcome the degradation problem, a new material was developed to replenish the FSAM layer at exposed areas, two of which are described below [5].

6.2.2 Stability in Imprint Formulation

For a SeRFSAM to be useful, it must be stable in the imprint formulation. The compatibility and stability was evaluated by GC/MS (Agilent Technologies 6890N equipped with an Agilent HP-5MS capillary column and an Agilent 5973N Mass Selective Detector). Imprint formulations were prepared and two such formulations consisting of two possible SeRFSAM are shown in Table 6.2 [5].

	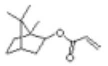	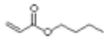	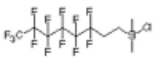	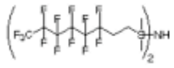
17%	**33%**	**33%**	**17%**	**0%**
17%	**33%**	**33%**	**0%**	**17%**

Table 6.2: Imprint formulations for GC analysis. An increased loading of SeRFSAM simplifies the observation of decomposition taking place [5].

Additive concentrations were tested as a function of time in order to observe whether decomposition occurs. Results indicate that FSAM decomposes upon storage in the imprint formulations, and is unsuitable as a SeRFSAM. However, no noticeable change was observed in the formulations containing F-Silazane.

6.2.3 Surface Analysis

F-Silazane successfully passed the stability test, so the water contact angle was measured to compare the surface energy to that of FSAM. The first step was to clean the surface by treating a one square inch glass plate with piranha solution[2] (2:1 ratio of concentrated sulfuric acid and 30 wt.% hydrogen peroxide in water) for 30 minutes followed by a thorough DI water rinse. A gentle stream of nitrogen gas was used to remove residual water droplets. The glass plate was then immersed in a toluene solution with 20 wt.% of the surface treatment material for 100 minutes then rinsed with toluene and dried with a gentle stream of nitrogen gas. The water contact angle was measured on a goniometer (Ramé-Hart m100). Control samples were only exposed to the piranha solution, rinsed thoroughly with DI water, and then immersed in toluene, which left the surface very hydrophilic as indicated by the water contact angle shown in Figure 6.6.

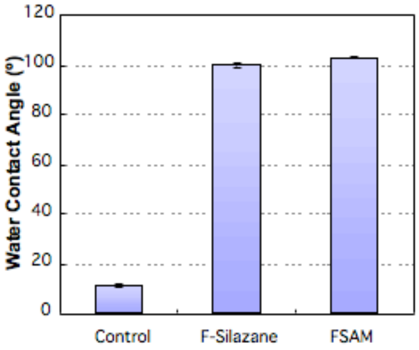

Figure 6.6: Water contact angle of FSAM and SeRFSAM treated quartz surfaces. Control surface is only exposed to a rigorous cleaning process and an Oxygen RIE [5].

---

[2] Extreme caution must be taken when mixing and handling piranha solution as it is an extremely dangerous substance. It is recommended that a thick chemical apron, goggles, and a face shield be used, along with heavy-duty long sleeved gloves to avoid any skin exposure [13] http://www.stanford.edu/dept/EHS/prod/researchlab/lab/safety_sheets/08-111.pdf. **2011.**

As expected, the contact angle of FSAM indicates a hydrophobic surface (highest contact angle, and as shown, SeRFSAM treatment generates a similar hydrophobic surface.

6.2.4 Elemental Analysis by XPS

X-ray photoelectron spectroscopy (XPS), also referred to as Electron Spectroscopy for Chemical Analysis (ESCA), is a widely used surface science technique. It allows for an elemental analysis of the surface to a depth of roughly 1-10 nm, which, in general terms, occurs through monochromatic X-ray irradiation of known energy that causes displacement of electrons from the sample surface [14]. The kinetic energies of the ejected electrons are then recorded with an electron spectrometer. The binding energy of the emitted electrons can then be calculated because they function as a fingerprint of the atom and orbital from which they originated. One such spectrum is provided in Figure 6.7 where the analysis for carbon, nitrogen, chlorine, and sulfur was carried out. The area under the peaks can then be integrated and ratios calculated.

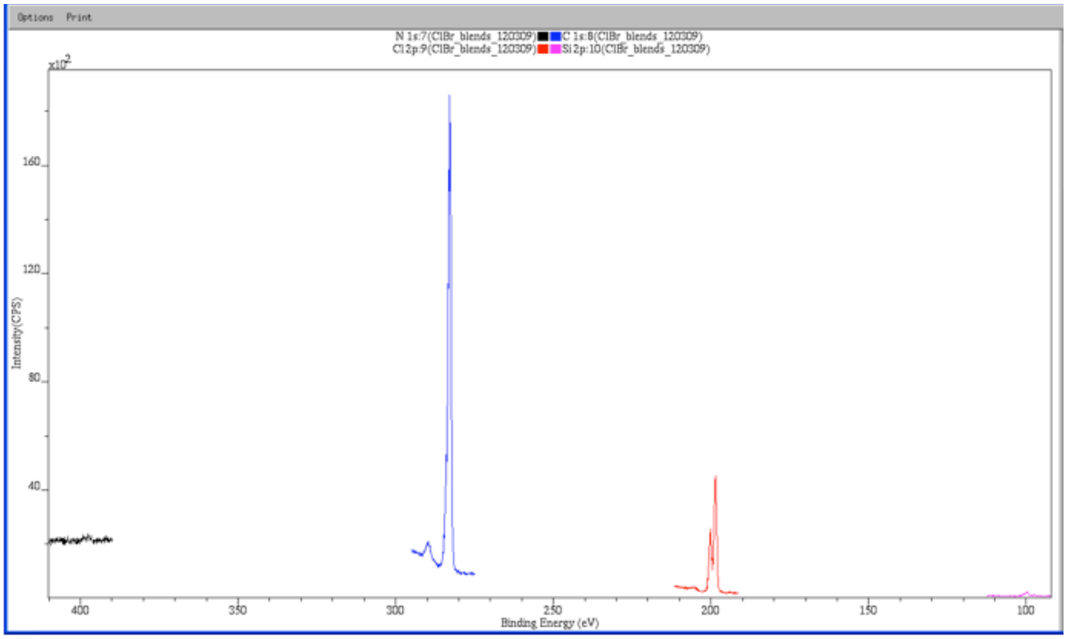

Figure 6.7: XPS spectrum analyzing for nitrogen (black), carbon (blue), chlorine (red), and silicon (pink).

Figure 6.8 illustrates a simplified version of the X-ray incident beam and emitted electrons. The incident angle is normally set to 45°, which corresponds to an analysis depth of approximately 8 nm.

Rotating the sample changes the depth that photons penetrate the surface and thereby the depth from which electrons is emitted yielding a concentration profile.

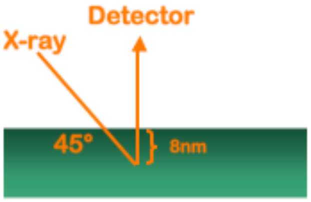

Figure 6.8: Incident X-ray beam angle controls the depth of analysis [15].

Films were prepared by imprinting formulations as illustrated by Table 6.3. The samples were analyzed under ultra high vacuum (10^{-8} Torr) with a Kratos Axis Ultra Photoelectron Spectrometer. An aluminum target was used to generate X-ray photons that were then filtered through a monochromator.

Component	Structure	1	2
EGDA		**37.0**	**36.0**
nBA	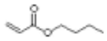	**19.6**	**19.0**
IBA	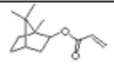	**37.0**	**36.0**
F-silazane	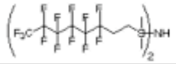	**2.5**	**5.1**
Darocur® 1173	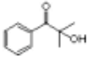	**3.9**	**4.1**

Table 6.3: Imprint formulations for XPS analysis.

In previous experiments conducted by Lin *et al.*, it was found that the unreactive surfactant (methyl perfluorooctanoate) tested was well below the anticipated value [3]. It is believed that the fluorinated molecule‘s vapor pressure was too high, evaporating under the high vacuum conditions in which XPS operates. However, in a separate experiment in which a surfactant (2-(perfluorodecyl)ethyl acrylate) was covalently bound to the polymer film, migration was observed, and a higher concentration of fluorine was located by the resist-air interface rather than in the bulk of the material as seen in Figure 6.9 [3].

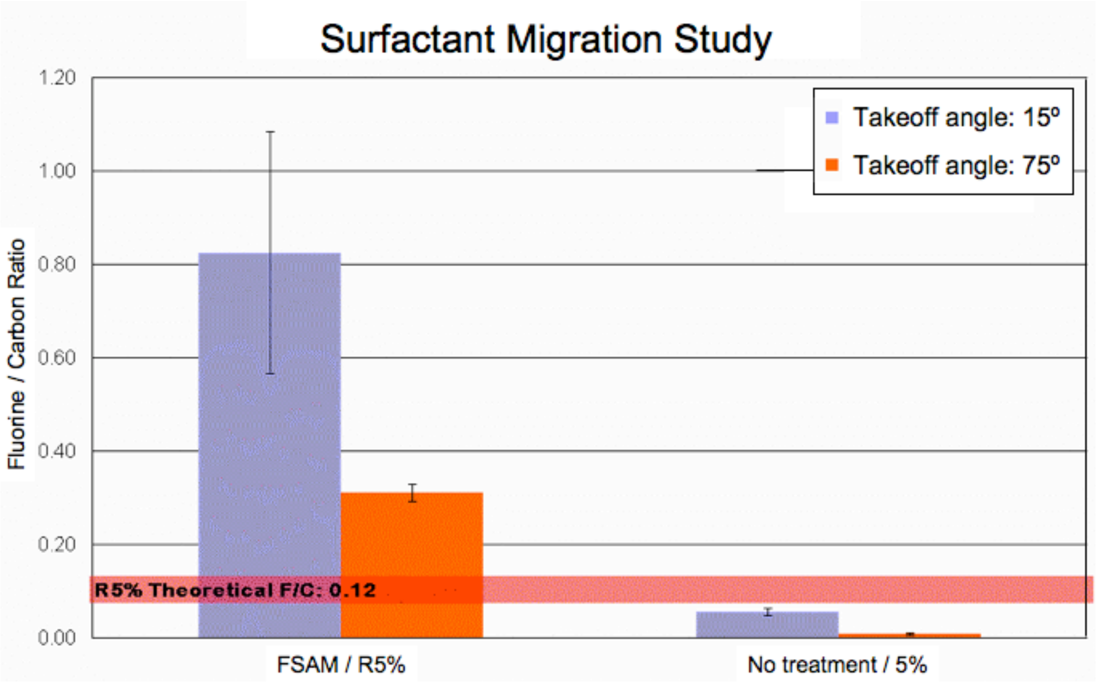

Figure 6.9: Illustrates the migration and inclusion of a fluorinated surfactant into the resist surface [4] (Courtesy of Dr. M. Lin).

Several films of two different compositions containing fluorinated silazane were prepared and analyzed by XPS. The results are illustrated in Figure 6.10.

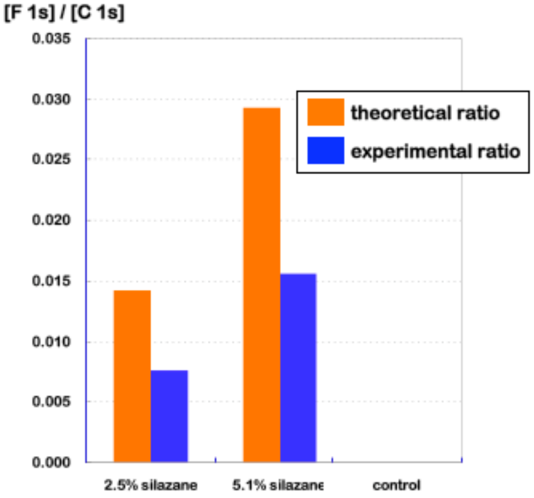

Figure 6.10: XPS data for a non-covalently bonded surfactant illustrates the lower than anticipated F/C ratio.

While F-Silazane has higher molecular weight and lower vapor pressure than previously tested materials, the presence of fluorine was well below the expected ratio in all of the samples similar to what Lin *et al.* discovered. It is believed that, while migration may take place of set fluorinated molecules, evaporation of non-covalently bound molecules causes the lower than anticipated ratio in the film (shown in Figure 6.11).

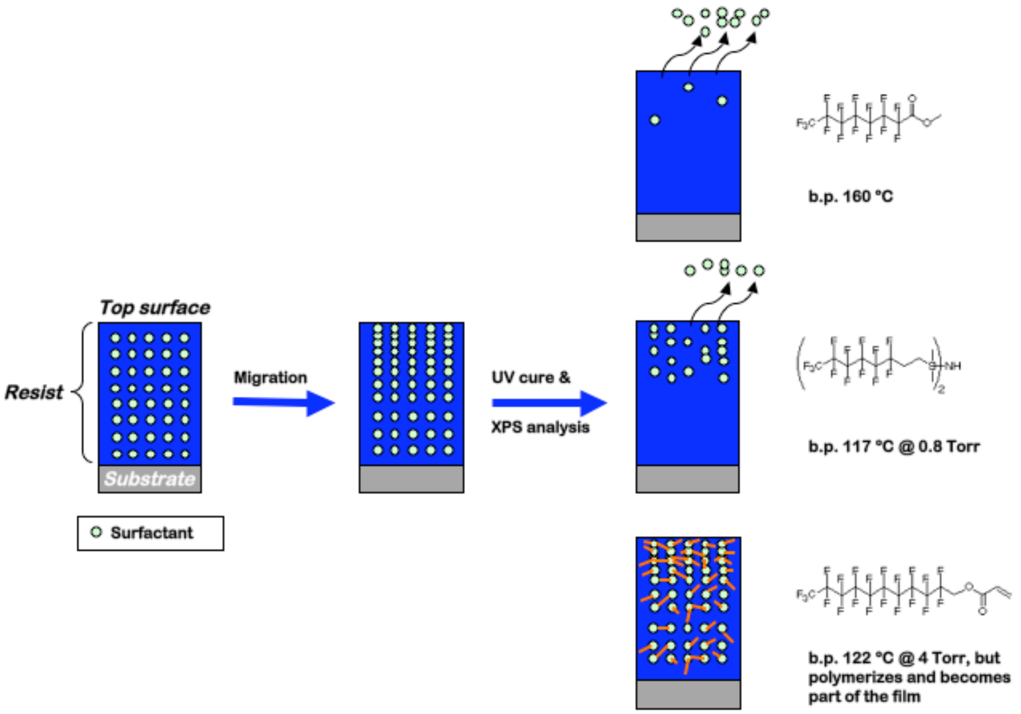

Figure 6.11: Migration of surfactant towards the surface. The high vacuum exerted by the XPS instrument can cause the evaporation of smaller molecules.

In order to confirm the migration for non-covalently bound species, it is evident that either a low-vacuum method for analysis has to be employed or a completely different technology must be used.

6.2.5 Multiple Imprint Study

After completing all analytical experiments, the material was tested in an imprint study. The study was carried out on an Imprio 100 (Molecular Imprints, Inc.) installed at The University of Texas at Austin. Non-patterned 25 mm^2 mesa templates were used after they had been cleaned and pre-treated with FSAM. Bare silicon substrates were cleaned and then coated with BT20 (Brewer Science, USA) as an adhesion-promoter layer. Water contact angles were used to verify template surface uniformity. The formulations depicted in Table 6.4 were used in these experiments.

	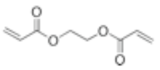	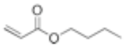	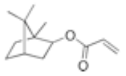	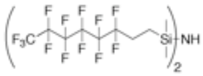	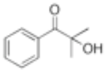
Formulation 1	**19.8 %**	**38.0 %**	**38.2 %**	**0 %**	**4.0 %**
Formulation 2	**19.8 %**	**35.4 %**	**35.4 %**	**5.1 %**	**4.0 %**

Table 6.4: Two resist formulations tested in a multiple imprint experiment [5].

It is clear that the control formulation caused a significantly faster degradation of the FSAM layer on the imprint as the quality of the imprinted images worsened to the point that no more imprints could be carried out. However, as Figure 6.12 illustrates, the SeRFSAM addition to the resist formulation did not cause the release layer to degrade to any noticeable degree. The water contact angle stayed fairly constant above 90°.

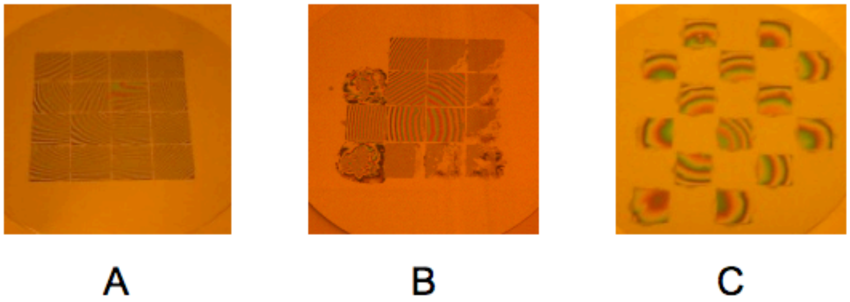

Figure 6.12: Confirming F-Silazanes characteristics of replenishing the degraded FSAM in a multiple imprint study [5]. A and B are images of SeRFSAM free formulation taken after 50 and 80 imprints respectively, whereas C contains F-Silazane and was taken after 100 imprints.

6.3 RESULTS AND CONCLUSIONS

F-Silazane shows promise as a candidate for SeRFSAM. It behaves similarly to FSAM, but is also miscible and stable in imprint formulations. Although the XPS and ATR-IR experiments were inconclusive, it is believed that the silazane undergoes a migration towards the air or template interface and minimizes the unfavorable interaction between the fluorinated SeRFSAM and the remainder of the resist components. The multiple imprint study demonstrates much slower degradation.

6.4 FUTURE WORK

A replenishing material has been demonstrated. However, it has not directly been confirmed that migration takes place and that there is a concentration gradient in the bulk of the material. Currently, instruments capable of carrying out elemental analysis of a surface under ambient conditions are available. Some of these instruments also have the ability to etch away at the surface and, if our hypothesis stands true, a gradient could be observed. Additionally, a much longer imprint study must also be carried out in order to test the capability of the SeRFSAM. The SeRFSAM works well for 100 imprints in MonoMat, but should be tested to failure, and the stability in other imprint formulations must be verified, especially in DPD formulations. Lastly, as the loading of SeRFSAM is fairly low, additives remain in the film after curing and will cause changes in physical and chemical properties. Full materials characterization of the imprinted films must be carried out in order to determine whether physical and/or chemical properties are altered beyond acceptable limits.

6.5 REFERENCES

[1] K. Wu, X. Wang, E. K. Kim, C. G. Willson and J. G. Ekerdt. "Experimental and Theoretical Investigation on Surfactant Segregation in Imprint Lithography". *Langmuir,* 23, 1166-1170, 2007.

[2] T. Bailey, B. J. Choi, M. Colburn, M. Meissl, S. Shaya, J. G. Ekerdt, S. V. Sreenivasan and C. G. Willson. "Step and flash imprint lithography: Template surface treatment and defect analysis". *J. Vac. Sci. Technol. B,* 18, 3572-3577, 2000.

[3] M. W. Lin, D. J. Hellebusch, K. Wu, E. K. Kim, K. Lu, L. Tao, K. M. Liechti, J. G. Ekerdt, P. S. Ho, W. Hu and C. G. Willson. "Interfacial adhesion studies for step and flash imprint lithography". *SPIE*, 6921, Emerging Lithographic Technologies XII, 2008.

[4] M. W. Lin. "Simulation and Design of Planarizing Materials and Interfacial Adhesion Studies for Step and Flash Imprint Lithography". *Ph.D. University of Texas at Austin,* 2008**.**

[5] T. Ogawa, D. J. Hellebusch, M. W. Lin, B. M. Jacobsson, W. Bell and C. G. Willson. "Reactive fluorinated surfactant for step and flash imprint lithography". *SPIE*, 7970, Alternative Lithographic Technologies III, 2011.

[6] E. G. Shafrin and W. A. Zisman. "Constitutive Relations in the Wetting of Low Energy Surfaces and the Theory of the Retraction Method of Preparing Monolayers". *J. Phys. Chem.,* 64, 519-524, 1960.

[7] M. W. Lin, D. J. Hellebusch, K. Wu, E. K. Kim, H. L. Kuan, K. M. Liechti, J. G. Ekerdt, P. S. Ho and C. G. Willson. "Role of surfactants in adhesion reduction for step and flash imprint lithography". *Journal of Micro/Nanolithography, MEMS and MOEMS,* 7, 033005, 2008.

[8] D. Truffier-Boutry, A. Beaurain, R. Galand, B. Pelissier, J. Boussey and M. Zelsmann. "XPS study of the degradation mechanism of fluorinated anti-sticking treatments used in UV nanoimprint lithography". *Microelectronic Engineering,* 87, 122-124, 2010.

[9] T. C. Bailey. "Imprint Template Advances and Surface Modification, and Defect Analysis for Step and Flash Imprint Lithography". *Ph.D. University of Texas at Austin,* 2003**.**

[10] S. Garidel, M. Zelsmann, N. Chaix, P. Voisin, J. Boussey, A. Beaurain and B. Pelissier. "Improved release strategy for UV nanoimprint lithography". *Journal of Vacuum Science and Technology B,* 25, 2430-2434, 2007.

[11] K. Wu. "Interface Study for Template Release in Step and Flash Imprint Lithography". *Ph.D. Dissertation, The University of Texas at Austin,* 2006**.**

[12] M. Bender, M. Otto, B. Hadam, B. Spangenberg and H. Kurz. "Multiple imprinting in UV-based nanoimprint lithography: related material issues". *Microelectronic Engineering,* 61-62, 407-413, 2002.

[13] http://www.stanford.edu/dept/EHS/prod/researchlab/lab/safety_sheets/08-111.pdf. **2011.**

[14] D. A. Skoog, F. J. Holler and T. A. Nieman. "Principles of Instrumental Analysis"; 5 Ed.; Brooks Cole; 1997.

[15] M. W. Lin. Personal Communication. 2008.

Appendix A: MALDI of Q_8^{OSiH}

A.1 MATRIX ASSISTED LASER DESORPTION/IONIZATION OF Q_8^{OSiH}

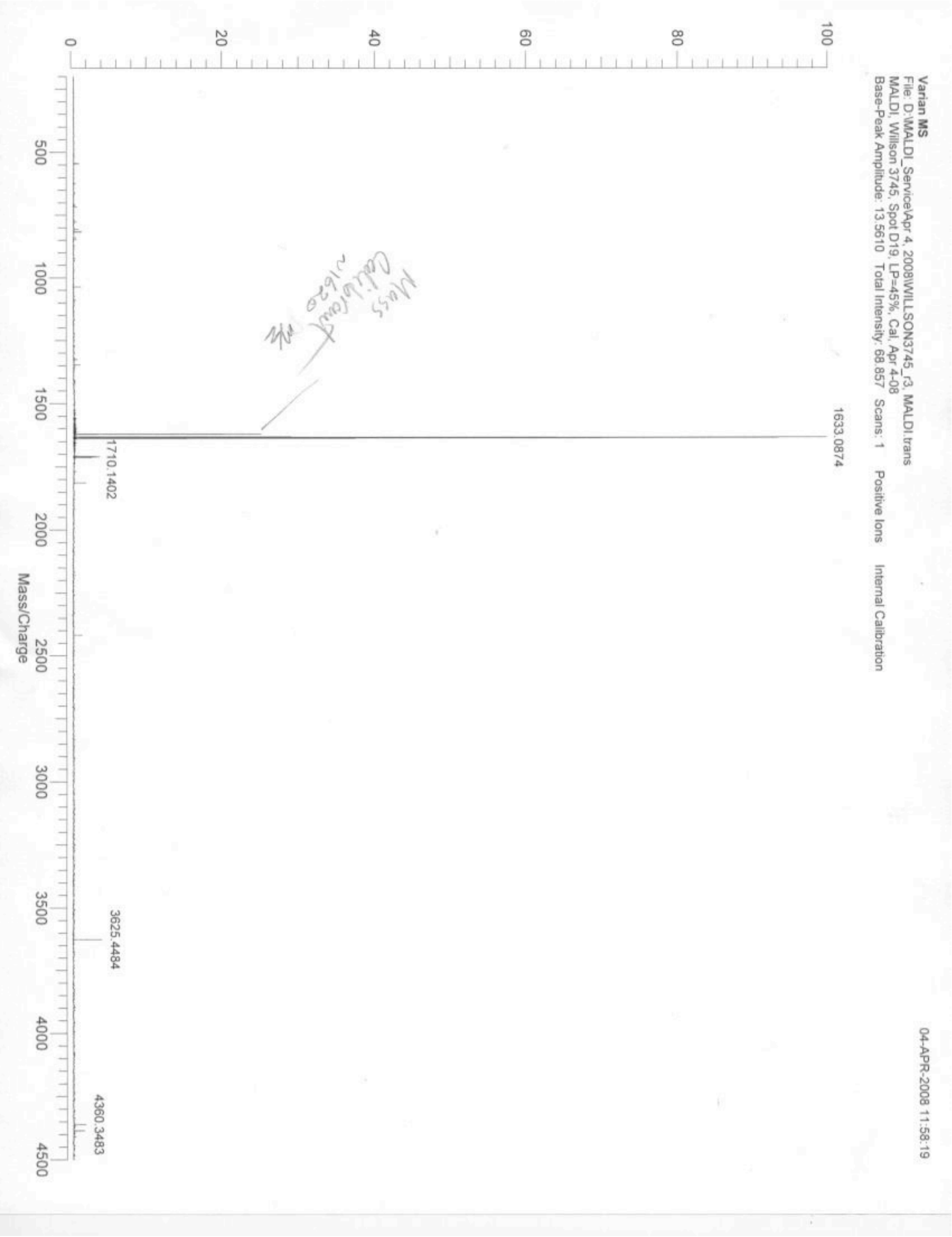

Figure A.1: MALDI spectra of fully substituted Q_8^{OSiH}.

Appendix B: *p*-Tolyl-POSS X-ray Crystal Analysis

B.1 Crystal Information

Figure B.1: ORTEP diagram of the cube shaped *p*-tolyl-POSS.

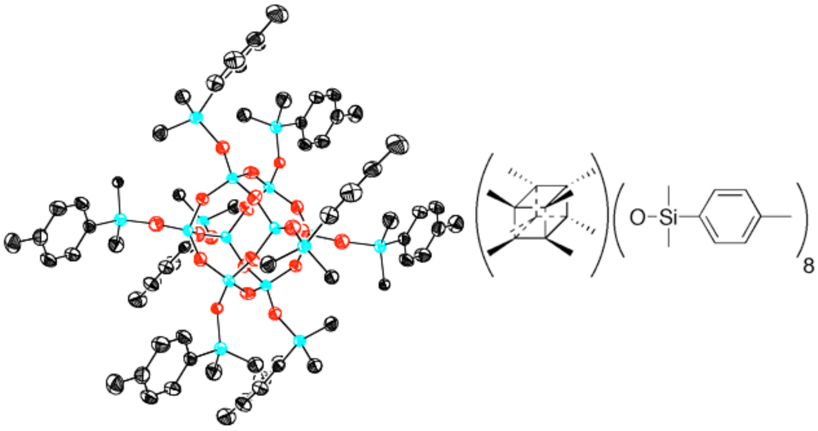

X-ray Experimental for $C_{72}H_{104}Si_{16}O_{20}$: Crystals grew as colorless, cube shaped prisms by precipitating from 1,3-bis(*p*-tolyl)-1,1,3,3-tetramethyldisiloxane. The data crystal had approximate dimensions; 0.24 x 0.22 x 0.16 mm. The data were collected on a Nonius Kappa CCD diffractometer using a graphite monochromator with MoKa radiation (1 = 0.71073 Å). A total of 520 frames of data were collected using w-scans with a scan range of 1.2° and a counting time of 74 seconds per frame. The data were collected at 153 K using an Oxford Cryostream low temperature device. Details of crystal data, data collection and structure refinement are listed in Table B.1. Data reduction were performed using DENZO-SMN [1]. The structure was solved by direct methods using SIR97 [2] and refined by full-matrix least-squares on F^2 with anisotropic displacement parameters for the non-H atoms using SHELXL-97 [3]. Structure analysis was aided by use of the programs PLATON98 [4] and WinGX [5]. The hydrogen atoms were observed in a ΔF map and refined with isotropic displacement parameters.

The initial unit cell assignment showed the c-axis to be 7.693 Å or ½ the value reported here. The cell volume with the 7.693 Å axis is too small to contain the octasilicate silane. Solution of the structure resulted in a highly disordered silane that had all the substituents of the target molecule. Further analysis of the raw data revealed highly diffuse scattering halfway along the 7.693 Å axis, indicating that the true cell length should be doubled. The stacking of the molecule and its geometry resulted in highly diffuse scattering for hkl reflections where l is odd in the 15.386 Å cell. The structure was refined using only those reflections where l is even. The net effect of this strategy is that the calculated data completeness is only 50%.

The function, $\Sigma w(|F_O|^2 - |F_C|^2)^2$,was minimized, where $w = 1/[(s(F_O))^2 + (0.0543*P)^2 + (2.0523*P)]$ and $P = (|F_O|^2 + 2|F_C|^2)/3$. $R_W(F^2)$ refined to 0.112, with R(F) equal to 0.0434 and a goodness of fit, S, = 1.03. Definitions used for calculating R(F),$R_W(F^2)$ and the goodness of fit, S, are given below. The data were corrected for secondary extinction but no correction was necessary. Neutral atom scattering factors and values used to calculate the linear absorption coefficient are from the International Tables for X-ray Crystallography (1992) [6]. All figures were generated using SHELXTL/PC [7]. Tables of positional and thermal parameters, bond lengths and angles, torsion angles and figures are found elsewhere.

Table B.1: Crystal data and structure refinement for B.1.

Empirical formula	C72 H104 O20 Si16
Formula weight	1738.99
Temperature	153(2) K
Wavelength	0.71075 Å

Crystal system	Triclinic	
Space group	P-1	
Unit cell dimensions	a = 12.5575(5) Å	α= 75.734(2)°.
	b = 12.7807(5) Å	β= 74.746(2)°.
	c = 15.3862(7) Å	γ = 86.369(2)°.
Volume	2308.92(17) Å^3	
Z	1	
Density (calculated)	1.251 Mg/m^3	
Absorption coefficient	0.282 mm^{-1}	
F(000)	920	
Crystal size	0.24 x 0.22 x 0.16 mm	
Theta range for data collection	2.35 to 27.45°.	
Index ranges	-16<=h<=16, -16<=k<=16, -18<=l<=18	
Reflections collected	9918	
Independent reflections	5237 [R(int) = 0.0226]	
Completeness to theta = 27.45°	49.7 %	
Absorption correction	Semi-empirical from equivalents	
Max. and min. transmission	1.00 and 0.93	
Refinement method	Full-matrix least-squares on F^2	
Data / restraints / parameters	5237 / 691 / 421	
Goodness-of-fit on F^2	1.030	
Final R indices [I>2sigma(I)]	R1 = 0.0434, wR2 = 0.1046	
R indices (all data)	R1 = 0.0595, wR2 = 0.1123	
Largest diff. peak and hole	0.376 and -0.285 e.Å^{-3}	

Table B.2: Atomic coordinates (x 10^4) and equivalent isotropic displacement parameters (Å^2 x 10^3) for B.1. U(eq) is defined as one third of the trace of the orthogonalized U^{ij} tensor.

	x	y	z	U(eq)

Si1	3228(1)	5462(1)	6257(1)	21(1)
Si2	4506(1)	3297(1)	6468(1)	21(1)
Si3	6706(1)	4548(1)	5770(1)	21(1)
Si4	5430(1)	6715(1)	5559(1)	21(1)
O1	3646(2)	4261(2)	6637(2)	34(1)
O2	5731(2)	3703(2)	6360(2)	32(1)
O3	6275(2)	5754(2)	5800(2)	32(1)
O4	4190(2)	6316(2)	6104(2)	32(1)
O9	2937(2)	5556(2)	5287(2)	32(1)
O10	4455(2)	2968(2)	5537(2)	32(1)
Si5	1588(4)	5462(3)	8085(3)	26(1)
O5	2152(2)	5724(3)	6972(2)	34(1)
C1	2631(4)	5699(4)	8661(3)	40(1)
C2	1130(5)	4048(4)	8463(5)	40(1)
C3	453(7)	6449(7)	8224(11)	34(2)
C4	-547(9)	6209(9)	8891(10)	33(2)
C5	-1368(10)	6971(8)	8993(11)	39(2)
C6	-1199(11)	8036(8)	8506(11)	35(2)
C7	-186(11)	8304(9)	7887(10)	46(3)
C8	638(10)	7538(8)	7762(10)	39(3)
C9	-2048(11)	8912(10)	8648(12)	50(3)
Si6	4530(2)	1653(3)	8302(2)	26(1)
O6	4230(4)	2266(2)	7301(3)	34(1)
C10	4300(4)	2665(3)	8995(3)	40(1)
C11	5958(4)	1193(4)	8038(5)	40(1)
C12	3494(6)	549(6)	8817(11)	30(2)
C13	2411(6)	671(7)	8715(9)	29(2)
C14	1642(6)	-154(7)	9099(8)	35(2)
C15	1917(8)	-1154(9)	9603(14)	34(2)
C16	2998(7)	-1323(7)	9627(9)	34(2)
C17	3772(8)	-500(7)	9241(10)	33(2)
C18	1058(10)	-2024(10)	10051(13)	52(3)
Si7	8445(4)	4466(3)	6883(3)	26(1)

O7	7737(2)	4301(3)	6174(2)	34(1)
C19	7527(4)	4230(5)	8055(3)	40(1)
C20	9045(5)	5845(4)	6457(5)	40(1)
C21	9539(6)	3415(7)	6811(10)	23(2)
C22	9367(9)	2375(7)	7385(10)	31(2)
C23	10145(10)	1569(8)	7285(10)	36(2)
C24	11149(11)	1755(9)	6620(12)	38(2)
C25	11363(9)	2791(8)	6103(11)	42(2)
C26	10603(9)	3618(9)	6225(11)	38(2)
C27	11991(11)	874(11)	6470(12)	61(4)
Si8	5591(2)	8412(3)	6649(2)	26(1)
O8	5714(3)	7746(2)	5841(2)	34(1)
C28	5834(7)	7518(4)	7679(4)	40(1)
C29	4164(4)	8982(4)	6825(5)	40(1)
C30	6643(6)	9506(6)	6137(10)	28(2)
C31	7754(7)	9297(8)	6127(9)	38(3)
C32	8556(7)	10081(8)	5742(9)	39(2)
C33	8293(9)	11129(9)	5333(15)	37(2)
C34	7239(8)	11312(8)	5233(10)	41(2)
C35	6422(7)	10529(8)	5624(10)	38(2)
C36	9145(11)	12010(9)	4957(12)	50(3)

Table B.3: Bond lengths [Å] and angles [°] for B.1.

Si1-O5	1.579(3)	Si2-O2	1.610(2)
Si1-O9	1.603(2)	Si2-O1	1.610(2)
Si1-O1	1.609(2)	Si3-O7	1.562(3)
Si1-O4	1.611(2)	Si3-O9#1	1.605(3)
Si2-O6	1.578(4)	Si3-O3	1.609(2)
Si2-O10	1.606(2)	Si3-O2	1.609(2)

Si4-O8	1.574(3)	Si6-C12	1.858(5)
Si4-O10#1	1.604(3)	C10-H10A	0.98
Si4-O3	1.609(2)	C10-H10B	0.98
Si4-O4	1.609(2)	C10-H10C	0.98
O9-Si3#1	1.605(3)	C11-H11A	0.98
O10-Si4#1	1.604(3)	C11-H11B	0.98
Si5-O5	1.630(5)	C11-H11C	0.98
Si5-C2	1.837(5)	C12-C13	1.404(6)
Si5-C1	1.840(5)	C12-C17	1.405(5)
Si5-C3	1.848(5)	C13-C14	1.384(6)
C1-H1A	0.98	C13-H13	0.95
C1-H1B	0.98	C14-C15	1.397(6)
C1-H1C	0.98	C14-H14	0.95
C2-H2A	0.98	C15-C16	1.369(6)
C2-H2B	0.98	C15-C18	1.503(6)
C2-H2C	0.98	C16-C17	1.386(6)
C3-C4	1.394(7)	C16-H16	0.95
C3-C8	1.400(7)	C17-H17	0.95
C4-C5	1.377(7)	C18-H18A	0.98
C4-H4	0.95	C18-H18B	0.98
C5-C6	1.382(7)	C18-H18C	0.98
C5-H5	0.95	Si7-O7	1.635(4)
C6-C7	1.378(7)	Si7-C19	1.830(5)
C6-C9	1.511(6)	Si7-C20	1.856(5)
C7-C8	1.388(7)	Si7-C21	1.861(4)
C7-H7	0.95	C19-H19A	0.98
C8-H8	0.95	C19-H19B	0.98
C9-H9A	0.98	C19-H19C	0.98
C9-H9B	0.98	C20-H20A	0.98
C9-H9C	0.98	C20-H20B	0.98
Si6-O6	1.674(4)	C20-H20C	0.98
Si6-C11	1.824(4)	C21-C22	1.396(7)
Si6-C10	1.834(5)	C21-C26	1.400(7)

C22-C23	1.382(7)	C28-H28C	0.98
C22-H22	0.95	C29-H29A	0.98
C23-C24	1.390(7)	C29-H29B	0.98
C23-H23	0.95	C29-H29C	0.98
C24-C25	1.368(7)	C30-C31	1.400(6)
C24-C27	1.512(6)	C30-C35	1.404(6)
C25-C26	1.393(7)	C31-C32	1.375(6)
C25-H25	0.95	C31-H31	0.95
C26-H26	0.95	C32-C33	1.391(6)
C27-H27A	0.98	C32-H32	0.95
C27-H27B	0.98	C33-C34	1.371(6)
C27-H27C	0.98	C33-C36	1.501(6)
Si8-O8	1.642(4)	C34-C35	1.388(6)
Si8-C28	1.796(5)	C34-H34	0.95
Si8-C30	1.862(5)	C35-H35	0.95
Si8-C29	1.869(4)	C36-H36A	0.98
C28-H28A	0.98	C36-H36B	0.98
C28-H28B	0.98	C36-H36C	0.98
O5-Si1-O9	108.21(15)	O7-Si3-O2	110.26(15)
O5-Si1-O1	109.84(16)	O9#1-Si3-O2	109.68(14)
O9-Si1-O1	110.19(14)	O3-Si3-O2	109.24(14)
O5-Si1-O4	110.32(15)	O8-Si4-O10#1	107.79(14)
O9-Si1-O4	108.85(14)	O8-Si4-O3	110.15(14)
O1-Si1-O4	109.40(14)	O10#1-Si4-O3	109.51(14)
O6-Si2-O10	108.49(16)	O8-Si4-O4	110.52(15)
O6-Si2-O2	108.77(19)	O10#1-Si4-O4	109.75(14)
O10-Si2-O2	109.56(14)	O3-Si4-O4	109.10(14)
O6-Si2-O1	111.62(17)	Si1-O1-Si2	148.53(18)
O10-Si2-O1	109.35(14)	Si3-O2-Si2	146.47(17)
O2-Si2-O1	109.03(14)	Si3-O3-Si4	148.96(17)
O7-Si3-O9#1	108.23(15)	Si4-O4-Si1	146.55(17)
O7-Si3-O3	110.05(16)	Si1-O9-Si3#1	150.26(18)
O9#1-Si3-O3	109.37(14)	Si4#1-O10-Si2	150.23(17)

O5-Si5-C2	108.0(3)	C8-C7-H7	119.3
O5-Si5-C1	108.0(3)	C7-C8-C3	121.2(7)
C2-Si5-C1	111.4(3)	C7-C8-H8	119.4
O5-Si5-C3	104.5(5)	C3-C8-H8	119.4
C2-Si5-C3	114.1(4)	C6-C9-H9A	109.5
C1-Si5-C3	110.4(6)	C6-C9-H9B	109.5
Si1-O5-Si5	140.3(3)	H9A-C9-H9B	109.5
Si5-C1-H1A	109.5	C6-C9-H9C	109.5
Si5-C1-H1B	109.5	H9A-C9-H9C	109.5
H1A-C1-H1B	109.5	H9B-C9-H9C	109.5
Si5-C1-H1C	109.5	O6-Si6-C11	108.1(3)
H1A-C1-H1C	109.5	O6-Si6-C10	105.9(3)
H1B-C1-H1C	109.5	C11-Si6-C10	113.0(3)
Si5-C2-H2A	109.5	O6-Si6-C12	103.5(4)
Si5-C2-H2B	109.5	C11-Si6-C12	114.3(4)
H2A-C2-H2B	109.5	C10-Si6-C12	111.1(5)
Si5-C2-H2C	109.5	Si2-O6-Si6	142.7(3)
H2A-C2-H2C	109.5	Si6-C10-H10A	109.5
H2B-C2-H2C	109.5	Si6-C10-H10B	109.5
C4-C3-C8	116.1(6)	H10A-C10-H10B	109.5
C4-C3-Si5	122.9(6)	Si6-C10-H10C	109.5
C8-C3-Si5	120.1(6)	H10A-C10-H10C	109.5
C5-C4-C3	121.5(7)	H10B-C10-H10C	109.5
C5-C4-H4	119.2	Si6-C11-H11A	109.5
C3-C4-H4	119.2	Si6-C11-H11B	109.5
C4-C5-C6	121.6(7)	H11A-C11-H11B	109.5
C4-C5-H5	119.2	Si6-C11-H11C	109.5
C6-C5-H5	119.2	H11A-C11-H11C	109.5
C7-C6-C5	117.4(6)	H11B-C11-H11C	109.5
C7-C6-C9	119.3(8)	C13-C12-C17	115.1(5)
C5-C6-C9	123.3(8)	C13-C12-Si6	122.2(5)
C6-C7-C8	121.5(7)	C17-C12-Si6	122.3(5)
C6-C7-H7	119.3	C14-C13-C12	122.0(6)

C14-C13-H13	119.0	Si7-C20-H20A	109.5
C12-C13-H13	119.0	Si7-C20-H20B	109.5
C13-C14-C15	121.0(6)	H20A-C20-H20B	109.5
C13-C14-H14	119.5	Si7-C20-H20C	109.5
C15-C14-H14	119.5	H20A-C20-H20C	109.5
C16-C15-C14	117.7(5)	H20B-C20-H20C	109.5
C16-C15-C18	122.0(7)	C22-C21-C26	115.2(5)
C14-C15-C18	120.3(7)	C22-C21-Si7	121.6(6)
C15-C16-C17	121.2(6)	C26-C21-Si7	123.1(6)
C15-C16-H16	119.4	C23-C22-C21	121.7(7)
C17-C16-H16	119.4	C23-C22-H22	119.1
C16-C17-C12	122.3(6)	C21-C22-H22	119.1
C16-C17-H17	118.8	C22-C23-C24	121.8(7)
C12-C17-H17	118.8	C22-C23-H23	119.1
C15-C18-H18A	109.5	C24-C23-H23	119.1
C15-C18-H18B	109.5	C25-C24-C23	116.9(6)
H18A-C18-H18B	109.5	C25-C24-C27	120.4(8)
C15-C18-H18C	109.5	C23-C24-C27	122.7(8)
H18A-C18-H18C	109.5	C24-C25-C26	121.6(7)
H18B-C18-H18C	109.5	C24-C25-H25	119.2
O7-Si7-C19	108.5(3)	C26-C25-H25	119.2
O7-Si7-C20	108.0(3)	C25-C26-C21	121.8(7)
C19-Si7-C20	113.2(3)	C25-C26-H26	119.1
O7-Si7-C21	104.5(5)	C21-C26-H26	119.1
C19-Si7-C21	110.8(4)	C24-C27-H27A	109.5
C20-Si7-C21	111.4(4)	C24-C27-H27B	109.5
Si3-O7-Si7	150.8(2)	H27A-C27-H27B	109.5
Si7-C19-H19A	109.5	C24-C27-H27C	109.5
Si7-C19-H19B	109.5	H27A-C27-H27C	109.5
H19A-C19-H19B	109.5	H27B-C27-H27C	109.5
Si7-C19-H19C	109.5	O8-Si8-C28	109.8(3)
H19A-C19-H19C	109.5	O8-Si8-C30	105.0(5)
H19B-C19-H19C	109.5	C28-Si8-C30	112.0(5)

O8-Si8-C29	105.3(3)	C32-C31-H31	118.8
C28-Si8-C29	113.3(3)	C30-C31-H31	118.8
C30-Si8-C29	110.9(3)	C31-C32-C33	120.9(6)
Si4-O8-Si8	148.6(2)	C31-C32-H32	119.6
Si8-C28-H28A	109.5	C33-C32-H32	119.6
Si8-C28-H28B	109.5	C34-C33-C32	117.3(6)
H28A-C28-H28B	109.5	C34-C33-C36	121.0(7)
Si8-C28-H28C	109.5	C32-C33-C36	121.6(7)
H28A-C28-H28C	109.5	C33-C34-C35	121.8(6)
H28B-C28-H28C	109.5	C33-C34-H34	119.1
Si8-C29-H29A	109.5	C35-C34-H34	119.1
Si8-C29-H29B	109.5	C34-C35-C30	121.2(6)
H29A-C29-H29B	109.5	C34-C35-H35	119.4
Si8-C29-H29C	109.5	C30-C35-H35	119.4
H29A-C29-H29C	109.5	C33-C36-H36A	109.5
H29B-C29-H29C	109.5	C33-C36-H36B	109.5
C31-C30-C35	115.5(5)	H36A-C36-H36B	109.5
C31-C30-Si8	120.8(5)	C33-C36-H36C	109.5
C35-C30-Si8	123.0(6)	H36A-C36-H36C	109.5
C32-C31-C30	122.3(6)	H36B-C36-H36C	109.5

—

Symmetry transformations used to generate equivalent atoms: #1 -x+1, -y+1, -z+1

Table B.4: Anisotropic displacement parameters ($Å^2 \times 10^3$) for A.1. The anisotropic displacement factor exponent takes the form: $-2\pi^2 [h^2 a^{*2} U^{11} + ... + 2 h k a^* b^* U^{12}]$

	U^{11}	U^{22}	U^{33}	U^{23}	U^{13}	U^{12}
Si1	20(1)	19(1)	23(1)	-5(1)	-2(1)	1(1)
Si2	22(1)	17(1)	23(1)	-1(1)	-4(1)	1(1)

Si3	20(1)	21(1)	24(1)	-4(1)	-9(1)	1(1)
Si4	22(1)	17(1)	27(1)	-8(1)	-7(1)	0(1)
O1	34(1)	24(1)	36(1)	-4(1)	-2(1)	8(1)
O2	26(1)	32(1)	33(1)	1(1)	-7(1)	-6(1)
O3	31(1)	25(1)	43(2)	-10(1)	-16(1)	6(1)
O4	26(1)	31(1)	38(1)	-13(1)	-3(1)	-5(1)
O9	28(1)	42(2)	27(1)	-10(1)	-6(1)	0(1)
O10	39(2)	27(1)	28(1)	-6(1)	-9(1)	0(1)
Si5	25(1)	26(1)	28(1)	-7(1)	-6(1)	-1(1)
O5	34(1)	31(1)	37(1)	-7(1)	-10(1)	2(1)
C1	41(1)	38(1)	38(1)	-7(1)	-8(1)	0(1)
C2	41(1)	38(1)	38(1)	-7(1)	-8(1)	0(1)
C3	34(4)	32(3)	34(4)	-1(3)	-11(3)	-9(3)
C4	26(3)	31(3)	33(4)	4(2)	-2(3)	5(2)
C5	36(4)	37(4)	35(3)	2(3)	-3(2)	1(3)
C6	33(3)	38(4)	30(4)	-5(3)	-6(2)	11(3)
C7	54(4)	35(4)	40(5)	5(3)	-9(3)	3(3)
C8	30(3)	42(4)	37(5)	-4(3)	0(3)	6(3)
C9	56(5)	46(4)	48(4)	-12(3)	-17(3)	13(3)
Si6	25(1)	26(1)	28(1)	-7(1)	-6(1)	-1(1)
O6	34(1)	31(1)	37(1)	-7(1)	-10(1)	2(1)
C10	41(1)	38(1)	38(1)	-7(1)	-8(1)	0(1)
C11	41(1)	38(1)	38(1)	-7(1)	-8(1)	0(1)
C12	29(3)	31(4)	27(3)	-3(3)	-8(3)	7(2)
C13	30(3)	25(3)	28(3)	-2(2)	-2(3)	-4(2)
C14	28(3)	42(3)	33(4)	-8(2)	-4(3)	1(2)
C15	40(4)	29(3)	29(4)	-2(2)	-3(4)	-7(3)
C16	35(3)	26(3)	32(4)	3(2)	-1(3)	2(2)
C17	29(3)	25(3)	35(4)	2(2)	2(3)	-2(2)
C18	51(5)	55(6)	49(5)	-10(4)	-15(4)	-7(3)
Si7	25(1)	26(1)	28(1)	-7(1)	-6(1)	-1(1)
O7	34(1)	31(1)	37(1)	-7(1)	-10(1)	2(1)

C19	41(1)	38(1)	38(1)	-7(1)	-8(1)	0(1)
C20	41(1)	38(1)	38(1)	-7(1)	-8(1)	0(1)
C21	15(3)	27(3)	28(4)	-12(3)	-6(2)	8(2)
C22	30(3)	30(3)	25(3)	3(2)	-5(2)	-2(3)
C23	36(3)	30(3)	32(4)	3(2)	-5(2)	8(2)
C24	37(4)	37(4)	39(5)	-3(3)	-14(3)	7(3)
C25	21(3)	48(5)	47(5)	-6(4)	3(3)	10(3)
C26	31(3)	38(4)	39(4)	4(3)	-12(3)	-2(3)
C27	46(5)	69(6)	65(7)	-21(5)	-14(4)	36(5)
Si8	25(1)	26(1)	28(1)	-7(1)	-6(1)	-1(1)
O8	34(1)	31(1)	37(1)	-7(1)	-10(1)	2(1)
C28	41(1)	38(1)	38(1)	-7(1)	-8(1)	0(1)
C29	41(1)	38(1)	38(1)	-7(1)	-8(1)	0(1)
C30	39(4)	20(3)	26(3)	-7(2)	-4(3)	-11(3)
C31	36(3)	31(3)	38(5)	-1(3)	-5(3)	9(2)
C32	30(3)	39(3)	40(4)	-4(3)	1(3)	-3(2)
C33	37(4)	40(4)	32(4)	-10(3)	-4(4)	-8(3)
C34	46(5)	30(3)	35(4)	2(2)	1(3)	-1(3)
C35	37(4)	42(4)	30(4)	-1(2)	-8(3)	7(3)
C36	61(5)	36(4)	48(5)	3(4)	-13(5)	-31(4)

Table B.5: Hydrogen coordinates (x 10^4) and isotropic displacement parameters (Å^{2}x10^3) for B.1.

	x	y	z	U(eq)
H1A	3255	5209	8539	59
H1B	2304	5566	9331	59
H1C	2890	6448	8420	59

H2A	558	3953	8161	59
H2B	829	3858	9137	59
H2C	1758	3579	8291	59
H4	-666	5504	9285	40
H5	-2067	6759	9409	47
H7	-49	9028	7538	55
H8	1341	7756	7356	47
H9A	-1814	9379	8983	75
H9B	-2762	8582	9010	75
H9C	-2120	9343	8044	75
H10A	4824	3261	8687	59
H10B	4408	2332	9612	59
H10C	3545	2941	9058	59
H11A	6019	607	7718	59
H11B	6187	929	8615	59
H11C	6436	1794	7637	59
H13	2199	1341	8374	35
H14	916	-39	9017	42
H16	3222	-2018	9913	41
H17	4516	-650	9264	40
H18A	1417	-2709	10262	77
H18B	662	-2102	9601	77
H18C	536	-1829	10584	77
H19A	6937	4770	8069	59
H19B	7949	4288	8494	59
H19C	7204	3506	8228	59
H20A	9571	5906	5850	59
H20B	9427	5983	6897	59
H20C	8454	6376	6399	59
H22	8697	2218	7856	37
H23	9989	869	7682	43
H25	12047	2950	5650	51

H26	10811	4339	5901	45
H27A	12065	740	5857	91
H27B	11748	211	6949	91
H27C	12705	1101	6508	91
H28A	5325	6904	7880	59
H28B	5713	7907	8172	59
H28C	6597	7257	7548	59
H29A	4090	9483	6248	59
H29B	4025	9368	7321	59
H29C	3627	8394	6997	59
H31	7961	8587	6396	45
H32	9299	9906	5755	47
H34	7063	11995	4886	49
H35	5700	10687	5542	46
H36A	9177	12331	4303	74
H36B	9867	11708	5013	74
H36C	8946	12566	5311	74

Table B.6: Torsion angles [°] for B.1.

O5-Si1-O1-Si2	176.2(3)	O1-Si2-O2-Si3	-62.1(4)
O9-Si1-O1-Si2	57.1(4)	O7-Si3-O3-Si4	176.5(3)
O4-Si1-O1-Si2	-62.6(4)	O9#1-Si3-O3-Si4	57.7(4)
O6-Si2-O1-Si1	-177.2(4)	O2-Si3-O3-Si4	-62.3(4)
O10-Si2-O1-Si1	-57.2(4)	O8-Si4-O3-Si3	-176.4(3)
O2-Si2-O1-Si1	62.6(4)	O10#1-Si4-O3-Si3	-58.1(4)
O7-Si3-O2-Si2	-177.0(3)	O4-Si4-O3-Si3	62.1(4)
O9#1-Si3-O2-Si2	-57.9(4)	O8-Si4-O4-Si1	177.5(3)
O3-Si3-O2-Si2	62.0(4)	O10#1-Si4-O4-Si1	58.8(4)
O6-Si2-O2-Si3	176.0(3)	O3-Si4-O4-Si1	-61.2(4)
O10-Si2-O2-Si3	57.5(4)	O5-Si1-O4-Si4	-177.5(3)

O9-Si1-O4-Si4	-58.9(4)	O1-Si2-O6-Si6	-93.5(5)
O1-Si1-O4-Si4	61.6(4)	C11-Si6-O6-Si2	-67.8(5)
O5-Si1-O9-Si3#1	-177.1(4)	C10-Si6-O6-Si2	53.5(5)
O1-Si1-O9-Si3#1	-57.0(4)	C12-Si6-O6-Si2	170.5(6)
O4-Si1-O9-Si3#1	63.0(4)	O6-Si6-C12-C13	-35.5(14)
O6-Si2-O10-Si4#1	-179.6(4)	C11-Si6-C12-C13	-152.9(11)
O2-Si2-O10-Si4#1	-61.0(4)	C10-Si6-C12-C13	77.8(13)
O1-Si2-O10-Si4#1	58.4(4)	O6-Si6-C12-C17	137.1(13)
O9-Si1-O5-Si5	153.6(4)	C11-Si6-C12-C17	19.7(15)
O1-Si1-O5-Si5	33.3(4)	C10-Si6-C12-C17	-109.7(13)
O4-Si1-O5-Si5	-87.4(4)	C17-C12-C13-C14	6.8(19)
C2-Si5-O5-Si1	-71.8(5)	Si6-C12-C13-C14	179.9(10)
C1-Si5-O5-Si1	48.8(5)	C12-C13-C14-C15	-0.3(19)
C3-Si5-O5-Si1	166.4(6)	C13-C14-C15-C16	-6(2)
O5-Si5-C3-C4	144.9(15)	C13-C14-C15-C18	177.2(17)
C2-Si5-C3-C4	27.2(18)	C14-C15-C16-C17	6(2)
C1-Si5-C3-C4	-99.2(15)	C18-C15-C16-C17	-177.5(18)
O5-Si5-C3-C8	-46.3(16)	C15-C16-C17-C12	1(2)
C2-Si5-C3-C8	-164.0(13)	C13-C12-C17-C16	-7(2)
C1-Si5-C3-C8	69.6(16)	Si6-C12-C17-C16	179.9(12)
C8-C3-C4-C5	9(3)	O9#1-Si3-O7-Si7	150.6(5)
Si5-C3-C4-C5	178.3(15)	O3-Si3-O7-Si7	31.2(6)
C3-C4-C5-C6	-7(3)	O2-Si3-O7-Si7	-89.4(6)
C4-C5-C6-C7	2(3)	C19-Si7-O7-Si3	51.1(6)
C4-C5-C6-C9	-175.4(19)	C20-Si7-O7-Si3	-71.9(6)
C5-C6-C7-C8	-1(3)	C21-Si7-O7-Si3	169.4(5)
C9-C6-C7-C8	177.1(18)	O7-Si7-C21-C22	-88.4(14)
C6-C7-C8-C3	4(3)	C19-Si7-C21-C22	28.3(15)
C4-C3-C8-C7	-8(3)	C20-Si7-C21-C22	155.2(12)
Si5-C3-C8-C7	-177.1(14)	O7-Si7-C21-C26	95.3(14)
O10-Si2-O6-Si6	145.9(4)	C19-Si7-C21-C26	-148.0(13)
O2-Si2-O6-Si6	26.8(5)	C20-Si7-C21-C26	-21.1(16)

C26-C21-C22-C23	-9(2)	O8-Si8-C30-C31	-80.4(12)
Si7-C21-C22-C23	174.9(13)	C28-Si8-C30-C31	38.7(14)
C21-C22-C23-C24	1(2)	C29-Si8-C30-C31	166.3(11)
C22-C23-C24-C25	4(3)	O8-Si8-C30-C35	89.9(13)
C22-C23-C24-C27	-177.3(19)	C28-Si8-C30-C35	-151.1(12)
C23-C24-C25-C26	-1(3)	C29-Si8-C30-C35	-23.4(15)
C27-C24-C25-C26	179.9(19)	C35-C30-C31-C32	8(2)
C24-C25-C26-C21	-7(3)	Si8-C30-C31-C32	179.0(11)
C22-C21-C26-C25	11(2)	C30-C31-C32-C33	-1(2)
Si7-C21-C26-C25	-172.3(14)	C31-C32-C33-C34	-8(2)
O10#1-Si4-O8-Si8	156.4(4)	C31-C32-C33-C36	176.5(17)
O3-Si4-O8-Si8	-84.2(4)	C32-C33-C34-C35	8(2)
O4-Si4-O8-Si8	36.5(5)	C36-C33-C34-C35	-176.0(18)
C28-Si8-O8-Si4	46.9(5)	C33-C34-C35-C30	0(2)
C30-Si8-O8-Si4	167.5(5)	C31-C30-C35-C34	-8(2)
C29-Si8-O8-Si4	-75.4(5)	Si8-C30-C35-C34	-178.3(11)

Symmetry transformations used to generate equivalent atoms: #1 -x+1,-y+1,-z+1

B.2 REFERENCES

[1] Z. Otwinoski and W. Minor. "Methods in Enzymology". 1997.

[2] A. Altomare, M. C. Burla, M. Camalli, G. L. Cascarano, C. Giacovazzo, A. Guagliardi, A. G. G. Moliterni, G. Polidori and R. Spagna. "*SIR97*: a new tool for crystal structure determination and refinement". *Journal of Applied Crystallography,* 32, 115-119, 1999.

[3] G. M. Sheldrick. "A short history of *SHELX*". *Acta Cryst.,* A64, 112-122, 2008.

[4] A. L. Spek. "PLATON, A Multipurpose Crystallographic Tool". Utrecht University. Utrecht, The Netherlands. 1998.

[5] L. J. Farrugia. "*WinGX* suite for small-molecule single crystallography". *Journal of Applied Crystallography,* 32, 837-838, 1999.

[6] "International Tables for X-ray Crystallography"; Vol. C Ed.; Kluwer Academic Press; Boston, 1992.

[7] G. M. Sheldrick. "SHELTX/PC (Version 5.03)". Siemens Analytical X-ray Instruments, Inc. Madison, Wisconsin, USA. 1994.

Appendix C: Keithley 4200 Settings

Site Coordinate	0,0				
Last Executed	03/31/2011 12:56:18				
Library Name	KI590ulib				
Module Name	CvSweep590				
Return Type	INT				
Parameter Name	**In/Out**	**Type**	**Value**		
CabCompFile	Input	CHAR_P	c:\\S4200\\kiuser\\usrlib\\		
			ki590ulib\\misc\\ki590CableComp.dat		
InstIdStr	Input	CHAR_P	CMTR1		
InputPin	Input	INT	0		
OutPin	Input	INT	0		
OffsetCorrect	Input	INT	1		
Waveform	Input	INT	1		
FirstBias	Input	DOUBLE	5.000000e+000		
LastBias	Input	DOUBLE	-5.000000e+000		
StepV	Input	DOUBLE	-1.000000e-001		
Frequency	Input	INT	0		
DefaultBias	Input	DOUBLE	0		
StartTime	Input	DOUBLE	2.000000e+000		
StepTime	Input	DOUBLE	1.000000e-001		
Range	Input	DOUBLE	2.000000e-009		
Model	Input	INT	0		
Filter	Input	INT	1		
ReadingRate	Input	INT	3		
C	Output	DBL_ARRAY	N/A		
Csize	Input	INT	1350		
V	Output	DBL_ARRAY	N/A		
Vsize	Input	INT	1350		
G_or_R	Output	DBL_ARRAY	N/A		
G_or_Rsize	Input	INT	1350		
T	Output	DBL_ARRAY	N/A		
Tsize	Input	INT	1350		

Table C.1: CV instrument settings [8-10].

C.1 REFERENCES

[8] I. Keithley Instruments. "Model 590 CV Analyzer Instruction Manual".

[9] I. Keithley Instruments. "Model 590 CV Analyzer, Quick Reference Guide".

[10] I. Keithley Instruments. "Gate Dielectric Capacitance-Voltage Characterization Using the Model 4200 Semiconductor Characterization System".

Glossary

AFM – Atomic Force Microscopy (Microscope)

AP – Adhesion Promoter

CAR – Chemically Amplified Resist

CMOS – Complimentary metal-oxide-semiconductor

CMP – Chemical Mechanical Polishing

CoO – Cost of Ownership

CV – Capacitance vs Volt

CVD – Chemical Vapor Deposition

DCM – Dichloromethane

DMF – Dimethyl Formamide

DPD – Directly Patternable Dielectric

DUV – Deep UV

EUV – Extreme Ultra Violet

FSAM – Fluorinated Self Assembled Monolayer

HDD – Hard Disk Drive

HRMS – High Resolution Mass Spectrometry

IC – Interconnect

IFM – Interfacial Force Microscopy

ILD – Interlayer Dielectric

IR – Infra Red

LAH – Lithium Aluminum Hydride

MER – The University of Texas Microelectronics Research Center

MIM – Metal-Insulator-Metal

NGL – Next Generation Lithography

NIL – Nanoimprint Lithography

NMR – Nuclear Magnetic Resonance Spectroscopy

PAG – Photoacid Generator

PBG – Photobase Generator

PI – Photo Initiator

PMMA – Polymethyl Methacrylate

POSS – Polyhedral Oligomeric Silsesquioxane

PS – Polystyrene

PS2V – Vinyl Terminated

PVD – Physical Vapor Deposition

Q_8 – Octakis(dimethylsilyloxy)silsesquioxane

RD – Reactive Diluent

SAM – Self Assembling Monolayer

SAWS – Surface Acoustic Wave Spectroscopy

SEM – Scanning Electron Microscope

SFIL – Step and Flash Imprint Lithography

SFIL-R – Reverse Tone SFIL

SeRFSAM – Self Replenishing Fluorinated Self Assembling Monolayer

TAMU MCF – Texas A&M Material Characterization Facility

THF - Tetrahydrofuran

UV – Ultra Violet

Bibliography

[1] M. Campbell-Kelly. "Computing". *Scientific American,* 301, 62-69, 2009.

[2] L. F. Thompson, C. G. Willson and M. J. Bowden. "Introduction to Microlithography"; Ed.; American Chemical Society; Washington D.C., 1983.

[3] G. E. More. "Cramming more components onto integrated circuits". *Electronics,* 38, 1965.

[4] http://www.intel.com/museum/archives/history_docs/moore.htm. **2011.**

[5] http://www.wisegeek.com/how-long-do-cell-phone-batteries-last.htm. **2011.**

[6] J. R. Adams. "Organic Materials Development for Advanced Lithographic Applications". *Ph.D. Dissertation, The University of Texas,* 2009**.**

[7] C. Mack. "Fundamental Principles of Optical Lithography"; 1st Ed.; John Wiley & Sons, Ltd.; Chichester, West Sussex, 2007.

[8] J. V. Crivello. "The discovery and development of onium salt cationic photoinitiators". *Journal of Polymer Science Part A: Polymer Chemistry,* 37, 4241-4254, 1999.

[9] S. A. MacDonald, C. G. Willson and J. M. J. Frechet. "Chemical Amplification in High-Resolution Imaging Systems". *Accounts of Chemical Research,* 27, 151-158, 1994.

[10] C. G. Willson, R. A. Dammel and A. Reiser. "Photoresist Materials: A Historical Perspective". *Advances in Resist Technology and Processing XIV*, 3049, 1997.

[11] https://asml.picturepark.com/Website/Publisher.aspx?Page=ASML.

[12] http://newsroom.intel.com/community/intel_newsroom/blog/2011/05/04/intel-reinvents-transistors-using-new-3-d-structure. **2011.**

[13] M. E. Colburn. "Step and Flash Imprint Lithography: A Low-Pressure, Room-Temperature Nanoimprint Lithography". *Ph.D. University of Texas at Austin,* 2001**.**

[14] E. A. Costner. "The Refractive Index and Absorbance of Aqueous and Organic Fluids for Immersion Lithography". *Ph.D. Dissertation, The University of Texas,* 2009**.**

[15] X. Gu, C. Bates, Y. Cho, E. Costner, F. Marzuka, T. Nagai, T. Ogata, C. Shi, A. K. Sundaresan, N. J. Turro, R. Bristol, P. Zimmerman and C. G. Willson. "A New Materials-based Pitch Division Technique". *Journal of Photopolymer Science and Technology,* 22, 773-781, 2009.

[16] X. Gu, Y. Cho, T. Kawakami, Y. Hagawara, B. Rawlings, R. Mesch, T. Ogata, T. Kim, T. Seshimo, W. Wang, A. K. Sundaresan, N. J. Turro, R. Gronheid, J. Blackwell, R. Bristol and C. G. Willson. "Photobase Generator Enabled Pitch Division: A Progress Report". *Advances in Resist Materials and Processing Technology XXVIII*, 7972, 2011.

[17] X. Gu, C. M. Bates, Y. Cho, T. Kawakami, T. Nagai, T. Ogata, A. K. Sundaresan, N. J. Turro, R. Bristol, P. Zimmerman and C. G. Willson. "Photobase generator assisted pitch division". *Advances in Resist Materials and Processing Technology XXVII*, 7639, 2010.

[18] Y. Cho, X. Gu, Y. Hagiwara, T. Kawakami, T. Ogata, B. Rawlings, Y. Li, A. K. Sundaresan, N. J. Turro, R. Bristol, J. M. Blackwell and C. G. Willson. "Polymer Bound Photobase Generators and Photoacid Generators for Pitch Division Lithography". *Advances in Resist Materials and Processing Technology XXVIII*, 7972, 2011.

[19] G. Xinyu. *Ph.D. Dissertation, The University of Texas,* 2011**.**

[20] F. L. Palmieri. "Step and Flash Imprint Lithography: Materials and Applications for The Manufacture of Advanced Integrated Circuits". *Ph.D. University of Texas at Austin,* 2008**.**

[21] D. J. Resnick, S. V. Sreenivasan and C. G. Willson. "Step & flash imprint lithography". *Materials Today,* 8, 34-42, 2005.

[22] S. Y. Chou, P. R. Krauss and P. J. Renstrom. "Imprint of sub-25 nm vias and trenches in polymers". *Appl. Phys. Lett.,* 67, 1995.

[23] S. Y. Chou, P. R. Krauss and P. J. Renstrom. "Nanoimprint lithography". *The 40th international conference on electron, ion, and photon beam technology and nanofabrication*, 14, 1996.

[24] M. Colburn, S. C. Johnson, M. D. Stewart, S. Damle, T. C. Bailey, C. Bernard, M. Wedlake, T. B. Michaelson, S. V. Sreenivasan, J. G. Ekerdt and C. G. Willson. "Step and flash imprint lithography: a new approach to high-resolution patterning". 3676, 1999.

[25] F. Hua, Y. Sun, A. Gaur, M. A. Meitl, L. Bilhaut, L. Rotkina, J. Wang, P. Geil, M. Shim, J. A. Rogers and A. Shim. "Polymer Imprint Lithography with Molecular-Scale Resolution". *Nano Lett.,* 4, 2467-2471, 2004.

[26] W. M. Tong, S. D. Hector, G.-Y. Jung, W. Wu, R. S. Williams, J. Ellenson, K. Kramer, T. Hostetler and S. K. Richards. "Nanoimprint lithography: the path toward high-tech, low-cost devices". *Emerging Lithographic Technologies IX*, SPIE, 2005.

[27] B. J. Choi, S. V. Sreenivasan, S. Johnson, M. Colburn and C. G. Willson. "Design of orientation stages for step and flash imprint lithography". *Journal of the International Societies for Precision Engineering and Nanotechnology,* 25, 192-199, 2001.

[28] B. J. Choi, M. Meissl, M. Colburn, T. Bailey, P. Ruchhoeft, S. V. Sreenivasan, F. Prins, S. Banerjee, J. G. Ekerdt and C. G. Willson. "Layer-to-Layer Alignment for

Step and Flash Imprint Lithography". *Emerging Lithographic Technologies V*, 2001.

[29] C. Perret, C. Gourgon, G. Micouin and J. P. Grolier. "Influence of Thermal Properties of Polymers on NanoImprint Lithography Performance". *Jpn. J. Appl. Phys.,* 41, 4203-4207, 2002.

[30] L.-R. Bao, X. Cheng, X. D. Huang, L. J. Guo, S. W. Pang and A. F. Yee. "Nanoimprinting over topography and multilayer three-dimensional printing". *J. Vac. Sci. Technol. B,* 20, 2881-2886, 2002.

[31] M. Vogler, S. Wiedenberg, M. Muhlberger, I. Bergmair, T. Glinsner, H. Schmidt, E.-B. Kley and G. Grutzner. "Development of a novel, low-viscosity UV-curable polymer system for UV-nanoimprint lithography". *Microelectronic Engineering,* 84, 984-988, 2007.

[32] B. H. Chao, F. Palmieri, W.-L. Jen, D. H. McMichael, C. G. Willson, J. Owens, R. Berger, K. Sotoodeh, B. Wilks, J. Pham, R. Carpio, E. LaBelle and J. Wetzel. "Dual damascene BEOL processing using multilevel step and flash imprint lithography". *Emerging Lithographic Technologies XII*, 6921, 2008.

[33] S. Johnson, D. J. Resnick, D. Mancini, K. Nordquist, W. J. Dauksher, K. Gehoski, J. H. Baker, L. Dues, A. Hooper, T. C. Bailey, S. V. Sreenivasan, J. G. Ekerdt and C. G. Willson. "Fabrication of multi-tiered structures on step and flash imprint lithography templates". *Microelectronic Engineering,* 67-68, 221-228, 2003.

[34] S. Sasaki, T. Hiraka, J. Mizuochi, Y. Nakanishi, S. Yusa, Y. Morikawa, H. Mohri and N. Hayashi. "UV-NIL template making and imprint evaluation". 7271, 2009.

[35] M. Pritschow, J. Butschke, M. Irmscher, L. Parisoli, T. Oba, T. Iwai and T. Nakamura. "Evaluation of the CD-SEM Vistec LWM90xx for line-width measurement of nanoimprint templates". *Alternative Lithographic Technologies*, 7271, 2009.

[36] W. H. Heath, F. Palmieri, J. R. Adams, B. K. Long, J. Chute, T. W. Holcombe, S. Zieren, M. J. Truitt, J. L. White and C. G. Willson. "Degradable Cross-Linkers

and Strippable Imaging Materials for Step-and-Flash Imprint Lithography". *Macromolecules,* 2008.

[37] F. Palmieri, J. Adams, B. Long, W. Heath, P. Tsiartas and C. G. Willson. "Design of Reversible Cross-Linkers for Step and Flash Imprint Lithography Imprint Resists". *ACS Nano,* 1, 307-312, 2007.

[38] M. D. Stewart and C. G. Willson. "Imprint Materials for Nanoscale Devices". *MRS Bulletin,* 30, 947-951, 2005.

[39] W.-L. K. Jen. "Materials and Processes for Advanced Lithography Applications". *Ph.D. Dissertation, The University of Texas at Austin,* 2009**.**

[40] T. Bailey, B. Smith, B. J. Choi, M. Colburn, M. Meissl, S. V. Sreenivasan, J. G. Ekerdt and C. G. Willson. "Step and flash imprint lithography: Defect analysis". *J. Vac. Sci. Technol. B,* 19, 2806-2810, 2001.

[41] T. Bailey, B. J. Choi, M. Colburn, M. Meissl, S. Shaya, J. G. Ekerdt, S. V. Sreenivasan and C. G. Willson. "Step and flash imprint lithography: Template surface treatment and defect analysis". *Papers from the 44th international conference on electron, ion, and photon beam technology and nanofabrication*, 18, 2000.

[42] M. W. Lin. "Simulation and Design of Planarizing Materials and Interfacial Adhesion Studies for Step and Flash Imprint Lithography". *Ph.D. University of Texas at Austin,* 2008**.**

[43] M. McCoy. "Deciding on a Dielectric". *Chemical & Engineering News,* 79, 43-46, 2001.

[44] M. D. Stewart, J. T. Wetzel, G. M. Schmid, F. Palmieri, E. Thompson, E. K. Kim, D. Wang, K. Sotoodeh, K. Jen, S. C. Johnson, J. Hao, M. D. Dickey, Y. Nishimura, R. M. Laine, D. J. Resnick and C. G. Willson. "Direct Imprinting of Dielectric Materials for Dual Damascene Processing". *Emerging Lithographic Technologies IX*, 5751, 2005.

[45] G. M. Schmid, M. D. Stewart, J. Wetzel, F. Palmieri, J. Hao, Y. Nishimura, K. Jen, E. K. Kim, D. J. Resnick, J. A. Liddle and C. G. Willson. "Implementation of an imprint damascene process for interconnect fabrication". *Journal of Vacuum Science & Technology B: Microelectronics and Nanometer Structures,* 24, 1283-1291, 2006.

[46] F. Palmieri, M. D. Stewart, J. Wetzel, J. Hao, Y. Nishimura, K. Jen, C. Flannery, B. Li, H.-L. Chao, S. Young, W. C. Kim, P. S. Ho and C. G. Willson. "Multi-level Step and Flash Imprint Lithography for Direct Patterning of Dielectrics ". *Proc. of SPIE,* 6151, 2006.

[47] M. A. Wahab, K. Y. Mya and C. He. "Synthesis, Morphology, and Properties of Hydroxyl Terminated-POSS/Polyimide Low-*k* Nanocomposite Films". *Journal of Polymer Science Part A: Polymer Chemistry,* 46, 5887-5896, 2008.

[48] J. Hao, M. W. Lin, F. Palmieri, Y. Nishimura, H.-L. Chao, M. D. Stewart, A. Collins, K. Jen and C. G. Willson. "Photocurable Silicon-Based Materials for Imprint Lithography". *Proc. of SPIE,* 6517, 2007.

[49] C. E. Hoyle, T. Y. Lee and T. Roper. "Thiol–Enes: Chemistry of the Past with Promise for the Future". *J. Polym. Sci. Part A: Polym. Chem.,* 42, 5301-5338, 2004.

[50] W. A. Pryor and E. G. Olsen. "Homolytic Displacement at Sulfur by the Hydrogen Atom. Formation of Hydrogen Sulfide in the Liquid-Phase Photolysis of Thiols". *J. Am. Chem. Soc.,* 100, 2852-2856, 1978.

[51] J. D. Coyle. "Photochemistry of Organic Sulphur Compounds". *Chemical Society Reviews,* 523-532, 1975.

[52] M. Moran, C. M. Casado and I. Cuadrado. "Ferrocenyl Substituted Octakis(dimethylsiloxy)octasilsesquioxanes: A New Class of Supramolecular Organometallic Compounds. Synthesis, Characterization, and Electrochemistry". *Organometallics,* 12, 4327-4333, 1993.

[53] A. Provatas, M. Luft, J. C. Mu, A. H. White, J. G. Matisons and B. W. Skelton. "Silsesquioxanes: Part I: A key intermediate in the building of molecular composite materials". *Journal of Organometallic Chemistry,* 565, 159-164, 1998.

[54] H. Uchida, Y. Kabe, K. Yoshino, A. Kawamata, T. Tsumuraya and S. Masamune. "General Strategy for the Systematic Synthesis of Oligosiloxanes. Silicone Dendrimers". *Journal of American Chemistry Society,* 112, 7077-7079, 1990.

[55] E. Markovic, M. Ginic-Markovic, S. Clarke, J. Matisons, M. Hussain and G. P. Simon. "Poly(ethylene glycol)-Octafunctionalized Polyhedral Oligomeric Silsesquioxane: Synthesis and Thermal Analysis". *Macromolecules,* 40, 2694-2701, 2007.

[56] L. N. Lewis and N. Lewis. "Platinum-Catalyzed Hydrosilylation-Colloid Formation as the Essential Step". *J. Am. Chem. Soc.,* 108, 7228-7231, 1986.

[57] W. B. Motherwell, G. Begis, D. E. Cladingboel, L. Jerome and T. D. Sheppard. "Observations on the direct amidocyclopropanation of alkenes using organozinc carbenoids". *Tetrahedron,* 63, 6462-6476, 2007.

[58] L. Barr, S. F. Lincoln and C. J. Easton. "A Cyclodextrin Molecular Reactor for the Regioselective Synthesis of 1,5-disubstituted-1,2,3-triazoles". *Supramolecular Chemistry,* 17, 547-555, 2005.

[59] L. Campbell-Verduyn, P. H. Elsinga, L. Mirfeizi, R. A. Dierckx and B. L. Feringa. "Copper-free 'click': 1,3-dipolar cycloaddition of azides and arynes". *Organic & Biomolecular Chemistry,* 6, 3461-3463, 2008.

[60] V. V. Dorsselaer, D. Schirlin, P. Marchal, F. Weber and C. Danzin. "Silicon-Mediated Inactivation of Diamine Oxidase". *Bioorganic Chemistry,* 24, 178-193, 1996.

[61] N.-H. Nguyen, J. W.Apriletti, J. D. Baxter and T. S. Scanlan. "Hammett Analysis of Selective Thyroid Hormone Receptor Modulators Reveals Structural and Electronic Requirements for Hormone Antagonists". *J. Am. Chem. Soc.,* 127, 4599-4608, 2005.

[62] J. T. Spletstoser, P. T. Flaherty, R. H. Himes and G. I. Georg. "Synthesis and Anti-Tubulin Activity of a 3'-(4-Azidophenyl)-3'-dephenylpaclitaxel Photoaffinity Probe". *J. Med. Chem.,* 47, 6459-6465, 2004.

[63] E. Block, J.-A. Laffitte and V. Eswarakrishnan. "Synthesis and Reactions of 3-Mercaptocyclobutanol and Derivatives. Preparation of a 2,4-Dithiabicyclo[3.1.1]heptane". *JOC,* 51, 1986.

[64] D. D. Perrin and W. L. F. Armarego. "Purification of Laboratory Chemicals"; 3rd Ed.; Butterworth-Heinemann Ltd; 1988.

[65] J. P. Wolfe, R. A. Rennels and S. L. Buchwald. "Intramolecular Palladium-Catalyzed Aryl Amination and Aryl Amidation". *Tetrahedron,* 52, 7525-7546, 1996.

[66] M. G. Banwell, B. L. Flynn, D. C. R. Hockless, R. W. Longmore and A. D. Rae. "Assessment of Double-Barrelled Heck Cyclizations as a Means for Construction of the 14-Phenyl-8,9-dihydro-6H-[1]benzopyrano[4',3':4,5]pyrrolo[2,1-a]isoquinolin-6-one Core Associated with Certain Members of the Lamellarin Class of Marine Natural Product". *Aust. J. Chem.,* 52, 755-765, 1998.

[67] F. Bilodeau, M.-C. Brochu, N. Guimond, K. H. Thesen and P. Forgione. "Palladium-Catalyzed Decarboxylative Cross-Coupling Reaction Between Heteroaramatic Carboxylic Acids and Aryl Halides". *Journal of Organic Chemistry,* 75, 1550-1560, 2010.

[68] J. B. F. Lloyd and P. A. Ongley. "The Electrophilic Substitution of Benzocyclobutene-II". *Tetrahedron,* 21, 245-254, 1965.

[69] A. R. Bassindale, C. Eaborn and D. R. M. Walton. "Aromatic Reactivity. Part XXXVIII. Protodesilylation of 1,2-Dihydrobenzocyclobutene, Indan, and Tetralin". *J. Chem. Soc. (B),* 12-15, 1969.

[70] J. T. Spletstoser, P. T. Flaherty, R. H. Himes and G. I. Georg. *J. Med. Chem.,* 47, 2004.

[71] C. Zhang and R. M. Laine. "Silsesquioxanes as synthetic platforms. II. Epoxy-functionalized inorganic-organic hybrid species". *Journal of Organometallic Chemistry,* 521, 199-201, 1996.

[72] T. I. Ito and W. P. Weber. "Synthesis and Mass Spectra of *w*-(trimethylsilyl)alkyl Methyl Sulfides and Sulfones". *JOC,* 39, 1694-1697, 1974.

[73] A. L. Schwan, D. Brillon and R. Dufault. "Synthesis, reactions, and interconversions of some 2-(trimethylsilyl)ethyl substituted sulfur compounds". *Can. J. Chem.,* 72, 325, 1994.

[74] S. Napolitano, A. Pilleri, P. Rolla and M. Wubbenhorst. "Unusual Deviations from Bulk Behavior in Ultrathin Films of Poly(tert-butylstyrene): Can Dead Layers Induce a Reduction of Tg?" *ACS Nano,* 4, 841-848, 2010.

[75] J. Domke and M. Radmacher. "Measuring the Elastic Properties of Thin Polymer Films with the Atomic Force Microscope". *Langmuir,* 14, 3320-3325, 1998.

[76] A. C.-M. Yang. "Young's moduli of materials in polymer deformation zones by an AFM deflection technique". *Materials Chemistry and Physics,* 41, 295-298, 1995.

[77] D. J. Shuman, A. L. M. Costa and M. S. Andrade. "Calculating the elastic modulus from nanoindentation and microindentation reload curves". *Materials Characterization,* 58, 380-389, 2007.

[78] M. Wang, K. M. Liechti, J. M. White and R. M. Winter. "Nanoindentation of polymeric thin films with an interfacial force microscope". *Journal of the Mechanics and Physics of Solids,* 52, 2329-2354, 2004.

[79] H. J. Hertz. "Ueber die Berührung fester elastischer Körper". *Journal Fur Die Reine Und Angewandte Mathematik,* 156-171, 1882.

[80] I. N. Sneddon. "The relation between load and penetration in the axisymmetric boussinesq problem for a punch of arbitrary profile". *International Journal of Engineering Science,* 3, 47-57, 1965.

[81] K. M. Liechti. Personal Communication. 2011.

[82] G. M. Schmid. Personal Communication. 2011.

[83] A. Henkes-Young. Personal Communication. 2011.

[84] S. Franssila. "Introduction to Microfabrication"; 2nd Ed.; John Wiley & Sons, Ltd.; Chichester, West Sussex, 2010.

[85] G. Odian. "Principles of Polymerization"; 4 Ed.; John Wiley & Sons, Ltd.; Chichester, 2004.

[86] H. Lin, X. Wan, X. Jiang, Q. Wang and J. Yin. "A Nanoimprint Lithography Hybrid Photoresist Based on the Thiol-Ene System". *Advanced Functional Materials,* 21, 2011.

[87] S. V. Sreenivasan, I. McMackin, F. Xu, D. Wang, N. Stacey and D. Resnick. "Reverse Tone Bi-Layer Etch in UV Nanoimprint Lithography". *Micro Magazine,* 2005.

[88] M. W. Lin, H.-L. Chao, J. Hao, E. K. Kim, F. Palmieri, W. C. Kim, M. Dickey, P. S. Ho and C. G. Willson. "Planarization for Reverse-Tone Step and Flash Imprint Lithography". *SPIE*, 6151, Emerging Lithographic Technologies X, 2006.

[89] T. Ogawa, S. Takei, B. M. Jacobsson, R. Deschner, W. Bell, M. W. Lin, Y. Hagiwara, M. Hanabata and C. G. Willson. "Planarizing material for reverse-tone step and flash imprint lithography". *Alternative Lithographic Technologies II*, 7637, 2010.

[90] J. E. L. III, M. Daffron, R. Hopper, M. Whittaker and S. Scott. "Planarizing Difficult Topographies Using Contact Planarization". *Solid State Technology,* 46, 2003.

[91] M. W. Lin, B. Chao, J. Hao, K. Osberg, P. S. Ho and C. G. Willson. "Simulation and design of planarizing materials for reverse-tone step and flash imprint lithography". *Journal of Micro/Nanolithography, MEMS and MOEMS,* 7, 023008, 2008.

[92] W.-L. Jen, F. Palmieri, B. Chao, M. Lin, J. Hao, J. Owens, K. Sotoodeh, R. Cheung and C. G. Willson. "Multi-level Step and Flash Imprint Lithography for Direct Patterning of Dielectrics". *Proc. of SPIE,* 6517, 2007.

[93] S. Boileau. "Anionic Polymerization of Cyclosiloxanes with Cryptates as Counterions". Ring-Opening Polymerization. 1985.

[94] T. Ogawa, B. M. Jacobsson and C. G. Willson. "Novel synthetic route to UV curable branched siloxanes for nano imprint lithography". *239th ACS National Meeting*, 2010.

[95] K. Yoshino, A. Kawamata, H. Uchida and Y. Kabe. "A Convenient Synthesis of a,w-Difunctionalized Linear Dimethylsiloxanes with Definite Chain Lengths". *Chemistry Letters,* 2133-2136, 1990.

[96] J. F. Miravet and J. M. J. Frechet. "New Hyperbranched Poly(siloxysilanes): Variation of the Branching Pattern and End-Functionalization". *Macromolecules,* 31, 3461-3468, 1998.

[97] Y. Xiao, R. A. Wong and D. Y. Son. "Synthesis of a New Hyperbranched Poly(silylenevinylene) with Ethynyl Functionalization". *Macromolecules,* 33, 7232-7234, 2000.

[98] K. Yoon and D. Y. Son. "Syntheses of Hyperbranched Poly(carbosilarylenes)". *Macromolecules,* 32, 5210-5216, 1999.

[99] J. V. Crivello and M. Ranjit. "Synthesis and photoinitiated cationic polymerization of monomers with the silsesquioxane core". *Journal of Polymer Science Part A: Polymer Chemistry,* 35, 407-425, 1997.

[100] A. De Camp Schuda, P. H. Mazzocchi, G. Fritz and T. Morgan. "A Short and Efficient Synthesis of 4,5-Disubstituted-1-pentenes". *Synthesis,* 1986, 309-312, 1986.

[101] J. V. Crivello and J. L. Lee. "The Synthesis, Characterization, and Photoinitiated Cationic Polymerization of Silicon-Containing Epoxy Resins". *Journal of Polymer Science Part A: Polymer Chemistry,* 28, 479-503, 1990.

[102] J. V. Crivello. "The Synthesis and Cationic Polymerization of Novel Epoxide Monomers". *Polymer Engineering and Science,* 32, 1662-1665, 1992.

[103] J. V. Crivello, M. Fan and D. Bi. "The Electron Beam-Induced Cationic Polymerization of Epoxy Resins". *Journal of Applied Polymer Science,* 44, 9-16, 1992.

[104] K. Wu, X. Wang, E. K. Kim, C. G. Willson and J. G. Ekerdt. "Experimental and Theoretical Investigation on Surfactant Segregation in Imprint Lithography". *Langmuir,* 23, 1166-1170, 2007.

[105] T. Bailey, B. J. Choi, M. Colburn, M. Meissl, S. Shaya, J. G. Ekerdt, S. V. Sreenivasan and C. G. Willson. "Step and flash imprint lithography: Template surface treatment and defect analysis". *J. Vac. Sci. Technol. B,* 18, 3572-3577, 2000.

[106] M. W. Lin, D. J. Hellebusch, K. Wu, E. K. Kim, K. Lu, L. Tao, K. M. Liechti, J. G. Ekerdt, P. S. Ho, W. Hu and C. G. Willson. "Interfacial adhesion studies for step and flash imprint lithography". *SPIE*, 6921, Emerging Lithographic Technologies XII, 2008.

[107] T. Ogawa, D. J. Hellebusch, M. W. Lin, B. M. Jacobsson, W. Bell and C. G. Willson. "Reactive fluorinated surfactant for step and flash imprint lithography". *SPIE*, 7970, Alternative Lithographic Technologies III, 2011.

[108] E. G. Shafrin and W. A. Zisman. "Constitutive Relations in the Wetting of Low Energy Surfaces and the Theory of the Retraction Method of Preparing Monolayers". *J. Phys. Chem.,* 64, 519-524, 1960.

[109] M. W. Lin, D. J. Hellebusch, K. Wu, E. K. Kim, H. L. Kuan, K. M. Liechti, J. G. Ekerdt, P. S. Ho and C. G. Willson. "Role of surfactants in adhesion reduction for step and flash imprint lithography". *Journal of Micro/Nanolithography, MEMS and MOEMS,* 7, 033005, 2008.

[110] D. Truffier-Boutry, A. Beaurain, R. Galand, B. Pelissier, J. Boussey and M. Zelsmann. "XPS study of the degradation mechanism of fluorinated anti-sticking treatments used in UV nanoimprint lithography". *Microelectronic Engineering,* 87, 122-124, 2010.

[111] T. C. Bailey. "Imprint Template Advances and Surface Modification, and Defect Analysis for Step and Flash Imprint Lithography". *Ph.D. University of Texas at Austin,* 2003**.**

[112] S. Garidel, M. Zelsmann, N. Chaix, P. Voisin, J. Boussey, A. Beaurain and B. Pelissier. "Improved release strategy for UV nanoimprint lithography". *Journal of Vacuum Science and Technology B,* 25, 2430-2434, 2007.

[113] K. Wu. "Interface Study for Template Release in Step and Flash Imprint Lithography". *Ph.D. Dissertation, The University of Texas at Austin,* 2006**.**

[114] M. Bender, M. Otto, B. Hadam, B. Spangenberg and H. Kurz. "Multiple imprinting in UV-based nanoimprint lithography: related material issues". *Microelectronic Engineering,* 61-62, 407-413, 2002.

[115] http://www.stanford.edu/dept/EHS/prod/researchlab/lab/safety_sheets/08-111.pdf. **2011.**

[116] D. A. Skoog, F. J. Holler and T. A. Nieman. "Principles of Instrumental Analysis"; 5 Ed.; Brooks Cole; 1997.

[117] M. W. Lin. Personal Communication. 2008.

[118] Z. Otwinoski and W. Minor. "Methods in Enzymology". 1997.

[119] A. Altomare, M. C. Burla, M. Camalli, G. L. Cascarano, C. Giacovazzo, A. Guagliardi, A. G. G. Moliterni, G. Polidori and R. Spagna. "*SIR97*: a new tool for crystal structure determination and refinement". *Journal of Applied Crystallography,* 32, 115-119, 1999.

[120] G. M. Sheldrick. "A short history of *SHELX*". *Acta Cryst.,* A64, 112-122, 2008.

[121] A. L. Spek. "PLATON, A Multipurpose Crystallographic Tool". Utrecht University. Utrecht, The Netherlands. 1998.

[122] L. J. Farrugia. "*WinGX* suite for small-molecule single crystallography". *Journal of Applied Crystallography,* 32, 837-838, 1999.

[123] "International Tables for X-ray Crystallography"; Vol. C Ed.; Kluwer Academic Press; Boston, 1992.

[124] G. M. Sheldrick. "SHELTX/PC (Version 5.03)". Siemens Analytical X-ray Instruments, Inc. Madison, Wisconsin, USA. 1994.

[125] I. Keithley Instruments. "Model 590 CV Analyzer Instruction Manual".

[126] I. Keithley Instruments. "Model 590 CV Analyzer, Quick Reference Guide".

[127] I. Keithley Instruments. "Gate Dielectric Capacitance-Voltage Characterization Using the Model 4200 Semiconductor Characterization System".

[128] I. Keithley Instruments. "Model 590 CV Analyzer Instruction Manual".

[129] I. Keithley Instruments. "Model 590 CV Analyzer, Quick Reference Guide".

[130] I. Keithley Instruments. "Gate Dielectric Capacitance-Voltage Characterization Using the Model 4200 Semiconductor Characterization System".

Vita

Börje Michael Jacobsson was born on January 15, 1979 in Täby, Sweden, the youngest son of Börje and Rose-Marie Jacobsson. After graduating from Åva Gymnasium in 1998, he enrolled at Southern Methodist University in Dallas, Texas. He graduated with a Bachelor's of Science in Biological Sciences and a Bachelor's of Art in Chemistry, after which he enrolled in the Master's of Science program in Chemistry under the supervision of Professor David Y. Son. Following graduation, he enrolled in the Chemistry and Biochemistry graduate program at The University of Texas at Austin and commenced doctoral studies under the supervision of Professor C. Grant Willson. While pursuing his doctoral degree, he completed a summer internship at Procter and Gamble in Cincinnati, Ohio. On November 6, 2010 he married Elizabeth A. McClure in Denton, Texas. After receiving his doctoral degree, he will be employed by Sid Richardson Carbon & Energy Co. at their research facility in Fort Worth, Texas.

Permanent address: Tranholmsvägen 21, 178 32 Ekerö, Sweden

This dissertation was typed by the author.